Institut für Theoretische Physik

Fakultät Mathematik und Naturwissenschaften

Technische Universität Dresden

Advanced electronic structure theory: From molecules to crystals

Dissertation

zur Erlangung des

Doktorgrades der Naturwissenschaften

(Doctor rerum naturalium)

vorgelegt von

CHRISTIAN BUTH

geboren am 15 Februar 1975 in Mönchengladbach

Dresden 2005

MAX-PLANCK-INSTITUT FÜR PHYSIK KOMPLEXER SYSTEME

Höhere Elektronenstrukturtheorie: Vom Molekül zum Kristall: In dieser Dissertation werden *ab initio* Theorien zur Beschreibung der Zustände von perfekten halbleitenden und nichtleitenden Kristallen, unter Berücksichtigung elektronischer Korrelationen, abgeleitet und angewandt. Als Ausgangsbasis dient hierzu die Hartree-Fock Approximation in Verbindung mit Wannier-Orbitalen. Darauf aufbauend studiere ich zunächst in Teil I der Abhandlung den Grundzustand der wasserstoffbrückengebundenen Fluorwasserstoff und Chlorwasserstoff zick-zack Ketten und analysiere die langreichweitigen Korrelationsbeiträge. Dabei mache ich die Basissatzextrapolationstechniken, die für kleine Moleküle entwickelt wurden, zur Berechnung von hochgenauen Bindungsenergien von Kristallen nutzbar.

In Teil II der Arbeit leite ich zunächst eine quantenfeldtheoretische *ab initio* Beschreibung von Elektroneneinfangzuständen und Lochzuständen in Kristallen her. Grundlage hierbei ist das etablierte algebraische diagrammatische Konstruktionsschema (ADC) zur Approximation der Selbstenergie für die Bestimmung der Vielteilchen-Green's-Funktion mittels der Dyson-Gleichung. Die volle Translationssymmetrie des Problems wird hierbei beachtet und die Lokalität elektronischer Korrelationen ausgenutzt. Das resultierende Schema wird Kristallorbital-ADC (CO-ADC) genannt. Ich berechne damit die Quasiteilchenbandstruktur einer Fluorwasserstoffkette und eines Lithiumfluoridkristalls. In beiden Fällen erhalte ich eine sehr gute Übereinstimmung zwischen meinen Resultaten und den Ergebnissen aus anderen Methoden.

Advanced electronic structure theory: From molecules to crystals: In this dissertation, theories for the *ab initio* description of the states of perfect semiconducting and insulating crystals are derived and applied. Electron correlations are treated thoroughly based on the Hartree-Fock approximation formulated in terms of Wannier orbitals. In part I of the treatise, I study the ground state of hydrogen-bonded hydrogen fluoride and hydrogen chloride zig-zag chains. I analyse the long-range contributions of electron correlations. Thereby, I employ basis set extrapolation techniques, which have originally been developed for small molecules, to also obtain highly accurate binding energies of crystals.

In part II of the thesis, I devise an *ab initio* description of the electron attachment and electron removal states of crystals using methods of quantum field theory. I harness the well-established algebraic diagrammatic construction scheme (ADC) to approximate the self-energy, used in conjunction with the Dyson equation, to determine the many-particle Green's function for crystals. Thereby, the translational symmetry of the problem and the locality of electron correlations are fully exploited. The resulting scheme is termed crystal orbital ADC (CO-ADC). It is applied to obtain the quasiparticle band structure of a hydrogen fluoride chain and a lithium fluoride crystal. In both cases, a very good agreement of my results to those determined with other methods is observed.

Den lieben Dresdnern.

Contents

Contents

II

List of Figures

List of Tables

1 Introduction

Solids are macroscopic objects of our sensuous reality; one can see, touch and taste them. However, their properties originate from the basic constituents, the electrons and nuclei. They form atoms which themselves form molecules that finally condense into solids [1,2]. Quantum mechanics is the fundamental physical theory which governs the microscopic world where the electrons and nuclei live in and has to be regarded to describe solids. This is one of the earliest theoretical insights gained by the failure of the classical Drude theory of metals which had to be replaced by the Sommerfeld theory [3].

The description of solids in terms of the electrostatic interaction among the constituents represents an example of physical systems which is not only complicated, i.e., composed of many interwoven subunits, but *complex*, i.e., inseparable into subunits [4]. This property can be traced back to the non-linear Coulomb interaction; the mutual influence of the movements of the electrons, of the nuclei and between electrons and nuclei leads to a correlated behavior which has to be accounted for appropriately in a meaningful description of solids. It has been very important to realize that, although electrostatic interactions are of infinite range, correlations are predominantly local and can be described with theories that account for them only in a finite fraction of a solid which encloses a volume of a few cubic-Ångstrom [1,2]. Within the fractions, correlations lead to inseparability and complex behavior. However, the particles in distinct fractions, i.e., subunits, of the solid exhibit vanishing spatial orbital overlaps and hence can be distinguished. However, there are also electron correlations in this regime, namely the long-range van der Waals dispersion interaction [Chapters 3, 4].

Crystals represent a special type of solids that is characterized by a small group of atoms which is repeated throughout space such that it forms a regular, translationally symmetric, three-dimensional structure [Chapter 2]. The most important characteristics of a crystal are its ground-state properties, predominantly binding energies, which immediately provide the crystal structure and various other energy derived quantities. Moreover, the ground-state expectation values of operators are also significant [Chapter 3]. Excited states of solids can be classified into excitonic states of N electrons and electron attachment and electron removal states of $N \pm 1$, $N \pm 2$, $N \pm 3$, ... electrons, respectively. Particularly $N \pm 1$ electron states are of great interest to the solid state physicist as they reveal fundamental properties of crystals [1–3,5–7]. Their determination on an *ab initio* level is therefore an important issue in solid state theory [Chapter 5]. States where initially more than a single electron is attached or removed are only rarely regarded.

Nowadays, solids are predominantly studied with two major approaches. On the one hand, model physics mostly heads for an *a posteriori* description of the main characteristics observed in experiments. Well established are the models of Hubbard, Anderson, Heisenberg and their derivatives. Devising models requires a profound expertise, experi-

ence and physical intuition and does not free one from a careful extraction of information from their solutions [1,3]. Models are typically chosen to be minimal which means that the model is the crudest approximation to the physical reality that shows the desired properties. There are also cases where several models are able to account for a certain experimental observation and it remains obscure which one is the most appropriate in the given situation without further information. This limits the usefulness of models to a purely explanatory device.

On the other hand, first principles approaches are meant to provide competitive accuracy with experimental investigations and to make reliable *a priori* predictions of observables. Density functional theory (DFT) [8,9] is an ubiquitous candidate and particular attention has been paid to the time-independent DFT in local density approximation (LDA), due to its numerical simplicity. It focuses on the ground-state electron density and yields ground-state properties [6,10].

DFT also provides Kohn-Sham orbital energies which are in several cases successfully interpreted to be energies of $N \pm 1$ excited states. These one-particle energies depend on the continuous crystal momentum quantum number which classifies them with respect to translational symmetry. Plotting the energies along certain paths through the Brillouin zone—which is the set of all unique crystal momenta—the energies arrange graphically into bands. Such a figure is typically referred to as a one-particle *band structure*.

It is well known that improvements on a general scale of the results of density functional theory computations are difficult to achieve because the underlying approximate density functionals need to be exchanged by other ones which have been devised under different model assumptions. As there is no systematic hierarchy of density functionals of increasing quality, such a replacement of the functional is not bound to yield improvements. It is the description of the $N \pm 1$ excited states where the insufficiencies of time-independent DFT become most apparent. In insulating materials, e.g., the LDA tends to significantly underestimate the band gap, e.g., Reference [11].

A number of ingenious methods have been devised to improve the description of $N \pm 1$ excited states from time-independent density functional theory. For example, the calculations have been supplemented by a GW treatment, e.g., References [1,12], or the so-called LDA+U method [13]. Other improvements concern the use of optimized effective potentials [14] such as the exact exchange potential [15] instead of its local, simplified form. Furthermore, DFT has been coupled with various extensions of the *coherent potential approximation (CPA)* like the *dynamical CPA* [16,17] or *dynamical mean field theory (DMFT)* [18–23]. Also Faddeev's method [24] of treating the three-particle t-matrix has been applied in conjunction with LDA band structure calculations [25]. The same holds true for different forms of the projection operator technique [1,2]. Within the conceptual framework of DFT, the time-dependent generalization is a route to treat excited states in a formally rigorous way. Yet, one must face the fact that the various approximations to time-independent and time-dependent DFT remain uncontrolled and therefore have to be reconsidered from case to case.

When one is aiming at controlled approximations, two different routes offer themselves which are wave-function-based, first-principles approaches, also referred to as *ab initio* theories. The *quantum Monte Carlo (QMC)* method, e.g., Reference [26], is a simple and straight forward way of dealing with the many-particle problem. Yet, it suffers from one

serious shortcoming, the so-called sign problem when treating fermions. Alternatively, emerging from the studies of atoms and molecules, polymers and crystals come more and more into the focus of quantum chemists [1, 2, 27, 28]. Bridging the gap between the study of molecules and the investigation of periodic systems is a fruitful endeavor to both quantum chemists and solid state physicists which will lead to a more profound understanding. Particularly, quantum chemical theories and methods are in a tradition of formal clarity and a great analytical and numerical care [29]. These are appealing benefits in comparison with the mostly trend oriented approaches of theoretical solid state physics [29]. I devote this thesis to a derivation of quantum chemical theories for periodic systems and their application to polymers and crystals. Part I considers the ground state of crystals and Part II treats their electron attachment and electron removal states.

I commence with the simplest *ab initio* wave function model of solids, which is provided by the Hartree-Fock approximation, in Chapter 2. With respect to the true, interacting, many-particle system, it represents the best antisymmetrized, independent-particle model. For most semiconducting or insulating substances, this approximation already provides a satisfactory accuracy and represents a very good starting point to treat electron correlations in the ground state and in the excited states. Meanwhile, the Hartree-Fock approximation can be employed routinely, thereby taking advantage of program packages like WANNIER which has been developed by Shukla *et al.* [30–32] in Dresden or CRYSTAL that originates from Torino [5, 7].

The Hartree-Fock wave function is invariant under unitary transformations of its constituting orbitals. I discuss two different views on these one-particle states, namely the completely delocalized plane-wave-like *Bloch orbitals* and the localized atomic-orbital-like *Wannier orbitals* which both provide a starting point for a subsequent treatment of electron correlations. For this purpose the whole range of quantum chemical correlation methods offers itself. Among those the *coupled-cluster theory (CC)* of Coester and Kümmel [33–35] is singled out. It is one of the most successful and manifold many-particle theories known [36]. CC naturally leads to a hierarchy of size-consistent methods which exhibit, in most cases, a strikingly rapid convergence to the *full configuration interaction (FCI)* limit [Chapter 3].

Molecular clusters [37] have been receiving a lot of attention because they can be seen as a bridge between the individual monomer and solids formed by many monomers. Consequently, a description of the infinite crystal using finite fractions of it, i.e., molecular clusters, should be possible. Indeed, the localized orbitals obtained for the center of the clusters can be shown in many cases to approximate well the Wannier orbitals of the infinite solid [1, 2, 38]. An *ab initio* correlated wave function model for molecules [39–42], e.g., the CC or FCI method, can now be used in conjunction with the *incremental scheme* [1, 2, 38, 43–45] to obtain a physically meaningful decomposition of the correlation energy of crystals in terms of non-additive many-body interactions, so-called *energy increments*, between groups of Wannier orbitals associated with individual fragments, e.g., atoms, in the unit cell of the crystal. The incremental scheme allows a detailed study of the origin and impact of electron correlations and, moreover, provides a convenient convergence criterion [1, 2, 38, 43–45].

The two most significant errors that deteriorate the correlation energy obtained from

ab initio calculations are given by the *N-electron error* and the *basis set error*. The *N*-electron error is caused by the truncation of the *N*-electron wave function model utilized while the basis set error refers to the incomplete one-particle basis set that is used. The *N*-electron error is approximately determined from the basis set limit of a correlation method by comparison with experimental results, the so-called *apparent error*, or a higher order wave function model [46]. In order to address the first source of error, the *N*-electron error, coupled-cluster singles and doubles has been employed which provides good accuracy.

The main source of the basis set error can be identified by investigating the behavior of many-particle wave functions for a nearly vanishing distance between two electrons r_{12} which remains regular. At $r_{12} = 0$, the divergence of the Coulomb repulsion is cancelled by the first derivative of the wave function, the so-called Kato *electron cusp condition* [42, 46, 47]. It yields a behavior of the (unnormalized) wave function for small r_{12} of the following type for the helium atom [42, 46]

$$\Psi(r_1, r_2, r_{12}) = 1 + \frac{1}{2}r_{12} + O(r_{12}^2) \tag{1.1}$$

where r_1 and r_2 denote the distance of electron one and two, respectively, to the nucleus of the atom. This wave function (1.1) exhibits the *Coulomb cusp* at $r_{12} = 0$ where its shape for r_{12} close to zero is referred to as the *Coulomb hole*. The accurate representation of the hole poses a difficult problem to the usual orbital basis sets and makes the largest contribution to the basis set error.

In order to achieve *chemical accuracy* in the theoretical binding energies of crystals, i.e., $1\frac{\text{kcal}}{\text{mol}} = 4.184\frac{\text{kJ}}{\text{mol}} = 0.0433641\frac{\text{eV}}{\text{unit}} = 1.5936\frac{\text{mE}_h}{\text{unit}}$ where unit denotes the group of atoms with respect to which the energy is given, the basis set convergence of Hartree-Fock and correlation energies should be studied systematically in the first place for *periodic* systems [Chapter 4]. To this end, the hierarchical series of correlation consistent basis sets [48] cc-pVXZ [49,50], aug-cc-pVXZ [49–51] and d-aug-cc-pVXZ [49,51,52], $X = $ D, T, Q, 5, 6 are especially well suited. The cardinal number X of the members of such a series is related to both, the highest angular momentum in the basis sets, and the number of basis functions which jointly increase with growing X. Hartree-Fock energies are well known to converge exponentially, e.g., Reference [53], towards the basis set limit, whereas correlation energies turn out to converge only with the third power of the highest angular momentum employed in a series of hierarchical basis sets [42,46,54]. This implies a disastrously slow convergence of the correlation energies with the quality of the one-particle basis set [42,46]. The time required for the calculations scales with the fourth power of the number of basis functions in the basis set because the number of two-electron integrals grows with this rate, implying that substantial improvements of the accuracy of the results cannot be achieved with acceptable effort. However, the convergence properties of the Hartree-Fock energy [53] and the correlation energy [42,46,55–59] can be exploited to extrapolate them towards the basis set limit [Chapter 3]. As only standard methods of quantum chemistry are required, basis set extrapolation of correlation energies provides an interesting alternative over the specialized, explicitly correlated (R12) methods, which per construction regard (1.1), generalized to molecular many-electron systems, and directly yield near basis set limit wave functions and correlation energies but have a high computational demand [42,46,60].

The powerful theory developed for basis set extrapolation of molecular ground-state

energies is harnessed to explore *hydrogen bonding* in crystals. This type of bonding has been a research topic for many years due to considerable difficulties encountered. A thorough treatment requires both a very good electron correlation method and a large one-particle basis set due to the low binding energy associated with it [57, 61]. In other words, a careful analysis of the sources of errors involved is required in the calculations. I need to come close to chemical accuracy in the binding energy. Hydrogen fluoride and hydrogen chloride crystals provide good initial candidates for an in depth analysis of hydrogen bonding because HF forms strong hydrogen bonds and HCl forms weak hydrogen bonds. Moreover, isolated infinite bent chains, $(HF)_\infty$ and $(HCl)_\infty$, already represent a realistic model of the corresponding crystals. An analysis has not been carried out so far using *ab initio* methods in conjunction with the incremental scheme. Therefore, the modeling of hydrogen-bonded crystals using oligomers has to be investigated carefully and the convergence of the incremental series needs to be studied [Chapter 4].

Excited states of solids, especially $N \pm 1$ excited states, are, by far, less well researched with *ab initio* theories than the ground state, despite the fact that a considerable effort has been invested [1, 2, 27, 28]. This has to be attributed mainly to the notably increased complexities of their description which require substantial theoretical advancements over theories to treat ground states [1, 2, 27, 28]. A series of attempts with wave-function-based methods has been undertaken [1, 2, 27, 28, 62–72]. They typically rely on the fact that the simple one-particle picture of $N \pm 1$ excited states does not change dramatically once electron correlations are fully considered for, typically, the outer valence states and the lowest virtual states. The symmetry classified $N \pm 1$ excited states, obtained from an accurate treatment of electron correlations, are already well-represented by the one-particle approximation. They form a so-called *quasiparticle band structure* which differs only by relative shifts and changes in bandwidths from the band structure of the underlying one-particle theory. Despite of their inherent many-particle description, a strict correspondence to the one-particle bands holds [1, 2]. However, particularly in the case of inner valence states of solids, a strong coupling to excited configurations leads to a break down of the quasiparticle picture [1, 3, 73–76]. One observes a multitude of so-called satellite peaks aside of the quasiparticle peak. Furthermore, on surfaces, core states and virtual states correspond to resonances which decay by electron emission. This leads to an abundance of states instead of a single one-particle peak [1, 73–76]. In both cases, the notion of band structures becomes inappropriate and only translational symmetry classification of excited states with respect to the crystal momentum remains [Chapters 5 and 7].

Previous *ab initio* theories for $N \pm 1$ excited states of crystals comprise a local Hamiltonian approach [2, 63–67, 69, 72] which has been shown to improve on the Hartree-Fock energy bands substantially but is presently only applicable to the valence bands of crystals. Moreover, based on Toyozawa's electronic polaron model [77], Suhai repartitions MP2 pair energies to estimate quasiparticle band structures [27, 28, 78–81]. By inserting the orbital energies into the energy-dependent self-energy, this model was shown to be a special case of *outer valence Green's functions (OVGF)* [82–84] that were derived in terms of crystal orbitals by Liegener [27, 28, 81, 85]. By applying the approximation to the self-energy of Igarashi *et al.* [62, 68], quasiparticle band structures were obtained by Albrecht *et al.* [68–70]. Many of these theories are only applicable under special, very

favorable, conditions and virtually all of them fail to describe strong correlations and electronic resonances appropriately. Hence a considerable theoretical and methodological advancement is required.

In the field of molecular physics, the *algebraic diagrammatic construction (ADC)* scheme [86–88] has been devised to represent diagrammatic series for propagators in a closed form which are ubiquitous in quantum field theory. In order to obtain band structures, the ADC scheme of the self-energy is used in conjuction with Dyson's equation to approximate the Feynman-Dyson perturbation series of the one-particle Green's function. It contains sums of certain proper and improper diagrams to infinite order [87, 89, 90] and converges to full configuration interaction with increasing order of the diagrammatic expansion. The basic properties of the ADC scheme and their derivations, as applied to molecules, are found in References [91–93]. Among those properties size-extensivity is an important one since it is crucial when solids are considered. Furthermore, the ADC method is known to be robust and also facilitates to study strong electron correlations due to the efficient and stable evaluation of the one-particle Green's function in terms of a Hermitian eigenvalue problem to obtain its spectral representation. In molecules strong correlations, for instance, occur when inner valence electrons are treated [73–76]. ADC has been shown to be superior to the OVGF method [84] and numerous works have been carried out over the last two decades, e.g., References [73–76], including studies of oligomers and clusters chosen to model infinite chains or crystals [94–96].

I devise an ADC scheme [86–88] for the self-energy of crystals which I denote by *crystal orbital ADC (CO-ADC)*. A formulation in crystal momentum and Wannier representation is given where the latter one is also suited to exploit the local character of electron correlations particularly for crystals with a large unit cell [Chapters 6, 6.4]. I have realized the ADC and CO-ADC method in terms of a computer program [97]. In the first place, the ionization potentials of a HF and a LiF molecule are computed and analyzed to obtain an understanding of the building blocks of the $(HF)_\infty$ chain and the LiF crystal which I have chosen for a first application. The band structure of the $(HF)_\infty$ chain is obtained and compared to results determined independently with the local Hamiltonian approach [98] and OVGF [99]. Similarly, the band structure of a LiF crystal is computed and compared to published results obtained by Albrecht [70] with the method of Igarashi *et al.* [62, 68] [Chapter 7].

Atomic units [39–42] are used throughout this dissertation: the reduced Planck constant $\hbar$, the electron charge magnitude and the electron mass are set to unity. The unit of length is the Bohr and the unit of energy is the Hartree. The conversion factors to *SI units* are $1\,\mathrm{Bohr} = 1\,E_b = 52.917\,721\,08\,\mathrm{pm}$ and $1\,\mathrm{Hartree} = 1\,E_h = 27.211\,384\,5\,\mathrm{eV}$ from the CODATA 2002 recommended values of Reference [100]. Additionally, the unit of length $1\,\text{Ångstrom} = 1\,\text{Å} = 0.1\,\mathrm{pm}$ is used.

Part I

Ground state

2 Ab initio foundation

The quantum mechanical basis for a first principles description of crystals is introduced here with special emphasis on the translational and point group symmetries which make up their appealing esthetics [Section 2.1]. Fundamental to crystals, in contrast to atoms and molecules, is the translational symmetry that I always incorporate explicitly into equations whereas point group symmetry affords a further classification of their states. Exploiting symmetry also allows notable computational savings.

As a foundation of a wave function based treatment, the Hartree-Fock independent particle model is discussed which has been devised in its main characteristics by Hartree [101], Slater [102] and Fock [103]. It already facilitates a lot of insights into an interacting many-particle system and provides the basis of more elaborate methods to describe the ground state and excited states [Section 2.2]. A one-particle basis set is introduced for practical applications and the basis set convergence rate of the Hartree-Fock method is discussed [Section 2.3 and 2.4].

Localized Hartree-Fock orbitals, i.e., Wannier orbitals, are determined, not only to provide an intuitive, chemical view on the crystal orbitals, in contrast to the abstract Bloch orbitals, but also because they are the ideal means to go beyond the one-particle model and head for greater accuracy and new effects. Rigorous proofs for an *a priori* determination of Wannier orbitals are given. The approach is shown to be computationally as efficient as the Bloch orbital based formulation [Sections 2.5 and 2.6].

2.1 Quantum mechanical description

Crystals are periodic systems which consist of a geometrical arrangement of atoms, the *unit cell*, that is repeated after certain distances, the *lattice constants* a_i, $i = 1, 2, 3$ in the three directions of periodicity, denoted by the noncoplanar *primitive lattice vectors* $\vec{a}_i$.[1] Mathematically, one defines a *crystal lattice*[2] by a set of fictitious points, associated with the unit cells and being related to each other by the *lattice vectors*

$$\vec{R} = u_1 \, \vec{a}_1 + u_2 \, \vec{a}_2 + u_3 \, \vec{a}_3 \tag{2.1}$$

with integer numbers u_i. Relative to $\vec{R}$, the M atoms in a unit cell are given by the displacements $\vec{d}_i$, $i = 1, \ldots, M$. By definition (2.1), the model of a crystal exhausts all space; a very appropriate assumption, if surface effects are not to be considered.

A convenient further simplification assumes a large parallelepiped with N_i unit cells along the three primitive vectors $\vec{a}_i$, $i = 1, 2, 3$ with a volume of $N_0 = N_1 \, N_2 \, N_3$ unit

---

[1]In this thesis, I formulate all the equations for three-dimensional crystals. Adaption to systems that are periodic in only one or two dimensions is straight forward.

[2]A crystal lattice constitutes an *affine space*. Yet, by arbitrarily choosing an origin, one obtains a *vector space*; this is tacitly assumed in what follows.

cells. The lattice indices which correspond to distinct unit cells in (2.1) are then given by $0 \le u_i \le N_i - 1$ where all other integer numbers $\tilde{u}_i$, are cyclically mapped to this range by $\tilde{u}_i \bmod N_i$. These definitions are termed *Born von Kármán* or *periodic boundary conditions*. The parallelepiped is also referred to as *Born von Kármán region*. In one-dimensional periodic systems, referred to as *chains* or less precise as *polymers*, Born von Kármán boundary conditions represent the topology of a ring, whereas the boundary conditions for systems with a periodicity in two dimensions, so-called *slabs* or colloquially *surfaces*, exhibit the topology of a torus. For three-dimensional crystals the topology of a toroid in four dimensional space is obtained. Meaningful results of bulk properties, which are derived by imposing periodic boundary conditions, are required to hold in the limit $N_0 \to \infty$.

To each crystal lattice (2.1) there exists a *reciprocal lattice* whose primitive vectors are defined by the conditions $\vec{a}_i \, \vec{b}_j = 2\pi \, \delta_{ij}$, $i, j = 1, 2, 3$. It consists of the vectors

$$\vec{K} = v_1 \, \vec{b}_1 + v_2 \, \vec{b}_2 + v_3 \, \vec{b}_3 \tag{2.2}$$

with integer numbers v_i. Furthermore, $\vec{R} \, \vec{K} = 2\pi \, n_{\vec{R}\vec{K}}$ holds with an integer number $n_{\vec{R}\vec{K}} = u_1 \, v_1 + u_2 \, v_2 + u_3 \, v_3$ [3, 6].

Implicitly, fixed nuclei are assumed in (2.1). In many cases this is a very good approximation as the coupled movement of the electrons and the nuclei in a molecule, cluster or solid frequently can be neglected in a first approximation because the electrons are moving more rapidly than the nuclei due to the mass ratio of 10^{-4}–10^{-5} [6, 39] between the former and the latter ones. Therefore, the electrons adjust almost instantly to the slow motion of the nuclei. This is utilized to separate the total Hamiltonian that depends on the combined electronic and nuclear coordinates into an electronic and a nuclear part which can thus be studied independently. The separation is called *Born-Oppenheimer approximation* [39, 104] and is assumed throughout. Only the electronic part is investigated here in the *fixed-nuclei approximation*. With the help of these so-called adiabatic solutions to the electronic problem, non-Born-Oppenheimer effects can, nevertheless, be studied.

Electronic structure theory is the branch of atomic, molecular and solid state physics that is concerned with the accurate description of the electronic states of many-particle systems: the ground state, the excited, electron attachment and electron removal states through which many further properties of the systems are accessible [39]. Since electrons are spin $\frac{1}{2}$ fermions, stationary states[3] lie in the *N-particle Hilbert space* that is a *tensorial product* of N *one-particle Hilbert spaces* [42, 105] which themselves are tensorial products of a one-particle spatial Hilbert space and a spin $\frac{1}{2}$ Hilbert space. Corresponding wave functions $\Psi^N(\vec{r}_1 \, s_1, \ldots, \vec{r}_N \, s_N)$ depend on the *spatial coordinates* $\vec{r}_1, \ldots, \vec{r}_N$ and the *spin coordinates* $s_1, \ldots, s_N$, and are eigenfunctions of the non-relativistic, time-independent, many-particle Schrödinger equation[4] with eigenenergies E^N [27, 28, 39–42]

$$\hat{H} \, \Psi^N(\vec{r}_1 \, s_1, \ldots, \vec{r}_N \, s_N) = E^N \, \Psi^N(\vec{r}_1 \, s_1, \ldots, \vec{r}_N \, s_N) \, . \tag{2.3}$$

---

[3]The theories in this thesis do not provide the lifetime of electronic resonances, like Auger decay on surfaces. This would require a non-Hermitian approach in terms of an extension of the Hilbert space treatment presented here.

[4]Relativistic electronic structure theory is based on the *Dirac equation* [27, 28, 106, 107].

where the Hamiltonian [27, 28, 39–42] is given by

$$\hat{H} = \sum_{n=1}^{N} \hat{h}_n + \frac{1}{2} \sum_{\substack{m,n=1 \\ m \neq n}}^{N} \frac{1}{|\vec{r}_m - \vec{r}_n|} + \hat{E}_{\text{nucl}} \tag{2.4a}$$

$$\hat{h}_n = -\frac{1}{2}\Delta_n - \sum_{i=1}^{N_0}\sum_{A=1}^{M} \frac{Z_{\vec{R}_i A}}{|\vec{r}_n - \vec{r}_{\vec{R}_i A}|} \tag{2.4b}$$

$$\hat{E}_{\text{nucl}} = \frac{1}{2} \sum_{\substack{i,j=1 \\ i \neq j \vee A \neq B}}^{N_0} \sum_{A,B=1}^{M} \frac{Z_{\vec{R}_i A} Z_{\vec{R}_j B}}{|\vec{r}_{\vec{R}_i A} - \vec{r}_{\vec{R}_j B}|} \ . \tag{2.4c}$$

Here N is the number of electrons in the crystal which is represented by a Born von Kármán region of N_0 unit cells. Moreover, M indicates the number of nuclei per unit cell, $Z_{\vec{R}_i A} \equiv Z_A$ stands for the charge of nucleus A in unit cell $\vec{R}_i$ and $|\vec{r}_n - \vec{r}_{\vec{R}_j A}|$ is the distance between the n-th electron and the A-th nucleus in unit cell $\vec{R}_j$. Finally, $|\vec{r}_m - \vec{r}_n|$ represents the distance between the m-th and the n-th electron and $|\vec{r}_{\vec{R}_i A} - \vec{r}_{\vec{R}_j B}|$ denotes the distance between the nuclei A and B of charge $Z_{\vec{R}_i A} \equiv Z_A$ and $Z_{\vec{R}_i B} \equiv Z_B$ in unit cells $\vec{R}_i$ and $\vec{R}_j$. The *core Hamilton operator* $\hat{h}_n$ of (2.4b) is a *one-particle operator* as it involves only the coordinates of a single electron n. Consequently, $|\vec{r}_m - \vec{r}_n|^{-1}$ in (2.4a) is a *two-particle operator*. As the nuclei are fixed, they make a constant electrostatic energy contribution.

The symmetry properties of the Hamiltonian (2.4) are described by a set of operators which commute with each other and with $\hat{H}$ [105]. Its eigenfunctions are simultaneous eigenstates to all these operators, and thus the energy eigenstates can be characterized further according to the symmetry of the system under study. By introducing basis functions which transform according to a specific symmetry operation, the whole problem can be divided into smaller subproblems.

The Hamiltonian (2.4) does not depend on spin, therefore the spin operator $\hat{\vec{s}}_i^2$ of electron i, the total spin operator $\hat{\vec{S}}^2 = \sum_{i=1}^{N} \hat{\vec{s}}_i^2$ and its z-component $\hat{S}_z$ which commute among each other, commute with $\hat{H}$. Furthermore, the Hamiltonian (2.4) is invariant under simultaneous translations of both electronic and nuclear coordinates by an arbitrary vector $\vec{r}$ which implies that the total momentum of the crystal is conserved [3, 6].

The underlying crystal lattice (2.1) imposes the most basic symmetry of crystals on $\hat{H}$, namely the invariance under arbitrary lattice translations $\vec{R}$ of the electrons alone, i.e., $[\hat{T}_{\vec{R}}, \hat{H}] = \hat{0}$. Thereby, the *translation operator* $\hat{T}_{\vec{R}}$ acts on the coordinates of all electrons $\vec{r}_1, \ldots, \vec{r}_N$. This observation has a fundamental consequence for the eigenstates of periodic systems—known as *Bloch's theorem* [3, 6, 108]—which obey[5]

$$\begin{aligned} \Psi_{\vec{k}n}(\vec{r}_1 + \vec{R}\, s_1, \ldots, \vec{r}_N + \vec{R}\, s_N) &= \hat{T}_{-\vec{R}}\, \Psi_{\vec{k}n}(\vec{r}_1\, s_1, \ldots, \vec{r}_N\, s_N) \\ &= \mathrm{e}^{\mathrm{i}\vec{k}\vec{R}}\, \Psi_{\vec{k}n}(\vec{r}_1\, s_1, \ldots, \vec{r}_N\, s_N) \ . \end{aligned} \tag{2.5}$$

---

[5]To formulate Bloch's theorem consistently with the established notation in the literature [3, 6, 108], I have to note that it is written in terms of active lattice translations. However, the translation operator $\hat{T}_{\vec{R}}$ refers to passive lattice translations. Therefore, I have to change the notation from $\hat{T}_{\vec{R}}$ to $\hat{T}_{-\vec{R}}$ in Equation (2.5).

Such functions are referred to as *Bloch functions (BF)*. In Equation (2.5), different states are enumerated by n to the *crystal momentum (wave vector)* quantum number which is denoted by $\vec{k}$. Crystal momenta are usually chosen to lie in the (first) *Brillouin zone* [3,6] which represents the region of space that is closer to the origin than to any other point of the reciprocal lattice (2.2). The whole surface of the resulting solid figure is conventionally also included [3,6]. Imposing Born von Kármán boundary conditions, the number of distinct crystal momenta $\vec{k}$ becomes discrete. They are given by the points [3,6]

$$\vec{k} = \frac{h_1}{N_1}\,\vec{b}_1 + \frac{h_2}{N_2}\,\vec{b}_2 + \frac{h_3}{N_3}\,\vec{b}_3 + \vec{K} \quad \text{for} \quad 0 \le h_i \le N_i \quad \text{with} \quad i = 1, 2, 3 \qquad (2.6)$$

folded back into the Brillouin zone by a suitable reciprocal lattice vector $\vec{K}$. Therefore, integrations over the whole zone, that occur frequently throughout, are replaced by finite summations.[6]

The remaining symmetry operations, which transform the crystal lattice (2.1) into itself, are given by proper and improper rotations represented in terms of orthogonal 3×3 matrices $\boldsymbol{\alpha}$ in conjunction with a translation $\vec{t}$. They can jointly be written as an *affine transformation* of the vector $\vec{r}$ [6,110]

$$\vec{r}\,' = \boldsymbol{\alpha}\,\vec{r} + \vec{t} \qquad (2.7)$$

and are frequently referred to by the symbol $\{\boldsymbol{\alpha}|\vec{t}\}$. The set of such operations with an invariant subgroup of pure lattice translations constitute a *space group*. From the rotational part $\boldsymbol{\alpha}$ of a space group, one can construct the *point group* [6].

2.2 Hartree-Fock approximation

The simplest ansatz for the wave function of an N-particle system $\Phi_0'^N(\vec{r}_1\,s_1, \ldots, \vec{r}_N\,s_N)$ is a so-called *Hartree product* [3,39–42,101] of N' independent normalized one-particle wave functions $\psi_{\vec{k}\,i}(\vec{r}\,s)$ to each crystal momentum $\vec{k}$

$$\Phi_0'^N(\vec{r}_1\,s_1, \ldots, \vec{r}_N\,s_N) = \prod_{\vec{k}} \prod_{i=1}^{N'} \psi_{\vec{k}\,i}(\vec{r}_j\,s_j) \qquad (2.8)$$

where $N' = \frac{N}{N_0}$ represents the number of electrons per unit cell. The $\psi_{\vec{k}\,i}(\vec{r}\,s)$ depend on the spin, i.e., they are two-component spinors [3,39–42,105,111]

$$\psi_{\vec{k}\,i}(\vec{r}\,s) = \begin{pmatrix} \psi_{\vec{k}\,i_\uparrow}^\uparrow(\vec{r}) \\ \psi_{\vec{k}\,i_\downarrow}^\downarrow(\vec{r}) \end{pmatrix}_s \qquad (2.9)$$

where $\psi_{\vec{k}\,i}^\uparrow(\vec{r}) = \psi_{\vec{k}\,i}(\vec{r}, \frac{1}{2}) \equiv \psi_{\vec{k}\,i}(\vec{r}, \uparrow)$ and $\psi_{\vec{k}\,i}^\downarrow(\vec{r}) = \psi_{\vec{k}\,i}(\vec{r}, -\frac{1}{2}) \equiv \psi_{\vec{k}\,i}(\vec{r}, \downarrow)$ represent *spatial one-particle wave functions* for the spin up and the spin down components, respectively.

---

[6]If Born von Kármán boundary conditions are not harnessed, a Monkhorst-Pack net can be used instead to carry out numerical integrations over the now continuous crystal momentum vector in terms of finite sums [5,7,109].

The indices i enumerate spinors whereas the indices $i_\uparrow$ and $i_\downarrow$ enumerate corresponding spatial components. Antisymmetrizing the product (2.8) to conform with the Pauli exclusion principle results in an expression which can be written in terms of the *Slater determinant* [27, 28, 39–42, 102, 112–115]

$$\Phi_0^N(\vec{r}_1\,s_1,\ldots,\vec{r}_N\,s_N) \;=\; \tfrac{1}{\sqrt{N!}}\det\begin{pmatrix} \phi_{1,1} & \cdots & \phi_{1,N_0} \\ \vdots & \ddots & \vdots \\ \phi_{N_0,1} & \cdots & \phi_{N_0,N_0} \end{pmatrix}. \tag{2.10}$$

I refer to the $N \times N$ matrix in (2.10) as *Slater matrix* $\boldsymbol{\mathcal{S}}^{\mathrm{BF}}$. It is composed of the $N' \times N'$ matrices

$$\phi_{lm} = \begin{pmatrix} \psi_{\vec{k}_m\,1}(\vec{r}_{1+(l-1)\,N'}\,s_{1+(l-1)\,N'}) & \cdots & \psi_{\vec{k}_m\,N'}(\vec{r}_{1+(l-1)\,N'}\,s_{1+(l-1)\,N'}) \\ \vdots & \ddots & \vdots \\ \psi_{\vec{k}_m\,1}(\vec{r}_{N'+(l-1)\,N'}\,s_{N'+(l-1)\,N'}) & \cdots & \psi_{\vec{k}_m\,N'}(\vec{r}_{N'+(l-1)\,N'}\,s_{N'+(l-1)\,N'}) \end{pmatrix} \tag{2.11}$$

to one of the N_0 crystal momenta which label the irreducible representations of the translational group.[7] The one-particle wave functions $\psi_{\vec{k}_i}(\vec{r}_j\,s_j)$, $i = 1,\ldots,N'$, $j = 1,\ldots,N$ in the Hartree product are now termed *spin orbitals*[8] and obey Bloch's theorem (2.5), individually. For this reason they are also frequently referred to as spin *Bloch orbitals*.

The energy expectation value with respect to the ansatz (2.10) for Φ_0^N always provides an upper bound to the exact ground state energy E_0^N

$$\mathcal{L}[\Phi_0^N(\vec{r}_1\,s_1,\ldots,\vec{r}_N\,s_N)] = \langle\,\Phi_0^N(\vec{r}_1\,s_1,\ldots,\vec{r}_N\,s_N)\,|\,\hat{H}\,|\,\Phi_0^N(\vec{r}_1\,s_1,\ldots,\vec{r}_N\,s_N)\,\rangle \geq E_0^N\,. \tag{2.12}$$

Minimizing the energy functional $\mathcal{L}$ with respect to $\Phi_0^N(\vec{r}_1\,s_1,\ldots,\vec{r}_N\,s_N)$, Equation (2.12), represents the *Ritz variational principle* [39, 111]. In this case, it implies a minimization with respect to the spin orbitals that constitute the Slater determinant (2.10). Without loss of generality, the additional constraint of orthonormality is imposed on the spin orbitals. One arrives at a set of coupled integro-differential equations, the *Hartree-Fock equations*. In their canonical form, they can formally be written in terms of an eigenvalue problem [39–42] for the orbitals that are used to form the Slater determinant (2.10), the so-called *occupied orbitals*

$$\hat{f}\,\psi_{\vec{k}\,i}(\vec{r}\,s) = \varepsilon_{\vec{k}\,i}\,\psi_{\vec{k}\,i}(\vec{r}\,s) \tag{2.13}$$

with the *Fock operator* [103]

$$\hat{f} = \hat{h} + \hat{v}^{(\mathrm{HF})}\,, \tag{2.14}$$

the core Hamilton operator (2.4b)

$$\hat{h}\,\psi_{\vec{k}\,i}(\vec{r}\,s) = \left[\sum_{\vec{k}'}\sum_{j=1}^{N'}\sum_{s'=-\frac{1}{2}}^{\frac{1}{2}}\int \psi_{\vec{k}'\,j}^*(\vec{r}'\,s')\,\hat{h}\,\psi_{\vec{k}'\,j}(\vec{r}'\,s')\,\,\mathrm{d}^3r'\right]\psi_{\vec{k}\,i}(\vec{r}\,s) \tag{2.15}$$

---

[7]Additional point group symmetries allow to further decompose the matrices $\phi(\vec{k})$ into subblocks until the full space group symmetry has been exploited in a similar fashion as for the translational symmetry.

[8](Spin-)orbitals are also frequently termed *one-particle wave functions*, a misnomer because the antisymmetrized Hartree product is no longer a simple product. In the Hartree-Fock equations, the orbitals couple via the exchange operator (2.18). Moreover, the energy expression (2.26) is not just a sum of the one-particle energies [3, 39–42].

and the *Hartree-Fock potential*

$$\hat{v}^{(\mathrm{HF})} = \sum_{\vec{k}'} \sum_{j=1}^{N'} (\hat{J}_{\vec{k}'\,j} - \hat{K}_{\vec{k}'\,j}) \tag{2.16}$$

where the *Coulomb operator* is

$$\hat{J}_{\vec{k}'\,j}\,\psi_{\vec{k}\,i}(\vec{r}\,s) = \Big[\sum_{s'=-\frac{1}{2}}^{\frac{1}{2}} \int \mathrm{d}^3 r'\, \psi_{\vec{k}'\,j}^*(\vec{r}'\,s')\, \frac{1}{|\vec{r}-\vec{r}'|}\, \psi_{\vec{k}'\,j}(\vec{r}'\,s') \Big] \psi_{\vec{k}\,i}(\vec{r}\,s) \tag{2.17}$$

and the *exchange operator* is

$$\hat{K}_{\vec{k}'\,j}\,\psi_{\vec{k}\,i}(\vec{r}\,s) = \Big[\sum_{s'=-\frac{1}{2}}^{\frac{1}{2}} \int \mathrm{d}^3 r'\, \psi_{\vec{k}'\,j}^*(\vec{r}'\,s')\, \frac{1}{|\vec{r}-\vec{r}'|}\, \psi_{\vec{k}\,i}(\vec{r}'\,s') \Big] \psi_{\vec{k}'\,j}(\vec{r}\,s)\,. \tag{2.18}$$

Here $\hat{v}^{(\mathrm{HF})}$ is the average one-particle potential experienced by an electron due to the presence of all the other electrons, a mean field, which replaces the two-particle operator $|\vec{r}_m - \vec{r}_n|^{-1}$, $m \neq n$, in the Hamiltonian (2.4). It represents a considerable approximation to the original interacting many-particle system. As $\hat{v}^{(\mathrm{HF})}$ depends on the coordinates of all electrons, one cannot solve (2.13) directly. Instead one has to start from an initial guess and then determine the wave function by iteratively solving the Hartree-Fock equations (2.13) until a self-consistent solution to arbitrary precision is found.

Once $\hat{v}^{(\mathrm{HF})}$ has been obtained, the functional dependence of the Fock operator (2.14) on the spin orbitals can be disregarded. Then $\hat{f}$ becomes an ordinary Hermitian one-particle operator with an infinite number of eigenfunctions. In this case, Equation (2.13) holds not only for occupied orbitals but also for orbitals which are not employed in the Slater determinant (2.10), the so-called *virtual orbitals*. For these reasons, the Hartree-Fock approximation is frequently referred to as a *one-particle approximation* or *independent particle approximation*. However, the ansatz of a Slater determinant (2.10) already accounts for the correlations among electrons with parallel spins. It prevents them to occupy the same region in space leading to the so-called *Fermi hole* or *exchange hole* [1,3,39,116].

In the previous paragraphs Hartree-Fock theory is derived in the Hilbert space which is a tensorial product of spin and spatial Hilbert spaces. As the Hamiltonian (2.4) does not depend on spin, spin-free equations can be obtained by considering the spatial parts of the spin orbitals (2.9) only which are denoted as *spatial orbitals*. For closed-shell ground states, i.e., crystals with an even number of electrons N in a spin singlet state, one needs $N/2$ spatial orbitals to construct the corresponding N spin orbitals. If

$$\psi_{\vec{k}\,i}^{\uparrow,\downarrow}(\vec{r}) := \psi_{\vec{k}\,i}^{\uparrow}(\vec{r}) = \psi_{\vec{k}\,i}^{\downarrow}(\vec{r}) \tag{2.19}$$

is assumed for all $\vec{k}\,i$ and $\vec{r}$, then the resulting spin-free Hartree-Fock equations are formally identical to (2.13) where spin orbitals are replaced by spatial orbitals. This is called the *restricted* Hartree-Fock approximation [39–42, 117, 118]. The *unrestricted* Hartree-Fock approximation [39, 119] assumes two different spatial components in (2.9). In this

case, two equations of the type (2.13) have to be solved in terms of spatial orbitals, one for each component of the spinor.

In atomic physics, Equation (2.13) can be solved numerically to arbitrary precision. Yet, for molecules and crystals this is not feasible. Therefore, one recognizes that the spatial orbitals are members of the spatial one-particle Hilbert space and can thus be expanded in terms of the complete set of one-particle basis functions

$$\chi_{\vec{R}\mu}(\vec{r}) \equiv \hat{T}_{\vec{g}_\mu + \vec{R}}\, \chi_\mu(\vec{r}) = \chi_\mu(\vec{r} - \vec{g}_\mu - \vec{R}) \tag{2.20}$$

for all $\vec{R}$ and $\mu = 1, \ldots, \infty$. Here $\vec{g}_\mu$ is an arbitrary displacement of the μ-th basis function in a unit cell. The $\vec{g}_\mu$ accounts for the fact that a $\chi_\mu(\vec{r})$ is frequently centred on some atom i which is displaced from the origin by some $\vec{d}_i$ inside the origin cell. Frequently the eigenfunctions of a Hermitian one-particle operator are taken as basis functions. Suitable basis sets are discussed in Section 2.3. Linear combinations of basis functions[9] are formed to obtain translational symmetry adapted basis functions which obey Bloch's theorem (2.5)

$$\varphi_{\vec{k}\mu}(\vec{r}) = \frac{1}{\sqrt{N_0}} \sum_{\vec{R}} \mathrm{e}^{\mathrm{i}\vec{k}\vec{R}}\, \hat{T}_{\vec{g}_\mu + \vec{R}}\, \chi_\mu(\vec{r}) \;. \tag{2.21}$$

The operator $\frac{1}{\sqrt{N_0}} \sum_{\vec{R}} \mathrm{e}^{\mathrm{i}\vec{k}\vec{R}}\, \hat{T}_{\vec{g}_\mu + \vec{R}}$ in (2.21) projects out the part of the basis function $\chi_\mu(\vec{r})$ which transforms according to the irreducible representation $\vec{k}$ where the basic *orthogonality relations* [3, 6]

$$\sum_{\vec{R}} \mathrm{e}^{\mathrm{i}\vec{k}\vec{R}} = N_0\, \delta_{\vec{k}, \vec{0}} \tag{2.22a}$$

$$\sum_{\vec{k}} \mathrm{e}^{\mathrm{i}\vec{k}\vec{R}} = N_0\, \delta_{\vec{R}, \vec{0}} \;, \tag{2.22b}$$

that hold under Born von Kármán boundary conditions for the translational subgroup, are utilized. Using these translational symmetry adapted basis functions (2.21), one arrives at a representation of the spatial Bloch orbitals which reads for restricted Hartree-Fock theory

$$\psi^{\uparrow,\downarrow}_{\vec{k}i}(\vec{r}) = \sum_{\mu=1}^{\infty} C_{\mu i}(\vec{k})\, \varphi_{\vec{k}\mu}(\vec{r}), \qquad i = 1, \ldots, \infty \tag{2.23}$$

---

[9]Consider, that one has further decomposed the block marices ϕ_{lm} of (2.11) into subblocks of irreducible representations according to point group symmetry. To the j-th row of the irreducible representation i, the proper symmetry adapted basis function $\varphi_{\vec{k}\mu,ij}(\vec{r})$ is obtained with the symmetry operation α of the group of the wave vector $\vec{k}$ applied to $\varphi_{\vec{k}\mu}(\vec{r})$ in (2.21) which projects out $\varphi_{\vec{k}\mu,ij}(\vec{r}) = \frac{d(i)}{g} \sum_\alpha [\alpha]^*_{i,jj}\, \hat{O}_\alpha\, \varphi_{\vec{k}}(\vec{r})$. Here g is the dimension of the group of the wave vector, $d(i)$ is the dimension of the i-th irreducible representation and $[\alpha]^*_{i,jl}$ indicates the jl-th element of the matrix representing the symmetry operation α in the i-th representation [6].

where $C_{\mu i}(\vec{k})$ are denoted as *orbital coefficients*. Such an expansion is usually termed *linear combination of atomic orbitals* (*LCAO*).[10] Expression (2.23) is inserted in the spin-free equivalent of (2.13) which transforms the Hartree-Fock equation into a generalized eigenvalue problem, the *Roothaan-Hall equations* [39–42, 117, 118]

$$\sum_{\nu=1}^{K} F_{\mu\nu}(\vec{k}) \, C_{\nu i}(\vec{k}) = \sum_{i,\nu=1}^{K} S_{\mu\nu}(\vec{k}) \, C_{\nu i}(\vec{k}) \, \varepsilon_i(\vec{k}) \tag{2.24}$$

for the spatial Bloch orbitals $\vec{k}\,i$, $i = 1, \ldots, K$ with crystal momentum $\vec{k}$ which are written compactly as matrix equations

$$\boldsymbol{F}(\vec{k})\boldsymbol{C}(\vec{k}) = \boldsymbol{S}(\vec{k})\boldsymbol{C}(\vec{k})\boldsymbol{\varepsilon}(\vec{k}) \, , \tag{2.25}$$

where $\boldsymbol{F}(\vec{k})$ is the matrix representation of the Fock operator. Furthermore, $S_{\mu\nu}(\vec{k}) = \langle \, \varphi_{\vec{k}\mu}(\vec{r}) \mid \varphi_{\vec{k}\nu}(\vec{r}) \, \rangle$ denotes the *overlap matrix* of the basis set (2.21). In the case of unrestricted Hartree-Fock theory, two equations of the type (2.23) and (2.25), one for each spinor component, result, which are then termed *Pople-Nesbet equations* [39, 119].

The self-consistent solution of (2.25) is interpreted as follows: $\boldsymbol{\varepsilon}(\vec{k}) = \mathbf{diag}(\cdots \varepsilon_{\vec{k}\,i} \cdots)$, $i = 1, \ldots, \infty$ is the matrix of *orbital energies* or *energy bands* and $\boldsymbol{C}(\vec{k})$ are the orbital coefficients in (2.23). Via Equations (2.9) and (2.23), twice as many spin orbitals than spatial orbitals result where the N spin orbitals which are lowest in energy are usually occupied according to the *aufbau principle*. The remaining orbitals are denoted as *unoccupied* or *virtual orbitals*. The energies of occupied and virtual Bloch orbitals are frequently also referred to as *valence* and *conduction bands*, respectively. Generally, I use the band indices i, j, m, n, ..., to denote occupied Hartree-Fock bands, a, b, c, d, ..., for virtual bands and p, q, r, s, ... for bands which may be both occupied or virtual. Finally, the Hartree-Fock energy of a crystal is given by the expectation value of the Hamiltonian Slater determinant (2.10)

$$E = \sum_{\vec{k}} \sum_{i=1}^{N'} [\varepsilon_{\vec{k}\,i} - \frac{1}{2} \, \langle \psi_{\vec{k}\,i}| \, \hat{v}^{(\mathrm{HF})} \, |\psi_{\vec{k}\,i}\rangle] + E_{\mathrm{nucl}} \, . \tag{2.26}$$

The energy expression is not only composed of a sum over independent particle energies $\varepsilon_{\vec{k}\,i}$ but also involves the expectation value of the Hartree-Fock potential (2.16) to avoid double counting of the two-electron interaction terms [27, 28, 39–42]. Therefore, this expression again clearly demonstrates that Hartree-Fock theory, strictly speaking, is not an independent particle approach. Moreover, the constant electrostatic energy of the nuclei E_{nucl} has to be accounted for in formula (2.26) to obtain total energies.

---

[10]Basis sets $\chi_\mu(\vec{r})$, $\mu = 1, \ldots, K$ are constructed by taking a finite number K of the wave functions for an electron in a central field [40, 42] [see Section 2.3 for details]. Such wave functions are less formally referred to as *atomic orbitals (AO)* which dwells on the fact that basis sets are occasionally optimized to represent the Hartree-Fock orbitals of isolated atoms [40, 42].

2.3 Basis sets

The choice of the basis set, used to expand the spatial orbitals in (2.23), is crucial for the rate of convergence with the number of basis functions. Only a few basis functions should be required to describe the many-particle system reasonably. In addition, the evaluation of the molecular integrals in (2.25) is required to be efficient.

The eigenfunctions of the one-particle operator

$$\hat{h}_{\text{GTO}} = -\frac{1}{2}\Delta + 2\zeta^2 r^2 + \frac{n(n-1) - l(l+1)}{2r^2} \tag{2.27}$$

are the so-called *Gaussian type orbitals (GTO)* or *Gaussian basis functions* [39,40,48,120] which have proven to be an efficient and accurate choice for basis sets. As the one-particle Hamiltonian (2.27) contains a central field potential, $\hat{h}_{\text{GTO}}$ commutes both with the squared *orbital angular momentum* $\vec{L}^2$ and its cartesian z-component L_z. Hence, the basis functions χ can be chosen to be simultaneous eigenfunctions of $\hat{h}_{\text{GTO}}$, $\vec{L}^2$ and $\hat{L}_z$ having the form

$$\chi_{nlm}(r, \vartheta, \varphi) = R_{nl}(r)\, Y_{lm}(\vartheta, \varphi) \tag{2.28}$$

with n, l, m denoting integer quantum numbers and r, ϑ, φ representing polar coordinates. One refers to n as the *principal quantum number,* to l as the *angular momentum quantum number* and finally to m as the *magnetic quantum number*. The eigenvalues are

$$\hat{h}_{\text{GTO}}\, \chi_{nlm} = \varepsilon_{nlm}\, \chi_{nlm} \tag{2.29a}$$

$$\vec{L}^2\, \chi_{nlm} = l\,(l+1)\, \chi_{nlm} \tag{2.29b}$$

$$\hat{L}_z\, \chi_{nlm} = m\, \chi_{nlm} \,. \tag{2.29c}$$

with $n \geq 1$, $l \leq n-1$ and $m = -l, -l+1, \ldots, l-1, l$. Eigenfunctions χ_{nlm} with $l = 0, 1, 2, 3, 4, \ldots$ are designated by $s, p, d, f, g, \ldots$ and are energetically $2\,l+1$ fold degenerate with respect to m. The radial parts of spherical Gaussian orbitals are of the form

$$R_{nl}(r) = C_n r^{n-1} \mathrm{e}^{-\zeta r^2}, \qquad C_n = \sqrt{\frac{2^{2n}(n-1)!}{2n-1}} \sqrt{\frac{(2\zeta)^{2n+1}}{\pi}} \tag{2.30}$$

and the spherical harmonics $Y_{lm}(\vartheta, \varphi)$ are defined as usual [40]. The functions χ_{nlm} with the same angular momentum quantum numbers are generally non-orthogonal.

Basis sets have been devised for essentially all elements of the periodic table and are tabulated in large collections [48] where fixed linear combinations of *primitive Gaussians* (2.28), so-called *contractions*, are used to represent the occupied orbitals of the free atom. *Minimal basis sets* provide only a single contraction for each occupied atomic orbital. The quality of larger basis sets is denoted by the attributes double-ζ, triple-ζ, $\ldots$ where the number of "ζ"s originally referred to the number of contractions assigned to each occupied atomic orbital. Nowadays, the number of "ζ"s indicates only the number of contractions utilized for the valence orbitals. Such basis sets also are referred to as *split-valence basis sets*. Finally, *polarization functions* are frequently added to the basis

sets which are diffuse Gaussian primitives of an angular momentum that is typically larger by one than the highest angular momentum in the remaining basis set. These functions allow for the change of the electronic structure of an atom caused by the anisotropic surrounding in a molecule or a crystal.

2.4 Convergence of Hartree-Fock energies

Hartree-Fock energies turn out to converge rapidly with increasing basis set quality towards the basis set limit. This fact can be attributed to the one-particle character of Hartree-Fock theory which hints at a good describability by a properly chosen one-particle basis set. The correlation consistent basis sets [48] cc-pVXZ [49,50], aug-cc-pVXZ [49–51] and d-aug-cc-pVXZ [49,51,52]—with the number of "ζ"s being given by their *cardinal numbers* $X = $ D, T, Q, 5, 6, i.e., double, triple, quadruple, quintuple and hextuple—form hierarchical series of basis sets of increasing quality. They are especially well suited to study the basis set convergence of Hartree-Fock energies of molecules and crystals.

The actual convergence behavior of Hartree-Fock energies has only empirically been determined in Reference [53] (and References therein) and has been shown to depend both on the number of basis functions and on the highest angular momentum in the basis sets. The cardinal number X of correlation consistent basis sets is related to both quantities. Hartree-Fock energies follow

$$E_{\mathrm{SCF}}(\infty) = E_{\mathrm{SCF}}(X) - A\,\mathrm{e}^{-BX}\;, \tag{2.31}$$

with the constants $A, B > 0$ and $E_{\mathrm{SCF}}(\infty)$ being the Hartree-Fock basis set limit while the Hartree-Fock energyobtained with a basis set X is denoted by $E_{\mathrm{SCF}}(X)$. The known functional dependence of $E_{\mathrm{SCF}}(X)$ can now be exploited to extrapolate Hartree-Fock energies obtained with a series of basis sets towards the basis set limit. This procedure will be used in Section 4.2 where the Hartree-Fock binding energies of infinite $(\mathrm{HF})_\infty$ and $(\mathrm{HCl})_\infty$ chains are studied.

2.5 Wannier functions

In the previous Sections 2.1 and 2.2, I discuss translational symmetry adapted equations using Bloch functions. Such functions are completely delocalized over the whole crystal. In this section, I would like to introduce a local view on one-particle states of crystals that comes much closer to the intuitively accessible concepts of chemical bonding.

2.5.1 Properties

Given a set of functions $w_{\vec{R}\,\varrho}(\vec{r}\,s)$, $\varrho = 1, \ldots, K$ which is associated with each unit cell $\vec{R}$ of a crystal; they are *translationally related*, i.e., related to each other by lattice translations $\hat{T}_{\vec{R}'}$, and are assumed to be orthonormal with respect to an integration over the entire crystal

$$w_{\vec{R}+\vec{R}'\,\varrho}(\vec{r}\,s) \equiv \langle\,\vec{r}\,s \mid \vec{R} + \vec{R}'\,\varrho\,\rangle \;=\; w_{\vec{R}\,\varrho}(\vec{r} - \vec{R}'\,s) = \hat{T}_{\vec{R}'}w_{\vec{R}\,\varrho}(\vec{r}\,s) \tag{2.32a}$$

$$\langle\, w_{\vec{R}\,\sigma}\,|\,w_{\vec{R}'\,\varrho}\,\rangle \;=\; \delta_{\vec{R}\,\sigma,\vec{R}'\,\varrho}\,. \tag{2.32b}$$

These two properties characterize the *Wannier functions (WF)*.

The *generalized* or *multi-band Wannier transformation* [1–3,6,10,27,28,30–32,121–123] and its inverse mediate between Bloch and Wannier functions[11]

$$w_{\vec{R}\,\varrho}(\vec{r}\,s) \;=\; \frac{1}{\sqrt{N_0}}\sum_{\vec{k}}\sum_{p=1}^{K}\mathcal{U}_{p\varrho}(\vec{k})\,\mathrm{e}^{-\mathrm{i}\vec{k}\vec{R}}\,\psi_{\vec{k}\,p}(\vec{r}\,s) = \sum_{\vec{k}}\sum_{p=1}^{K}\mathcal{W}_{\vec{k}\,p\;\vec{R}\,\varrho}\,\psi_{\vec{k}\,p}(\vec{r}\,s) \tag{2.33a}$$

$$\psi_{\vec{k}\,p}(\vec{r}\,s) \;=\; \frac{1}{\sqrt{N_0}}\sum_{\vec{R}}\sum_{\varrho=1}^{K}\mathcal{U}_{p\varrho}^{*}(\vec{k})\,\mathrm{e}^{\mathrm{i}\vec{k}\vec{R}}\,w_{\vec{R}\,\varrho}(\vec{r}\,s) = \sum_{\vec{R}}\sum_{\varrho=1}^{K}\mathcal{W}_{\vec{k}\,p\;\vec{R}\,\varrho}^{*}\,w_{\vec{R}\,\varrho}(\vec{r}\,s) \tag{2.33b}$$

where K denotes the number of functions involved in the transformations. I refer to the unitary matrix $\boldsymbol{\mathcal{U}}(\vec{k})$ as *band mixing matrix*.

The matrix representation (2.33) is compactly written in matrix notation [27,28]

$$\vec{w}(\vec{r}\,s) \;=\; \vec{\psi}(\vec{r}\,s)\,\boldsymbol{\mathcal{W}} \tag{2.34a}$$

$$\vec{\psi}(\vec{r}\,s) \;=\; \vec{w}(\vec{r}\,s)\,\boldsymbol{\mathcal{W}}^{\dagger} \tag{2.34b}$$

with the unitary $K\,N_0 \times K\,N_0$ matrix

$$\boldsymbol{\mathcal{W}} = \begin{pmatrix} \boldsymbol{\mathcal{W}}'_{\vec{k}_1\,\vec{R}_1} & \cdots & \boldsymbol{\mathcal{W}}'_{\vec{k}_1\,\vec{R}_{N_0}} \\ \vdots & \ddots & \vdots \\ \boldsymbol{\mathcal{W}}'_{\vec{k}_{N_0}\,\vec{R}_1} & \cdots & \boldsymbol{\mathcal{W}}'_{\vec{R}_{N_0}\,\vec{k}_{N_0}} \end{pmatrix} \tag{2.35}$$

which is recast as $N_0 \times N_0$ block matrix in terms of the $K \times K$ matrices $\boldsymbol{\mathcal{W}}'_{\vec{k}\,\vec{R}}$. The $K\,N_0$-row-vectors of Bloch and Wannier functions read

$$\begin{aligned}
\vec{\psi}(\vec{r}\,s) &= (\psi_{\vec{k}_1\,p_1}^{\mathrm{T}}(\vec{r}\,s)\cdots\psi_{\vec{k}_1\,p_K}^{\mathrm{T}}(\vec{r}\,s)\cdots\psi_{\vec{k}_{N_0}\,p_1}^{\mathrm{T}}(\vec{r}\,s)\cdots\psi_{\vec{k}_{N_0}\,p_K}^{\mathrm{T}}(\vec{r}\,s)) \\
\vec{w}(\vec{r}\,s) &= (w_{\vec{R}_1\,\varrho_1}^{\mathrm{T}}(\vec{r}\,s)\cdots w_{\vec{R}_1\,\varrho_K}^{\mathrm{T}}(\vec{r}\,s)\cdots w_{\vec{R}_{N_0}\,\varrho_1}^{\mathrm{T}}(\vec{r}\,s)\cdots w_{\vec{R}_{N_0}\,\varrho_K}^{\mathrm{T}}(\vec{r}\,s))\,.
\end{aligned} \tag{2.36}$$

They can be understood to be vectors composed of N_0 blocks where each block comprises K components. The unitarity of the matrix (2.35), $\boldsymbol{\mathcal{W}}\,\boldsymbol{\mathcal{W}}^{\dagger} = \boldsymbol{\mathcal{W}}^{\dagger}\,\boldsymbol{\mathcal{W}} = \mathbb{1}$, can be shown as follows

$$\begin{aligned}
\sum_{\vec{R}\,\varrho}\mathcal{W}_{\vec{k}\,p\;\vec{R}\,\varrho}\,\mathcal{W}_{\vec{k}'\,q\;\vec{R}\,\varrho}^{*} &= \sum_{\vec{R}\,\varrho}\left[\tfrac{1}{\sqrt{N_0}}\mathcal{U}_{p\varrho}(\vec{k})\mathrm{e}^{-\mathrm{i}\vec{R}\vec{k}}\right]\left[\tfrac{1}{\sqrt{N_0}}\mathcal{U}_{q\varrho}^{*}(\vec{k}')\,\mathrm{e}^{\mathrm{i}\vec{R}\vec{k}'}\right] \\
&= \left[\tfrac{1}{N_0}\sum_{\vec{R}}\mathrm{e}^{\mathrm{i}\vec{R}(\vec{k}'-\vec{k})}\right]\left[\sum_{\varrho}\mathcal{U}_{q\varrho}(\vec{k})\mathcal{U}_{p\varrho}^{*}(\vec{k})\right] \\
&= \delta_{\vec{k}\,\vec{k}'}\,\delta_{pq}
\end{aligned} \tag{2.37}$$

---

[11]Following the seminal paper of Wannier [121], most accounts of Wannier functions introduce them by means of (2.33a) leaving the band mixing matrix unspecified. Clearly, without fixing $\boldsymbol{\mathcal{U}}(\vec{k})$ properly, there correspond infinitely many Wannier [Bloch] functions to a given Bloch [Wannier] function, i.e., functions that obey Equation (2.32) [Equation (2.5)], which only differ by the choice of $\boldsymbol{\mathcal{U}}(\vec{k})$. Wannier functions are thus frequently characterized to be non-unique with a *gauge freedom* [122] in the choice of the band mixing matrix. In order to avoid this characterization of Wannier functions, I favor the more general definition given in (2.32).

with the orthogonality relation (2.22a) and the unitarity of the band mixing matrix at every $\vec{k}$-point. The other equality is proven similarly.

Equation (2.37) can be extended to arbitrary sets of translationally related functions, i.e., I can drop the orthonormality condition (2.32b). Let the $K \times K$ band mixing matrices be $\boldsymbol{\mathcal{U}}(\vec{k}) = \mathbb{1}$ for all $\vec{k}$; rewriting Equation (2.35) for spatial functions leads to the new transformation

$$\check{\mathcal{W}}_{\vec{k}\,p\,\vec{R}\,\varrho} = \frac{1}{\sqrt{N_0}}\,\delta_{p\varrho}\,\mathrm{e}^{-\mathrm{i}\vec{k}\,\vec{R}} \tag{2.38}$$

for the vectors

$$
\begin{aligned}
\vec{\varphi}(\vec{r}) &= \left(\varphi_{\vec{k}_1\,\mu_1}(\vec{r}) \cdots \varphi_{\vec{k}_1\,\mu_K}(\vec{r}) \cdots \varphi_{\vec{k}_{N_0}\,\mu_1}(\vec{r}) \cdots \varphi_{\vec{k}_{N_0}\,\mu_K}(\vec{r})\right) \\
\vec{\chi}(\vec{r}) &= \left(\chi_{\vec{R}_1\,\mu_1}(\vec{r}) \cdots \chi_{\vec{R}_1\,\mu_K}(\vec{r}) \cdots \chi_{\vec{R}_{N_0}\,\mu_1}(\vec{r}) \cdots \chi_{\vec{R}_{N_0}\,\mu_K}(\vec{r})\right).
\end{aligned}
\tag{2.39}
$$

which are the counterpart of $\vec{\psi}(\vec{r}\,s)$ and $\vec{w}(\vec{r}\,s)$ in (2.36) but with non-orthogonal spatial functions $\chi_{\vec{R}_1\,\mu_1}(\vec{r}), \ldots, \chi_{\vec{R}_{N_0}\,\mu_K}(\vec{r})$. The translational symmetry adaption of the basis set, as in (2.21), can be expressed immediately by $\vec{\varphi}(\vec{r}) = \vec{\chi}(\vec{r})\,\check{\boldsymbol{\mathcal{W}}}^{\dagger}$.

In order to derive the Hartree-Fock equations in Section 2.2, I made a special choice of crystal orbitals. The Slater matrix $\boldsymbol{\mathcal{S}}^{\mathrm{BF}}$ in (2.10) is formulated in terms of occupied Bloch orbitals which are eigenfunctions of the Fock operator (2.13). The Slater matrix $\boldsymbol{\mathcal{S}}^{\mathrm{BF}}$ can also be expressed in terms of occupied Wannier orbitals $\boldsymbol{\mathcal{S}}^{\mathrm{WF}}$ and the corresponding Slater determinant assumes the form

$$\check{\Phi}_0^N(\vec{r}_1\,s_1, \ldots, \vec{r}_N\,s_N) = \frac{1}{\sqrt{N!}}\,\det\begin{pmatrix} \boldsymbol{w}_{1,1} & \cdots & \boldsymbol{w}_{1,N_0} \\ \vdots & \ddots & \vdots \\ \boldsymbol{w}_{N_0,1} & \cdots & \boldsymbol{w}_{N_0,N_0} \end{pmatrix}. \tag{2.40}$$

The $N \times N$ block matrix in (2.40) is composed of the $N' \times N'$ matrices

$$\boldsymbol{w}_{lm} = \begin{pmatrix} w_{\vec{R}_m\,1}(\vec{r}_{1+(l-1)\,N'}\,s_{1+(l-1)\,N'}) & \cdots & w_{\vec{R}_m\,N'}(\vec{r}_{1+(l-1)\,N'}\,s_{1+(l-1)\,N'}) \\ \vdots & \ddots & \vdots \\ w_{\vec{R}_m\,1}(\vec{r}_{N'+(l-1)\,N'}\,s_{N'+(l-1)\,N'}) & \cdots & w_{\vec{R}_m\,N'}(\vec{r}_{N'+(l-1)\,N'}\,s_{N'+(l-1)\,N'}) \end{pmatrix} \tag{2.41}$$

for the N_0 lattice vectors in the Born von Kármán region.

In order to connect the Slater determinants in Bloch and Wannier representation, (2.10) and (2.40), respectively, let K in (2.35) become equal to the number of occupied Bloch orbitals for a certain crystal momentum which is given by N' and clearly is the same as the number of occupied Wannier orbitals per unit cell. Then, I observe, that the rows of $\boldsymbol{\mathcal{S}}^{\mathrm{BF}}$ in (2.10) are given by the vectors of Bloch functions $\vec{\psi}(\vec{r}\,s)$ in (2.34). Following Equation (2.34), the rows are transformed by $\boldsymbol{\mathcal{W}}^{\dagger}$ to the corresponding vectors of Wannier functions $\vec{w}(\vec{r}\,s)$ which represent the rows of $\boldsymbol{\mathcal{S}}^{\mathrm{WF}}$ in (2.40). One obtains the relation $\boldsymbol{\mathcal{S}}^{\mathrm{BF}} = \boldsymbol{\mathcal{S}}^{\mathrm{WF}}\,\boldsymbol{\mathcal{W}}^{\dagger}$. With this formula, I can prove an important theorem[12] which

---

[12]This theorem is a special case [6] of the general proposition that a determinantial many-particle wavefunction is—apart from a complex phase factor—invariant under unitary transformations of the constituting one-particle functions [39–42], particularly Section 3.2.3 in Reference [39].
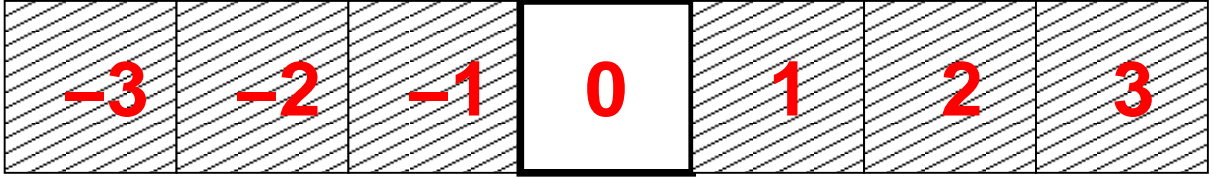
Figure 2.1: (Color) One-dimensional crystal lattice. The numbers in red denote the indices of the lattice vectors (2.1) which point from the origin cell "0" to the unit cell that is labelled by the number. The vectors are simply given by the integer numbers times the lattice constant.

establishes the connection between $\Phi_0^N(\vec{r}_1\, s_1, \ldots, \vec{r}_N\, s_N)$ and $\check{\Phi}_0^N(\vec{r}_1\, s_1, \ldots, \vec{r}_N\, s_N)$ of (2.10) and (2.40), respectively, as follows

$$
\begin{aligned}
\Phi_0^N(\vec{r}_1\, s_1, \ldots, \vec{r}_N\, s_N) &= \tfrac{1}{\sqrt{N!}}\, \det \boldsymbol{\mathcal{S}}^{\mathrm{BF}} = \tfrac{1}{\sqrt{N!}}\, \det(\boldsymbol{\mathcal{S}}^{\mathrm{WF}}\, \boldsymbol{\mathcal{W}}^{\dagger}) \\
&= \tfrac{1}{\sqrt{N!}}\, (\det \boldsymbol{\mathcal{S}}^{\mathrm{WF}})\, (\det \boldsymbol{\mathcal{W}}^{\dagger}) = \tfrac{1}{\sqrt{N!}}\, \mathrm{e}^{\mathrm{i}\theta}\, \det \boldsymbol{\mathcal{S}}^{\mathrm{WF}} \\
&= \mathrm{e}^{\mathrm{i}\theta}\, \check{\Phi}_0^N(\vec{r}_1\, s_1, \ldots, \vec{r}_N\, s_N)
\end{aligned}
\tag{2.42}
$$

where use is made of the rule for multiplying determinants and the unitarity property (2.37) of the inverse Wannier transformation (2.33b) which renders its determinant to be a complex number of modulus unity which can be written as $\mathrm{e}^{\mathrm{i}\theta}$ [6, 39–42].

Wannier functions are frequently termed *Wannier orbitals*, if they are Hartree-Fock orbitals, e.g., they result from a Wannier transformation of Bloch orbitals. Generally, I denote the Wannier orbital indices that result from occupied bands with κ, λ, μ, ν, ..., while the Wannier orbital indices of virtual bands are denoted by α, β, γ, δ, ... Indices of Wannier orbitals from occupied or virtual bands are referred to by ρ, σ, τ, υ, ...

2.5.2 A priori determination

2.5.2.1 Hartree-Fock equations in Wannier orbitals

In the previous Section 2.5.1, I showed that a Wannier transformation can be applied to the occupied orbitals which are used to construct the Slater determinant (2.42) without changing the wave function apart from a phase factor. In order to derive corresponding Hartree-Fock equations based on Wannier orbitals,[13] I note that the core Hamilton operator (2.15), the Hartree-Fock potential (2.16) and thus the Fock operator (2.14) are invariant under unitary transformations of the occupied orbitals [39–42] (particularly Section 3.2.3 in Reference [39]). Hence, they are the same for Bloch and Wannier orbitals. The expressions for the Coulomb (2.17) and the exchange operators (2.18) are replaced by corresponding formulas where Bloch orbitals are replaced by Wannier orbitals. The matrix elements of the Fock operator (2.14) with respect to occupied and virtual Wannier

---

[13]Alternatively, the line of arguments of Section 2.2 can be followed, replacing the Bloch orbitals in the Slater determinant (2.10) by Wannier orbitals (2.40). In fact this is undoing the unitary transformation that is required to obtain the *canonical* Hartree-Fock equations (2.13) [39–42] in a controlled way.

orbitals are given by

$$
\begin{aligned}
\langle w_{\vec{R}\varrho} | \hat{f} | w_{\vec{R}'\sigma} \rangle
&= \sum_{\vec{k}\,p,\ \vec{k}'\,q} \langle w_{\vec{R}\varrho} | \psi_{\vec{k}\,p} \rangle \langle \psi_{\vec{k}\,p} | \hat{f} | \psi_{\vec{k}'\,q} \rangle \langle \psi_{\vec{k}'\,q} | w_{\vec{R}'\sigma} \rangle \\
&= \sum_{\vec{k}\,p,\ \vec{k}'\,q} \mathcal{W}^*_{\vec{k}\,p\,\vec{R}\varrho}\, \varepsilon_{\vec{k}\,p}\, \delta_{\vec{k}\vec{k}'}\, \delta_{pq}\, \mathcal{W}_{\vec{k}'\,q\,\vec{R}'\sigma} \\
&= \sum_{\vec{k}\,p} \mathcal{W}^*_{\vec{k}\,p\,\vec{R}\varrho}\, \varepsilon_{\vec{k}\,p}\, \mathcal{W}_{\vec{k}\,p\,\vec{R}'\sigma} = \Lambda_{\vec{R}\varrho\,\vec{R}'\sigma}
\end{aligned}
\tag{2.43}
$$

and can be expressed compactly in matrix form by (2.35)

$$
\boldsymbol{\mathcal{W}}^\dagger \boldsymbol{\varepsilon}\, \boldsymbol{\mathcal{W}} = \boldsymbol{\Lambda} \,.
\tag{2.44}
$$

Multiplying Equation (2.43) with the operator $\sum_{\vec{R}\varrho} |w_{\vec{R}\varrho}\rangle$ and exploiting the completeness of the Wannier orbitals $\sum_{\vec{R}\varrho} |w_{\vec{R}\varrho}\rangle \langle w_{\vec{R}\varrho}| = \hat{\mathbb{1}}$, I arrive at the Hartree-Fock equations for Wannier orbitals

$$
\hat{f} | w_{\vec{R}'\sigma} \rangle = \sum_{\varrho=1}^{K} \Lambda_{\vec{R}'\varrho\,\vec{R}'\sigma} | w_{\vec{R}'\varrho} \rangle + \sum_{\vec{R}\neq\vec{R}'} \sum_{\varrho=1}^{K} \Lambda_{\vec{R}\varrho\,\vec{R}'\sigma} | w_{\vec{R}\varrho} \rangle \,.
\tag{2.45}
$$

They are no longer formally expressed in terms of a small eigenvalue problem (2.13) of the dimension of the number of bands K because the Fock matrix $\boldsymbol{\Lambda}$ obviously does no longer block with respect to the crystal momentum. Instead, the expressions (2.45) form a set of N equations which couple the Wannier orbitals in a unit cell to the Wannier orbitals in all other cells of a crystal.

Let me assume a restricted Hartree-Fock point of view to make the transition from spin orbitals to spatial orbitals. The spinors (2.9) and their components (2.19) are defined similarly for Wannier orbitals and the Hartree-Fock equations also formally retain the structure of (2.45). The spatial Wannier orbitals are expanded, similarly to (2.21), in terms of one-particle basis functions (2.28) and (2.30) [30, 31, 123, 124]

$$
\begin{aligned}
w_{\vec{R}\varrho}^{\uparrow,\downarrow}(\vec{r})
&= \hat{T}_{\vec{R}} \sum_{\vec{R}'} \sum_{\mu=1}^{\infty} C_{\vec{R}'\mu\,\vec{0}\varrho}\, \hat{T}_{R'+\vec{g}_\mu}\, \chi_\mu(\vec{r}) \\
&= \sum_{\vec{R}'} \sum_{\mu=1}^{\infty} C_{\vec{R}'+\vec{R}\mu\,\vec{R}\varrho}\, \chi_\mu(\vec{r} - \vec{g}_\mu - \vec{R}' - \vec{R}), \quad \varrho = 1, \dots, \infty
\end{aligned}
\tag{2.46}
$$

where I exploit the fact that both the spatial Wannier orbitals and the basis functions form sets of functions whose members are related by lattice translations (2.32a). The expansion coefficients, hence, are translationally symmetric $C_{\vec{R}'+\vec{R}\mu\,\vec{R}\varrho} = C_{\vec{R}'\mu\,\vec{0}\varrho} \equiv C_{\mu\varrho}(\vec{R}')$. The displacements $\vec{g}_\mu$ of the μ-th basis function in a unit cell are defined as in Equation (2.21). Assuming a truncated set of K basis functions (2.46), with the overlap matrix $S_{\vec{g}\mu\,\vec{g}'\nu} = \langle \chi_{\vec{g}\mu} | \chi_{\vec{g}'\nu} \rangle$ and the Fock matrix $F_{\vec{g}\mu\,\vec{g}'\nu} = \langle \chi_{\vec{g}\mu} | \hat{f} | \chi_{\vec{g}'\nu} \rangle$, I arrive at Roothaan-Hall equations [39–42, 117, 118]

$$
\sum_{\vec{g}'} \sum_{\nu=1}^{K} F_{\vec{g}\mu\,\vec{g}'\nu}\, C_{\vec{g}'\nu\,\vec{R}'\sigma} = \sum_{\vec{R}'',\vec{g}'} \sum_{\tau,\nu=1}^{K} S_{\vec{g}\mu\,\vec{g}'\nu}\, C_{\vec{g}'\nu\,\vec{R}''\tau}\, \Lambda_{\vec{R}''\tau\,\vec{R}'\sigma}
\tag{2.47}
$$

for the spatial Wannier orbitals $w_{\vec{R}\varrho}^{\uparrow,\downarrow}(\vec{r})$, $\varrho = 1, \dots, K$ in the unit cell $\vec{R}$, similarly to (2.24).

Equation (2.47) couples all unit cells of a crystal. To obtain a finite set of equations, I consider a large parallelepiped [a long oligomer for one-dimensional lattices] of N_0 unit cells. The matrices $\boldsymbol{F}$ and $\boldsymbol{S}$ that correspond to a one-dimensional lattice [Figure 2.1] adopt the particular block structure [27, 28]

$$
\begin{pmatrix}
\boldsymbol{0} & \boldsymbol{1} & \cdots & \boldsymbol{N_0} \\
-\boldsymbol{1} & \boldsymbol{0} & \cdots & \vdots \\
\vdots & & \ddots & \boldsymbol{1} \\
-\boldsymbol{N_0} & \cdots & -\boldsymbol{1} & \boldsymbol{0}
\end{pmatrix}
\tag{2.48}
$$

where the subblocks represent $K \times K$ matrices. For example, such a subblock of the Fock matrix is given by $F_{\vec{R}\sigma\,\vec{R}'\varrho} \equiv F_{\sigma\varrho}(\vec{R} - \vec{R}')$ for $\sigma, \varrho = 1, \dots, K$. The matrix $\boldsymbol{0}$ refers to interactions within unit cells, i.e., $\vec{R} = \vec{R}'$, whereas $-\boldsymbol{1} = \boldsymbol{1}^\dagger$ designates interactions with a nearest-neighbor cell and so forth until all interaction terms in the oligomer have been accumulated in (2.48). I am now in the position to rewrite (2.47) compactly as Roothaan-Hall equations [39–42, 117, 118]

$$
\boldsymbol{FC} = \boldsymbol{SC\Lambda} \,.
\tag{2.49}
$$

In contrast to (2.25), formula (2.49) is not a generalized eigenvalue problem but a complicated set of equations because $\boldsymbol{\Lambda}$ is a full matrix. As $\boldsymbol{\Lambda}$ is a Hermitian matrix, Equation (2.49) can be transformed into an eigenvalue problem by a similarity transformation with a unitary matrix $\boldsymbol{X}$. In analogy to formula (2.44) in terms of Wannier orbitals, it reads here in terms of the basis set $\boldsymbol{X}^\dagger \boldsymbol{\Lambda} \boldsymbol{X} = \boldsymbol{\varepsilon}$ where $\boldsymbol{X}$ is absorbed by the orbital coefficients $\boldsymbol{C} \boldsymbol{X}^\dagger = \bar{\boldsymbol{C}}$. The interactions are *not* translationally symmetric as the parallelepiped is isolated in vacuum. Hence, the crystal is modelled as a large molecular cluster and a self-consistent solution yields in this case *canonical* Hartree-Fock orbitals. The eigenvalues approximately discretize each of the energy bands of the perfect infinite crystal by N_0 values.

Affixing Born von Kármán boundary conditions to the parallelepiped [oligomer] restores translational symmetry of the interactions and the matrices $\boldsymbol{F}$ and $\boldsymbol{S}$ in (2.49) take following form for an oligomer

$$
\begin{pmatrix}
\boldsymbol{0} & \boldsymbol{1} & \cdots & \boldsymbol{N_0} \\
\boldsymbol{N_0} & \boldsymbol{0} & \cdots & \vdots \\
\vdots & & \ddots & \boldsymbol{1} \\
\boldsymbol{1} & \cdots & \boldsymbol{N_0} & \boldsymbol{0}
\end{pmatrix} \,.
\tag{2.50}
$$

I apply the similarity transformation (2.38) and (2.39) to (2.49) by multiplying from the right with the $\check{\boldsymbol{\mathcal{W}}}^\dagger$ of (2.38); inserting $\check{\boldsymbol{\mathcal{W}}}\check{\boldsymbol{\mathcal{W}}}^\dagger = \mathbb{1}$ yields [27, 28]

$$
\check{\boldsymbol{\mathcal{W}}}^\dagger \boldsymbol{F} \check{\boldsymbol{\mathcal{W}}} \check{\boldsymbol{\mathcal{W}}}^\dagger \bar{\boldsymbol{C}} = \check{\boldsymbol{\mathcal{W}}}^\dagger \boldsymbol{S} \check{\boldsymbol{\mathcal{W}}} \check{\boldsymbol{\mathcal{W}}}^\dagger \bar{\boldsymbol{C}} \check{\boldsymbol{\varepsilon}} \,.
\tag{2.51}
$$

I define the new block-diagonal matrices $\check{\boldsymbol{F}} = \check{\boldsymbol{\mathcal{W}}}^\dagger \boldsymbol{F} \check{\boldsymbol{\mathcal{W}}}$, $\check{\boldsymbol{C}} = \check{\boldsymbol{\mathcal{W}}}^\dagger \bar{\boldsymbol{C}} = \check{\boldsymbol{\mathcal{W}}}^\dagger \boldsymbol{C} \boldsymbol{X}^\dagger$, $\check{\boldsymbol{S}} = \check{\boldsymbol{\mathcal{W}}}^\dagger \boldsymbol{S} \check{\boldsymbol{\mathcal{W}}}$ and $\check{\boldsymbol{\varepsilon}} = \boldsymbol{\varepsilon} = \boldsymbol{X}^\dagger \boldsymbol{\Lambda} \boldsymbol{X}$ where the unitary transformation $\boldsymbol{X}$ is, as before,

defined to diagonalize $\mathbf{\Lambda}$ but this time under Born von Kármán boundary conditions. The matrices are composed of N_0 independent $K \times K$ blocks and can be written compactly as direct sums such that Equation (2.51) becomes

$$\bigoplus_{\vec{k}} \check{\boldsymbol{F}}(\vec{k}) \bigoplus_{\vec{k}} \check{\boldsymbol{C}}(\vec{k}) = \bigoplus_{\vec{k}} \check{\boldsymbol{S}}(\vec{k}) \bigoplus_{\vec{k}} \check{\boldsymbol{C}}(\vec{k}) \bigoplus_{\vec{k}} \check{\boldsymbol{\varepsilon}}(\vec{k}) \ . \tag{2.52}$$

I obtain the Roothaan-Hall equations [39–42,117,118] in terms of Bloch orbitals with the same equations for the $K \times K$ blocks as given by (2.25). The eigenvalues $\check{\varepsilon}$ in (2.52) now perfectly discretize the energy bands by N_0 values and are explicitly classified by the crystal momentum.

2.5.2.2 Orthogonalizing potential

Obviously, changing to Wannier representation in this direct way either complicates the equations and provides less information or represents an alternative derivation of the equations in terms of Bloch orbitals (2.25). The reason for this is simply given by (2.45) whose right hand side contains a coupling to all unit cells of the crystal. This is a consequence of the requirement to only consider orthonormal occupied orbitals imposed in course of the derivation of the Hartree-Fock equations by subtracting the Lagrangian multipliers [39–42]

$$\Lambda_{\vec{R}\kappa\,\vec{R}'\lambda} \left(\langle\, w_{\vec{R}\kappa} \mid w_{\vec{R}'\lambda} \,\rangle - \delta_{\vec{R}\vec{R}'}\, \delta_{\kappa\lambda} \right) \tag{2.53}$$

from the Hartree-Fock energy functional (2.12). The multipliers properly account for both intracell and intercell contributions, $\vec{R} = \vec{R}'$ and $\vec{R} \neq \vec{R}'$, respectively, yielding the occupied block of the Fock matrix in (2.45).

In order to make progress towards a more favorable form of the Hartree-Fock equations for Wannier orbitals, Shukla *et al.* [30,31] omit the intercell Lagrangian multipliers in (2.53) and thus arrive at

$$\Lambda_{\kappa\lambda} \left(\langle\, \tilde{w}_{\vec{R}\kappa} \mid \tilde{w}_{\vec{R}\lambda} \,\rangle - \delta_{\kappa\lambda} \right) \delta_{\vec{R}\vec{R}'} \ . \tag{2.54}$$

By this simplification, one does not pay attention to the mutual intercell orthogonality of the orbitals $\tilde{w}_{\vec{R}\lambda}(\vec{r}\,s)$, $\lambda = 1, \ldots, N'$ which is indicated by affixing the tilde accent.

In order to achieve orthogonality of the occupied orbitals in the origin cell to all other orbitals, i.e., their translational copies in all the other unit cells, I modify the Hartree-Fock energy functional $\mathcal{L}$ in (2.12) by adding an *orthogonalizing potential*

$$\mathcal{L}'[\Phi(\vec{r}_1\,s_1, \ldots, \vec{r}_N\,s_N)] = \mathcal{L}[\Phi(\vec{r}_1\,s_1, \ldots, \vec{r}_N\,s_N)] + V_{\text{Orth}} \tag{2.55}$$

which is given by

$$V_{\text{Orth}} = \frac{\bar{\lambda}}{2} \operatorname{Tr} \boldsymbol{\mathcal{S}}^2 = \frac{\bar{\lambda}}{2} \sum_{\substack{\vec{R},\vec{R}' \\ \vec{R}' \neq \vec{R}}} \sum_{\kappa,\xi=1}^{N'} \langle\, \tilde{w}_{\vec{R}\kappa} \mid \tilde{w}_{\vec{R}'\xi} \,\rangle \langle\, \tilde{w}_{\vec{R}'\xi} \mid \tilde{w}_{\vec{R}\kappa} \,\rangle \ . \tag{2.56}$$

where $\bar{\lambda} > 0$ denotes the *orthogonalizing potential strength* or *shift parameter*. The potential (2.56) is formed in terms of the off-diagonal elements of the overlap matrix between

translationally related orbitals $\tilde{S}_{\vec{R}\kappa\,\vec{R}'\xi} = (1 - \delta_{\vec{R}\vec{R}'}\,\delta_{\kappa\xi})\,\langle\,\tilde{w}_{\vec{R}\kappa}\mid\tilde{w}_{\vec{R}'\xi}\,\rangle$. The equality between the two expressions for V_{Orth} in (2.56) holds because the translationally related orbitals of a particular unit cell are orthonormal. I take the trace of $\tilde{S}^2$ in (2.56) as all summands in this definition of an orthogonalizing potential (2.55) are real and nonnegative causing an increase of energy proportional to $\bar{\lambda}$. The concept of introducing an artificial potential (2.56) into $\mathcal{L}$ is inspired by the ideas of *localizing potentials* that have been used from time to time, see References [31, 124–126].

Carrying out functional variation of $\mathcal{L}'$ with respect to the occupied orbitals, to minimize the modified functional (2.55), I arrive at

$$(\hat{f} + \hat{\mathcal{P}}_{\vec{R}})\,|\,\tilde{w}_{\vec{R}\lambda}\,\rangle = \sum_{\xi=1}^{N'} \Lambda_{\vec{R}\kappa\,\vec{R}\xi}\,|\,\tilde{w}_{\vec{R}\xi}\,\rangle \tag{2.57}$$

for the N' occupied Wannier orbitals in unit cell $\vec{R}$. The *penalty projection operator* is defined by

$$\hat{\mathcal{P}}_{\vec{R}} = \bar{\lambda}\sum_{\vec{R}'\neq\vec{R}}\sum_{\xi=1}^{N'}|\,\tilde{w}_{\vec{R}'\xi}\,\rangle\langle\,\tilde{w}_{\vec{R}'\xi}\,| \ . \tag{2.58}$$

The penalty projector (2.60) is *not* translationally symmetric. Instead, it holds the relation $\hat{T}_{\vec{g}}\hat{\mathcal{P}}_{\vec{R}} = \hat{\mathcal{P}}_{\vec{R}-\vec{g}}$. This way the unit cell $\vec{R}$ is distinguished from all other unit cells in the crystal lattice.

The translational relation of the orbitals in (2.57) implies that it is sufficient to formulate and solve (2.57) for the origin cell. The multipliers $\tilde{\Lambda}_{\vec{0}\kappa\,\vec{0}\lambda}$ constitute a Hermitian matrix which is diagonalizable by a unitary transformation $\boldsymbol{X}'^\dagger\tilde{\boldsymbol{\Lambda}}\boldsymbol{X}' = \boldsymbol{\varepsilon}'$. Both $\hat{f}$ and $\hat{\mathcal{P}}_{\vec{0}}$ are invariant under orbital rotations within a unit cell. I formally get a Hermitian $N' \times N'$ eigenvalue problem similarly to (2.13)

$$(\hat{f} + \hat{\mathcal{P}}_{\vec{0}})\,|\,\tilde{w}_{\vec{0}\kappa}\,\rangle = \varepsilon'_{\vec{0}\kappa}\,|\,\tilde{w}_{\vec{0}\kappa}\,\rangle \ . \tag{2.59}$$

The resulting orbitals are referred to as *pseudo-canonical Wannier orbitals*. In particular, they diagonalize the occupied block of the Fock matrix in the origin cell.[14] The functional dependence of $\hat{f} + \hat{\mathcal{P}}_{\vec{0}}$ on the occupied orbitals can now be disregarded. Consequently, the Fock operator becomes a conventional Hermitian operator. Then, the restriction of the penalty projection operator, to act only on occupied orbitals, can be released, i.e., N' in (2.58) is replaced by K. Now Equation (2.59) holds also for *virtual Wannier orbitals*.

I change to a closed-shell Slater determinant (2.40) to obtain spin free equations. A representation of the $\tilde{w}_{\vec{R}\varrho}^{\uparrow,\downarrow}(\vec{r})$ in terms of basis functions (2.46) is introduced. As the determination of the Wannier orbitals in the origin cell is decoupled with respect to the orbitals in all other unit cells of the crystal, clearly, only a basis set expansion of the orbitals in the origin cell is required. For sure this expansion also includes coefficients that refer, in principle, to all the other unit cells of the crystal (2.46) and describe the

---

[14]Pseudo-canonical Wannier orbitals are delocalized over the entire unit cell and thus implicate the same disadvantageous non-locality associated with Bloch orbitals when applying cutoff criteria to the Fock matrix and to the two-electron integrals.

tails of the Wannier orbitals. The basis set representation of the Fock operator $\boldsymbol{F}$ and the basis set overlap matrix $\boldsymbol{S}$ are the same as in (2.47). The basis set representation of the penalty projection operator (2.58), with N' replaced by K, is [30, 31, 124]

$$(\boldsymbol{\mathcal{P}}_{\vec{R}})_{\vec{g}_1\,\mu\,\vec{g}_2\,\nu} = \langle \chi_{\vec{g}_1\,\mu} | \hat{\mathcal{P}}_{\vec{R}} | \chi_{\vec{g}_2\,\nu} \rangle = \bar{\lambda} \sum_{\substack{\vec{R}',\vec{R}_1\vec{R}_2 \\ \vec{R}' \neq \vec{R}}} \sum_{\kappa,\lambda,\varrho=1}^{K} S_{\vec{g}_1\,\mu\,\vec{R}_1\,\kappa}\, C_{\vec{R}_1\,\kappa\,\vec{R}'\,\varrho}\, C^*_{\vec{R}_2\,\lambda\,\vec{R}'\,\varrho}\, S^*_{\vec{g}_2\,\nu\,\vec{R}_2\,\lambda} \,.$$

$$(2.60)$$

For sure the matrix elements of the penalty projector are also not translationally symmetric. Born von Kármán boundary conditions are typically not affixed [30, 31, 124] to the parallelepiped of unit cells which is used to derive the equations. The general structure of $\boldsymbol{F}$, $\boldsymbol{S}$ and $\boldsymbol{\mathcal{P}}_{\vec{R}}$ is described by (2.48). The fact that the boundary conditions break the relation by lattice translations of the orbitals of the parallelepiped does not represent a constraint because it is sacrificed already with the definition of the penalty projector (2.58) and (2.60).

In analogy to (2.47), I obtain Roothaan-Hall equations [30, 31, 39–42, 117, 118, 124]

$$(\boldsymbol{F} + \boldsymbol{\mathcal{P}}_{\vec{0}})\, \vec{C}_\varrho = \varepsilon'_\varrho\, \boldsymbol{S}\, \vec{C}_\varrho \tag{2.61}$$

for the occupied and virtual Wannier orbitals in the origin cell $\tilde{w}_{\vec{0}\,\varrho}(\vec{r})$ with $\varrho = 1, \ldots, K$ with expansion coefficients $(\vec{C}_\varrho)_{\vec{g}\,\mu} = C_{\vec{g}\,\mu\,\vec{0}\,\varrho}$ for all $K\,N_0$ indices $\vec{g}\,\mu$. Note that only a subset of K eigenvectors out of the $K\,N_0$ eigenvectors of (2.61) is required. By means of the basis set representation, the coupling of the Wannier orbitals in the origin cell to the Wannier orbitals in neighboring unit cells reappears which could be avoided by omitting the Lagrangian multipliers in (2.54). The Wannier orbitals in other but the origin cell are simply given by lattice translations (2.32a), exploiting that the expansion coefficients (2.46) are translationally symmetric. Therewidth, all Wannier orbitals of the crystal are determined.

Equation (2.61), as used in References [30, 31, 68–70, 124], exhibits an appreciable drawback. The conduct is highly inefficient due to the unfavorable cubic scaling with respect to the number of rows of a matrix of the algorithms for a full diagonalization of matrices [74, 127, 128]. The dimension of the matrices in (2.61) scales both with the number of basis functions in the origin cell and with the number of unit cells utilized to support the Wannier orbitals. The scaling of the eigenvalue problem represents a notable constraint over Bloch-orbital-based approaches described in Section 2.2 which scale only with the number of basis functions per unit cell. However, this constraint only is apparent but not immanent. Iterative eigenvalue solvers, particularly those of Davidson [129] or variants of filter diagonalization [130–132] can be employed to reduce the numerical effort. Thereby, the very favorable property of the spectrum of $\boldsymbol{F} + \boldsymbol{\mathcal{P}}_{\vec{0}}$ in (2.61) can be exploited. Namely, the lower K eigenvalues correspond to the Wannier orbitals in the origin cell. The other eigenvalues belong to the Wannier orbitals in other unit cells and are shifted to high values by means of $\bar{\lambda}$. Consequently, the latter eigenvalues are well separated from the the former ones.

The connection of the above ideas to a Bloch orbital based formalism can readily be achieved. To this end, the orthogonalizing potential (2.56) is defined anew to comprise
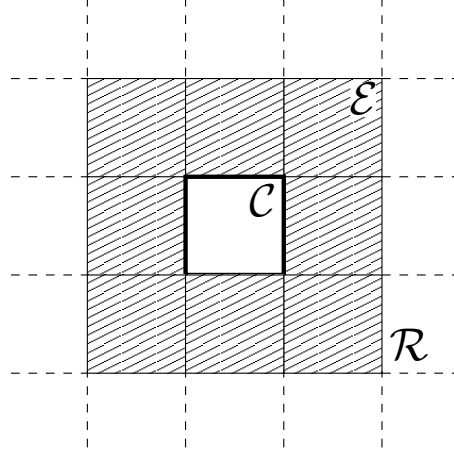
Figure 2.2: A cluster of the unit cells $\mathcal{N}$ which is utilized to support the Wannier orbitals of a crystal. The central cell $\mathcal{C}$ of the cluster is surrounded by several shells of environment cells $\mathcal{E}$. In this figure, first and second nearest-neighbor cells are shown. The remaining unit cells beyond $\mathcal{N} = \mathcal{C} \cup \mathcal{E}$, which are neglect, are designated by $\mathcal{R}$.

now the *full* overlap matrix $\check{V}_{\mathrm{Orth}} = \frac{\bar{\lambda}}{2} \operatorname{Tr} \boldsymbol{S}^2$. The modification virtually has no effect on the theory as the orthonormality of the Wannier functions in a unit cell is already put as a constraint to the minimization of the energy functional by means of the Lagrangian multipliers in (2.54). As the Wannier functions are normalized to unity, the additional contribution to the trace is simply $K N_0$. The changed definition of the orthogonalizing potential only amounts for a meaningless overall energetic shift of (2.55). Functional variation of $\mathcal{L}'$ with the new $\check{V}_{\mathrm{Orth}}$ yields that the summation in the penalty projector (2.58) and (2.60) no longer is restricted to the unit cells in the neighborhood, i.e., $\vec{R}' \neq \vec{R}$, but also contains the origin cell. I indicate this change by modifying the symbols for the projector to $\hat{\mathcal{P}}$ and $\boldsymbol{\mathcal{P}}$, respectively, because the previously utilized subscript which designated the unit cell to be dropped in the summations is now meaningless.

The minute alteration of V_{Orth} has the profound consequence to restore translational symmetry of the Equations (2.58) and (2.60). Therefore, Born von Kármán boundary conditions become beneficial. The Roothaan-Hall equations [30, 31, 39–42, 117, 118, 124] in (2.61) are changed to

$$(\boldsymbol{F} + \boldsymbol{\mathcal{P}}) \, \boldsymbol{C} = \boldsymbol{S} \, \boldsymbol{C} \, \boldsymbol{\varepsilon}' \; . \tag{2.62}$$

The $N_0 K \times N_0 K$ matrices $\boldsymbol{F}$, $\boldsymbol{S}$ and $\boldsymbol{\mathcal{P}}$ in (2.62) have the structure indicated in (2.50). Employing the unitary transformation (2.38) and (2.39) as for (2.51), the matrices in formula (2.62) are transformed into block-diagonal matrices [27, 28] in complete analogy to (2.52). They represent the N_0 independent $K \times K$ eigenvalue problems

$$(\check{\boldsymbol{F}}(\vec{k}) + \check{\boldsymbol{\mathcal{P}}}(\vec{k})) \, \check{\boldsymbol{C}}(\vec{k}) = \check{\boldsymbol{S}}(\vec{k}) \, \check{\boldsymbol{C}}(\vec{k}) \, \check{\boldsymbol{\varepsilon}}'(\vec{k}) \; . \tag{2.63}$$

Solving these equations yields Bloch orbitals which are orthonormal. Hence, apart from a constant shift of the Fock matrices $\check{\boldsymbol{F}}(\vec{k})$ by $\check{\boldsymbol{\mathcal{P}}}(\vec{k}) = \lambda \, \mathbb{1}$, Equation (2.63) becomes identical to (2.25).

A parallelepiped of N_0 unit cells which is cut out from an infinite crystal has been used so far as an intellectual device either with or without Born von Kármán boundary

conditions. In the end, the limit $N_0 \to \infty$ can be taken safely in all equations. However, in practical computations, the support of the Wannier orbitals (2.46) has to be restricted, i.e., the coefficients $C_{\mu\varrho}(\vec{R}')$ are considered only for a restricted number of unit cells $\vec{R}'$. To this end, a cluster $\mathcal{N}$ of unit cells is assumed for this purpose [Figure 2.2]. The Wannier orbitals in the *central cell* $\mathcal{C}$, thereby, are supported additionally by a certain number of environment cells $\mathcal{E}$, typically up to third nearest neighbors [30, 126].

Due to the orthogonalizing potential, the orbitals oscillate slightly in the environment which is referred to as *orthogonalization tails*. These tails reflect the Coulomb interaction of the electrons in the orbitals in the origin cell with the electrons in other unit cells. The physical impact of the tails is obvious, in contrast to overlapping orbitals whose extend is somewhat hidden in the overlap matrix.

A priori Wannier orbitals provide results for infinite solids as the Coulomb potential of the nuclei and electrons is evaluated not only on the cluster but is considered up to infinite distances by a summation due to Ewald [133, 134]. Thereby, the Coulomb potential is split into a short-range contribution that converges rapidly in direct space and a long-range contribution that converges rapidly in reciprocal space. Therefore, the full crystalline potential is accounted for. Yet, Wannier orbitals are allowed to vary only on a finite support, the cluster, which is expected to be sufficiently large.

In each iteration of the self-consistent solution of (2.61), the intermediate Hartree-Fock orbitals $\tilde{w}_{\vec{0}\varrho}(\bar{\lambda}, \vec{r}\, s)$ and multipliers $\varepsilon'_{\vec{0}\varrho}(\bar{\lambda})$ depend parametrically on $\bar{\lambda}$. One may take the limit $\bar{\lambda} \to \infty$ to determine solutions that do not involve any overlaps among orbitals in different unit cells. However, in practical computations, numerical stability requires a finite orthogonalization potential strength where the resulting Hartree-Fock energies do not show a noticeable dependence on $\bar{\lambda}$ in the range 10^3–$10^5\,\mathrm{E}_h$ [135].

The Hartree-Fock energy is given by the energy expectation value of the Slater determinant in Wannier orbitals (2.10) as follows[15] [30, 31, 124]

$$E = \sum_{\vec{R}} \sum_{\kappa=1}^{N'} [F_{\vec{R}\kappa\,\vec{R}\kappa} - \frac{1}{2} \langle w_{\vec{R}\kappa} | \hat{v}^{(\mathrm{HF})} | w_{\vec{R}\kappa} \rangle] + E_{\mathrm{nucl}} \,. \tag{2.64}$$

A simplified version of the above presented theory has been implemented in the WANNIER computer program. The polymers polyiminoborane, polyaminoborane [136] and the ionic crystals LiH [30, 32, 68, 69], LiF [31, 69, 70], LiCl [31], Li_2O, Na_2O [135] NaF [126], NaCl [126, 137] have been studied on the Hartree-Fock level. The correlation energy for the ground-state of LiH crystals [32], infinite LiH chains and the BeH_2 polymer [138] have been determined with full configuration interaction. The band structures of LiH [68, 69] and LiF [69, 70] have been investigated. Born effective charges have been studied for LiH, LiF, LiCl, NaF and NaCl [126].

---

[15]Equation (2.64) also follows immediately from (2.26) which is the trace of the matrix $\mathcal{T}_{\vec{k}\,i\,\vec{k}'\,j} = \varepsilon_{\vec{k}\,i}\,\delta_{\vec{k}\,i\,\vec{k}'\,j} - \frac{1}{2}\langle \psi_{\vec{k}\,i} | \hat{v}^{(\mathrm{HF})} | \psi_{\vec{k}'\,j} \rangle + \frac{1}{K\,N_0} E_{\mathrm{nucl}}\,\delta_{\vec{k}\,i\,\vec{k}'\,j}$. It transforms like the Fock matrix from a representation in terms of Bloch orbitals to a representation in terms of Wannier orbitals (2.34), i.e., $\tilde{\mathcal{T}}_{\vec{R}\kappa\,\vec{R}'\lambda} = \sum_{\vec{k},\vec{k}'} \sum_{i,j=1}^{K} \mathcal{W}^{\dagger}_{\vec{R}\kappa\,\vec{k}\,i}\, \mathcal{T}_{\vec{k}\,i\,\vec{k}'\,j}\, \mathcal{W}_{\vec{k}'\,j\,\vec{R}'\lambda}$. As the trace of a product of matrices is invariant under cyclic permutations of the factors, I obtain $\mathrm{Tr}\,\mathcal{T} = \mathrm{Tr}\,(\mathcal{W}\,\mathcal{W}^{\dagger}\,\mathcal{T}) = \mathrm{Tr}\,(\mathcal{W}^{\dagger}\,\mathcal{T}\,\mathcal{W}) = \mathrm{Tr}\,\tilde{\mathcal{T}}$. Here $\mathcal{W}$ only transforms the occupied orbitals among each other by letting $K = N'$ in (2.33), (2.34) and (2.35).

2.5.3 A posteriori determination

Wannier functions can also be determined *a posteriori* from the Bloch orbitals of a Hartree-Fock calculation utilizing (2.33) where the unitary matrix $\mathcal{U}_{\nu n}(\vec{k})$ can be chosen freely to determine a certain set of Wannier functions, e.g., those which are maximally localized with respect to the *Foster-Boys functional* [139, 140] as advocated by Marzari and Vanderbilt [122, 141] or by Zicovich *et al.* [123]. In one-dimensional models with non-crossing bands, these maximally localized Wannier functions were found to be real and to decay exponentially [6, 122] which is also conjectured to hold true in three-dimensional non-metallic crystals [122]. The semi-physical character of localized orbitals is reflected by the existence of various other orbital localization methods. There are, e.g., the method of Edmiston and Ruedenberg [125] or the recipe of Pipek and Mezey [142].

Most many-particle theories, like coupled-cluster discussed in the ensuing Chapter 3 or the one-particle Green's function of Chapters 5 and 6, rely on the strict separation between occupied and virtual Wannier orbitals; otherwise, Wick's theorem is not applicable [112–115]. The *a priori* determination of Wannier orbitals resorts to the Hartree-Fock approximation which yields an orthonormal set of orbitals that is partitioned, according to the aufbau principle, into occupied and virtual orbitals [Section 2.2]. In order to fulfill this requirement for an *a posteriori* applied Wannier transformation (2.33a), one considers the occupied and the virtual Bloch orbitals separately. This yields two independent unitary matrices, one for the occupied bands and one for the virtual bands, respectively. Hence $\mathcal{U}(\vec{k})$ in (2.33) is block-diagonal.

2.6 Crystal projected atomic orbitals

The Wannier transformation (2.33) introduced in Section 2.5.1 can also be applied to the virtual Bloch orbitals of a crystal. However, the typically large number of virtual Bloch orbitals makes the Wannier transformation computationally expensive and thus restricts its use to basis sets with only a few virtual functions. This computationally unfavorable situation is supplemented by conceptual considerations. Conduction bands of three-dimensional crystals are generally very sensitive to the basis set. In zero-, one- and two-dimensional systems they even represent a discretization of a continuum of scattering states, e.g., References [74, 128, 131, 132]. Therefore, in most cases only a suitable discretization of the virtual space in terms of Wannier functions (2.32) is needed.[16] They are not required to originate from eigenfunctions of the Fock operator. Finally, this does not impose any further constraints on the physical content of the virtual functions as Koopmans' theorem [39–42, 143] is not applicable to localized orbitals, either. A construction of virtual functions has been devised by Saebø and Pulay [144, 145]. It sets

---

[16]In Section 3.4, molecular clusters are used to model crystals. The translational relation (2.32a) of the localized occupied orbitals therein—which is only approximately fullfilled—is exploited to reduce the number of energy increments. In this approach, translational relation of the virtual orbitals is not required and they remain canonical and, generally, do not resemble Wannier or Bloch orbitals of the corresponding solid. For excited states, instead, occupied and virtual functions which are properly related to each other by lattice translations (2.32a) are required as, namely, the CO-ADC scheme fully exploits it.

out directly from the one-particle basis set of a molecular system which is motivated by its property to be inherently localized and translationally related (2.32a). The precise procedure described in what follows derives from the one of Hampel and Werner [146]. It has been extended to crystals by Shukla and Albrecht [147] and has been utilized to examine various polymers and crystals [32, 66–70, 138]. The scheme starts by constructing a set of orthonormal virtual functions in the origin which is, thereafter, translated and orthogonalized to all other unit cells of the crystal.

The N' occupied Wannier orbitals per unit cell can be obtained by the methods of Sections 2.5.2 and 2.5.3. The projector on the occupied space and its complement, which projects on the virtual space, read [146, 148]

$$\hat{P} = \sum_{\vec{R}} \sum_{\xi=1}^{N'} |w_{\vec{R}\xi}\rangle \langle w_{\vec{R}\xi}|, \qquad \hat{Q} = \hat{\mathbb{1}} - \hat{P}. \tag{2.65}$$

The crystal is described by K basis functions (2.20), (2.28) and (2.30) in each unit cell. To construct a translationally related (2.32a) set of virtual functions which solely describes the virtual space, I set out from the basis functions in the origin cell $\chi_{\vec{0}\mu}(\vec{r})$ of (2.20), (2.28) and (2.30). I apply the projector $\hat{Q}$ of (2.65) to them which projects out the virtual part of the $\chi_{\vec{0}\mu}(\vec{r})$

$$
\begin{aligned}
\tilde{\chi}_\mu(\vec{r}) &= \hat{Q}\,\chi_{\vec{0}\mu}(\vec{r}) = (\hat{\mathbb{1}} - \hat{P})\,\chi_{\vec{0}\mu}(\vec{r}) \\
&= \chi_{\vec{0}\mu}(\vec{r}) - \sum_{\vec{R}} \sum_{\xi=1}^{N'} \langle\,\vec{r}\,|\,w_{\vec{R}\xi}\,\rangle\langle\,w_{\vec{R}\xi}\,|\,\chi_{\vec{0}\mu}\,\rangle \\
&= \chi_{\vec{0}\mu}(\vec{r}) - \sum_{\vec{g}} \sum_{\nu=1}^{K} P_{\vec{g}\nu,\mu}\,\chi_{\vec{g}\nu}(\vec{r}) \\
&= \sum_{\vec{g}} \sum_{\nu=1}^{K} Q_{\vec{g}\nu,\mu}\,\chi_{\vec{g}\nu}(\vec{r}), \qquad \mu = 1, \ldots, K.
\end{aligned}
\tag{2.66}
$$

I refer to these virtual functions $\tilde{\chi}_\mu(\vec{r})$ as *crystal projected atomic orbitals (crystal PAO)*. The matrix representation of the projector $\hat{Q}$ in terms of the one-particle basis set is obtained by inserting the expansion of the occupied Wannier orbitals (2.46) into (2.66)

$$Q_{\vec{g}\nu,\mu} = \delta_{\vec{0}\mu\,\vec{g}\nu} - \sum_{\vec{R},\vec{R}'} \sum_{\xi=1}^{N'} \sum_{\varrho=1}^{K} C_{\nu\xi}(\vec{g} - \vec{R})\,C_{\varrho\xi}^*(\vec{R}')\,S_{\vec{R}+\vec{R}'\varrho\,\vec{0}\mu}. \tag{2.67}$$

Per construction the crystal PAOs $\tilde{\chi}_\mu(\vec{r})$ are strictly orthogonal to the occupied space [146, 148]. However, they are not orthogonal among themselves; the overlap matrix is

$$\tilde{S}_{\mu\nu} = \langle\,\tilde{\chi}_\mu\,|\,\tilde{\chi}_\nu\,\rangle = \sum_{\vec{g}_1,\vec{g}_2} \sum_{\mu',\nu'=1}^{K} Q_{\vec{g}_1\mu',\mu}^*\,S_{\vec{g}_1\mu'\,\vec{g}_2\nu'}\,Q_{\vec{g}_2\nu',\nu} = (\boldsymbol{Q}^\dagger\,\boldsymbol{S}\,\boldsymbol{Q})_{\mu\nu} \tag{2.68}$$

for $\mu, \nu = 1, \ldots, K$. It involves the overlap matrix of the basis set $S_{\vec{g}_1\mu'\,\vec{g}_2\nu'} = \langle\,\chi_{\vec{g}_1\mu'}|\chi_{\vec{g}_2\nu'}\,\rangle$. Unfortunately, (crystal) PAOs turn out to be somewhat less localized than the basis functions they originate from. Some of the functions $\tilde{\chi}_\mu(\vec{r})$ may even vanish, if the $\chi_{\vec{0}\mu}(\vec{r})$ do

not overlap with the virtual space. A pathological case immediately arises when $\hat{Q}$ is applied to $\hat{P}\chi_{\vec{0}\,\mu}(\vec{r})$ because $\hat{Q}\hat{P} = 0$ holds. This conclusion already indicates the problem of overcompleteness.

There are K basis functions per unit cell employed to represent occupied and virtual Wannier functions. Consequently, one expects $K - N'$ crystal PAOs to be required to describe the virtual space. The remaining N' crystal PAOs that are automatically produced by the procedure (2.66) lead to an overcomplete representation [146] and need to be identified and removed before basis functions for the virtual space of the whole crystal are constructed by applying lattice translations.

Hampel and Werner [146] describe three recipes to resolve the redundant description of the virtual space which they all find to perform approximately in the same way. The most "physical" one, that is also taken for the computations in Reference [146], has been extended to crystals and implemented into the WANNIER program by Shukla and Albrecht [147]. The overlap matrix $\tilde{\boldsymbol{S}}$ of (2.68) between crystal PAOs is formed. Let me denote the unitary matrix of its eigenvectors by $\tilde{\boldsymbol{Z}}$ and the matrix of its eigenvalues by $\tilde{\boldsymbol{\zeta}} = \mathbf{diag}(\tilde{\zeta}_1, \ldots, \tilde{\zeta}_K)$ yielding $\tilde{\boldsymbol{Z}}^\dagger \tilde{\boldsymbol{S}} \tilde{\boldsymbol{Z}} = \tilde{\boldsymbol{\zeta}}$. I assume that the eigenvectors in $\tilde{\boldsymbol{Z}}$ are arranged such that the eigenvalues are sorted in descending order $\tilde{\zeta}_1 > \ldots > \tilde{\zeta}_K$. The eigenvectors constitute an alternate set of basis functions for the virtual space

$$\chi'_\mu(\vec{r}) = \frac{1}{\sqrt{\tilde{\zeta}_\mu}} \sum_{\nu=1}^{K} Z_{\nu\mu}\, \tilde{\chi}_\nu(\vec{r}), \qquad \mu = 1, \ldots, K - N' \,. \tag{2.69}$$

I construct only $K - N'$ crystal PAOs, ignoring the eigenvectors of the matrix $\tilde{\boldsymbol{Z}}$ which correspond to the smallest N' eigenvalues that are arranged to occupy the positions $K - N'+1, \ldots, K$ in $\tilde{\boldsymbol{\zeta}}$. If they were not neglected, linear dependencies due to overcompleteness would arise when I derive, by means of lattice translations, the virtual functions of the entire crystal from those constructed in a single unit cell (2.66).

The new virtual space basis functions are orthonormal

$$S'_{\mu\nu} = \langle\, \chi'_\mu \mid \chi'_\nu \,\rangle = \frac{1}{\sqrt{\tilde{\zeta}_\mu\, \tilde{\zeta}_\nu}} \sum_{\kappa,\lambda=1}^{K} Z^*_{\kappa\mu}\, \tilde{S}_{\kappa\lambda}\, Z_{\lambda\nu} = \delta_{\mu\nu} \tag{2.70}$$

for $\mu, \nu = 1, \ldots, K - N'$. Translationally related (2.32a) virtual functions of the crystal are now constructed by applying all unique lattice translations to them which yields, similarly to (2.20), $\chi'_{\vec{g}\,\mu}(\vec{r}) \equiv \hat{T}_{\vec{g}}\, \chi'_\mu(\vec{r}) = \chi'_\mu(\vec{r} - \vec{g})$. The functions $\mu = 1, \ldots, K - N'$ to lattice vector $\vec{g}$ are orthonormal within the unit cell $\vec{g}$; they, are not orthogonal to virtual functions in other unit cells $\vec{g}' \neq \vec{g}$. Symmetric orthogonalization is, therefore, applied to all translationally related (2.32a) virtual functions of the crystal by means of

$$\check{\chi}_{\vec{R}\,\mu}(\vec{r}) = \sum_{\vec{g}} \sum_{\nu=1}^{K-N'} S'^{-\frac{1}{2}}_{\vec{g}\,\nu\,\vec{R}\,\mu}\, \chi'_{\vec{g}\,\nu}(\vec{r}) \tag{2.71}$$

using the following series expansion for the reciprocal of the square root of the overlap matrix

$$\boldsymbol{S}'^{-\frac{1}{2}} = (\mathbb{1} + (\boldsymbol{S}' - \mathbb{1}))^{-\frac{1}{2}} \approx \mathbb{1} - \frac{1}{2}\,(\boldsymbol{S}' - \mathbb{1})\,, \tag{2.72}$$

31

despite of its poor convergence properties [116], as this form can be applied without diagonalizing $\boldsymbol{S}'$. The functions in (2.71) are now normalized. Several iterations of transforming the virtual functions for the origin cell with (2.71) and using the expansion (2.72) leads, in many cases, to an orthogonalized set of translationally related (2.32a) virtual functions $\check{\chi}_{\vec{R}\,\mu}(\vec{r})$. Thus excitations into the crystal PAOs do not violate the *Pauli exclusion principle* [146, 148].

3 Ground state

In the previous Chapter 2, crystals are discussed from the point of view of an independent particle approximation [1, 3, 5–7, 149, 150] which is an appreciable simplification of the interacting many-particle system. It shall be overcome by a more elaborate treatment of correlation effects which is required for a reliable prediction of physical properties of crystals, like energies or structures. I have discussed two different views on one-particle states in Chapter 2, namely the completely delocalized plane-wave-like Bloch orbitals [Section 2.2] and the localized atomic-orbital-like Wannier orbitals [Section 2.5]. Both representations are suitable for a subsequent inclusion of correlation effects and are treated side by side.

Wave-function-based correlation treatments of the ground state of N electron systems need to represent the wave function Ψ_0^N, which lives in the N particle Hilbert space. To this end, an expansion in terms of antisymmetrized tensorial products of N Hartree-Fock orbitals, i.e., determinants, is utilized. Thereby, the occupied orbitals in the ground-state determinant are successively replaced by virtual orbitals which leads to the so-called *excited determinants* [39–42]. They are elegantly expressed using the formalism of second quantization which is introduced in Section 3.1. With such an ansatz for the ground-state wave function, optimal expansion coefficients are determined by applying the variational principle (2.12). This conceptually simple method is referred to as *configuration interaction (CI)*. If all possible excited determinants are included, the resulting scheme is referred to as *full CI (FCI)* otherwise as *truncated CI*. FCI exhibits a steep scaling of the computational effort with the number of electrons in the system and the one-particle basis set employed which rapidly makes its use prohibitively expensive. Truncated CI scales far less pronounced. The most common truncated CI method includes all singly and doubly excited determinants and is abbreviated as CISD. The hierarchy of truncated CI expansions shows a slow convergence with the order of excitations included raising the desire for an approximate FCI treatment with a more favorable truncation property [42]. To achieve this, one has to give up the variational determination of the wave function and resort to perturbative many-particle theories. Thereby, I introduce coupled-cluster theory in Section 3.2 which provides powerful correlation methods for the ground state of crystals with an N electron error which decays rapidly with the order of the excitations explicitly taken into account in the scheme.

The difference between the exact nonrelativistic ground-state energy and the energy in the independent particle model for the limit of a complete basis set is termed *correlation energy* [39]. It is given by

$$E_{\mathrm{corr}} = \langle \Psi_0^N \, | \, \hat{H} \, | \, \Psi_0^N \, \rangle - \langle \Phi_0^N \, | \, \hat{H} \, | \, \Phi_0^N \, \rangle \ . \tag{3.1}$$

As E_{corr} is an extensive quantity, $E_{\mathrm{corr}} = N_0 \, \mathcal{E}_{\mathrm{corr}}$ holds for a crystal where $\mathcal{E}_{\mathrm{corr}}$ is the correlation energy per unit cell and N_0 denotes the number of unit cells in the Born von

Kármán region [Section 2.1]. Although correlation energies are very small with respect to Hartree-Fock energies, they are very important for the properties of crystals which are in many cases given by energy differences where large absolute values nearly cancel, as for example in binding energies or analytical energy derivatives [39–42].

The localized occupied orbitals of molecular clusters, comprising a few monomers arranged in the geometry of the crystal, are found to be a good approximation to the occupied Wannier orbitals of the solid [1,2,38,43–45,138,151,152]. Introducing the incremental scheme [1,2,38,43–45] in Sections 3.3 and 3.4, the correlation energy of crystals can be determined from clusters which renders the study of crystals amenable to a treatment with conventional quantum chemical methods and existing computer programs [1,2,38,43–45]. The basis set convergence of correlation energies is regarded in Section 3.5.

3.1 Many-particle foundation

Having solved the independent particle problem, one already has gained considerable insights into the physics of an interacting many-particle system. It is a favorable starting point for more involved investigations. Up to now, quantum mechanics has been expressed in *first quantization*. For my further studies, it is beneficial to represent the Hamiltonian (2.4) in second quantization [39, 40, 42, 112–115]. This means that all one- and two-electron operators in (2.4) are represented in terms of the Hartree-Fock one-particle Bloch orbitals $\psi_{\vec{k}\,p}(\vec{r})$ thus incorporating the information already obtained by the Hartree-Fock treatment.

I introduce the operators $\hat{c}^{\dagger}_{\vec{k}\,p}$ ($\hat{c}_{\vec{k}\,p}$) which create (annihilate) electrons in $\psi_{\vec{k}\,p}(\vec{r})$ and, consequently, are referred to as *creators (annihilators)*. As electrons are fermions, these operators obey the anticommutation relations

$$\{\hat{c}_{\vec{k}_1\,p}, \hat{c}_{\vec{k}_2\,q}\} = 0, \qquad \{\hat{c}^{\dagger}_{\vec{k}_1\,p}, \hat{c}^{\dagger}_{\vec{k}_2\,q}\} = 0, \qquad \{\hat{c}^{\dagger}_{\vec{k}_1\,p}, \hat{c}_{\vec{k}_2\,q}\} = \delta_{\vec{k}_1\,\vec{k}_2}\,\delta_{pq} \qquad (3.2)$$

which properly account for the antisymmetry of the wave function required by the Pauli exclusion principle. The Hartree-Fock ground-state wave function (2.10) becomes

$$|\Phi_0^N\rangle = \prod_{\substack{\vec{k}\,i \\ n_{\vec{k}\,i}=1}} \hat{c}^{\dagger}_{\vec{k}\,i} |0\rangle \;. \qquad (3.3)$$

where the *occupation numbers* $n_{\vec{k}\,i}$ are unity for occupied and zero for virtual Bloch orbitals and $\bar{n}_{\vec{k}\,i} = 1 - n_{\vec{k}\,i}$. The *vacuum state* is represented by $|0\rangle$. Using second quantization, one obtains the so-called *Bloch* or *crystal momentum representation* (*CMR*) of

the Hamiltonian (2.4), introduced by Adams [6, 153, 154], which reads

$$
\begin{aligned}
\hat{H} &= \hat{H}_{\mathrm{HF}}^{\mathrm{BF}} + \hat{H}_{\mathrm{res}}^{\mathrm{BF}} \\
\hat{H}_{\mathrm{HF}}^{\mathrm{BF}} &= \sum_{\vec{k}\,p} \varepsilon_{\vec{k}\,p}\, \hat{c}_{\vec{k}\,p}^{\dagger}\, \hat{c}_{\vec{k}\,p} \\
\hat{H}_{\mathrm{res}}^{\mathrm{BF}} &= \sum_{\vec{k}_1\,p,\ \vec{k}_2\,q} W_{\vec{k}_1\,p\,\vec{k}_2\,q}\, \hat{c}_{\vec{k}_1\,p}^{\dagger}\, \hat{c}_{\vec{k}_2\,q} \\
&\quad + \tfrac{1}{2} \sum_{\substack{\vec{k}_1\,p,\ \vec{k}_2\,q, \\ \vec{k}_3\,r,\ \vec{k}_4\,s}} V_{\vec{k}_1\,p\,\vec{k}_2\,q\,\vec{k}_3\,r\,\vec{k}_4\,s}\, \hat{c}_{\vec{k}_1\,p}^{\dagger}\, \hat{c}_{\vec{k}_2\,q}^{\dagger}\, \hat{c}_{\vec{k}_4\,s}\, \hat{c}_{\vec{k}_3\,r}\ .
\end{aligned}
\tag{3.4}
$$

The decomposition according to Møller and Plesset [39–42] into the Hartree-Fock part $\hat{H}_{\mathrm{HF}}^{\mathrm{BF}}$ and the residual interaction $\hat{H}_{\mathrm{res}}^{\mathrm{BF}}$, i.e., the difference between the Hamiltonian and the Fock operator, emphasizes the relation between the known Hartree-Fock solution and the remaining correlation effects and turns out to be a suitable form to apply perturbation theory later on. In Equation (3.4), the energy bands or Bloch orbital energies are denoted by $\varepsilon_{\vec{k}\,p}$. The negative of the Hartree-Fock potential (2.16) is given by

$$
W_{\vec{k}_1\,p\,\vec{k}_2\,q} = -\sum_{\vec{k}\,i} V_{\vec{k}_1\,p\,\vec{k}\,i\,[\vec{k}_2\,q\,\vec{k}\,i]}\, n_{\vec{k}\,i}\ .
\tag{3.5}
$$

The *two-electron integrals* in (3.4) are defined with respect to Bloch orbitals by [39–42]

$$
V_{\vec{k}_1\,p\,\vec{k}_2\,q\,\vec{k}_3\,r\,\vec{k}_4\,s} = \iint \psi_{\vec{k}_1\,p}^{\dagger}(\vec{r}_1)\, \psi_{\vec{k}_2\,q}^{\dagger}(\vec{r}_2)\, \frac{1}{|\vec{r}_1 - \vec{r}_2|}\, \psi_{\vec{k}_3\,r}(\vec{r}_1)\, \psi_{\vec{k}_4\,s}(\vec{r}_2)\, \mathrm{d}^3 r_1\, \mathrm{d}^3 r_2\ .
\tag{3.6}
$$

The *antisymmetrized two-electron integrals* in (3.5) are

$$
V_{\vec{k}_1\,p\,\vec{k}_2\,q\,[\vec{k}_3\,r\,\vec{k}_4\,s]} = V_{\vec{k}_1\,p\,\vec{k}_2\,q\,\vec{k}_3\,r\,\vec{k}_4\,s} - V_{\vec{k}_1\,p\,\vec{k}_2\,q\,\vec{k}_4\,s\,\vec{k}_3\,r}\ .
\tag{3.7}
$$

They consist of a *Coulomb term* $V_{\vec{k}_1\,p\,\vec{k}_2\,q\,\vec{k}_3\,r\,\vec{k}_4\,s}$ and an *exchange term* $V_{\vec{k}_1\,p\,\vec{k}_2\,q\,\vec{k}_4\,s\,\vec{k}_3\,r}$. All crystal momentum vectors in (3.4), (3.6) and (3.7) are restricted to the Brillouin zone.

A different perspective on the one-particle states in a crystal is provided by Wannier orbitals [Section 2.5] which can be used equally well in the Hartree-Fock determinant (2.42). Consequently, Equations (3.2) and (3.3) remain formally the same with Bloch orbitals substituted by Wannier orbitals. Harnessing Wannier orbitals to express the Hamiltonian (2.4) yields its *Wannier representation* or *local representation* [6]. Frequently, it will turn out to be a more appropriate starting point in the ensuing sections. The inverse generalized Wannier transformation (2.33b) is applied to the Bloch orbitals of the creators and annihilators [115]; thereby it allows to recast (3.4). A creator transforms like the orbital it creates and the corresponding annihilator simply is the adjoint [115]. The transformation involves a mixing of bands via $\boldsymbol{\mathcal{U}}(\vec{k})$ and transforms the band energies into a block diagonal Fock matrix $\boldsymbol{F}$ with individual blocks for occupied and virtual bands.

The Hamiltonian in Wannier representation reads

$$
\begin{aligned}
\hat{H} &= \hat{H}_0^{\mathrm{WF}} + \hat{H}_1^{\mathrm{WF}} \\
\hat{H}_0^{\mathrm{WF}} &= \sum_{\vec{R}\,\varrho} \varepsilon_{\vec{R}\,\varrho}\, \hat{c}_{\vec{R}\,\varrho}^{\dagger}\, \hat{c}_{\vec{R}\,\varrho} \\
\hat{H}_1^{\mathrm{WF}} &= \sum_{\vec{R}_1\,\varrho,\ \vec{R}_2\,\sigma} W_{\vec{R}_1\,\varrho\,\vec{R}_2\,\sigma}\, \hat{c}_{\vec{R}_1\,\varrho}^{\dagger}\, \hat{c}_{\vec{R}_2\,\sigma} \\
&\quad + \tfrac{1}{2} \sum_{\substack{\vec{R}_1\,\varrho,\ \vec{R}_2\,\sigma,\\ \vec{R}_3\,\tau,\ \vec{R}_4\,\upsilon}} V_{\vec{R}_1\,\varrho\,\vec{R}_2\,\sigma\,\vec{R}_3\,\tau\,\vec{R}_4\,\upsilon}\, \hat{c}_{\vec{R}_1\,\varrho}^{\dagger}\, \hat{c}_{\vec{R}_2\,\sigma}^{\dagger}\, \hat{c}_{\vec{R}_4\,\upsilon}\, \hat{c}_{\vec{R}_3\,\tau}
\end{aligned}
\tag{3.8}
$$

with $\varepsilon_{\vec{R}\,\varrho} \equiv F_{\vec{R}\,\varrho\,\vec{R}\,\varrho} = F_{\vec{0}\,\varrho\,\vec{0}\,\varrho}$ being the diagonal elements of the Fock matrix $\boldsymbol{F}$. In the Wannier representation, the matrix elements of the one-particle operator are changed compared to the ones in the Bloch representation (3.5)

$$
W_{\vec{R}_1\,\varrho\,\vec{R}_2\,\sigma} = -\sum_{\vec{R}\,\tau} V_{\vec{R}_1\,\varrho\,\vec{R}\,\tau\,[\vec{R}_2\,\sigma\,\vec{R}\,\tau]}\, n_{\vec{R}\,\tau} + \slashed{F}_{\vec{R}_1\,\varrho\,\vec{R}_2\,\sigma}\ .
\tag{3.9}
$$

It now comprises the negative of the Hartree-Fock potential and, additionally, the off-diagonal elements of the Fock matrix. The latter contribution denotes $\slashed{F}_{\vec{R}_1\,\varrho\,\vec{R}_2\,\sigma} = (1 - \delta_{\vec{R}_1\,\varrho\,\vec{R}_2\,\sigma}) F_{\vec{R}_1\,\varrho\,\vec{R}_2\,\sigma}$. Note that $\slashed{\boldsymbol{F}}$ in (3.9) is block-diagonal and thus the Wannier orbitals are separated into occupied and virtual Wannier orbitals. The two-electron integrals in (3.8) and (3.9) are defined analogously to (3.6) and (3.7) with Bloch orbitals replaced by Wannier orbitals.

Inspecting the partition (3.4) of the Hamiltonian, one observes that it has the same form and meaning as the Møller-Plesset partition for canonical molecular orbitals [39–42] which is used frequently in molecular physics. Therefore, all equations derived on the basis of the molecular Møller-Plesset partition are in complete analogy to the equations in the case of crystals. The only difference between molecules and crystals is the occurrence of *composite indices* in the Hamiltonian (3.4), consisting of a crystal momentum vector $\vec{k}$ and a band index p which vary independently. Given an equation in terms of molecular orbitals, it can be written immediately in terms of Bloch orbitals by replacing all molecular orbital indices by composite indices. Afterwards one can exploit (translational) symmetry to simplify the equation.

Employing localized orbitals instead of canonical orbitals, complicates the derivation of molecular equations somewhat because the block-diagonal Fock matrix has always to be considered. However, replacing localized molecular orbitals by generalized Wannier orbitals remains trivial.

3.2 Coupled-cluster approximation

The family of coupled-cluster theories are a class of electron correlation methods which have proven to be very accurate and reliable. In what follows, I formulate the theory in terms of Wannier orbitals. Corresponding formulas employing Bloch orbitals are obtained simply by replacing lattice vectors by crystal momenta and Wannier orbital indices by

band indices. Coupled-cluster theories originate from the famous exponential ansatz for the exact ground-state wave function of an N particle system

$$\Psi_0^N = e^{\hat{T}}\Phi_0^N = \left[\sum_{\nu=0}^{\infty}\frac{1}{\nu!}\hat{T}^{\nu}\right]\Phi_0^N \tag{3.10}$$

of Coester and Kümmel [33–35] which has been introduced to quantum chemistry by Čížek [36, 39, 41, 42, 155–157]. Expression (3.10) relates the Hartree-Fock ground-state wave function Φ_0^N to the intermediately normalized, exact ground-state wave function Ψ_0^N employing the non-Hermitian *cluster operator* [39, 41, 42]

$$\hat{T} = \sum_{j=1}^{N}\hat{T}_j = \sum_{j=1}^{N}\sum_{\substack{\vec{R}_1'\,\alpha_1<...<\vec{R}_j'\,\alpha_j \\ \vec{R}_1\,\kappa_1<...<\vec{R}_j\,\kappa_j}} t_{\vec{R}_1\,\kappa_1,...,\vec{R}_j\,\kappa_j}^{\vec{R}_1'\,\alpha_1,...,\vec{R}_j'\,\alpha_j}\prod_{i=1}^{j}\hat{c}_{\vec{R}_i'\,\alpha_i}^{\dagger}\hat{c}_{\vec{R}_i\,\kappa_i}\,. \tag{3.11}$$

Here N is the number of electrons in the system, so $N \to \infty$ for crystals, and $t_{\vec{R}_1\,\kappa_1,...,\vec{R}_j\,\kappa_j}^{\vec{R}_1'\,\alpha_1,...,\vec{R}_j'\,\alpha_j}$ are referred to as *coupled-cluster amplitudes* or as *excitation amplitudes*. One series of indices runs over occupied Wannier orbitals $\vec{R}_1\,\kappa_1,\ldots,\vec{R}_j\,\kappa_j$ whereas the other series runs over virtual Wannier orbitals $\vec{R}_1'\,\alpha_1,\ldots,\vec{R}_j'\,\alpha_j$. The $\hat{T}_j$, $j = 1,\ldots,N$ are called *j particle excitation operators* which describe all unique j fold excitations. Since there are N electrons in the system, the cluster operator (3.11) terminates exactly after the summand $\hat{T}_N$.

The coupled-cluster amplitudes $t_{\vec{R}_1\,\kappa_1,...,\vec{R}_j\,\kappa_j}^{\vec{R}_1'\,\alpha_1,...,\vec{R}_j'\,\alpha_j}$ in formula (3.11) are obtained from the Schrödinger equation (2.3) with energy E_0^N and the exponential ansatz (3.10) for the exact ground-state wave function Ψ_0^N. To this end, I form the hierarchy of equations [39, 41, 42]

$$\langle\,|\,(\hat{H} - E_0^N)\,e^{\hat{T}}\,|\,\Phi_0^N\,\rangle = 0 \tag{3.12}$$

with the general state vector $\langle\,|$ for which, successively, the Hartree-Fock ground state and the excited Hartree-Fock states are inserted $\langle\,| = \langle\Phi_0^N|,\ \langle\Phi_{\vec{R}_1\,\kappa_1}^{\vec{R}_1'\,\alpha_1}|,\ \ldots,\ \langle\Phi_{\vec{R}_1\,\kappa_1...\vec{R}_j\,\kappa_j}^{\vec{R}_1'\,\alpha_1...\vec{R}_j'\,\alpha_j}|,$ $\ldots$ for all $\vec{R}_1\,\kappa_1 < \vec{R}_j\,\kappa_j < \ldots$ and $\vec{R}_1'\,\alpha_1 < \ldots < \vec{R}_j'\,\alpha_j < \ldots$ There are as many state vectors $\langle\,|$ utilized in (3.12) as there are single, double, $\ldots$ excitations in the cluster operator (3.11). The exponential in the matrix elements (3.12) is expanded into a series. The resulting sum of contributions to the quantities (3.12) terminates exactly because Equation (3.11) contains only excitations from occupied into virtual Hartree-Fock ground-state orbitals and the Hamiltonian (2.4) comprises only one- and two-particle operators. If the sum in the cluster operator (3.11) is not truncated, coupled-cluster finally becomes identical to full configuration interaction [39, 41, 42], i.e., the many-particle problem is solved exactly for the Hamiltonian (2.4).

Applying coupled-cluster theory in practice requires two further approximations. Firstly, the complete and thus infinite one-particle basis set is truncated to a finite one [Section 2.3]. Secondly, the sum of the excitation operators in $\hat{T}$ (3.11) is truncated after a few orders $n \ll N$ where a particularly rapid convergence with the order n is found. Although only n fold excitations are explicitly taken into account in the cluster operator (3.11), higher order excitations are accounted for implicitly by the series expansion

of $\mathrm{e}^{\hat{T}}$ in (3.10). The resulting amplitudes which correspond to the m fold excitations, $m > n$, are thereby approximated by products of amplitudes from lower excitations. This turns out to be an excellent estimate and, furthermore, guarantees the size-consistency of the theory which remains under truncation to any order n.

A workable coupled-cluster model of molecular physics usually sums only single and double excitation operators in the cluster operator (3.11), i.e., $\hat{T} \approx \hat{T}_1 + \hat{T}_2$, to approximate the exact energy $E_0^N \approx E_{\mathrm{CCSD}}^N$ of a N particle system. The hierarchy of equations (3.12) now, successively, projects on the Hartree-Fock ground state, the singly and the doubly excited Hartree-Fock states $\langle \, | = \langle \Phi_0^N |,\ \langle \Phi_{\vec{R}_1 \kappa_1}^{\vec{R}_1' \alpha_1} |,\ \langle \Phi_{\vec{R}_1 \kappa_1\ \vec{R}_2 \kappa_2}^{\vec{R}_1' \alpha_1\ \vec{R}_2' \alpha_2} |$, for all $\vec{R}_1' \alpha_1 < \vec{R}_2' \alpha_2,\ \vec{R}_1 \kappa_1 < \vec{R}_2 \kappa_2$. The resulting scheme is termed *coupled-cluster singles and doubles (CCSD)* [42, 158, 159]. The CCSD energy expression is obtained from the projection (3.12) on the Hartree-Fock ground state [158] to be

$$
\begin{aligned}
E_{\mathrm{CCSD}}^N &= \langle \Phi_0^N | \, \hat{H} \, \mathrm{e}^{\hat{T}_1 + \hat{T}_2} | \Phi_0^N \rangle \big/ \langle \Phi_0^N | \, \mathrm{e}^{\hat{T}_1 + \hat{T}_2} | \Phi_0^N \rangle \\
&= \langle \Phi_0^N | \, \hat{H} | \Phi_0^N \rangle + \sum_{\vec{R}\kappa, \vec{R}'\alpha} F_{\vec{R}\kappa\ \vec{R}'\alpha}\, t_{\vec{R}\kappa}^{\vec{R}'\alpha} \\
&\quad + \sum_{\substack{\vec{R}_1 \kappa > \vec{R}_2 \lambda \\ \vec{R}_1' \alpha > \vec{R}_2' \beta}} V_{\vec{R}_1 \kappa\ \vec{R}_2 \lambda\ [\vec{R}_1' \alpha\ \vec{R}_2' \beta]} \left(t_{\vec{R}_1 \kappa\ \vec{R}_2 \lambda}^{\vec{R}_1' \alpha\ \vec{R}_2' \beta} + t_{\vec{R}_1 \kappa}^{\vec{R}_1' \alpha}\, t_{\vec{R}_2 \lambda}^{\vec{R}_2' \beta} - t_{\vec{R}_1 \kappa}^{\vec{R}_2' \beta}\, t_{\vec{R}_2 \lambda}^{\vec{R}_1' \alpha} \right).
\end{aligned}
\tag{3.13}
$$

The remaining projections on single and double excitations in (3.12) provide a coupled set of nonlinear equations which have to be solved simultaneously to determine the coupled-cluster amplitudes [42, 158, 159].

CCSD has been devised for molecules by Purvis and Bartlett [158]. It yields accurate energies (3.13) and the equations for the cluster amplitudes are computationally managable [42, 158, 159]. The scheme contains all terms that couple directly to Φ_0^N. Frequently, the influence of the indirect coupling of triple excitations to the Hartree-Fock ground state is, additionally, accounted for perturbatively utilizing the cluster amplitudes of a converged CCSD calculation. This leads to the CCSD(T) method [160] which is known to deliver highly accurate correlation energies.

The last step to devise a practical coupled-cluster scheme for crystals is a translational symmetry adaption of the above equations by analyzing the individual terms therein. Several schemes have been derived and studied thoroughly. Fink and Staemmler [161, 162] consider CEPA-0, CCD is regarded by Förner *et al.* [163, 164] and Hirata *et al.* [165] deduce CCSD.

3.3 Configuration selection

The coupled-cluster energy expression (3.13) contains several lattice sums that run over the entire crystal. To obtain a meaningful approximation of coupled-cluster energies for crystals, the convergence of these lattice sums must be granted. Sun and Bartlett [166] have proven the convergence of Møller-Plesset perturbation theory, of the one-particle Green's functions and, in particular, of the coupled-cluster method. All of these methods are based on the Møller-Plesset partition of the Hamiltonian (3.4). Although the convergence of lattice sums is granted principally, I have to devise an algorithm for their proper

truncation [1]. The configuration space is the set of all single, double, ... excitations from occupied into virtual Wannier orbitals that are considered in the lattice sums for a specific crystal. It is built dynamically which means to meet a chosen accuracy in the lattice sums for a given crystal that transfers to a given accuracy in the coupled-cluster energy. In this section I discuss only equations for ground-state energies in terms of Wannier orbitals. Following the reasoning of Reference [166], the lattice sums in coupled-cluster theory in terms of Wannier orbitals also converge as they evolve from the equations in crystal momentum representation by means of the inverse Wannier transformation (2.33b).

The occupied Wannier orbitals in the unit cell $\vec{R}$ of a crystal are grouped in terms of n_{one} pairwise disjunct *one-body orbital sets* which are defined by

$$\vec{R}\,I_l \equiv \{w_{\vec{R}\alpha}(\vec{r}) \mid \alpha \in I_l\} \tag{3.14}$$

for $l = 1, \ldots, n_{\text{one}}$. Such a set is understood to be translationally symmetric, i.e., applying the operator $\hat{T}_{\vec{R}'}$ to $\vec{R}\,I_l$ yields $(\vec{R} - \vec{R}')\,I_l$. Hence, all Wannier orbitals of a crystals are partitioned.

The expression for the correlation energy (3.1) of a crystal is rearranged to decompose in terms of the correlation energies $\varepsilon_{\vec{R}_1\,I_1\cdots\vec{R}_K\,I_K}$ of the electrons out of the one-body orbital sets $\vec{R}_1\,I_1 \cdots \vec{R}_K\,I_K$. The resulting formula reads for the correlation energy of the crystal per unit cell $\mathcal{E}_{\text{corr,U.C.}}$

$$
\begin{aligned}
N_0\,\mathcal{E}_{\text{Corr,U.C.}} \;=\; & \frac{1}{1!}\sum_{\vec{R}_1\,I_1}\Delta\varepsilon_{\vec{R}_1\,I_1} + \frac{1}{2!}\sum_{\vec{R}_1\,I_1\neq\vec{R}_2\,I_2}\Delta\varepsilon_{\vec{R}_1\,I_1\,\vec{R}_2\,I_2} \\
& + \ldots + \frac{1}{K!}\sum_{\substack{\vec{R}_1\,I_1\cdots\vec{R}_K\,I_K \\ \text{pairwise disjunct}}}\Delta\varepsilon_{\vec{R}_1\,I_1\cdots\vec{R}_K\,I_K} + \ldots
\end{aligned}
\tag{3.15}
$$

where N_0 is the number of unit cells in the Born von Kármán region. The one-body, two-body, ..., K-body energy increments, ... $\Delta\varepsilon_{\vec{R}_1\,I_1}$, $\Delta\varepsilon_{\vec{R}_1\,I_1\,\vec{R}_2\,I_2}$, ..., $\Delta\varepsilon_{\vec{R}_1\,I_1\cdots\vec{R}_K\,I_K}$, ... are defined recursively by [1, 2, 38, 43–45, 138, 151, 152]

$$\Delta\varepsilon_{\vec{R}_1\,I_1} \;=\; \varepsilon_{\vec{R}_1\,I_1} \tag{3.16a}$$

$$\Delta\varepsilon_{\vec{R}_1\,I_1\,\vec{R}_2\,I_2} \;=\; \varepsilon_{\vec{R}_1\,I_1\,\vec{R}_2\,I_2} - \Delta\varepsilon_{\vec{R}_1\,I_1} - \Delta\varepsilon_{\vec{R}_2\,I_2} \tag{3.16b}$$

$$\vdots$$

$$\Delta\varepsilon_{\vec{R}_1\,I_1\cdots\vec{R}_K\,I_K} \;=\; \varepsilon_{\vec{R}_1\,I_1\cdots\vec{R}_K\,I_K} - \sum_{n=1}^{K-1}\frac{1}{n!}\sum_{\substack{\{\vec{R}'_1\,I'_1\cdots\vec{R}'_n\,I'_n\} \\ \subset\{\vec{R}_1\,I_1\cdots\vec{R}_K\,I_K\} \\ \vec{R}'_1\,I'_1\cdots\vec{R}'_n\,I'_n \\ \text{pairwise disjunct}}}\Delta\varepsilon_{\vec{R}'_1\,I'_1\cdots\vec{R}'_n\,I'_n}. \tag{3.16c}$$

$$\vdots$$

The factors $\frac{1}{1!}$, $\frac{1}{2!}$, ..., $\frac{1}{K!}$, ... in front of the sums on the right hand side of (3.15) account for permutations among the one-body orbital sets (3.14) of a certain K-body energy increment ($K \geq 2$) which for sure does not alter its value. By introducing an ordering relation "$<$" among the one-body orbital sets, i.e., $\vec{R}_1\,I_1 < \vec{R}_2\,I_2$, one eliminates all permutations that lead to the same values of an energy increment and thus the sums in (3.15)

only run over distinct ordered tuples of one-body orbital sets (3.14). $\mathcal{E}_{\mathrm{corr,U.C.}}$ becomes the full correlation energy per unit cell of the crystals with respect to a certain basis set and a certain correlation method, if all energy increments in (3.15) are calculated in the limit $N_0 \to \infty$.

There are three major advantages of the resummation of the correlation energy in terms of energy increments in (3.15):

1. Symmetry can be exploited to enormously reduce the number of distinct energy increments of significant magnitude to be calculated.

2. Correlation effects are partitioned in terms of non-additive one-body, two-body, three-body, ... contributions allowing for an analysis of the contributions to the correlation energy and their exact summation to infinite distances [Section 4.3.3].

3. A simple convergence check is given by monitoring the decay of the energy increments.

Point 1 is demonstrated best by considering that Wannier orbitals are translationally related (2.32a) which renders the energy increments translationally symmetric, i.e., they obey $\Delta\varepsilon_{\vec{0}\,I_1 \cdots \vec{R}_K - \vec{R}_1\,I_K} = \Delta\varepsilon_{\vec{R}_1\,I_1 \cdots \vec{R}_K\,I_K}$. This can be exploited to make the right hand side of (3.15) independent of the first lattice sum $\sum_{R_1}$ which, for this reason, is N_0 times the sum of the translational symmetry adapted energy increments. It allows to eliminate the factor N_0 in front of the left hand side of (3.15) which enormously reduces the number of energy increments to be calculated in order to describe a crystal with a given accuracy

$$
\begin{aligned}
\mathcal{E}_{\mathrm{Corr,U.C.}} \;=\; & \sum_{I_1} \Delta\varepsilon_{\vec{0}\,I_1} + \sum_{\vec{0}\,I_1 < \vec{R}_2\,I_2} \Delta\varepsilon_{\vec{0}\,I_1\,\vec{R}_2\,I_2} \\
& + \ldots + \sum_{\vec{0}\,I_1 < \vec{R}_2\,I_2 < \cdots < \vec{R}_K\,I_K} \Delta\varepsilon_{\vec{0}\,I_1\,\vec{R}_2\,I_2\,\cdots\,\vec{R}_K\,I_K} + \ldots .
\end{aligned}
\tag{3.17}
$$

Consider assigning an *electron pair*, i.e., two spin orbitals, to a one-body orbital set (3.14). In this case, coupled-cluster singles and doubles is equivalent to employing the correlation method full CI [39]; summing over all two-body energy increments or *pair energies* yields the *independent electron pair approximation (IEPA)* [39, 167], an approximation which is known to provide a first glance on correlation energies [39]. Higher order energy increments substantially improve on the IEPA and, in the end, provide the full CCSD correlation energy of a crystal.

The coupled-cluster method of the Sec 3.2 is formulated both in crystal momentum representation and in Wannier representation. Localized Wannier orbitals are essential to apply cutoff criteria within unit cells [1, 2, 27, 28, 43–45, 168] in complete analogy to the calculation of correlation energies of large molecules [148]. In order to investigate the asymptotic scaling of the determination of ground-state energies by means of the incremental series (3.16) and (3.17), I assume a crystal with macroscopic lattice constants. All one- and two-electron integrals between different unit cells become vanishingly small and are set to exactly zero. This implies that only a finite range of the Coulomb interaction between the electrons is regarded. Consequently, energy increments that involve Wannier orbitals in different unit cells vanish. Now, I form a *superlattice* which is constituted of

supercells, i.e., unit cells that consist here of two of the original unit cells. Clearly, the number of energy increments which is required to describe the total energy per unit cell of the crystal only doubles upon going over to the superlattice. Upon doubling the system size, the computational effort thereby also *only* doubles. Invoking the incremental scheme renders the underlying correlation theory to become a *linear scaling method* [152, 168] for ground-state energies of crystals. Once the incremental scheme is applied to study large molecules[1] this conclusion is transferred. An extension of these ideas to a configuration selection scheme for band structures is given in Section 6.4.

3.4 Finite-cluster approximation

The Wannier orbitals of polymers, surfaces and crystals [1, 2, 38, 43–45, 138, 151, 152] are found to be approximated well by the localized occupied molecular orbitals in the center of clusters that, e.g., result from the Foster-Boys method [139, 140], which comprise a few properly chosen monomers, that are arranged in the geometry of the infinite systems. To show that the particular localized molecular orbitals of such a cluster really approximate the Wannier orbitals of the solid well, the localized occupied molecular orbitals have to be approximately translationally related (2.32a) within the cluster and should not differ substantially among clusters of varying size. These two properties of the localized occupied molecular orbitals are termed *transferability*. The virtual orbitals of the finite clusters which are utilized to calculate the individual energy increments are not altered and remain canonical molecular orbitals. The finite-cluster approximation thus corresponds to a sort of domain decomposition of the virtual space which is also applied in other local correlation methods [168]. They are a source of finite-size effects but extended diffuse virtual orbitals that are influenced most by the cluster approximation give only a small contribution to the correlation energy.

The so far discussed combination of a correlation method, here CCSD [Section 3.2], configuration selection (3.16), (3.17) and a finite-cluster approximation to determine ground-state correlation energies of crystals is frequently referred to as *incremental scheme* [1, 2, 38, 43–45]. As the underlying correlation method can be chosen from among the variety of wave-function-based quantum chemical methods, the incremental scheme classifies as a meta-method. A favorable property of suitable correlation methods is size-consistency as, e.g., the two-body increments describe some sort of a dissociation process within the crystal [Section 4.3.3] and do not vanish completely, if the two one-body orbital sets (3.14) are infinitely far apart (Reference [169], page 21). In practice, a lack of size-consistency of the underlying correlation method turns out to be less severe, the convergence properties of the incremental series (3.16) and (3.17) only is degraded (Reference [170], page 21).

A simple recipe for practical calculations using the incremental scheme with standard

---

[1]Basing on the partitioning of the coupled-cluster correlation energy (3.16) and (3.17) for crystals in terms of Wannier orbitals, I can immediately derive an analogous configuration selection scheme for molecules. To this end, I assume a crystal with macroscopic lattice constants. The energy increments which involve one-body orbital sets (3.14) in different unit cells become vanishingly small, implying that one can restrict all lattice sums to the origin cell and, subsequently, omit lattice vectors in (3.16) and (3.17).

quantum chemical program packages is given by Albrecht [66] on pages 28 and 29. If the correlation energy of a large molecule, like the Buckminsterfullerene [171] or *closo*-hydroborate dianions [172], is computed with the incremental scheme and no truncation of the series [the molecular version of Equations (3.16) and (3.17)] is applied, this way of calculating the total correlation energy of the molecule $E_{\text{corr,cluster}}$ is in fact significantly more expensive than a direct calculation, if only standard quantum chemical program packages are harnessed, because all possible energy increments are needed which means that, in particular, $E_{\text{corr,cluster}}$ is anyhow required for the energy increment that contains excitations from all occupied orbitals of the cluster. The enormous redundancies involved with the calculations, utilizing the incremental scheme, could in principle be reduced to a negligible amount by directly identifying and regrouping the terms of the correlation method such that they contribute to the various energy increments in the calculation of correlation energies of solids. In a study of poly(para-phenylene) [152], in fact, a transition from one-body orbital sets (3.14) that only comprise a single bond to larger sets containing the occupied orbitals of a whole phenylene ring led to managable and rapidly convergent incremental series (3.16) and (3.17).

All types of crystals [1–3,38,173], i.e., molecular, ionic, covalent and metallic solids have been investigated, and prerequisites for their proper approximation using finite clusters have been devised [1,2,38]. The prototype of *"molecular" crystals* are the van-der-Waals-bonded rare gas solids which have been studied by Rościszewski *et al.* [174,175]. Bare clusters of a few atoms have been found to be sufficient, taking the full set of valence orbitals as one-body orbital sets (3.14) [174,175].

Hydrogen-bonded crystals are another type of molecular crystals which are frequently considered somewhat separately due to their unique physicochemical properties. Such solids are studied in this thesis for the first time with the incremental scheme in the case of the infinite $(\text{HF})_\infty$ and $(\text{HCl})_\infty$ chains. Appropriate cluster approximations are discussed in detail in the ensuing Chapter 4.

For *ionic crystals*, it turned out to be essential to surround clusters with several shells of point charges chosen according to Evjen [3,176] to ensure that a proper Madelung field is created [169,177–180]. The cations are described well by basis sets of moderate, double-ζ, quality but the anions in such crystals required a very accurate representation of their diffuse electron distribution [169,177,178]. The full set of valence orbitals are usually selected as one-body orbital sets (3.14) [169,177,178]. Many ionic compounds have been studied: the oxides MgO [177,178], CaO [178], rutile (TiO_2) [181] and NiO [182]. Light and heavy alkali halides [179,180] up to AgCl and AuCl [183] have been regarded as well as GdN [184], hydroborates [172], bulk LiH [32], the infinite lithium hydride chain [138] and the beryllium hydride polymer [138].

Covalent crystals are usually partitioned in terms of individual bonds [167,170,185]. Bonds that would be connected to other atoms in the infinite crystal, so-called dangling bonds, are required to be saturated with hydrogen atoms to yield the proper electronic structure of the crystal in the molecular clusters [66,167]. This procedure is analyzed and criticized by Paulus [167], on pages 46–48, who finds a charge redistribution. The ground-state binding energies of diamond [43], group-IV semiconductors [44,186,187], III-V semiconductors [188,189] and II-VI semiconductors [190] could be obtained. The *trans*-polyacetylene polymer [151] and a semiconducting polymer with an aromatic π-

system, poly(para-phenylene) [152], have been studied.

Despite of the well-known slow decay of Wannier orbitals of metals that originate from partially-filled bands [3,6,10,122], attempts are made to treat *metallic crystals* with the incremental scheme. Breathtakingly accurate results have been published so far that highly encourage further investigations. The first studies are graphite [45], one-dimensional lithium rings [191] and mercury crystals [192].

In finite clusters, energy increments which are equivalent due to space group symmetry in the infinite crystal, should also be calculated and utilized where appropriate to allow the cancellation of errors which are introduced by the finite-cluster approximation, Paulus [167], pages 46–48 and Albrecht [66], page 28. Moreover, Paulus [167] noted that the impact of finite-size effects on one-body energy increments are predominantly responsible for errors in the correlation energy of crystals among a set of clusters. Inaccuracies of the cluster approximation on two-body (and higher-body) energy increments are found to be compensated to a large extent.

Moreover, as the Hamiltonian (2.4) contains only one- and two-particle interactions, three-body and higher increments are only described by an indirect coupling [66], page 19. In the above studies of crystals, it has been found that three-body energy increments frequently are larger than zero. They represent the correction due to electron repulsion by the Pauli exclusion principle. The three-body energy increments tend to compensate space group symmetry breaking observed for the localized molecular orbitals with respect to Wannier orbitals of the infinite crystals, Reference [170], page 20 and Reference [66], page 19.

Let me conclude this section with the words of the originator of the incremental scheme, Hermann Stoll (with coworkers), taken from Reference [137]: "[...] The main drawback of the incremental scheme [...] is the derivation of the correlation increments from finite-cluster instead of infinite-solid calculations. By consistently and rigorously taking into account the periodicity of the lattice, at all stages of the calculations, we now strive to provide an improved procedure." I engage with this program in Part II of this dissertation but stay with the finite-cluster approximation to study the ground-state of infinite $(HF)_\infty$ and $(HCl)_\infty$ chains in the following Chapter 4 which will turn out to be an adequate pursuit for these systems.

3.5 Convergence of correlation energies

The incomplete one-particle basis sets, which are used in practical computations, lead to the basis set truncation error, in addition to the N electron error of the correlation method. The convergence of correlation energies with the quality of the underlying one-particle basis set has been investigated carefully [42, 46, 54, 193, 194]. The analysis of the partial-wave expansion of the correlation energy of the helium atom due to Hill [42, 46, 54] establishes the dependence of the correlation energy on the highest angular momentum ℓ in the basis set

$$E_{\text{corr}}(\ell) - E_{\text{corr}}(\ell - 1) = a_4 \left(\ell + \frac{1}{2}\right)^{-4} + a_5 \left(\ell + \frac{1}{2}\right)^{-5} + \dots \qquad (3.18)$$

The basis set is assumed to be saturated with respect to basis functions of lower angular momenta than ℓ. A similar convergence behavior has been found in the case of MP2 theory for many-electron atoms by Kutzelnigg and Morgan [195, 196].

Let $E_{\text{corr}}(\ell)$ be given for $\ell = L$, then the difference to $E_{\text{corr}}(\infty)$ can be derived by summing up the leading terms in (3.18) as follows

$$E_{\text{corr}}(\infty) = E_{\text{corr}}(L) + a_4 \sum_{\ell=L+1}^{\infty} \left(\ell + \frac{1}{2}\right)^{-4} + \dots \tag{3.19}$$

This sum is approximated by replacing the summation by an integration [42, 55]

$$\sum_{\ell=L+1}^{\infty} \left(\ell + \frac{1}{2}\right)^{-4} = \int_{L+\frac{1}{2}}^{\infty} \left(\ell + \frac{1}{2}\right)^{-4} = \frac{1}{3}(L+1)^{-3} \tag{3.20}$$

and truncating the series (3.19) after the leading correction term. Let $X = L + 1$ and $A' = \frac{a_4}{3}$, the relation

$$E_{\text{corr}}(\infty) = E_{\text{corr}}(X) - A' X^{-3} \tag{3.21}$$

follows. Here $E_{\text{corr}}(\infty)$ is the *basis set limit correlation energy* of the respective correlation method and $E_{\text{corr}}(X)$ represents the correlation energy obtained with basis set X. Expression (3.21) is derived for the asymptotic behavior, i.e., large X, of the correlation energy of the helium atom, assuming that basis sets of highest angular momentum X are centered on the nucleus. The basis sets are supposed to be complete for all angular momenta $\leq X$ and are required to be complete with respect to their radial part [54].

Writing Equation (3.21) for two different basis sets X and Y, I obtain

$$\begin{aligned} E_{\text{corr}}(\infty) &= E_{\text{corr}}(X) - A' X^{-3} \\ E_{\text{corr}}(\infty) &= E_{\text{corr}}(Y) - A' Y^{-3} \, . \end{aligned} \tag{3.22}$$

This allows one to eleminate the unknown constant A' which yields a simple two-point fit [42, 46, 56]

$$E_{\text{corr}}(\infty) = \frac{E_{\text{corr}}(X)\, X^3 - E_{\text{corr}}(Y)\, Y^3}{X^3 - Y^3} \, . \tag{3.23}$$

Equation (3.23) is derived under considerable constraints. However, the fit turns out to provide highly accurate molecular binding energies as I will demonstrate in the following Chapter 4 [42, 46, 55–57].

The extrapolation scheme for correlation energies of Park, Huh and Lee [58, 59] is a more flexible basis set extrapolation which has not been derived under the prerequisites of the X^{-3} scheme (3.23) but sets out from the approximation

$$\frac{E_{\text{corr}}^{\text{crystal}}(X) - E_{\text{corr}}^{\text{crystal}}(\infty)}{E_{\text{corr}}^{\text{crystal}}(Y) - E_{\text{corr}}^{\text{crystal}}(\infty)} \approx \gamma_{X,Y} = \frac{E_{\text{corr}}^{\text{monomer}}(X) - E_{\text{corr}}^{\text{monomer}}(\infty)}{E_{\text{corr}}^{\text{monomer}}(Y) - E_{\text{corr}}^{\text{monomer}}(\infty)} \, . \tag{3.24}$$

The *basis set convergence rate* $\gamma_{X,Y}$ is assumed to be the same for a monomer and a crystal formed by many monomers. $\gamma_{X,Y}$ is the ratio of the absolute error in the correlation

energy of the monomer described by two different basis sets X and Y. If the electronic structure of a monomer does not change substantially upon crystallization, a given basis set represents both the monomer and the crystal equally well. Expression (3.24) is recast to yield

$$E_{\text{corr}}^{\text{crystal}}(\infty) \quad = \quad \frac{E_{\text{corr}}^{\text{crystal}}(X) - \gamma_{X,Y} E_{\text{corr}}^{\text{crystal}}(Y)}{1 - \gamma_{X,Y}} \tag{3.25a}$$

$$\gamma_{X,Y} \quad = \quad \frac{E_{\text{corr}}^{\text{monomer}}(X) - E_{\text{corr}}^{\text{monomer}}(\infty)}{E_{\text{corr}}^{\text{monomer}}(Y) - E_{\text{corr}}^{\text{monomer}}(\infty)} \tag{3.25b}$$

which is interpreted [58] to optimize not only the linear parameter A' in (3.21) but also to consider the exponent of X as well, i.e.,

$$E_{\text{corr}}(\infty) = E_{\text{corr}}(X) - A' X^{-p} . \tag{3.26}$$

I consider it to cope slightly better with the increasing radial and angular completeness of hierarchical basis set series.

4 Hydrogen fluoride and hydrogen chloride chains

Hydrogen fluoride [61, 197–202] and hydrogen chloride [203–205] are representatives of *molecular crystals*, i.e., the electronic structure of the monomers is essentially preserved upon crystallization [3]. The monomers in both crystals are hydrogen bonded [61, 173, 206–208]. Such bonds are formed between two electronegative units X and Y which act as donor and acceptor, respectively, of a hydrogen atom [173, 209]

$$R–X–H \cdots :Y–R' \,. \tag{4.1}$$

In this thesis, X, Y stand for F, Cl and $R' = H$ whereas R is not needed here. Therefore, the hydrogen bond is formed between the separately identifiable monomers HF and HCl, respectively. Only a bare, tiny proton would remain, if a hydrogen atom was completely ionized. Therefore, a high electronegativity of the donor X is only able to withdraw charge partially from the hydrogen atom which leads to the additional formation of a directional and anisotropic bonding to the acceptor Y [61, 173, 206–209]. Hydrogen bonds are intermediates between purely ionic bonds and van der Waals bonds and are of great importance for the physical and chemical properties of many organic and inorganic crystals. Moreover, they turn out to be crucial for the structure of many biopolymers such as proteins or nucleic acids [61, 173, 206–209].

At low temperatures, HF and HCl are structurally very similar, with the differences between both crystals arising exclusively from the different halogenide atoms involved. While hydrogen fluoride forms very strong hydrogen bonds, hydrogen chloride forms only weak hydrogen bonds [173]. Therefore, HF and HCl represent good candidates for a thorough analysis of this special type of bonding in crystals. The monomers in both solids are found to be arranged in terms of parallel infinite zig-zag chains [Figure 4.1] with a large interchain distance and, hence, a weak interchain interaction [Section 4.1]. Frequently, a single infinite chain is considered as a simple but realistic model of these crystals. The isolated $(HF)_\infty$ chain has fascinated many theoreticians. Selected works are: model studies [210–212], the semiempirical [intermediate neglect of differential overlap (INDO)] examination of Zunger [213], DFT calculations (LDA) of Springborg [211, 212] and the *ab initio* investigations in References [99, 214–226]. Infinite $(HCl)_\infty$ chains, in contrast, have not been considered extensively. There are a model study [210] and a few *ab initio* examinations [216, 217, 227, 228]. For both, isolated $(HF)_\infty$ and $(HCl)_\infty$ chains, the zig-zag geometry of Figure 4.1 is the energetically favored arrangement in comparison to the linear geometry. For $(HF)_\infty$ this has been shown in early studies by Karpfen *et al.* [215, 219] and Beyer and Karpfen [221]. The structure of isolated $(HCl)_\infty$ chains has been investigated in Reference [228].

The large number of *ab initio* studies which have been carried out for the chains exhibits how challenging hydrogen bonded systems are. A thorough investigation requires
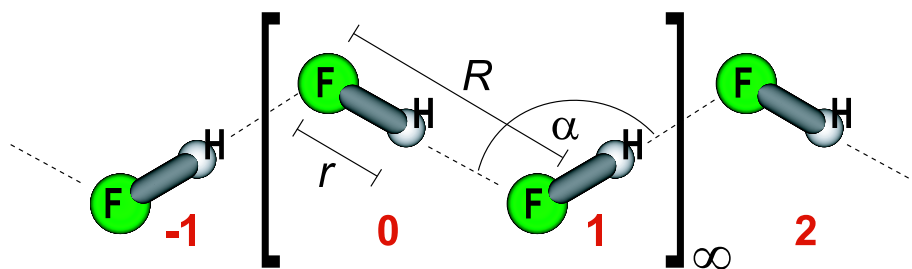
Figure 4.1: (Color) Geometry of infinite $(HF)_\infty$ and $(HCl)_\infty$ zig-zag chains. The numbers below the monomers indicate the relative position of a monomer in the chain with respect to an origin monomer "0". The figure is based on a rendering of $(HF)_{10}$ created with the MOLDEN program [229].

both very good electron correlation methods and large one-particle basis sets [57, 61]. Therefore, a periodic Hartree-Fock treatment [Section 2.2] is accompanied by sophisticated correlation calculations [Section 4.3]. To this end, I use the correlation method coupled-cluster singles and doubles (CCSD) [Section 3.2] in conjunction with the incremental scheme [Section 3.4]. Moreover, I apply the basis set extrapolation schemes for Hartree-Fock energies of Section 2.4 in Section 4.2 and the scheme for correlation energies of Section 3.5 in Section 4.3.4 to finally arrive at accurate binding energies in Section 4.4.

4.1 Computational details

Hydrogen fluoride and hydrogen chloride crystallize in an orthorhombic low-temperature phase described by the space groups $Bm2_1b$ for HF [197–199] and $Bb2_1m$ for HCl [203–205]. The unit cells of both crystals contain four monomers which are arranged in terms of two weakly interacting, parallel zig-zag chains [Figure 4.1] along the b-axis. They are described by a unit cell which comprises two monomers and are considered as an excellent one-dimensional model for HF and HCl crystals [99, 210–228]. The geometry of the single chains is determined by three parameters, the H—X distance r, the X$\cdots$X distance R and the angle $\alpha = \angle(HXH)$, X = F,Cl. Experimental values for the parameters are $r = 0.92\,\text{Å}$, $R = 2.50\,\text{Å}$, $\alpha = 120°$ for $(HF)_\infty$ [197, 230] and $r = 1.25\,\text{Å}$, $R = 3.688\,\text{Å}$, $\alpha = 93.3°$ for $(DCl)_\infty$ [203]. HCl and DCl crystals have very similar lattice constants and are considered to be isomorphous [203]. Unfortunately, further structural information for HCl crystals is unavailable.

Periodic Hartree-Fock calculations for binding energies (4.2) of infinite $(HF)_\infty$ and $(HCl)_\infty$ chains [Section 4.2] are carried out with the CRYSTAL program [5, 7, 231]. Short fractions of the chains, the oligomers $(HF)_n$ and $(HCl)_n$, $n = 2, 4, 6, 9, 10$, are treated with the program package MOLPRO [232]. Correlation calculations for the energy increments in (3.16), (3.17) are carried out for oligomers only, employing Foster-Boys localization [139, 140] of the molecular orbitals and the CCSD correlation method [158, 159, 232] [Section 3.2]. The chains are described by the hierarchical series of correlation consistent basis sets [48] cc-pVXZ [49, 50], aug-cc-pVXZ [49–51] and d-aug-cc-pVXZ [49, 51, 52], $X = D, T, Q, 5, 6$.

As Hartree-Fock energies converge rapidly towards the basis set limit (2.31)—in contrast
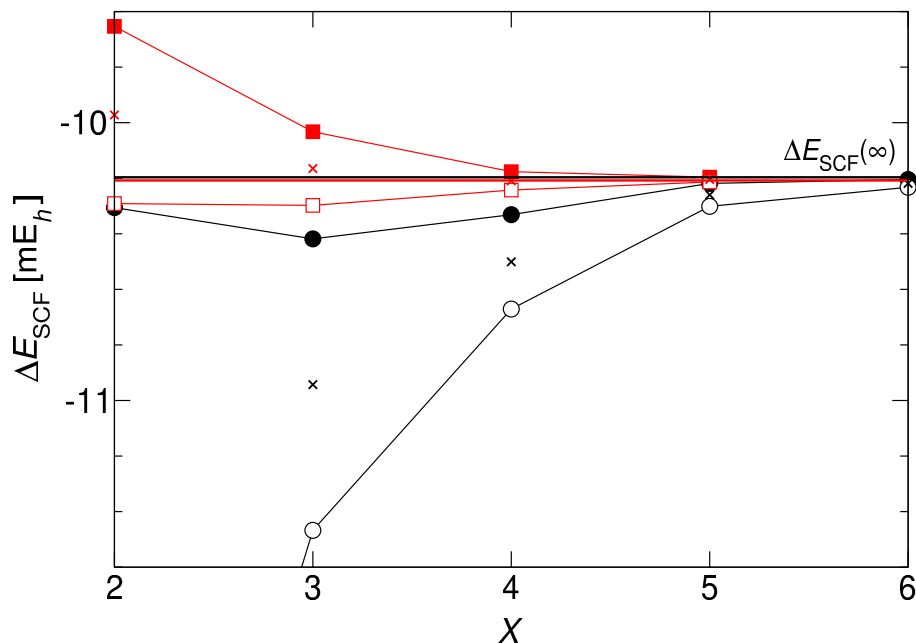
Figure 4.2: (Color) Basis set convergence of the Hartree-Fock binding energy per monomer ΔE_{SCF} in a $(HF)_\infty$ chain. Circles and squares represent $\Delta E_{SCF}(X)$ of the cc-pVXZ and aug-cc-pVXZ basis sets, respectively, where open and closed symbols denote bare and CP corrected Hartree-Fock binding energies. The straight line results from two nearly coinciding lines which indicate the extrapolated Hartree-Fock binding energies $\Delta E_{SCF}(\infty)$, the upper and the lower line referring to the cc-pVXZ and the aug-cc-pVXZ basis sets, respectively. The crosses indicate the mean of the CP corrected and the corresponding bare Hartree-Fock binding energies.

to correlation energies (3.23)—these two contributions (4.2) and (4.6) to the total binding energy (4.7) can thus be treated separately and one may even use a smaller basis set for the Hartree-Fock than for the correlation calculations. In fact, I exploit the different rates of convergence by dropping f, g, h, i basis functions in periodic Hartree-Fock calculations. This is required because CRYSTAL [5, 7, 231] is unable to handle f, g, h, i basis functions. However, the full basis sets are utilized in calculations for oligomers with MOLPRO [232]. To estimate the influence of the neglected basis functions on the binding energy (4.7) of the chains, I examine the Hartree-Fock binding energy per monomer for $(HF)_9$ and $(HCl)_9$ both with and without f, g, h functions in a cc-pV5Z [48–50] basis set which is close to completeness with respect to basis functions with the angular momenta s, p, d. The binding energies with f, g, h functions are smaller by $\approx 13\,\mu E_h$ than those excluding f, g, h functions for both chains which turns out to be sufficiently small to be neglected in the successive calculation of total binding energies in Section 4.4.

The behavior of the two-body energy increments for big separations of the two monomers is studied in Section 4.3.3 using the oligomers $(HF)_{10}$ and $(HCl)_{10}$. The aug-cc-pVDZ [48–51] basis set is employed which yields somewhat less accurate total binding energies than larger basis sets. Yet, the long-range behavior of the energy increments in the hydrogen-bonded chains is well described. In fact, the two-body energy increment for third nearest neighbors ε_{03} [Section 4.3] as obtained with the aug-cc-pVDZ [48–51] basis set is smaller

by 2% for $(HF)_\infty$ and by 4% for $(HCl)_\infty$ than ε_{03} in the larger aug-cc-pVTZ [48–51] basis set. Similarly, K-body energy increments for $K \geq 3$ agree well as soon as the spatial orbital overlap between the one-body orbital sets (3.14) become negligible.

The calculation of binding energies should always include a thorough investigation of the *basis set superposition error (BSSE)* [233–235] as they are defined with respect to the monomer energy [Equations (4.2) and (4.6)]. In weakly bound systems like $(HF)_\infty$ and $(HCl)_\infty$, BSSE can not only lower the accuracy of the results but also may yield artefacts. The situation is severe, if poor basis sets are employed. Basis sets for three-dimensional crystals are frequently chosen considerably less diffuse with respect to a certain accuracy of the binding energy than those for molecular calculations [5, 7], as there is no need to describe any vacuum properly. However, the definition of the binding energy involves a calculation of the monomer energy which implies that a proper description of the vacuum is also required. A balanced representation of the atoms in the crystal and the atoms in the monomer is therefore imperative. In single chains, the vacuum for the two remaining directions vertically to the chain axis needs to be accounted for which requires more diffuse basis sets.

BSSE is removed using the *counterpoise correction (CP)* [42, 234, 235], by surrounding a HF or a HCl monomer, respectively, with additional *ghost basis functions*, i.e., basis functions that are not centered on atoms but are freely placed in space, arranged to form short fractions (oligomers) of the infinite chains. By this procedure, I am able to include the effect of *basis set extension (BSE)* [235], i.e., the improved description of the atoms in the origin cell due to the basis sets in neighboring unit cells, which leads to BSSE if unaccounted for. The impact of BSE is not as severe in the Hartree-Fock approximation as it is for the correlation methods, due to the exponential convergence of Hartree-Fock energies towards the basis set limit (2.31) with respect to the cardinal number X of correlation consistent basis sets while correlation energies only converge with X^{-3} (3.21) [Sections 2.4 and 3.5]. Hence, even the smaller correlation consistent basis sets yield reasonable Hartree-Fock binding energies per monomer even if the BSSE is not regarded.

4.2 Independent particles

Treating the electrons in the infinite $(HF)_\infty$ and $(HCl)_\infty$ chains in Hartree-Fock approximation, yields the following contribution to the binding energy per monomer

$$\Delta E_{\mathrm{SCF}} = \frac{1}{2}\,\mathcal{E}^{\mathrm{SCF}}_{\mathrm{chain}} - \mathcal{E}^{\mathrm{SCF}}_{\mathrm{monomer}} \qquad (4.2)$$

where $\mathcal{E}^{\mathrm{SCF}}_{\mathrm{chain}}$ is the Hartree-Fock energy of a chain per unit cell and $\mathcal{E}^{\mathrm{SCF}}_{\mathrm{monomer}}$ is the corresponding Hartree-Fock energy of the monomer. In Figures 4.2 and 4.3, $\mathcal{E}^{\mathrm{SCF}}_{\mathrm{chain}}$ of $(HF)_\infty$ and $(HCl)_\infty$ are plotted for series of correlation consistent basis sets. For each series, there is an upper curve for the CP corrected[1] binding energies and a corresponding lower curve giving the bare binding energies without CP correction of the monomer energies. Both

---

[1]The BSSE is removed beyond microhartree accuracy with the CP correction [234, 235], [Section 4.1], by surrounding the monomer additionally with the basis functions of eight neighboring monomers.
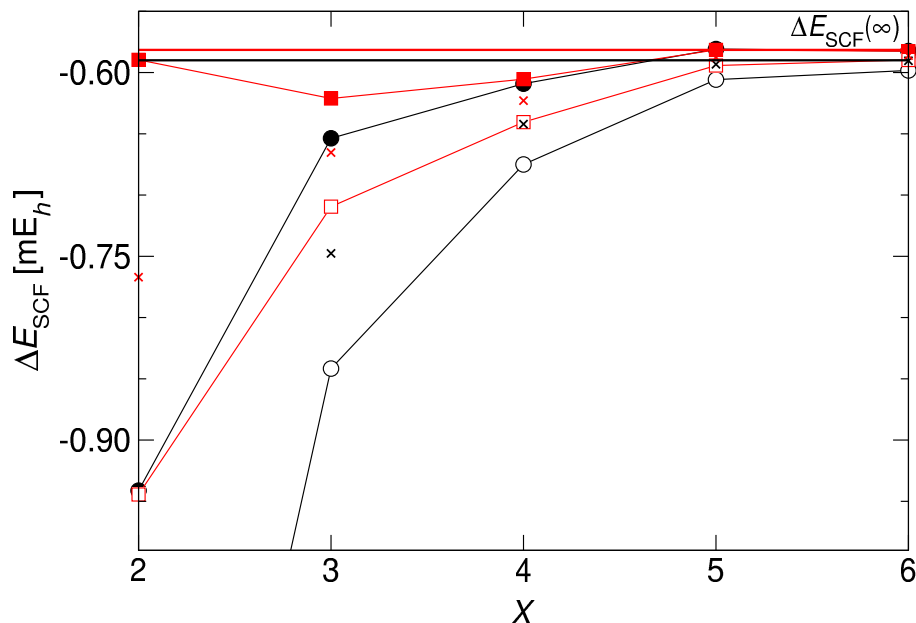
Figure 4.3: (Color) Basis set convergence of the Hartree-Fock binding energy per monomer ΔE_{SCF} of a $(HCl)_\infty$ chain. Symbols are chosen as in Figure 4.2. The upper and the lower straight lines now refer to the aug-cc-pVXZ and the cc-pVXZ basis sets limits $\Delta E_{SCF}(\infty)$, in reverse order compared to Figure 4.2.

curves converge unsystematically towards the Hartree-Fock basis set limit; especially, they do not converge monotonically.

The deviation of the lower curve from the upper curve of the same basis set series yields an estimate of the error of the approximation introduced by the finite basis sets as this deviation is the size of the BSSE [235] and an estimate of the incompleteness of a one-particle basis set. It is very small, 0.27% for $(HF)_\infty$ and 2.7% for $(HCl)_\infty$, utilizing the cc-pV6Z basis set. Nevertheless, I would like to elucidate whether, in the case of an infinite chain, the Hartree-Fock energies follow (2.31) as well, i.e., whether the packing in infinite periodic systems has an unexpected impact on Hartree-Fock basis set convergence. The Table 4.1 gives Hartree-Fock binding energies (4.2) at the basis set limit for the infinite chains as obtained by a least squares fit using (2.31). It turns out that the fit describes the Hartree-Fock energies, underlying Figures 4.2 and 4.3, excellently. A three-point fit based on (2.31) to the Hartree-Fock energies, obtained with three basis sets X, Y and Z, also yields convincing results that converge rapidly with the quality of the three basis sets used. For the basis set convergence of the Hartree-Fock binding energy of several hydrogen-bonded complexes, including $(HF)_2$ and $(HCl)_2$, Halkier *et al.* [57] found that the mean of the bare and the counterpoise corrected Hartree-Fock binding energies frequently provides a decent extrapolation to the basis set limit. This behavior of the mean Hartree-Fock binding energy is solely observed for the aug-cc-pVXZ series for $(HF)_\infty$.

In Table 4.6, I communicate the mean of the basis set extrapolated Hartree-Fock binding energies $\Delta E_{SCF}(\infty)$ for the chains of Table 4.1. At the Hartree-Fock equilibrium geometry

Compound	BSSE correction	$\Delta E_{\text{SCF}}(\infty)$	
		cc-pVXZ	aug-cc-pVXZ
$(\text{HF})_\infty$	Non	-10.199	-10.194
	CP	-10.194	-10.222
$(\text{HCl})_\infty$	Non	-0.596	-0.586
	CP	-0.584	-0.577

Table 4.1: Basis set extrapolated Hartree-Fock binding energies per monomer $\Delta E_{\text{SCF}}(\infty)$ of $(\text{HF})_\infty$ and $(\text{HCl})_\infty$ chains as obtained by least squares fits to (2.31) of their Hartree-Fock energies for the cc-pVXZ ($X = $ D, ..., 6) and aug-cc-pVXZ ($X = $ D, ..., 5 for $(\text{HF})_\infty$ and $X = $ D, ..., 6 for $(\text{HCl})_\infty$) series of basis sets. All data are given in millihartree.

of $(\text{HF})_\infty$, Bayer and Karpfen give $-10.360\,\text{mE}_h$ for basis set three in Reference [221] and Hirata and Iwata find $-10.855\,\text{mE}_h$ for the 6-311++G(d,p) basis set [225]. Both numbers are in good agreement with my result of $-10.202\,\text{mE}_h$. Yet, Berski and Latajka report $-9.696\,\text{mE}_h$ for $(\text{HF})_\infty$, using the 6-311G(d,p) basis set [224], and $-2.073\,\text{mE}_h$ for $(\text{HCl})_\infty$ employing the DZ(d,p) basis set [228]. Especially the latter number deviates considerably from my result, $-0.586\,\text{mE}_h$. One reason for that is most likely the fact that Berski and Latajka did not remove the BSSE [224, 228].

4.3 Electron correlations

4.3.1 Transferability

In order to ensure that the localized occupied molecular orbitals of oligomers in the geometry of the infinite chains are a good approximation to the Wannier orbitals of $(\text{HF})_\infty$ and $(\text{HCl})_\infty$, the orbitals obtained by the Foster-Boys procedure [139, 140] have to be approximately translationally related (2.32a) within a certain oligomer and must not differ substantially among oligomers of varying length. In other words, the localized occupied molecular orbitals are required to be transferable [Section 3.4]. In order to achieve transferability for moderately sized molecular clusters, one is frequently obliged to account for the omitted monomers in terms of an appropriate substitute. In the case of $(\text{HF})_\infty$ and $(\text{HCl})_\infty$, two options offer themselves. On the one hand, both chains are cut out from a molecular crystal, implying no substitutes as in rare-gas crystals [174, 175]. On the other hand, particularly $(\text{HF})_\infty$, is rather ionic and a surrounding by point charges can be envisaged [176–180]. I explore both possibilities to elucidate what kind of procedure is adequate for hydrogen bonded solids.

In the case of $(\text{HF})_\infty$ and $(\text{HCl})_\infty$, the outer and inner valence orbitals of a HF and a HCl monomer, i.e., eight electrons, are assigned to a one-body orbital set (3.14). To test the transferability prerequisite, I calculated all one-body energy increments and all two-body energy increments between two adjacent monomers, the so-called *connected two-body energy increments*, in isolated oligomers $(\text{HF})_n$ and $(\text{HCl})_n$, $n = 2, 4, 6, 10$. They are compared to the energy increments in the oligomers which I surround by point charges q up to twentieth nearest neighbors. The hydrogen atoms are represented by $q = +1$;
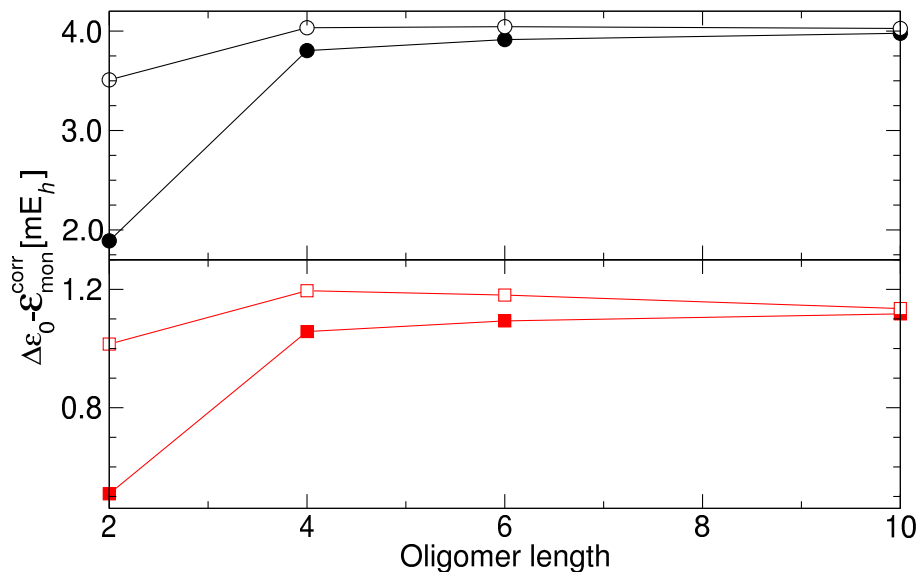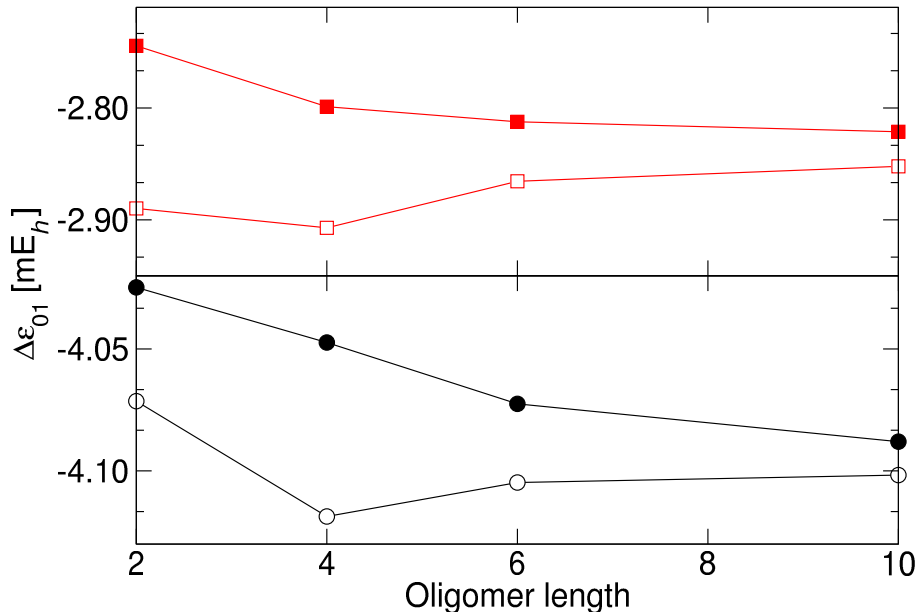
Figure 4.4: (Color) One-body energy increments $\Delta\varepsilon_0$ of $(HF)_\infty$ and $(HCl)_\infty$ chains as determined in oligomers of varying length reduced by the CP-corrected correlation energy $\mathcal{E}_{mon}^{corr}$ of the respective monomer. Circles stand for $(HF)_\infty$ and squares for $(HCl)_\infty$ data obtained with the aug-cc-pVDZ basis set [48–51]. Open symbols refer to oligomers surrounded by point charges whereas closed symbols denote isolated oligomers.

fluorine and chlorine atoms are described by $q = -1$ in the interior whereas the charge of the outermost left and right fluorine and chlorine atoms is set to $q = -\frac{1}{2}$ [176–180].

Comparing the mean of the innermost one-body and the innermost connected two-body energy increments among oligomers of varying length in Figures 4.4 and 4.5, I observe a rapid convergence towards the limit of the infinite chain where the values for the isolated oligomers and the values for the point-charge embedded oligomers also approach each other quickly. The energy increments taken from the isolated oligomers increase (decrease) in Figure 4.4 (Figure 4.5) monotonically while additional point charges cause an unsystematic but somewhat accelerated convergence. Obviously, the choice whether to employ point charges or not has only little impact. The one-body (two-body) energy increments differ by $67\,\mu E_h$ ($14\,\mu E_h$) in $(HF)_\infty$ and by $22\,\mu E_h$ ($31\,\mu E_h$) in $(HCl)_\infty$. In the following only energy increments taken from isolated oligomers are regarded. The observed convergence behavior of the individual curves in Figures 4.4 and 4.5 is explained by a small variation in the localized orbitals, and, predominantly, by the improvement of the electronic structure as it rapidly approaches the electronic structure of the infinite chains upon increasing length of the oligomers. This underlines the transferability of the underlying orbitals.

The error introduced on the binding energy due to the only approximate translational relation (2.32a) of the Wannier orbitals in the finite length oligomers can be estimated by investigating the numerical differences between energy increments which should be identical due to translational symmetry. The connected two-body increments, for exam-

Figure 4.5: (Color) Two-body energy increments $\Delta\varepsilon_{01}$ of $(HF)_\infty$ and $(HCl)_\infty$ chains as determined in oligomers of varying length. Symbols are chosen as in Figure 4.4.

ple, vary at most by $40\,\mu E_h$ in $(HF)_{10}$ and at most by $11\,\mu E_h$ in $(HCl)_{10}$.[2] I conclude that the transferability prerequisite of the energy increments is fulfilled in good accuracy. The agreement between the electronic structure of the chains obtained in the two different ways described, corroborates the applicability of oligomers to represent the electronic structure of infinite $(HF)_\infty$ and $(HCl)_\infty$ chains.

4.3.2 Short-range correlations

Let me discuss the short-range correlation contributions first. The most relevant energy increments of $(HF)_\infty$ and $(HCl)_\infty$ are summarized in Table 4.2. The one-body energy increments incorporate excitations of electrons out of the Wannier orbitals associated with a single monomer to all virtual orbitals in the oligomer and thus include, in addition to the short-range correlations close to the nuclei of the monomer, the energy lowering due to a delocalization of the valence electrons of a monomer over the whole chain. The electronic structure of the HF and HCl monomers is essentially preserved in $(HF)_\infty$ and $(HCl)_\infty$ as can be seen from the CP corrected correlation energy of the HF monomer $(-227.3406\,mE_h)$ and the HCl monomer $(-176.2151\,mE_h)$ which are by 1.8% and 0.6% smaller, respectively, than the corresponding one-body energy increments $\Delta\varepsilon_0$ [Table 4.2]. The one-body energy increments are a bit larger than the correlation energies of the corresponding free monomers which reflects the *Pauli repulsion* that is exerted by the electrons of the neighboring monomers.

The K-body increments, $K \geq 2$, describe the mutual correlations of the valence elec-

---

[2] The two first and the two last monomers at the ends of the oligomers are not regarded as they are appreciably influenced by finite-size effects.

Increment	$(HF)_\infty$	$(HCl)_\infty$
$\Delta\varepsilon_0$	-223.3632	-175.0985
$\Delta\varepsilon_{01}$	-4.0879	-2.8213
$\Delta\varepsilon_{02}$	-0.0861	-0.1347
$\Delta\varepsilon_{012}$	-0.0163	0.0014
$\Delta\varepsilon_{03}$	-0.0063	-0.0092
$\Delta\varepsilon_{013}$	-0.0015	-0.0016
$\Delta\varepsilon_{0123}$	0.0003	0.0006

Table 4.2: Exemplary energy increments of $(HF)_\infty$ and $(HCl)_\infty$ chains taken from $(HF)_{10}$ and $(HCl)_{10}$ oligomers. The energy increments are extracted from the innermost monomers in the oligomers employing the aug-cc-pVDZ basis set [48–51]. All data are given in millihartree.

trons of several monomers. They give rise to a pronounced non-linear increase of the binding energy of small clusters and short oligomers which is termed *bond cooperativity* (References [61, 236] and references therein) and is a manifestation of electron correlations. The connected two-body energy increment of $(HCl)_\infty$ ε_{01}^{HCl} is 31% smaller than the corresponding energy increment ε_{01}^{HF} in $(HF)_\infty$. The connected three-body energy increment ε_{012}^{HCl} even is repulsive, i.e., greater than zero, but ε_{012}^{HF} is attractive. The reverse trend is observed for the remaining energy increments. The energy increment ε_{02}^{HCl} is 57% larger than ε_{02}^{HF}. The connected four-body increment ε_{0123}^{HCl} even is 100% larger than ε_{0123}^{HF} and both are repulsive. These two trends of the energy increments can be explained by two effects. Firstly, short-range correlations are effective for nearest neighbors which is apparently stronger in $(HF)_\infty$ than in $(HCl)_\infty$ due to the tighter packing of the monomers in $(HF)_\infty$ and the greater compactness of the HF monomer itself. Secondly, chlorine atoms have a higher *polarizability* than fluorine atoms. This causes the van der Waals interaction to be stronger in $(HCl)_\infty$ than in $(HF)_\infty$ leading the more distant energy increments to be larger in $(HCl)_\infty$ compared to $(HF)_\infty$ despite of the bigger intermonomer distances in $(HCl)_\infty$.

However, one should not interpret the energy increments of the incremental scheme too extensively and especially one should not associate too much physics with their individual values. The energy increments depend on the specific unitary transformation used to localize the occupied orbitals (here determined by the Foster-Boys method [139, 140]). Therefore, their values depend on this transformation. Only the binding energy, which is the sum of these energy increments, is a physical observable and thus invariant under unitary transformations of the orbitals. For an analysis of the individual energy increments to be meaningful and of semi-quantitative quality, the energy increments are required to be fairly independent of the underlying localization procedure. This is well-fulfilled for hydrogen-bonded systems.

4.3.3 Long-range correlations

At separations of two isolated monomers where the spatial orbital overlap between the orbitals in the one-body orbital sets of the monomers becomes negligible, only van der
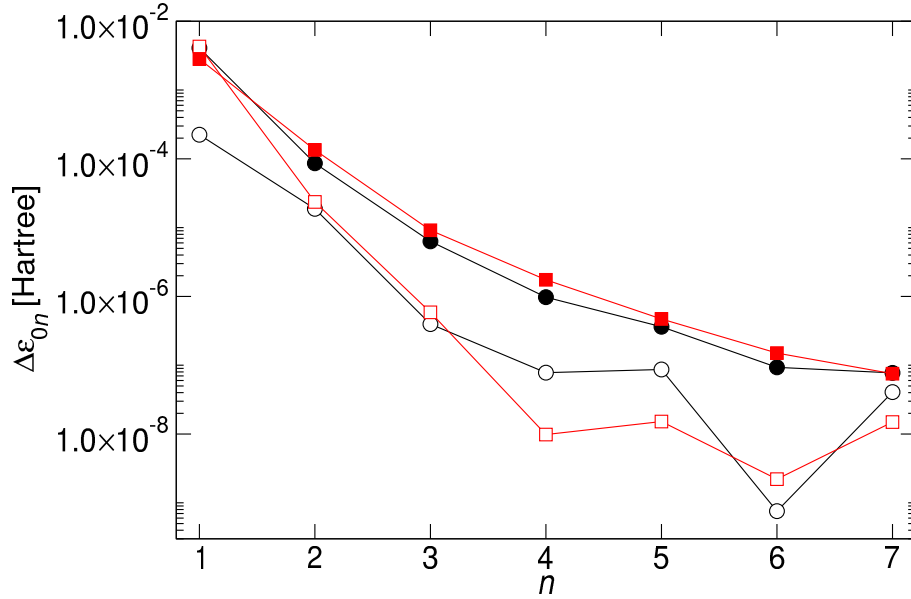
Figure 4.6: (Color) Absolute values of two-body energy increments $|\Delta\varepsilon_{0\,n}|$ (closed symbols) and van-der-Waals-reduced two-body energy increments $|\Delta\varepsilon_{0\,n}^{\mathrm{vdW}}|$ (open symbols) using (4.3) and the constants in Table 4.3 for both $(\mathrm{HF})_\infty$ (circles) and $(\mathrm{HCl})_\infty$ (squares) chains.

Waals dispersion interaction remains. This is also the case for the interaction between two separated monomers in the infinite chains which is correspondingly described by the two-body energy increments [177–180]. The two-body energy increments of $(\mathrm{HF})_\infty$ and $(\mathrm{HCl})_\infty$ up to seventh nearest neighbors are displayed in Figure 4.6. The curves decay rapidly with the distance between the two contributing monomers.

The monomers in Figure 4.1 which are labelled by odd cardinal numbers are tilted with respect to monomer 0. Likewise, monomers with even cardinal numbers are arranged parally to the origin monomer. I will refer to the two types of two-body energy increments that result from a parallel or tilted setting of monomers as odd or even energy increments, respectively. The long-range interaction between monomers is approximated by the leading term of two-body van der Waals dispersion interaction [237]

$$
\varepsilon_{0\,n}^{\mathrm{vdW}} = \begin{cases} -\dfrac{C_6^{\mathrm{odd}}}{\left(\frac{n}{2}\,a\right)^6} & ;\ n\ \text{odd} \\[2ex] -\dfrac{C_6^{\mathrm{even}}}{\left(\frac{n}{2}\,a\right)^6} & ;\ n\ \text{even} \end{cases} , \tag{4.3}
$$

where individual van der Waals constants C_6^{odd} and C_6^{even} are affixed for odd and even energy increments with cardinal number n, respectively. Here a represents the lattice constant of the $(\mathrm{HF})_\infty$ or the $(\mathrm{HCl})_\infty$ chain. The van der Waals constants are obtained by a weighted fit with the Levenberg-Marquardt algorithm [238] of the data in Figure 4.6 for either the odd or the even energy increments. The weights are chosen such that the fit reproduces the energy increments with large n best as for them spatial orbital overlaps between the orbitals from the two one-body orbital sets (3.14) are negligible. The van der Waals constants for the fits of the two sets of translationally equivalent monomers are given in Table 4.3.

Compound	C_6^{odd}	C_6^{even}
$(\mathrm{HF})_\infty$	-23.354	-20.225
$(\mathrm{HCl})_\infty$	-120.81	-120.08

Table 4.3: Van der Waals constants C_6^{odd} and C_6^{even} of two-body dispersion interaction for $(\mathrm{HF})_\infty$ and $(\mathrm{HCl})_\infty$ chains. They are obtained by fitting the two-body energy increments of Figure 4.6 with either odd or even cardinal numbers n, respectively, for the aug-cc-pVDZ basis set [48–51] to (4.3). All data are given in Hartree Bohr[6].

Now the van der Waals contribution (4.3) can be subtracted from the two-body energy increments yielding *van-der-Waals-reduced energy increments*

$$\Delta\varepsilon_{0\,n}^{\mathrm{vdW}} = \Delta\varepsilon_{0\,n} - \varepsilon_{0\,n}^{\mathrm{vdW}} \ . \tag{4.4}$$

Their absolute values $|\Delta\varepsilon_{0\,n}^{\mathrm{vdW}}|$ are shown aside of the absolute values of the two-body energy increments $|\Delta\varepsilon_{0\,n}|$ in Figure 4.6.

Two regions can be identified in Figure 4.6. Firstly, nearest to second-next-nearest neighbors, the *local correlation zone*, where, due to spatial orbital overlaps, short-range electron correlations are effective. There, the decay of two-body energy increments with the distance between the two monomers is slower than what would result from a pure van der Waals interaction (4.3). I observe that the contribution to $|\Delta\varepsilon_{0\,1}^{\mathrm{vdW}}|$ of $(\mathrm{HCl})_\infty$ is appreciably larger than in $(\mathrm{HF})_\infty$ as the curves for $|\Delta\varepsilon_{0\,1}|$ and $|\Delta\varepsilon_{0\,1}^{\mathrm{vdW}}|$ are much closer for $(\mathrm{HCl})_\infty$ than for $(\mathrm{HF})_\infty$. Secondly, the *van der Waals zone* reaching from the third up to the seventh nearest neighbor. Here a typical r^{-6}-decay is observed, leading to van-der-Waals-reduced energy increments which are numerically zero. A slight deviation of the two-body energy increments from a perfect r^{-6} behavior is perceived beyond fifth nearest neighbors which can most likely be attributed to inaccuracies caused by the oligomer approximation. The Wannier orbitals in $(\mathrm{HCl})_\infty$ are more precisely related by lattice translations (2.32a) compared with $(\mathrm{HF})_\infty$ [Section 4.3.1] which leads to a lower absolute value of the fourth to seventh van-der-Waals-reduced energy increment. The low magnitude of $\Delta\varepsilon_{0\,6}^{\mathrm{vdW}}$ for both chains is an artefact of the fitting process. Figure 4.6 also reveals that the two-body energy increments are of satisfactory accuracy even beyond the estimates given in Section 4.3.1 of $40\,\mu\mathrm{E_h}$ for $(\mathrm{HF})_{10}$ and $11\,\mu\mathrm{E_h}$ for $(\mathrm{HCl})_{10}$ due to a considerable error cancellation.

Given the van der Waals constants in Table 4.3, I can employ (4.3) to sum up the van der Waals contribution of the two-body energy increments to the binding energy to infinite distances between the two monomers $\sum_{n=3}^{\infty}\varepsilon_{0n}^{\mathrm{vdW}}$ which yields $-8\,\mu\mathrm{E_h}$ for $(\mathrm{HF})_\infty$ and $-12\,\mu\mathrm{E_h}$ for $(\mathrm{HCl})_\infty$. The better polarizability of chlorine atoms compared to fluorine atoms leads to larger long-range correlations in $(\mathrm{HCl})_\infty$ than in $(\mathrm{HF})_\infty$ [Section 4.3.2]. The van der Waals contribution of two distant monomers is comparable in magnitude to the connected three-body energy increment $\Delta\varepsilon_{0\,1\,2}$ in Table 4.2. The contribution of two-body energy increments between monomers being separated beyond third-nearest neighbors is in both cases $\approx 30\%$ of $\Delta\varepsilon_{0\,3}$.

The decomposition of the energy increments into a short-range and a long-range van der Waals contribution allows to focus on the short-range part (4.4), if a good description

Figure 4.7: (Color) Basis set convergence of the correlation contribution to the binding energy per monomer ΔE_{corr} of a $(\text{HF})_\infty$ chain. Symbols are chosen as in Figure 4.2, with diamonds showing data for the d-aug-cc-pVXZ basis sets.

of the long-range part, i.e., the dispersive interaction, is amenable via (4.3). This reduces considerably the number of energy increments to be calculated by the correlation method and hence allows to reduce the computational demand. As spatial orbital overlaps are negligible between monomers being further apart than third-nearest neighbors, the correlation contribution to their interaction energy does not require supporting monomers beyond this separation. Leaving out all unnecessary monomers in the infinite chain,[3] one arrives at the setting of a molecular *dissociation process* which can be described with moderate computational effort. This observation opens a perspective for accelerated calculations of correlation energies of crystals with the incremental scheme.

4.3.4 Basis set convergence

To determine the correlation energy per monomer of the infinite chains $\mathcal{E}_{\text{corr}}$, I inspect the energy increments in Table 4.2 which converge rapidly both with the distance among the monomers involved and with the order of the many-body expansion, i.e., with the number of monomers taken into account for a specific energy increment. To obtain an accuracy of $\approx 50\,\mu E_{\text{h}}$ for $(\text{HF})_\infty$ and an accuracy of $\approx 11\,\mu E_{\text{h}}$ for $(\text{HCl})_\infty$, respectively, in $\mathcal{E}_{\text{corr}}$ from Table 4.2, I see that it is enough to include the following energy increments

$$\mathcal{E}_{\text{corr}} \approx \Delta\varepsilon_0 + \Delta\varepsilon_{0\,1} + \Delta\varepsilon_{0\,2} \,. \tag{4.5}$$

---

[3]Doll *et al.* [177] utilize point charges to represent left-out ions in their determination of the van der Waals constants of ionic crystals.

Figure 4.8: (Color) Basis set convergence of the correlation contribution to the binding energy per monomer ΔE_{corr} of a $(HCl)_{\infty}$ chain. Symbols are chosen as in Figure 4.2.

Hence, it is sufficient to correlate the electrons in the Wannier orbitals of only two monomers at a time for $(HF)_{\infty}$ and $(HCl)_{\infty}$ where more distant two-body energy increments contribute only $-8\,\mu E_{\text{h}}$ for $(HF)_{\infty}$ and $-12\,\mu E_{\text{h}}$ for $(HCl)_{\infty}$ as shown in Section 4.3.3. In three-dimensional crystals, three-body terms become more important according to the thorough analyses in References [162, 175, 239] and the much larger number of three-body energy increments compared to the number of two-body energy increments in this case. Rościszewski *et al.* [175] stress in their *ab initio* study of rare-gas solids that it is required to sum up van der Waals contributions of two- and three-body terms to large distances.

Having determined $\mathcal{E}_{\text{chain}}^{\text{corr}}$, I can give the contribution of electron correlations to the binding energy per monomer in $(HF)_{\infty}$ and $(HCl)_{\infty}$

$$\Delta E_{\text{corr}} = \frac{1}{2}\,\mathcal{E}_{\text{chain}}^{\text{corr}} - \mathcal{E}_{\text{monomer}}^{\text{corr}} \tag{4.6}$$

where the correlation energy of a chain per unit cell is $\mathcal{E}_{\text{chain}}^{\text{corr}}$ and the correlation energy for the monomer is $\mathcal{E}_{\text{monomer}}^{\text{corr}}$.

I obtain ΔE_{corr} of $(HF)_{\infty}$ and $(HCl)_{\infty}$ for series of correlation consistent basis sets, shown in Figures 4.7 and 4.8. For each series, there is an upper curve for the CP corrected binding energies and an lower curve giving the bare binding energies without CP correction of the monomer energies. One notes that the CP corrected energies drop monotonically with improving basis set quality but the corresponding bare energies behave unsystematically. The binding energy curves of $(HF)_{\infty}$ in Figure 4.7 for the aug-cc-pVXZ and d-aug-cc-pVXZ basis sets are essentially parallel, if CP correction is applied, but the associated curves for the bare binding energies differ considerably, an effect which is exclusively caused by the behavior of the monomer energies employed for the bare and

X–Y		$\Delta E_{\text{corr}}(\infty)$ cc-pVXZ	$\Delta E_{\text{corr}}(\infty)$ aug-cc-pVXZ
X^{-3}	D–T	-1.037	-1.337
	D–Q	-1.433	-1.547
	T–Q	-1.637	-1.655
	Q–5	-1.606	
Park *et al.*	D–T	-1.215	-1.475
	D–Q	-1.496	-1.593
	T–Q	-1.620	-1.646
	Q–5	-1.585	

Table 4.4: Basis set extrapolation of the CP corrected correlation contribution to the binding energy per monomer ΔE_{corr} of a $(HF)_\infty$ chain by means of (3.21) and (3.25). All data are given in millihartree.

CP corrected curves. The small difference between the two CP corrected curves indicates the small improvement of the description of the ground state of a HF monomer and $(HF)_\infty$ by the second set of diffuse functions in d-aug-cc-pVXZ basis sets.

The error of the correlation contribution to the binding energy (4.6), introduced by the finite basis sets, can be estimated as the differences of the bare and the CP corrected values corresponding to the same basis set series in Figures 4.7 and 4.8. Using the cc-pV5Z binding energies, the deviation of the bare binding energy from the CP corrected binding energy is $\approx 20\%$ for $(HF)_\infty$ and $\approx 5\%$ for $(HCl)_\infty$, the error being considerably larger for $(HF)_\infty$ compared to $(HCl)_\infty$. The basis set error is far too large for a definitive value of the correlation contribution to the binding energy of the infinite chains.

To get the basis set limit correlation contribution to the binding energies (4.6), firstly, I apply a two-point fit based on (3.21), involving the correlation energies for the infinite chains and the CP corrected ones for the respective monomers [56]. Secondly, Equation (3.25) is employed, where the correlation energy of the monomer is required in a very good approximation. As there are no suitable R12 data for HF and HCl, I determine the correlation energy of the monomers by X^{-3} extrapolation (3.23). For HF, I extrapolate the correlation energies of calculations with a cc-pV5Z and a cc-pV6Z basis set, where basis set extension [235], [Section 4.1], is accounted for by surrounding the HF monomer by the basis sets of four additional monomers which yields $E_{\text{corr, HF}} = -314.530\,\text{mE}_h$. For the HCl monomer, the basis sets of only two neighboring HCl monomers is utilized in the extrapolation of aug-cc-pV5Z and aug-cc-pV6Z correlation energies, yielding $E_{\text{corr, HCl}} = -254.373\,\text{mE}_h$.

Two-point extrapolations for $(HF)_\infty$ and $(HCl)_\infty$ are displayed in Tables 4.4 and 4.5, and are found to converge rapidly towards a limit with increasing quality of the involved basis sets. The most reliable extrapolations to the limit are obtained, if basis sets of largest X and $X + 1$ are employed. For several molecules, this fit was shown to yield the best approximation to the basis set limit, with respect to accurate R12 data [46], for the correlation contribution to the binding energy [56]. The extrapolations obtained with cc-pVXZ and aug-cc-pVXZ series are found to approach each other as they should. Inspecting Figures 4.7 and 4.8, I observe that the extrapolations involving the best basis

X–Y		$\Delta E_{\text{corr}}(\infty)$ cc-pVXZ	$\Delta E_{\text{corr}}(\infty)$ aug-cc-pVXZ
X^{-3}	D–T	-2.300	-2.681
	D–Q	-2.604	-2.742
	T–Q	-2.760	-2.773
	Q–5	-2.747	
Park *et al.*	D–T	-2.409	-2.742
	D–Q	-2.642	-2.764
	T–Q	-2.750	-2.774
	Q–5	-2.762	

Table 4.5: Basis set extrapolation of the CP corrected correlation contribution to the binding energy per monomer ΔE_{corr} of a $(HCl)_\infty$ chain by means of (3.21) and (3.25). All data are given in millihartree.

sets, i.e., with largest X and $X + 1$, lie well in the range where they are expected to be, leading to the conclusion that the basis set limit is nearly reached. The very good agreement of the best extrapolated values [Q–5 for cc-pVXZ and T–Q for aug-cc-pVXZ] indicates reliability for the correlation contribution to the binding energies of both chains. Especially X^{-3} extrapolations involving double-ζ quality basis sets in Tables 4.4 and 4.5 are found to be less accurate than corresponding extrapolations by Park *et al.* with respect to the values of Q–5 extrapolation [cc-pVXZ] or the ones of T–Q extrapolation [aug-cc-pVXZ], as the latter extrapolation method is independent of the convergence properties of the series [54,55] underlying X^{-3} extrapolation (3.23). The mean of corresponding bare and CP corrected energies [57] does only provide a decent approximation to the basis set limit binding energies for $(HF)_\infty$ [Figure 4.7], the results for $(HCl)_\infty$ are contradictory [Figure 4.8].

The accuracy of the resulting correlation contribution to the binding energies in Table 4.6 is estimated by the deviation of the extrapolated binding energies for the aug-cc-pVXZ series from the ones for the cc-pVXZ series, where the largest basis sets of the respective series [T–Q for aug-cc-pVXZ and Q–5 for cc-pVXZ] are utilized. The deviation is $\approx 3\%$ or $\approx 4\%$ for $(HF)_\infty$ and $\approx 1\%$ or $\approx 0.4\%$ for $(HCl)_\infty$ depending on the extrapolation method employed, i.e., X^{-3} (3.23) or the method of Park *et al.* (3.25).

I would like to point out further, that Equations (3.23) and (3.25) facilitate to extrapolate the individual energy increments occurring in the decomposition of the correlation energy in terms of the incremental scheme, separately. Thus, energy increments with close nearby one-body orbital sets can be treated with larger basis sets than energy increments with a large distance among the one-body orbital sets. The latter energy increments can be described with basis sets of moderate quality as mentioned in Section 4.1. This is advantageous for treating, e.g., hydrogen bonds in larger molecules and facilitates a more accurate treatment of different atoms or fragments in crystals.

	$(HF)_\infty$	$(HCl)_\infty$
$\Delta E_{SCF}(\infty)$	-10.202	-0.586
$\Delta E_{corr}(\infty)$	-1.623	-2.764
$\Delta E(\infty)$	-11.826	-3.350

Table 4.6: Basis set extrapolated binding energies per monomer $\Delta E(\infty)$ of $(HF)_\infty$ and $(HCl)_\infty$ chains and their decomposition into basis set extrapolated Hartree-Fock $\Delta E_{SCF}(\infty)$ and electron correlation $\Delta E_{corr}(\infty)$ contributions. $\Delta E_{SCF}(\infty)$ is the mean of the four extrapolated energies for each infinite chain, respectively, in Table 4.1 and $\Delta E_{corr}(\infty)$ is the mean of the two Q–5 (cc-pVXZ) and the two T–Q (aug-cc-pVXZ) extrapolated energies for each infinite chain, respectively, in Tables 4.4 and 4.5. All data are given in millihartree.

4.4 Binding energy

Having understood the impact of electron correlations in the infinite $(HF)_\infty$ and $(HCl)_\infty$ chains, I am in the position to examine the total binding energy per monomer ΔE of the chains which is given by

$$\Delta E = \Delta E_{SCF} + \Delta E_{corr} \tag{4.7}$$

It consists of the Hartree-Fock contribution ΔE_{SCF} and a contribution due to electron correlations ΔE_{corr} which have already been discussed in (4.2) and (4.6), respectively.

I report ΔE_{corr} in Table 4.6 as obtained by basis set extrapolation [Sections 4.2 and 4.3.4]. Using density functional theory, Hirata and Iwata find, at optimized geometries, for the total binding energies ΔE of $(HF)_\infty$ $-13.521\,\mathrm{mE}_h$ (BLYP) and $-13.864\,\mathrm{mE}_h$ (B3LYP) [utilizing the 6-311++G(d,p) basis set] [225] which is larger by 14% and 17% than my results for the experimental geometry.

Part II

Excited states

5 Band structures

The accurate *ab initio* description of the ground state of crystalline solids has been discussed in the first part of this dissertation. This second part is devoted to treat excited states of crystals where I focus on *electron removal* and *electron attachment states* of crystals. In course of this, especially, the difference of the energies associated with such states in relation to the ground-state energy are regarded and the resulting relative energies are translational symmetry classified with respect to crystal momentum.

Excited states of solids can be calculated by means of a configuration interaction expansion similarly to the one mentioned in the introduction of Chapter 3 for a correlated description of ground state wave functions. However, such an expansion is extremely sensitive to the truncation employed, e.g., References [131, 132], because electron correlations have to be treated in a consistent manner both in the ground state and the excited states. In contrast, the one-particle Green's function enables the direct calculation of energy differences without a need for inaccurate subtractions between particle removal (addition) states and the ground state, harnessing quantum field theoretical techniques [112–115].

I assume a *quasiparticle* point of view for the discussion of the states in the outer valence region and the lowest virtual states of crystals. This means that the symmetry classified energy differences which are obtained from an accurate treatment of electron correlations by means of Green's functions in this and the ensuing Chapter 6 are predominantly characterized by the independent particle approximation. They still arrange in a band structure, which is referred to as *quasiparticle band structure*, despite of their inherent many-particle description [1, 2, 27, 28] and a strict correspondence to Hartree-Fock bands holds [1]. For core-hole states, inner valence states and high lying conduction bands of solids, a strong coupling to excited configurations leads to a break down of the quasiparticle picture. Then band structures are no longer a meaningful concept and only the translational symmetry classification of the excited states with respect to the crystal momentum remains [73–76].

5.1 Green's functions

The exact ground state of the N particle system $|\Psi_{\mathrm{H},0}^N\rangle$ and the creation and annihilation operators $\hat{c}_{\mathrm{H},\vec{k}p}(t)$ and $\hat{c}_{\mathrm{H},\vec{k}'q}^\dagger(t')$ are be expressed in the *Heisenberg picture* [112–115] instead of the more familiar *Schrödinger picture*, which is utilized in the crystal momentum representation of the Hamiltonian (3.4). State vectors in Heisenberg picture $|\Psi_{\mathrm{H}}^N\rangle$ are related to the state vectors in the Schrödinger picture $|\Psi^N\rangle$ by the transformation $|\Psi_{\mathrm{H}}^N\rangle = \mathrm{e}^{\mathrm{i}\hat{H}t}|\Psi^N\rangle$ whereas corresponding operators transform like $\hat{O}_{\mathrm{H}}(t) = \mathrm{e}^{\mathrm{i}\hat{H}t}\,\hat{O}\,\mathrm{e}^{-\mathrm{i}\hat{H}t}$.

The *one-particle Green's function* (or *particle propagator*) in terms of Bloch orbitals [6,

87, 112–115] reads

$$G_{\vec{k}\,p\,\vec{k}'\,q}(t,t') = (-\mathrm{i})\,\langle \Psi_{\mathrm{H},0}^N |\, \hat{T}[\hat{c}_{\mathrm{H},\vec{k}\,p}(t)\,\hat{c}_{\mathrm{H},\vec{k}'\,q}^\dagger(t')]\,| \Psi_{\mathrm{H},0}^N \rangle\,. \tag{5.1}$$

Wick's *time-ordering operator* $\hat{T}$ reorders a product of time-dependent operators, e.g., Heisenberg-picture operators, chronologically such that the operator at largest time comes first. Applying $\hat{T}$ to $\hat{c}_{\mathrm{H},\vec{k}\,p}(t)\,\hat{c}_{\mathrm{H},\vec{k}'\,q}^\dagger(t')$ yields

$$\hat{T}[\hat{c}_{\mathrm{H},\vec{k}\,p}(t)\,\hat{c}_{\mathrm{H},\vec{k}'\,q}^\dagger(t')] = \hat{c}_{\mathrm{H},\vec{k}\,p}(t)\,\hat{c}_{\mathrm{H},\vec{k}'\,q}^\dagger(t')\,\Theta(t-t') - \hat{c}_{\mathrm{H},\vec{k}'\,q}^\dagger(t')\,\hat{c}_{\mathrm{H},\vec{k}\,p}(t)\,\Theta(t'-t) \tag{5.2}$$

with the *Heavyside step function*

$$\Theta(t-t') = \begin{cases} 0 & ;\ t < t' \\ 1 & ;\ t > t'\,. \end{cases} \tag{5.3}$$

Both $\Theta(t-t')$ and the time-ordered product (5.2) are undefined for equal times. Special care is required, if composite time-dependent operators, e.g., the Heisenberg-picture operator $\hat{H}_{\mathrm{H,res}}^{\mathrm{BF}} = \mathrm{e}^{\mathrm{i}\hat{H}t}\,\hat{H}_{\mathrm{res}}^{\mathrm{BF}}\,\mathrm{e}^{-\mathrm{i}\hat{H}t}$ of (3.4), are replaced by their definition in terms of Heisenberg-picture creation and annihilation operators in time-ordered products. The proper ordering of the constituting creators and annihilators at equal times has to be maintained by infinitesimally changing time variables appropriately. The decomposition of the time-ordered product (5.2) into two parts transfers immediately to the Green's function (5.1)

$$G_{\vec{k}\,p\,\vec{k}'\,q}(t,t') = G_{\vec{k}\,p\,\vec{k}'\,q}^+(t,t') + G_{\vec{k}\,p\,\vec{k}'\,q}^-(t,t')\,. \tag{5.4}$$

The summands are known as *retarded* and *advanced one-particle Green's functions*, $G_{\vec{k}\,p\,\vec{k}'\,q}^+(t,t')$ and $G_{\vec{k}\,p\,\vec{k}'\,q}^-(t,t')$, respectively.

Due to translational symmetry of the Hamiltonian (2.4), the one-particle Green's function only depends on one crystal momentum [6], i.e., $G_{\vec{k}\,p\,\vec{k}'\,q}(t,t') = \delta_{\vec{k},\vec{k}'}\,G_{pq}(\vec{k},t,t')$. Similarly, as the Hamiltonian (2.4) does not depend on time and thus is invariant under temporal translations, the Green's function only depends on the difference between t and t'. Fourier transforming $G_{pq}(\vec{k},t,t')$ with respect to $t - t'$ yields the one-particle Green's function in energy space

$$G_{pq}(\vec{k},\omega) = \int_{-\infty}^{\infty} G_{pq}(\vec{k},t,t')\,\mathrm{e}^{\mathrm{i}\omega(t-t')}\,\mathrm{d}(t-t')\,, \tag{5.5}$$

which can be recast in terms of the *spectral* or *Lehmann representation* [112–115] as

$$\begin{aligned} G_{pq}(\vec{k},\omega) &= \sum_{n\in\{N+1\}} \frac{y_p^{(n)}(\vec{k})\,y_q^{(n)*}(\vec{k})}{\omega + A_n(\vec{k}) + \mathrm{i}\eta} + \sum_{n\in\{N-1\}} \frac{x_p^{(n)}(\vec{k})\,x_q^{(n)*}(\vec{k})}{\omega + I_n(\vec{k}) - \mathrm{i}\eta} \tag{5.6a}\\ &= G_{pq}^+(\vec{k},\omega) + G_{pq}^-(\vec{k},\omega)\,. \tag{5.6b} \end{aligned}$$

The negative of the pole positions in (5.6a) is given by either the *electron affinities (EA)* $A_n(\vec{k}) = E_0^N - E_n^{N+1}(\vec{k})$ or the *ionization potentials (IP)* $I_n(\vec{k}) = E_n^{N-1}(-\vec{k}) - E_0^N$. Here

$E_n^{N\pm 1}(\pm \vec{k})$ is the energy of the n-th excited state of the $N \pm 1$ particle system.[1] The imaginary parts $\pm i\eta$ in (5.6a) are necessary to ensure the convergence of the integral in (5.5). The *pole strengths* in (5.6a) are given in terms of the *transition amplitudes*

$$x_p^{(n)}(\vec{k}) = \langle \Psi_{\mathrm{H},n}^{N-1}(-\vec{k}) | \, \hat{c}_{\vec{k}p} \, | \Psi_{\mathrm{H},0}^N \rangle \quad \text{and} \quad y_p^{(n)}(\vec{k}) = \langle \Psi_{\mathrm{H},0}^N | \, \hat{c}_{\vec{k}p} \, | \Psi_{\mathrm{H},n}^{N+1}(\vec{k}) \rangle \, , \qquad (5.7)$$

where $|\Psi_{\mathrm{H},n}^{N\pm 1}(\pm \vec{k})\rangle$ denote excited states of the $N \pm 1$ particle system with crystal momenta $\pm \vec{k}$. The pole strengths can be interpreted in terms of the spectral intensities observed in photoelectron spectroscopy experiments, similarly to the molecular case discussed in Reference [83]. Moreover, $G_{pq}^{\pm}(\vec{k}, \omega)$ designate the Fourier transforms of the retarded (advanced) Green's functions (5.4).

To obtain electron affinities and ionization potentials from the energies of electron attachment and electron removal states of three-dimensional crystals, one has to specify the energy of the added (removed) electron at the Fermi level of the neutral crystal [240, 241]. This is usually done by introducing chemical potentials $\mu^{\pm}$ which are added to the pole positions of the one-particle Green's function, i.e., $A_n(\vec{k}) + \mu^+$ and $I_n(\vec{k}) + \mu^-$.

The (fundamental) *band gap* is the smallest difference between the energies for removing an electron from and attaching an electron to an N particle system:

$$E_{\mathrm{gap}} = I - A + \mu^+ - \mu^- = (E^{N-1} - E_0^N) - (E_0^N - E^{N+1}) \, . \qquad (5.8)$$

Here A stands for the largest electron affinity and I designates the smallest ionization potential. Correspondingly, $E^{N\pm 1}$ denote the energies of the electron attachment (removal) state with the lowest (highest) energy and E_0^N represents the ground-state energy.

5.2 Feynman-Dyson perturbation series

The one-particle Green's function (5.1) cannot be determined exactly in most cases but has to be approximated. This can be achieved by relating the eigenstates of the non-interacting system, which are known and are here the solution of the Hartree-Fock equations [Section 2.2], to the eigenstates of the interacting system. In the first place, one introduces an artificial time dependence into the time-independent Hamiltonian (3.4) such that the many-particle system becomes non-interacting at $t \to -\infty$. Evolving from the ultimate past, the interaction is gradually switched on and acquires its full strength at the present $t = 0$. Afterwards, it is gradually switched off until the non-interacting many-particle system is rereached in the ultimate future $t \to \infty$.

The mathematical formulation of the process of *adiabatic switching on and off* of the interaction starts with the following modification of the Hamiltonian (3.4) in the Schrödinger picture [112–115]

$$\hat{H}(t) = \hat{H}_0 + \mathrm{e}^{-\varepsilon |t|} \hat{H}_1 \, , \qquad (5.9)$$

where $\varepsilon > 0$ is a constant characterizing the speed of this process. In the end, the thus determined eigenstates of the interacting many-particle system must be independent of

---

[1]Following Kramers' theorem, time reversal symmetry implies $E_n^{N\pm 1}(\vec{k}) = E_n^{N\pm 1}(-\vec{k})$ [6].

this parameter to be meaningful. To proceed one changes from the Heisenberg picture into the *interaction picture*. The state vectors in the latter picture $|\Psi^N\rangle_{\mathrm{I}}$ are related to the state vectors in the Schrödinger picture $|\Psi^N\rangle$ by $|\Psi^N_{\mathrm{I}}\rangle \equiv \mathrm{e}^{\mathrm{i}\hat{H}_0 t}|\Psi^N\rangle$ and operators transform like $\hat{O}_{\mathrm{I}}(t) \equiv \mathrm{e}^{\mathrm{i}\hat{H}_0 t}\hat{O}\,\mathrm{e}^{-\mathrm{i}\hat{H}_0 t}$. The unitary *time-evolution operator* $\hat{U}_{\mathrm{I},\varepsilon}(t,t')$ takes a wave function in the interaction picture from time t' to time t. With the Hartree-Fock ground state $|\Phi^N_{\mathrm{I},0}\rangle \equiv |\Phi^N_0\rangle$ representing the non-interacting system in the ultimate past or future, it adiabatically transforms eigenstates of the non-interacting many-particle system into eigenstates of the interacting many-particle system upon going from $t' = \pm\infty$ to $t = 0$, i.e.,

$$|\Psi^N_{\mathrm{H},0}(0)\rangle = |\Psi^N_{\mathrm{I},0}(0)\rangle = \hat{U}_{\mathrm{I},\varepsilon}(0,-\infty)|\Phi^N_0\rangle \quad \text{and} \quad |\Phi^N_0\rangle = \hat{U}_{\mathrm{I},\varepsilon}(\infty,0)|\Psi^N_{\mathrm{I},0}(0)\rangle \ . \quad (5.10)$$

Until now, the problem has been reformulated without introducing any approximations. The time-evolution operator can be expanded into a perturbation series [112–115]

$$\hat{U}_{\mathrm{I},\varepsilon}(t,t') = \sum_{n=0}^{\infty} \frac{(-\mathrm{i})^n}{n!} \int_t^{t'} \cdots \int_t^{t'} \mathrm{e}^{-\varepsilon(|t_1|+\ldots+|t_n|)}\, \hat{T}[\hat{H}_{\mathrm{I},1}(t_1)\cdots\hat{H}_{\mathrm{I},1}(t_n)]\,\mathrm{d}t_1\cdots\mathrm{d}t_n \quad (5.11)$$

with closed-form expressions for any order n in the perturbation $\hat{H}_{\mathrm{I},1}(t)$.

Relating the eigenstates of the non-interacting many-particle system to those of the interacting system via adiabatic switching on and off of the interaction (5.10), Gell-Mann and Low [112–115, 242] found that the limit $\varepsilon \to 0$ only is meaningful for the quantity

$$\lim_{\varepsilon\to 0^+} \frac{\hat{U}_{\mathrm{I},\varepsilon}(0,-\infty)|\Phi^N_0\rangle}{\langle\Phi^N_0|\hat{U}_{\mathrm{I},\varepsilon}(0,-\infty)|\Phi^N_0\rangle} \ , \quad (5.12)$$

if it exists to all orders in perturbation theory, i.e., truncations of the series (5.11) after arbitrary orders; then expression (5.12) represents an eigenstate of $\hat{H}$. However, this eigenstate needs not necessarily to be the ground state of the interacting system. The numerator and denominator of (5.12) do *not* exist separately in the limit $\varepsilon \to 0^+$.

A basic theorem [112–115], e.g., Reference [113], pages 83–85, relates the matrix elements of products of Heisenberg-picture operators to the corresponding matrix elements of products of operators in the interaction picture in terms of a closed-form series expansion via formulas (5.11) and (5.12). Application to the one-particle Green's function (5.1) yields

$$G_{pq}(t,t') = -\mathrm{i}\sum_{n=0}^{\infty}\frac{(-\mathrm{i})^n}{n!}\int_{-\infty}^{\infty}\cdots\int_{-\infty}^{\infty}\frac{\langle\Phi^N_0|\hat{T}[\hat{H}_{\mathrm{I},1}(t_1)\cdots\hat{H}_{\mathrm{I},1}(t_n)]\hat{c}_{\mathrm{I},p}(t)\hat{c}^\dagger_{\mathrm{I},q}(t)|\Phi^N_0\rangle}{\langle\Phi^N_0|\hat{U}_\varepsilon(\infty,-\infty)|\Phi^N_0\rangle}\ \mathrm{d}t_1\cdots\mathrm{d}t_n \ . \quad (5.13)$$

Replacing the interacting ground state $|\Psi^N_{\mathrm{H},0}\rangle$ in (5.1) by the Hartree-Fock ground state $|\Phi^N_0\rangle$ corresponds to the zeroth order approximation of the one-particle Green's function by (5.13)

$$\begin{aligned} G^0_{pq}(\vec{k},\omega) &= (-\mathrm{i})\,\langle\Phi^N_0|\hat{T}[\hat{c}_{\mathrm{H},\vec{k}\,p}(t)\,\hat{c}^\dagger_{\mathrm{H},\vec{k}'\,q}(t')]|\Phi^N_0\rangle \\ &= \delta_{\vec{k}\,p,\,\vec{k}\,q}\left[\frac{\bar{n}_{\vec{k}\,p}}{\omega-\varepsilon_{\vec{k}\,p}+\mathrm{i}\eta} + \frac{n_{\vec{k}\,p}}{\omega-\varepsilon_{\vec{k}\,p}-\mathrm{i}\eta}\right] \ . \end{aligned} \quad (5.14)$$
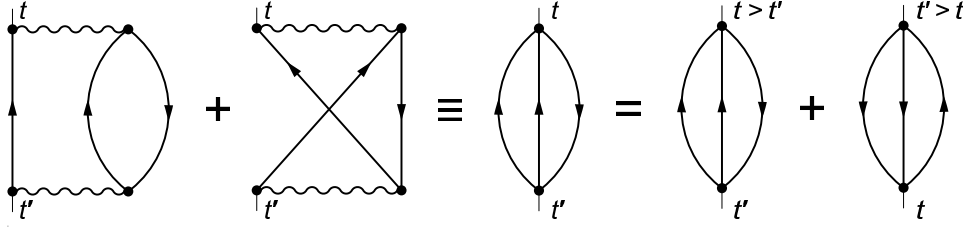
Figure 5.1: Decomposition of a second order Feynman diagram of the self-energy in Abrikosov notation (middle) in terms of two Feynman diagrams in Feynman notation (left) and its two time orderings in terms of two Goldstone diagrams in Abrikosov notation (right).
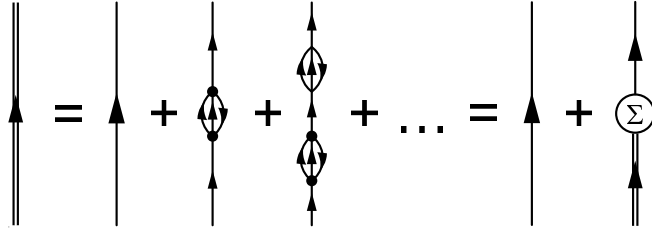
Figure 5.2: Dyson equation (5.15) depicted diagrammatically in terms of the second order self-energy diagram from the middle of Figure 5.1.

This formula is referred to as *free Green's function* or *free propagator*. A Møller-Plesset partition of the Hamiltonian (3.4) is assumed in (5.14). For crystals with a band gap, the occupation numbers in (5.14) are independent of $\vec{k}$, i.e., $n_{\vec{k}p} = n_p$ and $\bar{n}_{\vec{k}p} = \bar{n}_p$.

The evaluation of the time-ordered products of creation and annihilation operators in (5.13) can be simplified by *Wick's theorem* [112–115, 243]. A diagrammatic representation of the resulting terms is provided by the so-called *Feynman diagrams* [112–115, 244, 245]. The route to, first, draw all diagrams of a certain order and afterwards to translate them into analytic expressions is, in general, an easier approach than to apply Wick's theorem directly. Moreover, Feynman diagrams provide a pictorial representation of the individual terms of the perturbation series that facilitates an understanding of the dominant physical contributions in a many-particle system. Examples of Feynman diagrams are given in the figures of the ensuing Section 5.3. A dictionary of diagram elements is provided in Table 5.1 in conjunction with rules how to translate a Feynman diagram into its corresponding analytic expression. The diagrams consist of *interaction vertices*, depicted by points, blobs or wiggly lines, that represent the one- and two-electron interaction and interconnecting lines that depict the free Green's functions (5.14).

Looking thoroughly at the diagrammatic expansion of the numerator in (5.13), one observes that it can be decomposed into two factors. One factor reproduces the diagrammatic expansion of the denominator $\langle \Phi_0^N | \hat{U}_\varepsilon(\infty, -\infty) | \Phi_0^N \rangle$ leading to its cancellation. The other factor is a sum of so-called *connected diagrams*, i.e., diagrams that cannot be composed by two independent diagrams which are neither connected by an interaction line nor by a propagator line. This cancellation of the denominator with a factor of the numerator constitutes the famous *linked cluster theorem* [112–115, 246, 247] which was conjectured by Brueckner [113, 246] from an analysis of the first few orders of the

perturbation series (5.13) and has been proven to hold in general by Goldstone [113, 247].

Let me recast the infinite number of terms in the diagrammatic series for the Green's function (5.13) in a compact manner. Consider, for example, all Feynman diagrams which involve the diagrammatic element in the middle of Figure 5.1 and are connected by free propagator lines. They are shown in the middle of Figure 5.2. Taking off the two outmost free propagator lines from the left, middle and right diagrams in the middle of Figure 5.2 produce none, a single and two stacked diagram elements, respectively, of the type depicted in the middle of Figure 5.1. This diagram element is denoted *proper self-energy insertion* whereas the stack of two such elements is referred to as *improper self-energy insertion* because the latter one can be decomposed into twice the former one by cutting a single free propagator line (5.14). In what follows, the term self-energy diagram always denotes proper self-energy insertions.

The analytic expression, which represents the sum of the analytic expressions of a number of self-energy diagrams, is termed self-energy $\boldsymbol{\Sigma}(\vec{k}, \omega)$. It is introduced by the *Dyson equation* [6, 87, 112–115, 248, 249]

$$\boldsymbol{G}(\vec{k},\omega) = \boldsymbol{G}^0(\vec{k},\omega) \; + \; \boldsymbol{G}^0(\vec{k},\omega)\,\boldsymbol{\Sigma}(\vec{k},\omega)\,\boldsymbol{G}(\vec{k},\omega) \tag{5.15a}$$

$$= \boldsymbol{G}^0(\vec{k},\omega) \; + \; \boldsymbol{G}^0(\vec{k},\omega)\,\boldsymbol{\Sigma}(\vec{k},\omega)\,\boldsymbol{G}^0(\vec{k},\omega) + \dots \; , \tag{5.15b}$$

which can be solved formally by

$$\boldsymbol{G}(\vec{k},\omega) = [\boldsymbol{G}^0(\vec{k},\omega)^{-1} - \boldsymbol{\Sigma}(\vec{k},\omega)]^{-1} \; . \tag{5.16}$$

Equation (5.15) sums all improper self-energy insertions to infinite order in the perturbation that derive from the proper self-energy insertions used to approximate $\boldsymbol{\Sigma}(\vec{k}, \omega)$ [Figure 5.2].

The self-energy in (5.15) can be decomposed into an ω independent part, the static self-energy $\boldsymbol{\Sigma}^\infty(\vec{k})$, and an ω dependent part, the dynamic self-energy $\boldsymbol{M}(\vec{k}, \omega)$ [83, 87, 250, 251]

$$\boldsymbol{\Sigma}(\vec{k},\omega) = \boldsymbol{\Sigma}^\infty(\vec{k}) + \boldsymbol{M}(\vec{k},\omega) \; , \tag{5.17}$$

where $\lim\limits_{\omega\to\pm\infty} \boldsymbol{M}(\vec{k},\omega) = \boldsymbol{0}$ holds.

5.3 Diagrammatic evaluation

Because of the Dyson equation (5.15), the diagrammatic expansion of the one-particle Green's function (5.13) is generated by only considering all proper, connected Feynman diagrams of the self-energy. The order of the individual interaction vertices in a diagram is meaningless. Only the way the vertices are connected to each other by free propagators, i.e., the topology of the diagram, is relevant.

Diagrams drawn with respect to the form of the two-electron interaction used in the Bloch Hamiltonian (3.4) are denoted to be in *Feynman notation*. However, the interaction can be rewritten in terms of the antisymmetrized two-electron matrix elements (3.7)

$$\frac{1}{2} \sum_{\substack{\vec{k}_1\,p,\ \vec{k}_2\,q, \\ \vec{k}_3\,r,\ \vec{k}_4\,s}} V_{\vec{k}_1\,p\ \vec{k}_2\,q\ \vec{k}_3\,r\ \vec{k}_4\,s}\,\hat{c}^\dagger_{\vec{k}_1\,p}\,\hat{c}^\dagger_{\vec{k}_2\,q}\,\hat{c}_{\vec{k}_4\,s}\,\hat{c}_{\vec{k}_3\,r} = \frac{1}{4} \sum_{\substack{\vec{k}_1\,p,\ \vec{k}_2\,q, \\ \vec{k}_3\,r,\ \vec{k}_4\,s}} V_{\vec{k}_1\,p\ \vec{k}_2\,q\ [\vec{k}_3\,r\ \vec{k}_4\,s]}\,\hat{c}^\dagger_{\vec{k}_1\,p}\,\hat{c}^\dagger_{\vec{k}_2\,q}\,\hat{c}_{\vec{k}_4\,s}\,\hat{c}_{\vec{k}_3\,r} \tag{5.18}$$

$\vec{k}\,p$ | t $\mathrm{i}\,G^0_{pq}(\vec{k}, t, t')$ $\vec{k}\,p$ ‖ t $\mathrm{i}\,G_{pq}(\vec{k}, t, t')$

$\vec{k}\,q$ | t' $\vec{k}\,q$ ‖ t'

$\vec{k}\,p$ $-\mathrm{i}\,W_{\vec{k}\,p\,\vec{k}\,q}$ $\vec{R}_1\,\varrho$ $-\mathrm{i}\,F_{\vec{R}_1\,\varrho\,\vec{R}_2\,\sigma}$

$\vec{k}\,q$ $\vec{R}_2\,\sigma$

$\vec{k}_1\,r_1$ $\vec{k}_2\,r_2$ $-\mathrm{i}\,V_{\vec{k}_1\,r_1\,\vec{k}_2\,r_2\,[\vec{k}_3\,r_3\,\vec{k}_4\,r_4]}$ $\vec{k}_1\,r_1$ $\vec{k}_2\,r_2$ $-\mathrm{i}\,V_{\vec{k}_1\,r_1\,\vec{k}_2\,r_2\,\vec{k}_3\,r_3\,\vec{k}_4\,r_4}$

$\vec{k}_3\,r_3$ $\vec{k}_4\,r_4$ $\vec{k}_3\,r_3$ $\vec{k}_4\,r_4$

$\vec{k}\,p$ $\mathrm{i}\,G^0_{pq}(\vec{k}, t, t^+)$ $\vec{k}\,p$ $\mathrm{i}\,G_{pq}(\vec{k}, t, t^+)$

$\vec{k}\,q$ $\vec{k}\,q$ $\vec{k}\,p$ $= \mathrm{i}\,G^{0,-}_{pq}(\vec{k}, t, t)$ $\vec{k}\,q$ $\vec{k}\,q$ $\vec{k}\,p$ $= \mathrm{i}\,G^-_{pq}(\vec{k}, t, t)$

t' $\mathrm{e}^{-\mathrm{i}\omega(t'-t)}$ $\times(-1)$

t

$\vec{k}\,p$ | t $\sum$ $-\mathrm{i}\,\Sigma_{pq}(\vec{k}, t, t')$

$\vec{k}\,q$ | t'
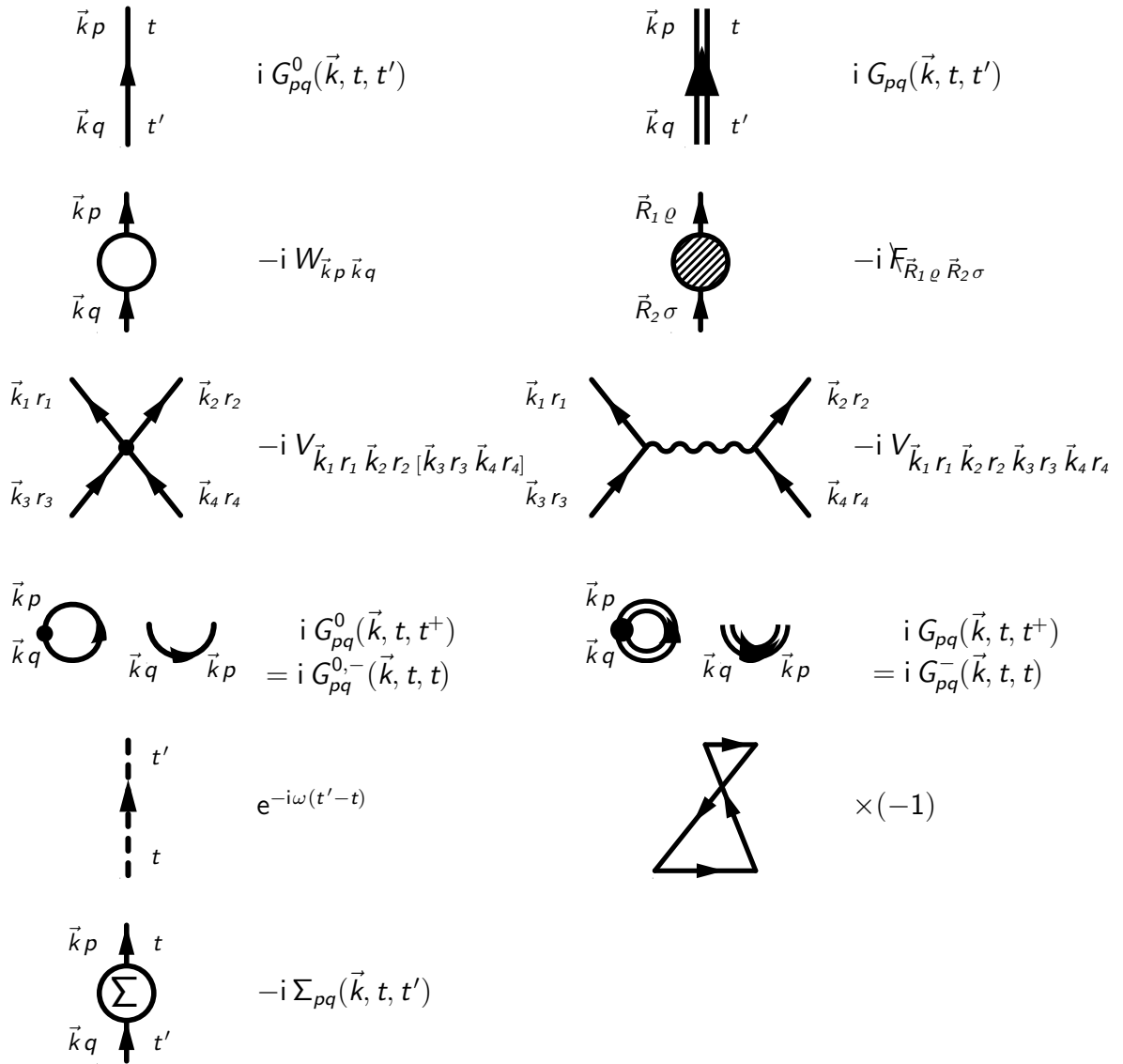
Table 5.1: Dictionary of diagram elements for Feynman diagrams and the corresponding analytic expressions. Two distinct one-particle vertices, the one in terms of Bloch orbitals $-\mathrm{i}\,W_{\vec{k}\,p\,\vec{k}\,q}$ from (3.5) and the other in terms of Wannier orbitals $-\mathrm{i}\,F_{\vec{R}_1\,\varrho\,\vec{R}_2\,\sigma}$ from (3.9) are assumed. Crystal momentum is also conserved at the two different two-particle vertices, i.e., $\vec{k}_1 + \vec{k}_2 = \vec{k}_3 + \vec{k}_4$. The prefactors $-\mathrm{i}$ of the one- and two-particle vertices accumulate to the factor $(-\mathrm{i})^n$ in (5.13) for an n-th order diagram. It is precisely cancelled by the prefactor i of the propagators. An example for a fermion loop is shown as the last diagram element in the right column. From the diagram elements and analytic expression for Bloch orbitals, I obtain corresponding terms for Wannier orbitals by simply replacing all crystal momenta by lattice vectors and all band indices by Wannier orbital indices. Note that the crystal momentum quantum number is no longer conserved at the vertices such that, for a one-particle vertex, two distinct lattice vectors are require whereas four distinct lattice vectors are needed in the case of a two-particle vertex.
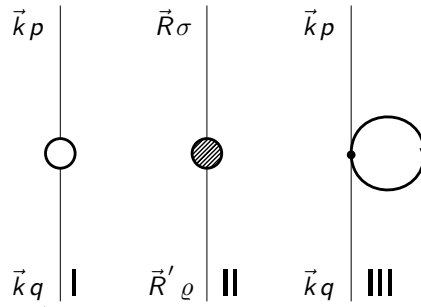
Figure 5.3: First order Feynman diagrams of the self-energy. The contribution of one-particle interactions is split into the two diagrams I and II, respectively, whereas the contribution of two-particle interactions is represented by diagram III. Diagram I is chosen to correspond to the negative of the Hartree-Fock potential, e.g., in (3.5) and (3.9). Then diagram II represents an additional contribution by one-particle operators as, e.g., in (3.9). The Feynman diagrams of this figure are pictorially identical to the corresponding Goldstone diagrams.

as the annihilators $\hat{c}_{\vec{k}_3\,r}$ and $\hat{c}_{\vec{k}_4\,s}$ anticommute (3.2). Diagrams for this form of the two-electron interaction are referred to as being depicted in *Abrikosov notation* [112, 114] or *Hugenholtz notation* [114, 252, 253]. In this notation, the interaction wiggles in the Feynman notation, e.g., Figures 5.1 (left) and 5.5 (left), are replaced by interaction points, e.g., Figures 5.1 (middle)–5.5 (right). Thereby, several diagrams in Feynman notation are combined in terms of a single diagram in Abrikosov notation, e.g., the two second order Feynman diagrams in Feynman notation yield a single Feynman diagram in Abrikosov notation in Figure 5.1. Therefore, less diagrams have to be drawn and evaluated in Abrikosov notation which saves a lot of work.

The evaluation of Feynman diagrams involves integrations over intermediate time variables in (5.13) which extend from $-\infty$ to ∞ thus requiring a careful handling of the time ordered products. This is inconvenient for the explicit evaluation of Feynman diagrams. It can be circumvented by explicitly expanding the time-ordered products in (5.13). For a Feynman diagram this means defining a time coordinate that runs from the past at the bottom of the diagram to the future at its top [Figure 5.1]. The vertical arrangement of the interaction points now becomes relevant and indicates a specific time-ordering. Diagrams with all possible arrangements of the wiggly interaction lines are drawn and one arrives at *time-ordered Feynman diagrams* which are also termed *Goldstone diagrams*. To a n-th order Feynman diagram, there are $n!$ possibilities to arrange the n interaction vertices vertically and thus $n!$ not necessarily different n-th order Goldstone diagrams which correspond to a single n-th order Feynman diagram.

Each permutation of the n interaction vertices of a Feynman diagram either exchanges the chronology of the external indices of the self-energy or leaves it unchanged. Therefore, the diagrams fall into two classes with $t_1 < t_2$ or $t_1 > t_2$ which are referred to as retarded and advanced dynamic self-energy diagrams, respectively. The first diagram on the left hand side of Figure 5.1 is advanced and the second diagram is retarded. The diagrams of the two classes can be transformed into each other by turning them upside down. The special case $t_1 = t_2$ holds for the diagrams of the static self-energy which do not depend on energy as the difference $t_1 - t_2$ vanishes and thus no dependence on ω is introduced by
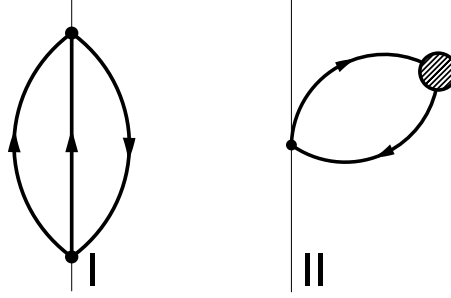
Figure 5.4: Second order Feynman diagrams of the self-energy. Inserting a two-particle and a one-particle vertex into diagram III of Figure 5.3 yields diagram I and II, respectively, of this figure.

a Fourier transformation with respect to this time difference.

Evaluating the diagrammatic series leads to a sum of time-dependent diagrams. Yet, at the very end one is only interested in energy dependent quantities because of the time-independence of the physical problem. Therefore, one carries out a Fourier transformation to energy space with respect to the times affixed to the external indices of the self-energy similarly to (5.5). This conduct can be incorporated directly into the rules for evaluating the self-energy diagrams. Note that the factor $e^{i\omega(t-t')}$ in the Fourier transformation (5.5) is the same as the time-dependent exponential factor in the advanced part $G_{pq}^{0,-}(\vec{k}, t, t')$ of the free propagator (5.14) in terms of time variables

$$
\begin{aligned}
G_{pq}^0(\vec{k}, t, t') &= \delta_{\vec{k}\,p,\,\vec{k}\,q}[n_{\vec{k}\,p}\,\theta(t-t') - \bar{n}_{\vec{k}\,p}\,\theta(t'-t)]e^{-i\varepsilon_{\vec{k}\,p}(t-t')} \\
&= G_{pq}^{0,+}(\vec{k}, t, t') + G_{pq}^{0,-}(\vec{k}, t, t') \ .
\end{aligned}
\tag{5.19}
$$

where $\theta(t - t')$ denotes the Heavyside step function (5.3). Thus by adding an additional auxiliary line which contributes the factor $e^{-i\omega(t'-t)}$ to a Goldstone diagram, one obtains a ground-state-like diagram that can be evaluated in complete analogy to the rules for ground-state Goldstone diagrams discussed in References [112–115].

The diagrammatic rules to evaluate Goldstone self-energy diagrams in Abrikosov notation for crystals are easily derived from those given explicitly for molecules in Reference [83]. In Section 3.1, two choices of one-particle orbitals are discussed to represent the Hamiltonian (2.4). Diagrams can be drawn in either case. The dictionary of diagram elements is given in Table 5.1. It is employed in conjunction with following rules for n-th order diagrams utilizing the Bloch representation (3.4) which are:

1. Draw n interaction vertices on a vertical line. Among these points, distinguish two *external points*[2] by labeling them with $\vec{k}\,p$ and $\vec{k}\,q$. The points correspond to the times t and t', respectively.[3]

2. Among the $n = m_1 + m_2$ interaction vertices, choose m_1 blobs to correspond to one-particle vertices and let m_2 points represent two-particle vertices.

---

[2]External points are those points in a self-energy diagram to which free propagator lines are attached automatically by means of the Dyson equation.

[3]The external points of the self-energy (5.17) depend on the same crystal momentum $\vec{k}$ as the Hamiltonian (2.4) is translationally symmetric.
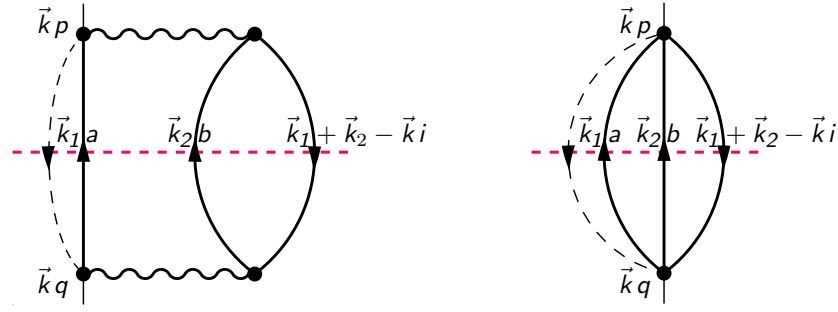
Figure 5.5: (Color) Second order Goldstone diagram of the retarded dynamic self-energy. The dashed black line depicts the $e^{-i\omega(t'-t)}$ auxiliary line. The dashed red line represents a horizontal line of rule 6.

3. Join the external points $\vec{k}\,p$ and $\vec{k}\,q$ with a $e^{-i\omega(t'-t)}$ auxiliary line. Connect all vertices by free propagator lines such that one (two) line(s) goes (go) in and one (two) line(s) comes out of a one-particle (two-particle) vertex.

4. Lines pointing downwards are called *hole lines*; otherwise they are termed *particle lines*. A hole line corresponds to an occupied Bloch orbital, a particle line to a virtual Bloch orbital. Label internal lines with intermediate crystal momenta in conjunction with particle (hole) band indices depending whether the line points upwards (downwards).

5. Conserve the crystal momentum quantum number at each vertex, i.e., for a one-particle interaction $W_{\vec{k}_1\,r_1\,\vec{k}_2\,r_2}$, the rule $\vec{k}_1 = \vec{k}_2$ holds; for a two-particle interaction $V_{\vec{k}_1\,r_1\,\vec{k}_2\,r_2\,\vec{k}_3\,r_3\,\vec{k}_4\,r_4}$ the rule $\vec{k}_1 + \vec{k}_2 = \vec{k}_3 + \vec{k}_4$ holds.

6. Draw a (dashed) horizontal line between every two consecutive interaction vertices. The horizontal line l ($l = 1, \ldots, n-1$) intersects several free propagator lines and frequently also intersects the $e^{-i\omega(t'-t)}$ auxiliary line. It represents the denominators A_l in the analytic expression of the diagram, i.e., the factors $\frac{1}{A_l}$. Each intersection of the horizontal line with a free propagator or auxiliary line supplies a summand to A_l, specifically[4] ω ($-\omega$) when the $e^{-i\omega(t'-t)}$ auxiliary line points downward (upward) and $\varepsilon_{\vec{k}\,r}$ ($-\varepsilon_{\vec{k}\,r}$), if the $G^0_{\vec{k}\,r\,\vec{k}\,r}$ line points downward (upward).

7. Multiply the contributions of the horizontal lines of rule 6 with the interaction matrix elements $W_{\vec{k}_1\,r_1\,\vec{k}_2\,r_2}$ for one-particle vertices and $V_{\vec{k}_1\,r_1\,\vec{k}_2\,r_2\,[\vec{k}_3\,r_3\,\vec{k}_4\,r_4]}$ for two-particle vertices; multiply with a factor of $(-1)^{n_{\mathrm{h}}+n_{\mathrm{l}}}$ where n_{h} is the number of hole lines and n_{l} is the number of *Fermion loops*,[5] see also rule 10; sum over the internal indices.

8. Multiply the above contribution by $2^{-n_{\mathrm{P}}}$ where n_{P} is the number of permutations of two free propagators which leave the diagram unchanged.

---

[4]This denotes the analogous change from an advanced to a retarded free propagator (5.19).

[5]Loops are formed by a few totally connected fermion lines that can be travelled along the specified direction of the lines reaching the point again where one started. See also Table 5.1 for an example.
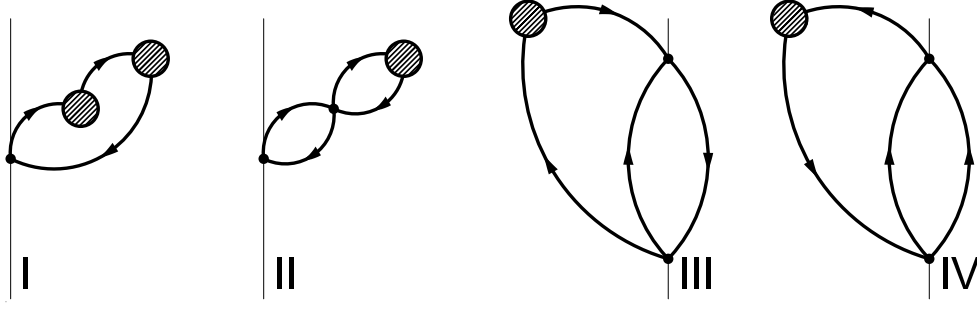
Figure 5.6: Third order Feynman diagrams of the self-energy which include a one-particle vertex. Diagrams I and II derive from diagram II in Figure 5.4 by inserting a one-particle vertex or a two-particle vertex, respectively. The diagrams III and IV derive from diagram I in Figure 5.4 by inserting a one-particle vertex.

9. The above rules 1 to 8 are also valid for Goldstone diagrams in Feynman notation; just replace the $V_{\vec{k}_1 r_1 \, \vec{k}_2 r_2 \, [\vec{k}_3 r_3 \, \vec{k}_4 r_4]}$ interaction points by $V_{\vec{k}_1 r_1 \, \vec{k}_2 r_2 \, \vec{k}_3 r_3 \, \vec{k}_4 r_4}$ interaction wiggles.

10. The sign of the $V_{\vec{k}_1 r_1 \, \vec{k}_2 r_2 \, [\vec{k}_3 r_3 \, \vec{k}_4 r_4]}$ interaction points and the number of loops is not uniquely determined in Abrikosov notation. To obtain the proper sign of the diagram compare with one of the diagrams in Feynman notation contained in it.

The evaluation of Goldstone diagrams with the above given rules shall now be illustrated. The three Feynman diagrams of the self-energy in first order are shown in Figure 5.3. There is only a single time-ordering of each of these Feynman diagrams. Therefore, they are pictorially identical with the corresponding Goldstone diagrams. Assuming the Møller-Plesset partition of the Hamiltonian in crystal momentum representation (3.4), diagram I corresponds to the *negative* of the Hartree-Fock potential $W_{\vec{k}_p \vec{k}_q}$ in (3.5). Diagram III originates from the two-particle interaction. Evaluating this diagram, with the help of the diagram rules given above, I obtain precisely the *positive* of the Hartree-Fock potential $-W_{\vec{k}_p \vec{k}_q}$. As the higher order diagrams can be constructed by inserting additional vertices into those of lower orders, there always arise two different diagrams from a single self-energy diagram; the one is produced by an insertion of diagram I and the other results from an insertion of diagram III. In other words, I obtain two diagrams with an equal contribution of opposite sign which consequently cancel. Therefore, insertions of diagrams I and III need not to be considered, leading to a significant reduction of the number of diagrams to be drawn in Hartree-Fock approximation. Yet, diagram II represents the matrix elements of an additional non-vanishing one-particle operator that has to be regarded. In the Bloch representation of the Hamiltonian (3.4), diagram II vanishes.

Let me consider the second order Feynman diagrams shown in Figure 5.4. Diagram I consists of two external points which can be time-ordered in two distinct ways displayed in Figure 5.1. I obtain the single second order Goldstone diagram of the advanced and the retarded self-energy, respectively. Diagram II vanishes because diagram II in Figure 5.3 is zero in crystal momentum representation (3.4). The second order Goldstone diagram for the retarded self-energy is shown in Figure 5.5. Firstly, I consider one of the diagrams in Feynman notation which is contained in the diagram in Abrikosov notation. Following
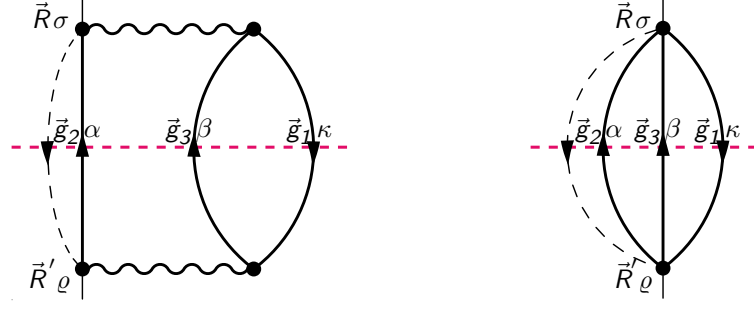
Figure 5.7: (Color) Second order Goldstone diagram of the retarded dynamic self-energy. One assumes that there is no particle-hole coupling in the one-particle interaction. Auxiliary lines are dashed where the $e^{-i\omega(t'-t)}$ auxiliary line is in black and the red line represents a horizontal line of rule 6.

rule 6, the horizontal line contributes $\frac{1}{\omega+\varepsilon_{\vec{k}_1+\vec{k}_2-\vec{k}\,i}-\varepsilon_{\vec{k}_2\,a}-\varepsilon_{\vec{k}_3\,b}}$. The interaction wiggles of the diagram in Feynman notation contribute $V_{\vec{k}\,p\,\vec{k}_1+\vec{k}_2-\vec{k}\,i\,\vec{k}_1\,a\,\vec{k}_2\,b}$ and $V_{\vec{k}_1\,a\,\vec{k}_2\,b\,\vec{k}\,q\,\vec{k}_1+\vec{k}_2-\vec{k}\,i}$. There are $n_{\mathrm{h}} = 1$ hole lines and $n_{\mathrm{l}} = 1$ loops in the diagram and one can permute the two particle lines without changing it, so $n_{\mathrm{P}} = 1$; the proper sign and prefactor thus is $\frac{1}{2}(-1)^2$. The corresponding analytic expression for the diagram reads

$$\frac{1}{2}(-1)^2 \sum_{\substack{\vec{k}_1,\vec{k}_2 \\ a,b,i}} \frac{V_{\vec{k}\,p\,\vec{k}_1+\vec{k}_2-\vec{k}\,i\,\vec{k}_1\,a\,\vec{k}_2\,b}\,V_{\vec{k}_1\,a\,\vec{k}_2\,b\,\vec{k}\,q\,\vec{k}_1+\vec{k}_2-\vec{k}\,i}}{\omega+\varepsilon_{\vec{k}_1+\vec{k}_2-\vec{k}\,i}-\varepsilon_{\vec{k}_2\,a}-\varepsilon_{\vec{k}_3\,b}} \tag{5.20}$$

Secondly, transfering these information, one immediately obtains the analytic expression of the second order Goldstone diagram in Figure 5.5 in Abrikosov notation by replacing the simple two electron integrals (3.6) by their antisymmetrized counterparts (3.7).

$$\frac{1}{2}(-1)^2 \sum_{\substack{\vec{k}_1,\vec{k}_2 \\ a,b,i}} \frac{V_{\vec{k}\,p\,\vec{k}_1+\vec{k}_2-\vec{k}\,i\,[\vec{k}_1\,a\,\vec{k}_2\,b]}\,V_{\vec{k}_1\,a\,\vec{k}_2\,b\,[\vec{k}\,q\,\vec{k}_1+\vec{k}_2-\vec{k}\,i]}}{\omega+\varepsilon_{\vec{k}_1+\vec{k}_2-\vec{k}\,i}-\varepsilon_{\vec{k}_2\,a}-\varepsilon_{\vec{k}_3\,b}}\,. \tag{5.21}$$

By this conduct, one has in fact evaluated two diagrams in Feynman notation simultaneously [Figure 5.5], due to the compact Abrikosov notation. The sum over $\vec{k}_1\,a$ and $\vec{k}_2\,b$ in (5.21) is simplified by exploiting $V_{\vec{k}_1\,a\,\vec{k}_2\,b\,[\vec{k}\,q\,\vec{k}_1+\vec{k}_2-\vec{k}\,i]} = V^*_{\vec{k}\,q\,\vec{k}_1+\vec{k}_2-\vec{k}\,i\,[\vec{k}_1\,a\,\vec{k}_2\,b]} = -V^*_{\vec{k}\,q\,\vec{k}_1+\vec{k}_2-\vec{k}\,i\,[\vec{k}_2\,b\,\vec{k}_1\,a]}$. The numerator is obviously invariant under interchanges of $\vec{k}_1\,a$ and $\vec{k}_2\,b$. The contributions to the sum in (5.21) of Bloch orbitals with $\vec{k}_1\,a < \vec{k}_2\,b$ is equal to contributions from those with $\vec{k}_1\,a > \vec{k}_2\,b$ whereas terms involving $\vec{k}_1\,a = \vec{k}_2\,b$ vanish. Restricting the summation in (5.21) to $\vec{k}_1\,a < \vec{k}_2\,b$ avoids double counting and the factor $\frac{1}{2}$ can be dropped yielding

$$\sum_{\substack{\vec{k}_1,\vec{k}_2,a,b,i \\ \vec{k}_1\,a<\vec{k}_2\,b}} \frac{V_{\vec{k}\,p\,\vec{k}_1+\vec{k}_2-\vec{k}\,i\,[\vec{k}_1\,a\,\vec{k}_2\,b]}\,V^*_{\vec{k}\,q\,\vec{k}_1+\vec{k}_2-\vec{k}\,i\,[\vec{k}_1\,a\,\vec{k}_2\,b]}}{\omega+\varepsilon_{\vec{k}_1+\vec{k}_2-\vec{k}\,i}-\varepsilon_{\vec{k}_2\,a}-\varepsilon_{\vec{k}_3\,b}} \tag{5.22}$$
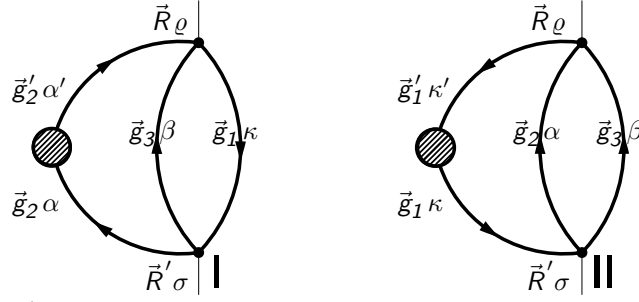
Figure 5.8: Third order Goldstone diagrams of the retarded dynamic self-energy which include a one-particle vertex. They derive from the Feynman diagrams in Figure 5.6 by time ordering. One assumes that there is no particle-hole coupling in the one-particle interaction. Diagram I represents particle-particle interaction and diagram II describes hole-hole interaction.

The corresponding second-order Goldstone diagram of the advanced dynamic self-energy is obtained by turning the diagram in Figure 5.5 upside down. Thereby the role of the propagator lines is exchanged where particle lines become hole lines. Vice versa hole lines become particle lines. The analytic expression is in this case formally identical to (5.22) replacing the band indices as follows $i \rightarrow a$, $a \rightarrow i$, and $b \rightarrow j$.

Let me switch to the Wannier representation of the Hamiltonian (3.8) now. The rules for evaluating Goldstone diagrams are just the same as the ones given above, if one merely replaces all crystal momenta by lattice vectors. The only exception concerns the conservation of crystal momentum in rule 5 to which there is no equivalent.

The first order Goldstone diagrams I and III in Figure 5.3 yield analytic expressions which correspond to those obtained in crystal momentum representation, i.e., diagram I represents the negative of the Hartree-Fock potential and is precisely cancelled in all orders of perturbation theory by diagram III which is the positive potential. However, the first order Goldstone diagram II in Figure 5.3, which designates the additional one-particle operator $\not{F}$ in (3.9), does no longer vanish. Instead, the analytic expression of diagram II reads

$$\not{F}_{\vec{R}' \sigma \, \vec{R} \varrho} \; . \tag{5.23}$$

Replacing the Bloch orbitals in the second order diagram of Figure 5.5 by Wannier orbitals, as in Figure 5.7, yields the analytic expression

$$\sum_{\substack{\vec{g}_1, \vec{g}_2, \vec{g}_3, \kappa, \alpha, \beta \\ \vec{g}_1 \, \alpha < \vec{g}_2 \, \beta}} \frac{V_{\vec{R} \varrho \, \vec{g}_1 \, \kappa \, [\vec{g}_2 \, \alpha \, \vec{g}_3 \, \beta]} \, V^*_{\vec{R}' \, \sigma \, \vec{g}_1 \, \kappa \, [\vec{g}_2 \, \alpha \, \vec{g}_3 \, \beta]}}{\omega + \varepsilon_{\vec{g}_1 \, \kappa} - \varepsilon_{\vec{g}_2 \, \alpha} - \varepsilon_{\vec{g}_3 \, \beta}} \; . \tag{5.24}$$

As $\not{F}$ is block-diagonal with respect to occupied and virtual orbitals, all time orderings of the second Feynman diagram II in Figure 5.4 couple particles and holes and thus vanish [90].

The Feynman diagrams in third order that involve $\not{F}$ are drawn in Figure 5.6. All time-orderings of the diagrams I and II vanish because they couple particles and holes. However, some time orderings of the diagrams III and V of Figure 5.6, which are displayed

in Figure 5.8, are the first non-vanishing diagrams that involve $\not{F}$. The contribution of the first diagram in Figure 5.8 is

$$
\sum_{\substack{\vec{g}_1,\vec{g}_1',\vec{g}_2,\vec{g}_3 \\ \alpha,\alpha',\beta,\kappa}} \frac{V_{\vec{R}\,\varrho\,\vec{g}_1\,\kappa\,[\vec{g}_2'\,\alpha'\,\vec{g}_3\,\beta]}}{\omega + \varepsilon_{\vec{g}_1\,\kappa} - \varepsilon_{\vec{g}_2'\,\alpha'} - \varepsilon_{\vec{g}_3\,\beta}}\, \not{F}_{\vec{g}_2'\,\alpha'\,\vec{g}_2\,\alpha}\, \frac{V^*_{\vec{R}'\,\sigma\,\vec{g}_1\,\kappa\,[\vec{g}_2\,\alpha\,\vec{g}_3\,\beta]}}{\omega + \varepsilon_{\vec{g}_1\,\kappa} - \varepsilon_{\vec{g}_2\,\alpha} - \varepsilon_{\vec{g}_3\,\beta}} \tag{5.25}
$$

and the analytic expression for the second diagram reads

$$
\begin{aligned}
&-\frac{1}{2} \sum_{\substack{\vec{g}_1,\vec{g}_2,\vec{g}_3,\vec{g}_3' \\ \alpha,\beta,\kappa,\kappa'}} \frac{V_{\vec{R}\,\varrho\,\vec{g}_1'\,\kappa'\,[\vec{g}_2\,\alpha\,\vec{g}_3\,\beta]}}{\omega + \varepsilon_{\vec{g}_1'\,\kappa'} - \varepsilon_{\vec{g}_2\,\alpha} - \varepsilon_{\vec{g}_3\,\beta}}\, \not{F}_{\vec{g}_1'\,\kappa'\,\vec{g}_1\,\kappa}\, \frac{V^*_{\vec{R}\,\varrho\,\vec{g}_1\,\kappa\,[\vec{g}_2\,\alpha\,\vec{g}_3\,\beta]}}{\omega + \varepsilon_{\vec{g}_1\,\kappa} - \varepsilon_{\vec{g}_2\,\alpha} - \varepsilon_{\vec{g}_3\,\beta}} \\
&= -\sum_{\substack{\vec{g}_1,\vec{g}_2,\vec{g}_3,\vec{g}_3' \\ \alpha,\beta,\kappa,\kappa' \\ \vec{g}_1\,\alpha < \vec{g}_2\,\beta}} \frac{V_{\vec{R}\,\varrho\,\vec{g}_1'\,\kappa'\,[\vec{g}_2\,\alpha\,\vec{g}_3\,\beta]}}{\omega + \varepsilon_{\vec{g}_1'\,\kappa'} - \varepsilon_{\vec{g}_2\,\alpha} - \varepsilon_{\vec{g}_3\,\beta}}\, \not{F}_{\vec{g}_1'\,\kappa'\,\vec{g}_1\,\kappa}\, \frac{V^*_{\vec{R}\,\varrho\,\vec{g}_1\,\kappa\,[\vec{g}_2\,\alpha\,\vec{g}_3\,\beta]}}{\omega + \varepsilon_{\vec{g}_1\,\kappa} - \varepsilon_{\vec{g}_2\,\alpha} - \varepsilon_{\vec{g}_3\,\beta}}\ .
\end{aligned} \tag{5.26}
$$

Turning the third-order Goldstone diagrams in Figure 5.8 upside down yields corresponding diagrams of the advanced dynamic self-energy where the analytic expressions are formally identical to those in (5.25) and (5.26) replacing $\alpha \to \kappa$, $\alpha' \to \kappa'$, $\beta \to \lambda$, and $\kappa \to \alpha$ in (5.25) and $\alpha \to \kappa$, $\beta \to \lambda$, $\kappa \to \alpha$, and $\kappa' \to \alpha'$ in (5.26).

6 Crystal orbital algebraic diagrammatic construction

The perturbative expansion of the self-energy derived in the previous Chapter 5 has well-known convergence problems for strong interactions. It usually is not systematically improvable, i.e., considering higher orders in the perturbation does not automatically lead to a higher accuracy. This has been studied intensively for the perturbative treatment of the ground-state correlation energy in terms of Møller-Plesset perturbation theory [42].

A simple evaluation of the propagator with the Dyson equation is troubled by the energy dependence of the self-energy. In many cases this requires a numerical pole search. Such algorithms work quite well for the outer valence region in atoms, molecules and crystals. Yet, strong many-particle effects manifest for the core states, inner valence states and virtual states and a simple pole search becomes hopeless.

By turning to the algebraic diagrammatic construction (ADC) scheme for the dynamic self-energy (5.17) in the ensuing Section 6.1, the above shortcomings of the diagrammatic method are overcome. This is because the static self-energy can then be determined using the former one as is shown in Section 6.2 before the two parts of the self-energy are combined in Section 6.3 to finally determine the poles of the one-particle Green's function with the help of the Dyson equation. The truncation of the configuration space for infinite crystals in practical computations is considered in Section 6.4.

6.1 Dynamic self-energy

6.1.1 Crystal momentum representation

The dynamic self-energy $\boldsymbol{M}(\vec{k}, \omega)$ is represented in terms of the $2p1h/2h1p$-propagator (two-particle-one-hole/two-hole-one-particle-propagator) and possesses the *spectral representation* [87, 250, 251]

$$
\begin{aligned}
M_{pq}(\vec{k}, \omega) &= \sum_{n \in \{N+1\}} \frac{m_p^{+,(n)}(\vec{k}) \, m_q^{+,(n)*}(\vec{k})}{\omega - \omega_n^+(\vec{k}) + \mathrm{i}\eta} + \sum_{n \in \{N-1\}} \frac{m_p^{-,(n)}(\vec{k}) \, m_q^{-,(n)*}(\vec{k})}{\omega - \omega_n^-(\vec{k}) - \mathrm{i}\eta} \\
&= M_{pq}^+(\vec{k}, \omega) + M_{pq}^-(\vec{k}, \omega) \,,
\end{aligned}
\tag{6.1}
$$

where $\omega_n^\pm(\vec{k})$ denote the pole positions of the $2p1h/2h1p$-propagator and the $m_p^{\pm,(n)}(\vec{k})$ are termed *Dyson amplitudes*. The *retarded dynamic self-energy* $M_{pq}^+(\vec{k}, \omega)$ and the *advanced dynamic self-energy* $M_{pq}^-(\vec{k}, \omega)$ are associated with excitations of the $N \pm 1$ particle system, respectively. Yet, the pole positions $\omega_n^\pm(\vec{k})$ do *not* directly correspond to the energies of physical states as the (dynamic) self-energy is only defined in conjunction with the Dyson equation (5.15).

The algebraic diagrammatic construction scheme is a stable and efficient method to determine the spectral representation of the dynamic self-energy (6.1). The construction starts by making the ansatz

$$M_{pq}^{\pm}(\vec{k},\omega) = \vec{U}_{p}^{\pm\dagger}(\vec{k})\,(\omega\,\mathbb{1} - \boldsymbol{K}^{\pm}(\vec{k}) - \boldsymbol{C}^{\pm}(\vec{k}))^{-1}\,\vec{U}_{q}^{\pm}(\vec{k})\;, \qquad (6.2)$$

which is termed *general algebraic form* or *ADC form*. The vector $\vec{U}_{q}^{\pm}(\vec{k})$ is called *modified coupling amplitude* for the crystal orbital $\vec{k}\,q$. Both $\boldsymbol{K}^{\pm}(\vec{k})$ and $\boldsymbol{C}^{\pm}(\vec{k})$ are Hermitian matrices, $\boldsymbol{C}^{\pm}(\vec{k})$ being referred to as *modified interaction matrix* [87] while $\boldsymbol{K}^{\pm}(\vec{k})$ is assumed to be diagonal.

The ADC form (6.2) can be expanded into a geometric series

$$M_{pq}^{\pm}(\vec{k},\omega) = \vec{U}_{p}^{\pm\dagger}(\vec{k})\sum_{n=0}^{\infty}[(\omega\,\mathbb{1} - \boldsymbol{K}^{\pm}(\vec{k}))^{-1}\,\boldsymbol{C}^{\pm}(\vec{k})]^{n}(\omega\,\mathbb{1} - \boldsymbol{K}^{\pm}(\vec{k}))^{-1}\,\vec{U}_{q}^{\pm}(\vec{k})\;. \qquad (6.3)$$

The approximation of the dynamic self-energy up to n-th order, $\boldsymbol{M}^{(n),\pm}(\vec{k},\omega)$, in terms of the ADC form (6.2) is denoted by ADC(n) and is constructed by inserting the perturbation expansions

$$\begin{aligned}
\boldsymbol{U}^{\pm}(\vec{k}) &= \boldsymbol{U}^{\pm\,(1)}(\vec{k}) + \boldsymbol{U}^{\pm\,(2)}(\vec{k}) + \ldots \\
\boldsymbol{C}^{\pm}(\vec{k}) &= \boldsymbol{C}^{\pm\,(1)}(\vec{k}) + \boldsymbol{C}^{\pm\,(2)}(\vec{k}) + \ldots
\end{aligned} \qquad (6.4)$$

into (6.3), retaining all contributions up to order n.

The link between the expansion of the ADC form (6.3) and (6.4) and the diagrammatic expansion of the dynamic self-energy in terms of the Feynman-Dyson perturbation series can now be established by noting that the analytic structure of the latter expansion is reproduced by the former series. Approximations to $\boldsymbol{U}^{\pm,(n)}(\vec{k})$, $\boldsymbol{K}^{\pm}(\vec{k})$, and $\boldsymbol{C}^{(n),\pm}(\vec{k})$ are obtained by comparing the n-th order summands, as determined by inserting (6.4) into (6.3), to the diagrammatic expansion of the dynamic self-energy up to n-th order where the analytic structure imposed by formula (6.3) either allows a one-to-one correspondence between the analytic expression of a diagram and one summand but occasionally requires one to associate linear combinations of the analytic expressions of several diagrams with particular summands in the above expansion (6.3).

Consequently, the expansion of $\boldsymbol{U}^{\pm}(\vec{k})$ in (6.4) starts earliest in first order, as Koopmans' theorem [39–42, 143], is accurate in zeroth and first order of perturbation theory and corrections arise first in second order [1, 3, 5–7, 39–42]. As $\boldsymbol{K}^{\pm}(\vec{k})$ already holds the zero order approximation to the modified coupling amplitudes the first term in the series for $\boldsymbol{C}^{\pm}(\vec{k})$ is also of first order.

Specifically, the ADC equations up to second order are given by

$$\boldsymbol{M}^{(2),\pm}(\vec{k},\omega) = \boldsymbol{U}^{\pm(1)\dagger}(\vec{k})(\omega\mathbb{1} - \boldsymbol{K}^{\pm}(\vec{k}))^{-1}\boldsymbol{U}^{\pm(1)}(\vec{k}) + O(3)\;. \qquad (6.5)$$

Considering the second order diagram in Figure 5.5, Equation (5.22), one observes that the internal summations run over two particle indices and a hole index. This advises the following specialization of the ADC form (6.2) which immediately carries over to the

second order terms (6.5)

$$
\begin{aligned}
M_{pq}^{+}(\vec{k},\omega) \; = \; & \sideset{}{'}\sum_{\substack{\vec{l}_1,\vec{l}_2,\vec{l}_1',\vec{l}_2' \\ i,a,b,i',a',b'}} U_{\vec{k}\,p\,;\,\vec{l}_1+\vec{l}_2-\vec{k}\,i\,\vec{l}_1\,a\,\vec{l}_2\,b}^{+*} \\
& \times \left(\omega\,\mathbb{1} - \boldsymbol{K}^{+}(\vec{k}) - \boldsymbol{C}^{+}(\vec{k})\right)^{-1}_{\substack{\vec{l}_1+\vec{l}_2-\vec{k}\,i\,\vec{l}_1\,a\,\vec{l}_2\,b\,; \\ \vec{l}_1'+\vec{l}_2'-\vec{k}\,i'\,\vec{l}_1'\,a'\,\vec{l}_2'\,b'}} \\
& \times U_{\vec{k}\,q\,;\,\vec{l}_1'+\vec{l}_2'-\vec{k}\,i'\,\vec{l}_1'\,a'\,\vec{l}_2'\,b'}^{+} \;.
\end{aligned}
\tag{6.6}
$$

The prime on the summation symbol indicates that the summation only runs over indices with $\vec{l}_1\,a < \vec{l}_2\,b$ and $\vec{l}_1'\,a' < \vec{l}_2'\,b'$ to avoid double counting of identical contributions. The corresponding ansatz for $\boldsymbol{M}^{-}(\vec{k},\omega)$ is formally identical to (6.6) apart from the changed occupation numbers of the band indices $i \rightarrow a$, $a \rightarrow i$, $b \rightarrow j$, $i' \rightarrow a'$, $a' \rightarrow i'$, and $b' \rightarrow j'$. The summation variables $\vec{l}_1$, $\vec{l}_1'$, $\vec{l}_2$, and $\vec{l}_2'$ are crystal momentum vectors like $\vec{k}$. The quantities $\boldsymbol{M}^{\pm}(\vec{k},\omega)$, $\boldsymbol{U}^{\pm}(\vec{k})$, $\boldsymbol{K}^{\pm}(\vec{k})$, and $\boldsymbol{C}^{\pm}(\vec{k})$ are invariant under translations by an arbitrary lattice vector, a property which is taken into account for the internal summations in the ADC form (6.6). This adaption to translational symmetry is carried out by translating each of the three matrices in (6.2) by the same but arbitrary lattice vector, using Bloch's theorem [3,6] which leads to three linear equations that can be used to eliminate two intermediate summations over crystal momentum vectors.

Inspecting again the second order diagram in Figure 5.5, Equation (5.22), the so-called crystal orbital ADC(2) [CO-ADC(2)] is obtained by making the assignments

$$
U_{\vec{k}\,p\,;\,\vec{l}_1+\vec{l}_2-\vec{k}\,i\,\vec{l}_1\,a\,\vec{l}_2\,b}^{+} \;=\; V_{\vec{k}\,p\,\vec{l}_1+\vec{l}_2-\vec{k}\,i\,[\vec{l}_1\,a\,\vec{l}_2\,b]}^{*}\, n_{\vec{l}_1+\vec{l}_2-\vec{k}\,i}\,\bar{n}_{\vec{l}_1\,a}\,\bar{n}_{\vec{l}_2\,b}
\tag{6.7a}
$$

$$
K_{\substack{\vec{l}_1+\vec{l}_2-\vec{k}\,i\,\vec{l}_1\,a\,\vec{l}_2\,b\,; \\ \vec{l}_1'+\vec{l}_2'-\vec{k}\,i'\,\vec{l}_1'\,a'\,\vec{l}_2'\,b'}}^{+} \;=\; \delta_{\substack{\vec{l}_1+\vec{l}_2-\vec{k}\,i\,\vec{l}_1\,a\,\vec{l}_2\,a\,; \\ \vec{l}_1'+\vec{l}_2'-\vec{k}\,i'\,\vec{l}_1'\,a'\,\vec{l}_2'\,b'}}\, \left(\varepsilon_{\vec{l}_1\,a} + \varepsilon_{\vec{l}_2\,b} - \varepsilon_{\vec{l}_1+\vec{l}_2-\vec{k}\,i}\right)
\tag{6.7b}
$$

$$
\times\, n_{\vec{l}_1+\vec{l}_2-\vec{k}\,i}\,\bar{n}_{\vec{l}_1\,a}\,\bar{n}_{\vec{l}_2\,b}
$$

$$
C_{\substack{\vec{l}_1+\vec{l}_2-\vec{k}\,i\,\vec{l}_1\,a\,\vec{l}_2\,b\,; \\ \vec{l}_1'+\vec{l}_2'-\vec{k}\,i'\,\vec{l}_1'\,a'\,\vec{l}_2'\,b'}}^{+} \;=\; 0
\tag{6.7c}
$$

to the ADC form (6.5), (6.6) which reproduces the diagram exactly. The equations for $\boldsymbol{U}^{-}(\vec{k})$, $\boldsymbol{K}^{-}(\vec{k})$, and $\boldsymbol{C}^{-}(\vec{k})$ are formally identical to (6.7) apart from the occupation numbers which are in this case $\bar{n}_{\vec{l}_1+\vec{l}_2-\vec{k}\,a}\,n_{\vec{l}_1\,i}\,n_{\vec{l}_2\,j}$. Equations (6.7) are derived in Reference [254] utilizing a Gaussian basis set expansion of the Bloch orbitals. Explicit molecular ADC equations up to fourth order are given in Reference [87].

Generally, in ADC(2) and ADC(3), each entry of the $\boldsymbol{U}^{\pm}(\vec{k})$ and the $\boldsymbol{K}^{\pm}(\vec{k}) + \boldsymbol{C}^{\pm}(\vec{k})$ in (6.2) is characterized by one or two arrangements, respectively, of two particles and one hole ($2p1h$) for $\boldsymbol{M}^{+}(\vec{k},\omega)$ and two holes and one particle ($2h1p$) for $\boldsymbol{M}^{-}(\vec{k},\omega)$. In brief notation these arrangements are referred to as $2p1h$- and $2h1p$-*configurations*. All such configurations that can be formed with the one-particle basis set underlying a Hartree-Fock calculation constitute the *configuration space* in ADC(2) and ADC(3). The configuration space is enlarged in ADC(4) by $3p2h$- and $3h2p$-configurations [87]. In general, every second order in ADC, the configuration space enlarges by the next higher excitation class.

The spectral representation (6.1) of the dynamic self-energy is obtained from the ADC form (6.2) by solving the Hermitian eigenvalue problem

$$
(\boldsymbol{K}^{\pm}(\vec{k}) + \boldsymbol{C}^{\pm}(\vec{k}))\boldsymbol{Y}^{\pm}(\vec{k}) = \boldsymbol{Y}^{\pm}(\vec{k})\boldsymbol{\Omega}^{\pm}(\vec{k}), \qquad \boldsymbol{Y}^{\pm\dagger}(\vec{k})\boldsymbol{Y}^{\pm}(\vec{k}) = \mathbb{1}\;.
\tag{6.8}
$$

The vector notation in (6.2) and (6.8) is a convenient means to sum over all intermediate crystal momenta and band indices. The diagonal matrix $\mathbf{\Omega}^{\pm}(\vec{k})$ contains the eigenvalues of the secular matrix $\mathbf{K}^{\pm}(\vec{k}) + \mathbf{C}^{\pm}(\vec{k})$ and $\mathbf{Y}^{\pm}(\vec{k})$ denotes the eigenvector matrix. The eigenvalues are the pole positions of the dynamic self-energy, i.e., $\omega_n^{\pm}(\vec{k}) = \Omega_{nn}^{\pm}(\vec{k})$, while the Dyson amplitudes (6.1) are obtained via

$$m_p^{\pm,(n)}(\vec{k}) = \vec{U}_p^{\pm\dagger}(\vec{k})\,\vec{Y}^{\pm,(n)}(\vec{k})\ , \tag{6.9}$$

where the n-th column vector $\vec{Y}^{(n),\pm}(\vec{k})$ of $\mathbf{Y}^{\pm}(\vec{k})$ is used here together with the adjoint of $\vec{U}_p^{\pm}(\vec{k})$. Unlike in CO-ADC(2), in CO-ADC(3) (and higher orders), the eigenvector matrices do no longer allow a simple interpretation of their row indices in terms of (Hartree-Fock) $2p1h$-, $2h1p$-, (or higher excited)-configurations because the individual eigenvectors $\vec{Y}^{(n),\pm}(\vec{k})$ couple to several entries of the modified coupling amplitudes (6.7c).

6.1.2 Wannier representation

I derive in the following an expansion of the dynamic self-energy with respect to orbitals which are localized within unit cells, i.e., generalized Wannier orbitals, which facilitates to apply cutoff criteria inside the origin cell and between the origin cell and other unit cells. This affords one the ability to apply fine grained configuration selection which is independent of the actual choice of the unit cell. That is especially helpful for systems with more than one atom per unit cell. In particular, it enables the treatment of crystals with large unit cells, not amenable to Bloch orbital based treatments [Section 6.4] [1, 2, 27, 28].

For an evaluation of the one-particle Green's function in terms of the Feynman-Dyson perturbation series, it is essential that there is no mixing between occupied and virtual Wannier orbitals; otherwise Wick's theorem can no longer be applied [112–115]. To fulfill this requirement, the Wannier transformation (2.33a) is applied to the occupied and virtual Bloch orbitals separately, yielding two independent unitary matrices, one for the occupied bands and one for the virtual bands, respectively [141]. Hence $\boldsymbol{\mathcal{U}}(\vec{k})$ in (2.33) is block-diagonal.

On the one hand, I want to evaluate the CO-ADC equations entirely in terms of Wannier orbitals; on the other hand, band structures are defined with respect to the crystal momentum quantum number. In what follows, three different transformation schemes to switch between the Wannier representation and the crystal momentum representation are applied to the CO-ADC formalism and their physical and methodological implications are discussed.

The dynamic self-energy $M_{nm}^{\pm}(\vec{k},\omega) \equiv M_{\vec{k}\,n\,\vec{k}\,m}^{\pm}(\omega)$ depends on *two* external Bloch orbitals $\psi_{\vec{k}n}^*(\vec{r}s)$ and $\psi_{\vec{k}m}(\vec{r}s)$. Hence carrying out the inverse Wannier transformation (2.33b) for the external orbitals in (6.6) leads to

$$M_{pq}^{\pm}(\vec{k},\omega) = \frac{1}{N_0}\sum_{\varrho,\sigma}\mathcal{U}_{p\varrho}(\vec{k})\,\mathcal{U}_{q\sigma}^*(\vec{k})\sum_{\vec{R},\vec{R}'}\mathrm{e}^{i\vec{k}(\vec{R}'-\vec{R})}\,M_{\vec{R}\,\varrho\,\vec{R}'\,\sigma}^{\pm}(\omega)\ , \tag{6.10}$$

for the left-hand side of (6.6) and a similar expression for the right-hand side where the internal summations $\vec{l}_1$, $\vec{l}_2$, $\vec{l}_1'$, and $\vec{l}_2'$ still run over all $\vec{k}$-points in the Brillouin zone.

To obtain a representation of the dynamic self-energy $M_{nm}^{\pm}(\vec{k}, \omega)$ entirely in terms of Wannier orbitals, it is important to note that, although matrix elements such as the modified coupling amplitudes $U_{\vec{k}\,p\,;\,\vec{l}_1 + \vec{l}_2 - \vec{k}\,i\,\vec{l}_1\,a\,\vec{l}_2\,b}^{+}(\vec{k})$ in (6.6) only depend on three *independent* crystal momenta, they actually describe quantities which depend on four Bloch orbitals, namely $\psi_{\vec{k}\,p}(\vec{r}\,s)$, $\psi_{\vec{l}_1 + \vec{l}_2 - \vec{k}\,i}(\vec{r}\,s)$, $\psi_{\vec{l}_1\,a}^{*}(\vec{r}\,s)$, and $\psi_{\vec{l}_2\,b}^{*}(\vec{r}\,s)$ and thus a fourfold inverse Wannier transformation (2.33b) has to be applied. This transformation of (6.6) to the Wannier representation yields

$$
M_{\vec{R}\,\varrho\,\vec{R}'\,\sigma}^{+}(\omega) = \sum_{\substack{\vec{g}_1\,\kappa\,\vec{g}_2\,\alpha\,\vec{g}_3\,\beta \\ \vec{g}_1'\,\kappa'\,\vec{g}_2'\,\alpha'\,\vec{g}_3'\,\beta'}}'\check{U}_{\vec{R}\,\varrho\,;\,\vec{g}_1\,\kappa\,\vec{g}_2\,\alpha\,\vec{g}_3\,\beta}^{+\,*}
$$
$$
\times\,(\omega\,\mathbb{1} - \check{\boldsymbol{K}}^{+} - \check{\boldsymbol{C}}^{+})_{\substack{\vec{g}_1\,\kappa\,\vec{g}_2\,\alpha\,\vec{g}_3\,\beta\,; \\ \vec{g}_1'\,\kappa'\,\vec{g}_2'\,\alpha'\,\vec{g}_3'\,\beta'}}^{-1} \qquad (6.11)
$$
$$
\times\,\check{U}_{\vec{R}'\,\sigma\,;\,\vec{g}_1'\,\kappa'\,\vec{g}_2'\,\alpha'\,\vec{g}_3'\,\beta'}^{+}\,,
$$

exploiting the unitarity of $\boldsymbol{\mathcal{U}}(\vec{k})$ and the basic orthogonality relations (2.22). The corresponding equation for $M_{\vec{R}\,\varrho\,\vec{R}'\,\sigma}^{-}(\omega)$ is formally identical to (6.11) apart from the changed occupation numbers $\kappa \to \alpha$, $\alpha \to \kappa$, $\beta \to \lambda$, $\kappa' \to \alpha'$, $\alpha' \to \kappa'$, and $\beta' \to \lambda'$. As for formula (6.6), the prime on the summation symbol indicates that $\vec{g}_2\,\alpha < \vec{g}_3\,\beta$ and $\vec{g}_2'\,\alpha' < \vec{g}_3'\,\beta'$ must hold to avoid double counting of contributions.

One obviously Hermitian form for the dynamic self-energy emerging from (6.10) and (6.11) is given by

$$
M_{pq}^{\pm}(\vec{k}, \omega) = \sum_{\varrho,\sigma} \mathcal{U}_{p\varrho}(\vec{k})\,\mathcal{U}_{q\sigma}^{*}(\vec{k})\,\vec{U}_{\varrho}^{\pm}(\vec{k})^{\dagger}(\omega\,\mathbb{1} - \check{\boldsymbol{K}}^{\pm} - \check{\boldsymbol{C}}^{\pm})^{-1}\vec{U}_{\sigma}^{\pm}(\vec{k}) \qquad (6.12a)
$$
$$
\vec{U}_{\sigma}^{\pm}(\vec{k}) = \frac{1}{\sqrt{N_0}}\sum_{\vec{R}} \mathrm{e}^{i\vec{k}\vec{R}}\,\vec{U}_{\vec{R}\,\sigma}^{\pm}\,. \qquad (6.12b)
$$

The vector notation in (6.12) combines the six internal summations over the intermediate lattice vectors and Wannier orbital indices $\vec{g}_1\,\kappa$, $\vec{g}_2\,\alpha$, $\vec{g}_3\,\beta$, $\vec{g}_1'\,\kappa'$, $\vec{g}_2'\,\alpha'$, and $\vec{g}_3'\,\beta'$ in formula (6.11). The check accent on the quantities $\check{\boldsymbol{U}}^{\pm}$, $\check{\boldsymbol{K}}^{\pm}$, and $\check{\boldsymbol{C}}^{\pm}$ indicates that the internal summation indices are lattice vectors and Wannier orbital indices rather than crystal momenta and band indices as in (6.6). I refer to (6.12) as the *supercell form* of CO-ADC.

The secular matrix $\check{\boldsymbol{K}}^{\pm} + \check{\boldsymbol{C}}^{\pm}$ in (6.12a) does not explicitly depend on $\vec{k}$ which implies that the $2p1h/2h1p$-propagator [analogous to (6.1)] contains *all* poles, i.e., poles for each $\vec{k}$-point. Hence, the resulting pole positions $\breve{\omega}_n$ do also not explicitly depend on $\vec{k}$. Multiplying with $\vec{U}_{\varrho}^{\pm\,\dagger}(\vec{k})$ from the left projects on the desired set of eigenvectors for a specific crystal momentum $\vec{k}$. Hence, the translational symmetry among the N_0 unit cells of the crystal is not exploited to reduce the size of the configuration space which is unfavorable in conjunction with the cutoff criteria discussed in Section 6.4. In practice, Equation (6.12) is applied to a large molecule formed by N_0 unit cells for which Born von Kármán boundary conditions are enforced. As a consequence, only N_0 discrete crystal momenta are in the Brillouin zone. The above given transformation from the Wannier

representation to the crystal momentum representation, is simple and robust and can be used in conjunction with almost any electron correlation method, but it suffers from finite-size effects due to the, usually, small number of unit cells which are considered in practice, see, e.g., Reference [26].

The translational symmetry of the dynamic self-energy (6.11) can be exploited by applying a translation by $-\vec{R}$ which removes the explicit dependence of $M_{\vec{R}\varrho\,\vec{R}'\sigma}(\omega)$ on two external lattice vectors such that it only depends on the difference of the lattice vectors according to

$$M_{\vec{R}\varrho\,\vec{R}'\sigma}(\omega) = M_{\vec{0}\varrho\,\vec{R}'-\vec{R}\sigma}(\omega) \equiv M_{\varrho\sigma}(\vec{R}'-\vec{R},\omega) \ . \tag{6.13}$$

This facilitates to remove the lattice summation over $\vec{R}$ and the prefactor $\frac{1}{N_0}$ in (6.10) which results in (dropping the prime on $\vec{R}'$)

$$M_{pq}^{\pm}(\vec{k},\omega) = \sum_{\varrho,\sigma} \mathcal{U}_{p\varrho}(\vec{k})\,\mathcal{U}_{q\sigma}^{*}(\vec{k}) \sum_{\vec{R}} \mathrm{e}^{i\vec{k}\vec{R}}\,M_{\varrho\sigma}(\vec{R},\omega) \ . \tag{6.14}$$

To continue, I give up the idea of an ADC form for $M_{\vec{0}\varrho\,\vec{R}\sigma}(\omega)$, where the modified coupling amplitudes on the left and on the right are related by Hermitian conjugation, as it is the case for (6.12), and arrive at

$$
\begin{aligned}
M_{pq}^{\pm}(\vec{k},\omega) &= \sum_{\varrho,\sigma} \mathcal{U}_{p\varrho}(\vec{k})\,\mathcal{U}_{q\sigma}^{*}(\vec{k})\,\vec{\tilde{U}}_{\vec{0}\varrho}^{\pm\dagger}(\omega\,\mathbb{1}-\tilde{\boldsymbol{K}}^{\pm}-\tilde{\boldsymbol{C}}^{\pm})^{-1}\,\vec{\tilde{U}}_{\sigma}^{\pm}(\vec{k}) && (6.15\mathrm{a}) \\
\vec{\tilde{U}}_{\sigma}^{\pm}(\vec{k}) &= \sum_{\vec{R}} \mathrm{e}^{i\vec{k}\vec{R}}\,\vec{\tilde{U}}_{\vec{R}\sigma}^{\pm} \ , && (6.15\mathrm{b})
\end{aligned}
$$

where a slightly changed definition of the transformed modified coupling amplitude $\vec{\tilde{U}}_{\sigma}^{\pm}(\vec{k}) = \sqrt{N_0}\,\vec{\check{U}}_{\sigma}^{\pm}(\vec{k})$ is employed which is indicated by a tilde accent on all quantities: $\tilde{\boldsymbol{U}}^{\pm} \equiv \check{\boldsymbol{U}}^{\pm}$, $\tilde{\boldsymbol{K}}^{\pm} \equiv \check{\boldsymbol{K}}^{\pm}$, and $\tilde{\boldsymbol{C}}^{\pm} \equiv \check{\boldsymbol{C}}^{\pm}$. Because of its asymmetric nature, I denote formula (6.15) as *semi-transformed form*.

By exploiting the translational symmetry (6.13), I remove the summation over all translationally equivalent octuples consisting of the two external Wannier orbitals $w_{\vec{R}\varrho}^{*}(\vec{r}s)$ and $w_{\vec{R}'\sigma}(\vec{r}s)$ of the dynamic self-energy $M_{\vec{R}\varrho\,\vec{R}'\sigma}(\omega)$ and two $2p1h$- or two $2h1p$-configurations entering the internal sixfold summation over Wannier orbitals in (6.11). I arrive at a summation over $\vec{0}\varrho$, $\vec{R}'-\vec{R}\sigma$ and the six internal lattice vectors and Wannier orbital indices. This formulation thus provides a far better starting point for reducing the number of configurations by means of the cutoff criteria of Section 6.4 than the supercell form. Using the unsymmetric form (6.15) implies that the spectral representation of the dynamic self-energy (6.1) has to be adjusted in order to be able to extract it directly from the ADC ansatz (6.15). In particular, the pole positions of the $2p1h/2h1p$-propagator [analogous to (6.1)] still do not dependent explicitly on $\vec{k}$ and the modified coupling amplitudes are no longer related by Hermitian conjugation; yet, for sure, the dynamic self-energy itself stays Hermitian. This way of exploiting translational symmetry in conjunction with the Wannier orbitals has already been applied successfully before to devise *ab initio* electron correlation methods for crystals like the local Hamiltonian approach of Gräfenstein *et al.* [63–67, 71, 72] or the Green's function based method of Albrecht *et al.* [68–70].

The internal structure of the dynamic self-energy is not regarded in the two formulas (6.12) and (6.15). Expression (6.15) results from (6.10) and (6.11) by exploiting the overall translational symmetry of $\boldsymbol{M}^{\pm}(\vec{k}, \omega)$ in (6.13) and utilizing its exclusive dependence on two external Wannier orbitals. However, the translational symmetry of the matrices $\tilde{\boldsymbol{K}}^{\pm}$ and $\tilde{\boldsymbol{C}}^{\pm}$ in (6.15) can also be exploited additionally, which already was harnessed to derive (6.6) from its original molecular orbital formulation. I obtain

$$
\begin{aligned}
M_{pq}^{+}(\vec{k}, \omega) &= \sum_{\varrho, \sigma} \mathcal{U}_{p\varrho}(\vec{k})\, \mathcal{U}_{q\sigma}^{*}(\vec{k}) \sum_{\vec{g}_1\, \vec{g}_2\, \vec{g}_1'\, \vec{g}_2'} \sum_{\substack{\kappa\, \alpha\, \beta, \\ \kappa'\, \alpha'\, \beta'}} \bar{U}_{\varrho\,;\, \vec{g}_1\, \vec{g}_2\, \kappa\, \alpha\, \beta}^{+\,*}(\vec{k}) \\
&\quad \times (\omega\, \mathbb{1} - \bar{\boldsymbol{K}}^{+}(\vec{k}) - \bar{\boldsymbol{C}}^{+}(\vec{k}))_{\substack{\vec{g}_1\, \vec{g}_2\, \kappa\, \alpha\, \beta\,; \\ \vec{g}_1'\, \vec{g}_2'\, \kappa'\, \alpha'\, \beta'}}^{-1} \qquad (6.16\text{a}) \\
&\quad \times \bar{U}_{\sigma\,;\, \vec{g}_1'\, \vec{g}_2'\, \kappa'\, \alpha'\, \beta'}^{+}(\vec{k})
\end{aligned}
$$

$$
\bar{U}_{\sigma\,;\, \vec{g}_1'\, \vec{g}_2'\, \kappa'\, \alpha'\, \beta'}^{+}(\vec{k}) = \sum_{\vec{R}} e^{i\vec{k}\vec{R}}\, \bar{U}_{\vec{R}\sigma\,;\, \vec{0}\, \kappa'\, \vec{g}_1'\, \alpha'\, \vec{g}_2'\, \beta'}^{+} \qquad (6.16\text{b})
$$

$$
(\bar{\boldsymbol{K}}^{+}(\vec{k}) + \bar{\boldsymbol{C}}^{+}(\vec{k}))_{\substack{\vec{g}_1\, \vec{g}_2\, \kappa\, \alpha\, \beta\,; \\ \vec{g}_1'\, \vec{g}_2'\, \kappa'\, \alpha'\, \beta'}} = \sum_{\vec{R}} e^{i\vec{k}\vec{R}}\, (\bar{\boldsymbol{K}}^{+} + \bar{\boldsymbol{C}}^{+})_{\substack{\vec{0}\, \kappa\, \vec{g}_1\, \alpha\, \vec{g}_2\, \beta\,; \\ \vec{R}\, \kappa'\, \vec{g}_1'+\vec{R}\, \alpha'\, \vec{g}_2'+\vec{R}\, \beta'}}\,, \qquad (6.16\text{c})
$$

where the identities $\bar{\boldsymbol{U}}^{+} \equiv \check{\boldsymbol{U}}^{+}$, $\bar{\boldsymbol{K}}^{+} \equiv \check{\boldsymbol{K}}^{+}$ and $\bar{\boldsymbol{C}}^{+} \equiv \check{\boldsymbol{C}}^{+}$ hold. The corresponding relations for $\boldsymbol{M}^{-}(\vec{k}, \omega)$ are formally identical to (6.16) apart from the changed occupation numbers $\kappa \to \alpha$, $\alpha \to \kappa$, $\beta \to \lambda$, $\kappa' \to \alpha'$, $\alpha' \to \kappa'$, and $\beta' \to \lambda'$. Alternatively, one can derive (6.16) by inserting the inverse Wannier transformation (2.33b) into the CO-ADC equations for Bloch orbitals (6.6) which already are fully adapted to translational symmetry. This transformation is referred to as *fully translational symmetry adapted form*.

The modified coupling amplitudes (6.16b) are constructed by considering only Wannier orbitals relative to an origin cell or reference cell where the hole with index κ is assumed to reside. The external orbital index σ of the modified coupling amplitude can be viewed to represent a Bloch orbital $\psi_{\vec{k}\sigma}(\vec{r}s)$. The external Bloch orbital interacts with the $2p1h$-configurations that are pinned with one lattice vector to the origin cell and extend with the two remaining lattice vectors $\vec{g}_1$ and $\vec{g}_2$ over up to two different unit cells. Alternatively, one can use the translational symmetry of the $\bar{U}_{\vec{R}\sigma\,;\, \vec{0}\, \kappa'\, \vec{g}_1'\, \alpha'\, \vec{g}_2'\, \beta'}^{+}$ to arrive at

$$
\bar{U}_{\sigma\,;\, \vec{g}_1'\, \vec{g}_2'\, \kappa'\, \alpha'\, \beta'}^{+}(\vec{k}) = \sum_{\vec{R}} e^{-i\vec{k}\vec{R}}\, \bar{U}_{\vec{0}\, \sigma\,;\, \vec{R}\, \kappa'\, \vec{g}_1'+\vec{R}\, \alpha'\, \vec{g}_2'+\vec{R}\, \beta'}^{+} \qquad (6.17)
$$

where the external orbital $w_{\vec{0}\, \sigma}(\vec{r}s)$ now is independent of $\vec{R}$ and Equation (6.17) describes the interaction of a Wannier orbital in the origin cell with $2p1h$-configurations centered around the origin cell and their translationally copies centered around $\vec{R}$ which are combined to give an intermediate $2p1h$-configuration with a total crystal momentum $-\vec{k}$.

The matrix (6.16c) describes the coupling among the $2p1h$-configurations. One of the lattice vectors of the first triple of orbitals is pinned to the origin cell and the two other lattice vectors $\vec{g}_1$ and $\vec{g}_2$ are offset to it. The remaining three lattice vectors denote a Wannier orbital in an arbitrary cell $\vec{R}$ and two further Wannier orbitals in the cells $\vec{g}_1' +$

$\vec{R}$ and $\vec{g}_2' + \vec{R}$ relative to the former. Obviously, the entire (6.16c) can be interpreted to describe the interaction of a $2p1h$-configuration of Wannier orbitals centered around the origin cell with another $2p1h$-configuration with crystal momentum $\vec{k}$. Due to the full exploitation of translational symmetry, also those of the matrices in terms of the intermediate $2p1h$-configurations, the fully translational symmetry adapted form yields the smallest configuration space in conjunction with the cutoff criteria of Section 6.4.

To derive explicit CO-ADC expressions for the matrices showing up in (6.16), one changes to the Wannier representation of the Hamiltonian (3.8). The matrices in (6.16) are transformed employing the inverse generalized Wannier transformation (2.33) which corresponds to utilizing the *full* Fock matrix as zero order Hamiltonian. A subsequently applied perturbative expansion with respect to the off-diagonal elements of the Fock matrix $\boldsymbol{F}$ is equivalent to employing the partitioning of the Hamiltonian in (3.8). Up to second order, this does not introduce any new diagrams involving $\boldsymbol{F}$ for the dynamic self-energy [83,90,131,132] [Section 5.3]. The expansion of the ADC form for the diagrammatic series in Wannier representation formally assumes the same structure as (6.5). However, there is no crystal momentum dependence of the individual matrices in this case yielding

$$\boldsymbol{M}^{(2),\pm}(\omega) = \bar{\boldsymbol{U}}^{\pm(1)\dagger}(\omega\mathbb{1} - \bar{\boldsymbol{K}}^{\pm})^{-1}\bar{\boldsymbol{U}}^{\pm(1)} + O(3) \; . \tag{6.18}$$

With the second order diagram, Figure 5.5, Equation (5.24), one obtains expressions for the matrices in (6.16) within a second order treatment of the one- and two-electron interaction

$$\bar{U}^{+}_{\vec{R}\,\varrho\,;\,\vec{g}_1\,\kappa\,\vec{g}_2\,\alpha\,\vec{g}_3\,\beta} = V^{*}_{\vec{R}\,\varrho\,\vec{g}_1\,\kappa\,[\vec{g}_2\,\alpha\,\vec{g}_3\,\beta]}\,n_{\vec{g}_1\,\kappa}\,\bar{n}_{\vec{g}_2\,\alpha}\,\bar{n}_{\vec{g}_3\,\beta} \tag{6.19a}$$

$$\bar{K}^{+}_{\substack{\vec{g}_1\,\kappa\,\vec{g}_2\,\alpha\,\vec{g}_3\,\beta\,;\\ \vec{g}_1'\,\kappa'\,\vec{g}_2'\,\alpha'\,\vec{g}_3'\,\beta'}} = \delta_{\substack{\vec{g}_1\,\kappa\,\vec{g}_2\,\alpha\,\vec{g}_3\,\beta\,;\\ \vec{g}_1'\,\kappa'\,\vec{g}_2'\,\alpha'\,\vec{g}_3'\,\beta'}}\,(\varepsilon_{\vec{g}_2\,\alpha} + \varepsilon_{\vec{g}_3\,p_3} - \varepsilon_{\vec{g}_1\,\kappa})\,n_{\vec{g}_1\,\kappa}\,\bar{n}_{\vec{g}_2\,\alpha}\,\bar{n}_{\vec{g}_3\,\beta} \tag{6.19b}$$

$$\bar{C}^{+}_{\substack{\vec{g}_1\,\kappa\,\vec{g}_2\,\alpha\,\vec{g}_3\,\beta\,;\\ \vec{g}_1'\,\kappa'\,\vec{g}_2'\,\alpha'\,\vec{g}_3'\,\beta'}} = 0 \tag{6.19c}$$

to which I refer as CO-ADC(2,2) *approximation*. The equations for $\bar{\boldsymbol{U}}^{-}$, $\bar{\boldsymbol{K}}^{-}$, and $\bar{\boldsymbol{C}}^{-}$ are formally identical to (6.19), apart from the occupation numbers, which are in this case $\bar{n}_{\vec{g}_1\,\alpha}\,n_{\vec{g}_2\,\kappa}\,n_{\vec{g}_3\,\lambda}$. Here $\bar{\boldsymbol{K}}^{\pm} + \bar{\boldsymbol{C}}^{\pm}$ are diagonal which is no longer the case, if the full Fock matrix is chosen to be the zeroth order Hamiltonian $\hat{H}_0^{\mathrm{WF}}$ in (3.8).

Goldstone diagrams involving $\boldsymbol{F}$ arise earliest in third order [Figure 5.8]. They are to be incorporated into the expansion of the ADC form up to third order which reads

$$\begin{aligned}\boldsymbol{M}^{(3)\pm}(\omega) =\;& \boldsymbol{M}^{(2)\pm}(\omega)\\ &+ \bar{\boldsymbol{U}}^{\pm(2)\dagger}(\omega\mathbb{1} - \bar{\boldsymbol{K}}^{\pm})^{-1}\bar{\boldsymbol{U}}^{\pm(1)}\\ &+ \bar{\boldsymbol{U}}^{\pm(1)\dagger}(\omega\mathbb{1} - \bar{\boldsymbol{K}}^{\pm})^{-1}\bar{\boldsymbol{U}}^{\pm(2)}\\ &+ \bar{\boldsymbol{U}}^{\pm(1)\dagger}(\omega\mathbb{1} - \bar{\boldsymbol{K}}^{\pm})^{-1}\bar{\boldsymbol{C}}^{\pm(1)}(\omega\mathbb{1} - \bar{\boldsymbol{K}}^{\pm})^{-1}\bar{\boldsymbol{U}}^{\pm(1)} + O(4)\end{aligned} \tag{6.20}$$

with the second order term $\boldsymbol{M}^{(2)\pm}(\omega)$ from (6.18). The Goldstone diagrams in Figure 5.8, Equations (5.25) and (5.26) fit nicely into the analytic structure of the summand that

precedes $O(4)$ in (6.20) upon making the assignments

$$
\begin{aligned}
\bar{C}^{+}_{\substack{\vec{g}_1\,\kappa\,\vec{g}_2\,\alpha\,\vec{g}_3\,\beta\,;\\ \vec{g}_1'\,\kappa'\,\vec{g}_2'\,\alpha'\,\vec{g}_3'\,\beta'}} \;\; &= \;\; (\not{F}_{\vec{g}_2\,\alpha\,\vec{g}_2'\,\alpha'}\,\delta_{\vec{g}_3\,\beta\,\vec{g}_3'\,\beta'} - \not{F}_{\vec{g}_2\,\alpha\,\vec{g}_3'\,\beta'}\,\delta_{\vec{g}_3\,\beta\,\vec{g}_2'\,\alpha'} \\
& \qquad - \not{F}_{\vec{g}_3\,\beta\,\vec{g}_2'\,\alpha'}\,\delta_{\vec{g}_2\,\alpha\,\vec{g}_3'\,\beta'} + \not{F}_{\vec{g}_3\,\beta\,\vec{g}_3'\,\beta'}\,\delta_{\vec{g}_2\,\alpha\,\vec{g}_2'\,\alpha'})\,\delta_{\vec{g}_1\,\kappa\,\vec{g}_1'\,\kappa'} \\
& \qquad - \not{F}_{\vec{g}_1\,\kappa\,\vec{g}_1'\,\kappa'}\,\delta_{\vec{g}_2\,\alpha\,\vec{g}_2'\,\alpha'}\,\delta_{\vec{g}_3\,\beta\,\vec{g}_3'\,\beta'}\,.
\end{aligned}
\tag{6.21}
$$

Corresponding expressions for $\boldsymbol{M}^{-}(\vec{k},\omega)$ are obtained by exchanging $\kappa \to \alpha$, $\alpha \to \kappa$, $\beta \to \lambda$, $\kappa' \to \alpha'$, $\alpha' \to \kappa'$, and $\beta' \to \lambda'$ in (6.21). In conjunction with (6.19a), (6.19b), the formula (6.21) constitutes the so-called CO-ADC(3,2) *approximation* which means being third order in the diagrams that involve the one-particle interaction, i.e., $\not{F}$, but only second order in the diagrams of exclusively the two-particle interaction, i.e., the two-electron integrals. The first summand in (6.21) describes coupling of holes i to i' and originates from diagram I in Figure 5.8, Equation (5.26).[1] The remaining terms in (6.21) originate from diagram II in Figure 5.8, Equation (5.25) and represent the coupling between two particles.

6.2 Static self-energy

6.2.1 Crystal momentum representation

The static self-energy has not been determined so far. It is represented by all those diagrams in the diagrammatic expansion of the self-energy where the external points of the diagrams correspond to equal times [83]. In a strict second order treatment of electron correlations, using Bloch orbitals (3.4), the static self-energy is zero because the first static self-energy diagrams arise the earliest in third order. Moreover, it turns out that the diagrammatic series for the static self-energy does not converge reasonably in many cases [89]. However, a self-consistent solution is possible [84, 87] utilizing [83, 250, 251]

$$
\Sigma^{\infty}_{pq}(\vec{k}) = W_{pq}(\vec{k}) + \sum_{\vec{k}'}\sum_{r,s} V_{\vec{k}\,p\,\vec{k}'\,r\,[\vec{k}\,q\,\vec{k}'s]}\left[\frac{1}{2\pi\mathrm{i}}\oint G_{sr}(\vec{k}',\omega)\,\mathrm{d}\omega\right],
\tag{6.22}
$$

here given in terms of Bloch orbitals. The contour integration in (6.22) runs along the real axis and closes in the upper complex ω-plane, hence enclosing only the poles of the advanced Green's function $\boldsymbol{G}^{-}(\vec{k}',\omega)$ in (5.6b).

The self-consistent solution of (6.22) is computationally expensive. Yet, a stable and efficient *Dyson expansion method (DEM)* to determine the static self-energy is devised in Reference [89]. There, the first two terms of the Dyson expansion (5.15b) are inserted into (6.22). The term $W_{pq}(\vec{k})$ in (6.22) cancels the result of the contour integration over the free Green's function $G^0_{sr}(\vec{k}',\omega)$. Carrying out the contour integration over the product

---

[1]This diagram vanishes in Reference [90] because, there, the one-particle operator—the complex absorbing potential—vanishes in the occupied-occupied block which minimizes the artefacts of the artificial potential.

of the two free Green's functions and the static self-energy yields

$$\Sigma_{pq}^{\infty}(\vec{k}) = \sum_{\vec{k}'} \sum_{r,s} A_{\vec{k}\,p\,\vec{k}\,q,\,\vec{k}'\,s\,\vec{k}'\,r}\, \Sigma_{sr}^{\infty}(\vec{k}') + b_{pq}(\vec{k}) \tag{6.23a}$$

$$A_{\vec{k}\,p\,\vec{k}\,q,\,\vec{k}'\,s\,\vec{k}'\,r} = V_{\vec{k}\,p\,\vec{k}'\,r\,[\vec{k}\,q\,\vec{k}'\,s]}\left[\frac{\bar{n}_{\vec{k}'\,s}\,n_{\vec{k}'\,r}}{\varepsilon_{\vec{k}'\,r} - \varepsilon_{\vec{k}'\,s}} + \frac{n_{\vec{k}'\,s}\,\bar{n}_{\vec{k}'\,r}}{\varepsilon_{\vec{k}'\,s} - \varepsilon_{\vec{k}'\,r}}\right] \tag{6.23b}$$

$$b_{pq}(\vec{k}) = \sum_{\vec{k}'} \sum_{r,s} V_{\vec{k}\,p\,\vec{k}'\,r\,[\vec{k}\,q\,\vec{k}'\,s]}\, Q_{rs}(\vec{k}') \tag{6.23c}$$

$$Q_{rs}(\vec{k}') = \frac{1}{2\pi\mathrm{i}}\oint G_{ss}^0(\vec{k}',\omega) M_{sr}(\vec{k}',\omega) G_{rr}^0(\vec{k}',\omega)\,\mathrm{d}\omega\,. \tag{6.23d}$$

The $Q_{rs}(\vec{k}')$ can now be determined by inserting the crystal momentum dependent spectral representation of the dynamic self-energy (6.1) into (6.23d) and carrying out the contour integration to yield for $Q_{rs}(\vec{k}') = Q_{rs}^+(\vec{k}') + Q_{rs}^-(\vec{k}')$

$$Q_{rs}^+(\vec{k}') = \sum_{n\in\{N+1\}} m_s^{+,(n)}(\vec{k}')\, m_r^{+,(n)*}(\vec{k}')\left[\frac{-n_{\vec{k}'\,s}\,n_{\vec{k}'\,r}}{(\varepsilon_{\vec{k}'\,s} - \omega_n^+(\vec{k}'))(\varepsilon_{\vec{k}'\,r} - \omega_n^+(\vec{k}'))}\right.$$

$$\left. + \frac{n_{\vec{k}'\,s}\,\bar{n}_{\vec{k}'\,r}}{(\varepsilon_{\vec{k}'\,s} - \varepsilon_{\vec{k}'\,r})(\varepsilon_{\vec{k}'\,s} - \omega_n^+(\vec{k}'))} - \frac{\bar{n}_{\vec{k}'\,s}\,n_{\vec{k}'\,r}}{(\varepsilon_{\vec{k}'\,s} - \varepsilon_{\vec{k}'\,r})(\varepsilon_{\vec{k}'\,r} - \omega_n^+(\vec{k}'))}\right] \tag{6.24a}$$

$$Q_{rs}^-(\vec{k}') = \sum_{n\in\{N-1\}} m_s^{-,(n)}(\vec{k}')\, m_r^{-,(n)*}(\vec{k}')\left[\frac{\bar{n}_{\vec{k}'\,s}\,\bar{n}_{\vec{k}'\,r}}{(\varepsilon_{\vec{k}'\,s} - \omega_n^-(\vec{k}'))(\varepsilon_{\vec{k}'\,r} - \omega_n^-(\vec{k}'))}\right.$$

$$\left. - \frac{n_{\vec{k}'\,r}\,\bar{n}_{\vec{k}'\,s}}{(\varepsilon_{\vec{k}'\,s} - \varepsilon_{\vec{k}'\,r})(\varepsilon_{\vec{k}'\,s} - \omega_n^-(\vec{k}'))} + \frac{\bar{n}_{\vec{k}'\,r}\,n_{\vec{k}'\,s}}{(\varepsilon_{\vec{k}'\,s} - \varepsilon_{\vec{k}'\,r})(\varepsilon_{\vec{k}'\,r} - \omega_n^-(\vec{k}'))}\right]. \tag{6.24b}$$

In order to evaluate (6.24), I resort to (6.6) [analogous equations result from (6.16)]. The direct usage of (6.24) is, in principle, very time consuming because the $\boldsymbol{K}^{\pm}(\vec{k}') + \boldsymbol{C}^{\pm}(\vec{k}')$ matrices have to be diagonalized *fully* to obtain the pole positions $\omega_n^{\pm}(\vec{k}')$. For the CO-ADC(2) form of the dynamic self-energy in crystal momentum representation (6.7), however, $\boldsymbol{K}^{\pm}(\vec{k}') + \boldsymbol{C}^{\pm}(\vec{k}')$ remains diagonal. This leads to $m_r^{\pm,(n)*}(\vec{k}') = U_{\vec{k}'\,r,n}^{\pm}$ and $\omega_n^{\pm}(\vec{k}') = K_{nn}^{\pm}(\vec{k}')$, where the n-th eigenvector of $\boldsymbol{K}^{\pm}(\vec{k}') + \boldsymbol{C}^{\pm}(\vec{k}')$ is only non-zero for a single $2p1h$- or $2h1p$-configuration, respectively. In general, the $Q_{rs}(\vec{k}')$ are determined efficiently from (6.24) by the *inversion method* or by a single vector *Lanczos diagonalization* to circumvent a full diagonalization of $\boldsymbol{K}^{\pm}(\vec{k}') + \boldsymbol{C}^{\pm}(\vec{k}')$ [89].

The inversion method has been found [89] to be more efficient than the single vector Lanczos diagonalization, so I concentrate on the former. I define auxiliary vectors $\vec{V}_r^{\pm}(\vec{k}')$ as the solution of the inhomogeneous systems of linear equations

$$(\varepsilon_{\vec{k}'\,i}\mathbb{1} - \boldsymbol{K}^+(\vec{k}') - \boldsymbol{C}^+(\vec{k}'))\,\vec{V}_i^+(\vec{k}') = \vec{U}_i^+(\vec{k}')\,, \qquad n_{\vec{k}'\,i} = 1 \tag{6.25a}$$

$$(\varepsilon_{\vec{k}'\,a}\mathbb{1} - \boldsymbol{K}^-(\vec{k}') - \boldsymbol{C}^-(\vec{k}'))\,\vec{V}_a^-(\vec{k}') = \vec{U}_a^-(\vec{k}')\,, \qquad \bar{n}_{\vec{k}'\,a} = 1\,. \tag{6.25b}$$

Inserting the eigenvectors $\boldsymbol{Y}^{\pm}(\vec{k}')$ of $\boldsymbol{K}^{\pm}(\vec{k}') + \boldsymbol{C}^{\pm}(\vec{k}')$ to solve (6.25) and using formula (6.9), reveals the usefulness of the new vectors

$$\vec{V}_r^{\pm}(\vec{k}') = \boldsymbol{Y}^{\pm}(\vec{k}')\,(\varepsilon_{\vec{k}'\,r}\mathbb{1} - \boldsymbol{\Omega}^{\pm}(\vec{k}'))^{-1}\,\vec{m}_r^{\pm\dagger}(\vec{k}')\,. \tag{6.26}$$

to rewrite the Equations (6.24) for $Q_{rs}^{\pm}(\vec{k}')$

$$
\begin{aligned}
Q_{rs}^{+}(\vec{k}') &= -\vec{V}_s^{+\dagger}(\vec{k}')\,\vec{V}_r^{+}(\vec{k}')\,n_{\vec{k}'\,s}\,n_{\vec{k}'\,r} + (\varepsilon_{\vec{k}'\,s} - \varepsilon_{\vec{k}'\,r})^{-1} \\
&\quad \times [\vec{V}_s^{+\dagger}(\vec{k}')\,\vec{U}_r^{+}(\vec{k}')\,\bar{n}_{\vec{k}'\,r}\,n_{\vec{k}'\,s} - \vec{U}_s^{+\dagger}(\vec{k}')\,\vec{V}_r^{+}(\vec{k}')\,\bar{n}_{\vec{k}'\,s}\,n_{\vec{k}'\,r}] \quad (6.27\text{a})
\end{aligned}
$$

$$
\begin{aligned}
Q_{rs}^{-}(\vec{k}') &= \vec{V}_s^{-\dagger}(\vec{k}')\,\vec{V}_r^{-}(\vec{k}')\,\bar{n}_{\vec{k}'\,s}\,\bar{n}_{\vec{k}'\,r} - (\varepsilon_{\vec{k}'\,s} - \varepsilon_{\vec{k}'\,r})^{-1} \\
&\quad \times [\vec{V}_s^{-\dagger}(\vec{k}')\,\vec{U}_r^{-}(\vec{k}')\,n_{\vec{k}'\,r}\,\bar{n}_{\vec{k}'\,s} - \vec{U}_s^{-\dagger}(\vec{k}')\,\vec{V}_r^{-}(\vec{k}')\,\bar{n}_{\vec{k}'\,r}\,n_{\vec{k}'\,s}] \;. \quad (6.27\text{b})
\end{aligned}
$$

I have reduced the problem of determining the $Q_{rs}^{\pm}(\vec{k}')$ to the problem of determining the $\vec{V}_r^{\pm}(\vec{k}')$. Inspecting the inhomogeneous systems of linear equations (6.25), I note that I have to solve for the $\vec{V}_i^{+}(\vec{k}')$ in the large $2p1h$-configuration space but only for the usually small set of all occupied orbitals. Conversely, the $\vec{V}_a^{-}(\vec{k}')$ have to be calculated in the small $2h1p$-configuration space but for the usually large set of all virtual orbitals.

The diagonal parts $\varepsilon_{\vec{k}'\,r}\mathbb{1} - \boldsymbol{K}^{\pm}(\vec{k}')$ in (6.25) are at least of a magnitude of twice the Hartree-Fock band gap, implying usually a diagonal dominance of the full matrices in (6.25). Therefore, a solution by *Jacobi iterations* [89, 127] is suggested

$$
\begin{aligned}
\vec{V}_r^{\pm,(0)}(\vec{k}') &= (\varepsilon_{\vec{k}'\,r}\mathbb{1} - \boldsymbol{K}^{\pm}(\vec{k}'))^{-1}\,\vec{U}_r^{\pm}(\vec{k}') \\
\vec{V}_r^{\pm,(n)}(\vec{k}') &= \vec{V}_r^{\pm,(0)}(\vec{k}') + (\varepsilon_{\vec{k}'\,r}\mathbb{1} - \boldsymbol{K}^{\pm}(\vec{k}'))^{-1}\boldsymbol{C}^{\pm}(\vec{k}')\vec{V}_r^{\pm,(n-1)}(\vec{k}')
\end{aligned}
\quad (6.28)
$$

which turns out to converge rapidly.

The inhomogeneous linear system of equations (6.23a) can now be solved for $\Sigma_{pq}^{\infty}(\vec{k})$ by a matrix inversion [84]

$$
\vec{\Sigma}^{\infty} = (\mathbb{1} - \boldsymbol{A})^{-1}\,\vec{b}\;, \quad (6.29)
$$

where Σ_i^{∞}, b_i and A_{ij} are composed by numerating the compound indices $(p, q, \vec{k})$ and $(s, r, \vec{k}')$ in $\Sigma_{pq}^{\infty}(\vec{k})$, $b_{pq}^{\infty}(\vec{k})$ and $A_{\vec{k}\,p\,\vec{k}\,q,\,\vec{k}'\,s\,\vec{k}'\,r}$ by integer numbers i and j, respectively. Inspecting Equation (6.23b), I note that $\boldsymbol{A}$ couples only to the components of $\Sigma_{sr}^{\infty}(\vec{k}')$, where the s, r indices denote ph- or hp-orbitals. As all quantities in (6.29) are Hermitian, I can further restrict the band indices to $p \leq q$. As soon as the number of $\vec{k}$-points becomes large, the solution of (6.29) gets cumbersome as the dimension of the system of linear equations is given by the number of entries of the upper triangle (including the diagonal entries) of the static self-energy matrix times the number of $\vec{k}$-points. Thus an iterative linear equations solver has to be employed [127].

6.2.2 Wannier representation

The static self-energy can also be determined directly in Wannier representation from which I obtain the static self-energy in crystal momentum representation by

$$
\Sigma_{pq}^{\infty}(\vec{k}) = \sum_{\varrho,\sigma} \mathcal{U}_{p\varrho}(\vec{k})\,\mathcal{U}_{q\sigma}^{*}(\vec{k}) \sum_{\vec{R}} e^{i\vec{k}\vec{R}}\,\Sigma_{\varrho\sigma}^{\infty}(\vec{R})\;. \quad (6.30)
$$

To find an approximation for $\Sigma_{\varrho\sigma}^{\infty}(\vec{R})$, I insert the inverse Wannier transformation (2.33b) and its Hermitian conjugate into (6.23) and arrive at

$$
\Sigma_{\varrho\sigma}^{\infty}(\vec{R}) = \sum_{\vec{R}'} \sum_{\tau,\upsilon} \left[\sum_{\vec{g}} A_{\vec{0}\,\varrho\,\vec{R}\,\sigma,\,\vec{g}\,\upsilon\,\vec{g}+\vec{R}'\,\tau} \right] \Sigma_{\upsilon\tau}^{\infty}(\vec{R}') + b_{\varrho\sigma}(\vec{R}) \quad (6.31\text{a})
$$

$$b_{\varrho\sigma}(\vec{R}) \;=\; \sum_{\vec{R}'} \sum_{\tau,\upsilon} \left[\sum_{\vec{g}} V_{\vec{0}\,\varrho\;\vec{g}+\vec{R}'\,\tau\;[\vec{R}\sigma\;\vec{g}\upsilon]} \right] Q_{\tau\upsilon}(\vec{R}') \,. \tag{6.31b}$$

Note that the translational symmetry of $A_{\vec{0}\,\varrho\;\vec{R}\sigma,\;\vec{g}\upsilon\;\vec{g}+\vec{R}'\,\tau}$ could only be utilized once to remove one lattice summation such that two lattice summations (one over $\vec{R}'$ and one over $\vec{g}$) show up in (6.31) while only one $\vec{k}'$ summation is necessary in (6.23). There is no first order contribution[2] to the static self-energy in (6.31) because the static self-energy used here evolves from an inverse Wannier transformation of the self-energy obtained in Møller-Plesset partition [39–42] (3.4) and a *subsequent* perturbative expansion with respect to the off-diagonal elements of the Fock matrix.

For the remaining equations (6.23b) and (6.23d), I switch from $M_{sr}(\vec{k}',\omega)$ to $M_{\upsilon\tau}(\vec{R}',\omega)$. Further, I assume the partition (3.8) of the Hamiltonian in Wannier representation and get

$$A_{\vec{0}\,\varrho\;\vec{R}\sigma,\;\vec{g}\upsilon\;\vec{g}+\vec{R}'\,\tau} \;=\; V_{\vec{0}\,\varrho\;\vec{g}+\vec{R}'\,\tau\;[\vec{R}\sigma\;\vec{g}\upsilon]} \left(\frac{\bar{n}_{\vec{g}\upsilon}\,n_{\vec{g}+\vec{R}'\,\tau}}{\varepsilon_{\vec{g}+\vec{R}'\,\tau} - \varepsilon_{\vec{g}\upsilon}} + \frac{n_{\vec{g}\upsilon}\,\bar{n}_{\vec{g}+\vec{R}'\,\tau}}{\varepsilon_{\vec{g}\upsilon} - \varepsilon_{\vec{g}+\vec{R}'\,\tau}} \right) \tag{6.32a}$$

$$Q_{\tau\upsilon}(\vec{R}') \;=\; \frac{1}{2\pi\mathrm{i}} \oint G^0_{\upsilon\upsilon}(\vec{0},\omega) M_{\upsilon\tau}(\vec{R}',\omega) G^0_{\tau\tau}(\vec{0},\omega) \,\mathrm{d}\omega \tag{6.32b}$$

with the free Green's function in Wannier representation

$$G^0_{\tau\upsilon}(\vec{R}',\omega) = \delta_{\vec{0}\,\tau,\;\vec{R}'\,\upsilon} \left[\frac{\bar{n}_{\vec{0}\,\tau}}{\omega - \varepsilon_{\vec{0}\,\tau} + \mathrm{i}\eta} + \frac{n_{\vec{0}\,\tau}}{\omega - \varepsilon_{\vec{0}\,\tau} - \mathrm{i}\eta} \right] \tag{6.33}$$

for the partition (3.8).

To determine the $Q_{\tau\upsilon}(\vec{R}')$, I introduce the spectral representation of the dynamic self-energy in Wannier representation [the analogue of Equation (6.1)]

$$\begin{aligned} M_{\upsilon\tau}(\vec{R}',\omega) &= \sum_{n\in\{N+1\}} \frac{\check{m}^{+,(n)}_{\upsilon}(\vec{0})\,\check{m}^{+,(n)*}_{\tau}(\vec{R}')}{\omega - \check{\omega}^+_n + \mathrm{i}\eta} + \sum_{n\in\{N-1\}} \frac{\check{m}^{-,(n)}_{\upsilon}(\vec{0})\,\check{m}^{-,(n)*}_{\tau}(\vec{R}')}{\omega - \check{\omega}^-_n - \mathrm{i}\eta} \\ &= M^+_{\upsilon\tau}(\vec{R}',\omega) + M^-_{\upsilon\tau}(\vec{R}',\omega) \,, \end{aligned} \tag{6.34}$$

which is obtained from the ADC form of the dynamic self-energy in Wannier representation (6.11) by letting $\vec{R} \to \vec{0}$ and diagonalizing $\check{\boldsymbol{K}}^{\pm} + \check{\boldsymbol{C}}^{\pm}$ analogously to (6.8). I would like to point out that the full configuration space of $2p1h$- and $2h1p$-configurations is necessary here, the $2p1h$- and $2h1p$-configurations of both the origin cell and the surrounding neighbor cells, because translational symmetry cannot be exploited in the internal summations as $\vec{R}'$—in contrast to $\vec{k}$—is not a good quantum number. This leads to the redundancies that have already been mentioned in conjunction with the supercell form of the dynamic self-energy in section 6.1.

The $Q_{\tau\upsilon}(\vec{R}')$ can now be determined by inserting the spectral representation of the dynamic self-energy in Wannier representation (6.34) into (6.32b) and carrying out the

---

[2]The first order contribution to the static self-energy is described by diagram II in Figure 5.3 which vanishes for the crystal momentum representation of the Hamiltonian (3.4). However, it arises in the Wannier representation of (3.8) where the corresponding analytic expression is (5.23).

contour integration to yield for $Q_{\tau\upsilon}(\vec{R}') = Q_{\tau\upsilon}^+(\vec{R}') + Q_{\tau\upsilon}^-(\vec{R}')$

$$
\begin{aligned}
Q_{\tau\upsilon}^+(\vec{R}') &= \sum_{n\in\{N+1\}} \check{m}_\upsilon^{+,(n)}(\vec{0})\, \check{m}_\tau^{+,(n)*}(\vec{R}') \left[\frac{-n_{\vec{R}'\,\tau}\, n_{\vec{0}\,\upsilon}}{(\varepsilon_{\vec{R}'\,\tau} - \check{\omega}_n^+)(\varepsilon_{\vec{0}\,\upsilon} - \check{\omega}_n^+)} \right. \\
&\quad \left. + \frac{n_{\vec{R}'\,\tau}\, \bar{n}_{\vec{0}\,\upsilon}}{(\varepsilon_{\vec{R}'\,\tau} - \varepsilon_{\vec{0}\,\upsilon})(\varepsilon_{\vec{R}'\,\tau} - \check{\omega}_n^+)} - \frac{\bar{n}_{\vec{R}'\,\tau}\, n_{\vec{0}\,\upsilon}}{(\varepsilon_{\vec{R}'\,\tau} - \varepsilon_{\vec{0}\,\upsilon})(\varepsilon_{\vec{0}\,\upsilon} - \check{\omega}_n^+)} \right] \quad \text{(6.35a)} \\
Q_{\tau\upsilon}^-(\vec{R}') &= \sum_{n\in\{N-1\}} \check{m}_\upsilon^{-,(n)}(\vec{0})\, \check{m}_\tau^{-,(n)*}(\vec{R}') \left[\frac{\bar{n}_{\vec{R}'\,\tau}\, \bar{n}_{\vec{0}\,\upsilon}}{(\varepsilon_{\vec{R}'\,\tau} - \check{\omega}_n^-)(\varepsilon_{\vec{0}\,\upsilon} - \check{\omega}_n^-)} \right. \\
&\quad \left. + \frac{n_{\vec{R}'\,\tau}\, \bar{n}_{\vec{0}\,\upsilon}}{(\varepsilon_{\vec{R}'\,\tau} - \varepsilon_{\vec{0}\,\upsilon})(\varepsilon_{\vec{0}\,\upsilon} - \check{\omega}_n^-)} - \frac{\bar{n}_{\vec{R}'\,\tau}\, n_{\vec{0}\,\upsilon}}{(\varepsilon_{\vec{R}'\,\tau} - \varepsilon_{\vec{0}\,\upsilon})(\varepsilon_{\vec{R}'\,\tau} - \check{\omega}_n^-)} \right] . \quad \text{(6.35b)}
\end{aligned}
$$

I proceed as before by defining the auxiliary vectors

$$
(\varepsilon_{\vec{R}'\,\kappa}\mathbb{1} - \check{\boldsymbol{K}}^+ - \check{\boldsymbol{C}}^+)\, \vec{V}_\kappa^+(\vec{R}') = \vec{U}_\kappa^+(\vec{R}'), \qquad n_{\vec{R}'\,\kappa} = 1 \quad \text{(6.36a)}
$$

$$
(\varepsilon_{\vec{R}'\,\alpha}\mathbb{1} - \check{\boldsymbol{K}}^- - \check{\boldsymbol{C}}^-)\, \vec{V}_\alpha^-(\vec{R}') = \vec{U}_\alpha^-(\vec{R}'), \qquad \bar{n}_{\vec{R}'\,\alpha} = 1 \quad \text{(6.36b)}
$$

setting $\vec{U}_\varrho^\pm(\vec{R}) \equiv \vec{U}_{\vec{R}\varrho}^\pm$, and rewrite Equation (6.35) for $Q_{\tau\upsilon}^\pm(\vec{R}')$

$$
\begin{aligned}
Q_{\tau\upsilon}^+(\vec{R}') &= -\vec{V}_\upsilon^{+\dagger}(\vec{0})\, \vec{V}_\tau^+(\vec{R}')\, n_{\vec{R}'\,\tau}\, n_{\vec{0}\,\upsilon} + (\varepsilon_{\vec{R}'\,\tau} - \varepsilon_{\vec{0}\,\upsilon})^{-1} \\
&\quad \times [\vec{U}_\upsilon^{+\dagger}(\vec{0})\, \vec{V}_\tau^+(\vec{R}')\, \bar{n}_{\vec{0}\,\upsilon}\, n_{\vec{R}'\,\tau} - \vec{V}_\upsilon^{+\dagger}(\vec{0})\, \vec{U}_\tau^+(\vec{R}')\, \bar{n}_{\vec{R}'\,\tau}\, n_{\vec{0}\,\upsilon}] \quad \text{(6.37a)} \\
Q_{\tau\upsilon}^-(\vec{R}') &= \vec{V}_\upsilon^{-\dagger}(\vec{0})\, \vec{V}_\tau^-(\vec{R}')\, \bar{n}_{\vec{R}'\,\tau}\, \bar{n}_{\vec{0}\,\upsilon} - (\varepsilon_{\vec{R}'\,\tau} - \varepsilon_{\vec{0}\,\upsilon})^{-1} \\
&\quad \times [\vec{U}_\upsilon^{-\dagger}(\vec{0})\, \vec{V}_\tau^-(\vec{R}')\, n_{\vec{0}\,\upsilon}\, \bar{n}_{\vec{R}'\,\tau} - \vec{V}_\upsilon^{-\dagger}(\vec{0})\, \vec{U}_\tau^-(\vec{R}')\, \bar{n}_{\vec{0}\,\upsilon}\, n_{\vec{R}'\,\tau}] . \quad \text{(6.37b)}
\end{aligned}
$$

The algorithm for Jacobi iterations now reads

$$
\begin{aligned}
\vec{V}_\varrho^{\pm,(0)}(\vec{R}') &= (\varepsilon_{\vec{R}'\,\varrho}\mathbb{1} - \check{\boldsymbol{K}}^\pm)^{-1}\, \vec{U}_\varrho^\pm(\vec{R}') \\
\vec{V}_\varrho^{\pm,(n)}(\vec{R}') &= \vec{V}_\varrho^{\pm,(0)}(\vec{R}') + (\varepsilon_{\vec{R}'\,\varrho}\mathbb{1} - \check{\boldsymbol{K}}^\pm)^{-1}\check{\boldsymbol{C}}^\pm \vec{V}_\varrho^{\pm,(n-1)}(\vec{R}')
\end{aligned} \quad \text{(6.38)}
$$

and the inhomogeneous linear system of equations (6.31a) can be solved for $\Sigma_{\varrho\sigma}^\infty(\vec{R})$ by a matrix inversion again (6.29) [84]

$$
\vec{\Sigma}^\infty = (\mathbb{1} - \boldsymbol{A})^{-1}\, \vec{b}, \quad \text{(6.39)}
$$

where a check accent is affixed to indicate that Wannier orbitals rather than Bloch orbitals are used. Note that $\boldsymbol{\Sigma}^\infty(\vec{R})$ is *not* Hermitian. Hence the full static self-energy matrix has to be included in $\vec{\Sigma}^\infty$ explicitly for several lattice vectors $\vec{R}$. However, the property $\boldsymbol{\Sigma}^{\infty\dagger}(\vec{R}) = \boldsymbol{\Sigma}^\infty(-\vec{R})$ holds which can be utilized to reduce the dimension of (6.39).

6.3 Dyson equation

Having determined approximations for the static (6.30) and the dynamic self-energy (6.16) in terms of Wannier orbitals, I can finally determine the positions and strengths of the

poles of the one-particle Green's function from formula (5.16). [The pole positions and strengths of the Green's function—using Bloch orbitals to represent the self-energy (6.23) and (6.6)—can be obtained following a nearly identical line of argument.] To this end, the small Hermitian eigenvalue problem

$$(\boldsymbol{\varepsilon}(\vec{k}) + \boldsymbol{\Sigma}^\infty(\vec{k}) + \boldsymbol{M}(\vec{k}, \omega))\, \vec{\breve{x}}_\mathrm{G}(\vec{k}, \omega) = \omega\, \vec{\breve{x}}_\mathrm{G}(\vec{k}, \omega)\,, \tag{6.40}$$

with $\boldsymbol{\varepsilon}(\vec{k})$ being the diagonal matrix of Bloch orbital energies and $\vec{\breve{x}}_\mathrm{G}(\vec{k}, \omega)$ denoting eigenvectors, has to be solved *self-consistently*, i.e., such that the energy ω entering the dynamic self-energy $\boldsymbol{M}(\vec{k}, \omega)$ is identical to the resulting eigenvalue ω.

Dropping the matrices $\boldsymbol{\mathcal{U}}(\vec{k})$, which arise by inserting (6.16) and (6.30) into (6.40) is allowed because eigenvalue problems are invariant under similarity transformations. Defining the *translational symmetry adapted Fock matrix* $\bar{F}_{\varrho\sigma}(\vec{k}) = \sum_{\vec{R}} \mathrm{e}^{\mathrm{i}\vec{k}\vec{R}}\, F_{\varrho\sigma}(\vec{R})$, one arrives at

$$(\bar{\boldsymbol{F}}(\vec{k}) + \bar{\boldsymbol{\Sigma}}^\infty(\vec{k}) + \bar{\boldsymbol{M}}(\vec{k}, \omega))\, \vec{x}_\mathrm{G}(\vec{k}, \omega) = \omega\, \vec{x}_\mathrm{G}(\vec{k}, \omega) \tag{6.41}$$

where the new quantities $\bar{\boldsymbol{F}}(\vec{k})$, $\bar{\boldsymbol{\Sigma}}^\infty(\vec{k})$, $\bar{\boldsymbol{M}}(\vec{k}, \omega)$, and $\vec{x}_\mathrm{G}(\vec{k}, \omega)$ are related to the original ones $\boldsymbol{\varepsilon}(\vec{k})$, $\boldsymbol{\Sigma}^\infty(\vec{k})$, $\boldsymbol{M}(\vec{k}, \omega)$, and $\vec{\breve{x}}_\mathrm{G}(\vec{k}, \omega)$ by

$$\varepsilon_{pq}(\vec{k}) = \sum_{\varrho,\sigma} \mathcal{U}_{p\varrho}(\vec{k})\, \mathcal{U}_{q\sigma}^*(\vec{k})\, \bar{F}_{\varrho\sigma}(\vec{k}) \tag{6.42a}$$

$$\Sigma_{pq}^\infty(\vec{k}) = \sum_{\varrho,\sigma} \mathcal{U}_{p\varrho}(\vec{k})\, \mathcal{U}_{q\sigma}^*(\vec{k})\, \bar{\Sigma}_{\varrho\sigma}^\infty(\vec{k}) \tag{6.42b}$$

$$M_{pq}(\vec{k}, \omega) = \sum_{\varrho,\sigma} \mathcal{U}_{p\varrho}(\vec{k})\, \mathcal{U}_{q\sigma}^*(\vec{k})\, \bar{M}_{\varrho\sigma}(\vec{k}, \omega) \tag{6.42c}$$

$$\breve{x}_{\mathrm{G},p}(\vec{k}, \omega) = \sum_{\varrho} \mathcal{U}_{p\varrho}(\vec{k})\, x_{\mathrm{G},\varrho}(\vec{k}, \omega)\,. \tag{6.42d}$$

Inserting the ADC form of the dynamic self-energy (6.16) into (6.41) and defining[3]

$$\vec{x}^\pm(\vec{k}, \omega) = (\omega\, \mathbb{1} - \bar{\boldsymbol{K}}^\pm(\vec{k}) - \bar{\boldsymbol{C}}^\pm(\vec{k}))^{-1}\, \bar{\boldsymbol{U}}^\pm(\vec{k})\, \vec{x}_\mathrm{G}(\vec{k}, \omega), \tag{6.43}$$

with the modified interaction matrices $\bar{\boldsymbol{U}}^\pm(\vec{k}) = (\cdots \vec{\bar{U}}_\sigma^\pm(\vec{k}) \cdots)$, yields the following form of the eigenvalue problem (6.41)

$$(\bar{\boldsymbol{F}}(\vec{k}) + \bar{\boldsymbol{\Sigma}}^\infty(\vec{k}))\, \vec{x}_\mathrm{G}(\vec{k}, \omega) + \bar{\boldsymbol{U}}^{+\dagger}(\vec{k})\, \vec{x}^+(\vec{k}, \omega) + \bar{\boldsymbol{U}}^{-\dagger}(\vec{k})\, \vec{x}^-(\vec{k}, \omega) = \omega\, \vec{x}_\mathrm{G}(\vec{k}, \omega)\,. \tag{6.44}$$

Rewriting Equation (6.43) as

$$\bar{\boldsymbol{U}}^\pm(\vec{k})\, \vec{x}_\mathrm{G}(\vec{k}, \omega) + (\bar{\boldsymbol{K}}^\pm(\vec{k}) + \bar{\boldsymbol{C}}^\pm(\vec{k}))\, \vec{x}^\pm(\vec{k}, \omega) = \omega\, \vec{x}^\pm(\vec{k}, \omega)\,, \tag{6.45}$$

it becomes evident that formulas (6.44) and (6.45) can be recast as a joint Hermitian eigenvalue problem

$$\boldsymbol{B}(\vec{k})\boldsymbol{X}(\vec{k}) = \boldsymbol{X}(\vec{k})\boldsymbol{E}(\vec{k}), \qquad \boldsymbol{X}^\dagger(\vec{k})\, \boldsymbol{X}(\vec{k}) = \mathbb{1}$$

$$\boldsymbol{B}(\vec{k}) = \begin{pmatrix} \bar{\boldsymbol{F}}(\vec{k}) + \bar{\boldsymbol{\Sigma}}^\infty(\vec{k}) & \bar{\boldsymbol{U}}^{+\dagger}(\vec{k}) & \bar{\boldsymbol{U}}^{-\dagger}(\vec{k}) \\ \bar{\boldsymbol{U}}^+(\vec{k}) & \bar{\boldsymbol{K}}^+(\vec{k}) + \bar{\boldsymbol{C}}^+(\vec{k}) & \boldsymbol{0} \\ \bar{\boldsymbol{U}}^-(\vec{k}) & \boldsymbol{0} & \bar{\boldsymbol{K}}^-(\vec{k}) + \bar{\boldsymbol{C}}^-(\vec{k}) \end{pmatrix}\,. \tag{6.46}$$

---

[3]Note the close relationship between the vectors $\vec{x}^\pm(\vec{k}, \omega)$ in (6.43) and the vectors $V_r^\pm(\vec{k})$ in (6.25).

The new matrix $\boldsymbol{B}(\vec{k})$ is called the *band structure matrix*. It has to be diagonalized for several $\vec{k}$-points yielding eigenvalues $e_n(\vec{k}) = (\boldsymbol{E}(\vec{k}))_{nn}$ and eigenvectors $\vec{X}_n(\vec{k}) = (\vec{x}_{\mathrm{G}}(\vec{k}, e_n(\vec{k}))^{\mathrm{T}}, \; \vec{x}^+(\vec{k}, e_n(\vec{k}))^{\mathrm{T}}, \; \vec{x}^-(\vec{k}, e_n(\vec{k}))^{\mathrm{T}})^{\mathrm{T}}$. Equation (6.46) is similar to the result for molecules [87] where the diagonalization of the ADC form (6.16) also sums, via the molecular equivalent of (6.3), infinitely many proper self-energy diagrams before its result is put into the Dyson equation (5.15) to sum all improper self-energy diagrams that derive from those contained in the ADC form.

The spectral representation of the one-particle Green's function (5.6) reads, in terms of the eigenpairs of (6.46),

$$G_{pq}(\vec{k}, \omega) = \sum_n \frac{\bar{x}_p^{(n)}(\vec{k}) \, \bar{x}_q^{(n)*}(\vec{k})}{\omega - e_n(\vec{k})} \; , \tag{6.47}$$

where $\bar{x}_p^{(n)}(\vec{k}) = (\boldsymbol{X}(\vec{k}))_{pn}$ denotes the transition amplitude of the n-th state which are given by either the $x_p^{(n)}(\vec{k})$ or the $y_p^{(n)}(\vec{k})$ in (5.7).

In some cases, the external Wannier orbitals of the dynamic self-energy are restricted to a single cell of the crystal, i.e., $\boldsymbol{M}(\vec{k}, \omega) \approx \boldsymbol{M}(\vec{R} = \vec{0}, \omega)$, the so-called *one-lattice-site approximation* for the dynamic self-energy. Note, however, that configurations in neighboring unit cells are not *entirely* excluded. The $\vec{k}$-dependence is *solely* mediated by the one-particle matrix $\bar{\boldsymbol{F}}(\vec{k}) + \bar{\boldsymbol{\Sigma}}^\infty(\vec{k})$. The static self-energy can also be evaluated in one-lattice-site approximation. Then the $\vec{k}$-dependence is exclusively due to $\bar{\boldsymbol{F}}(\vec{k})$ and this approximation to the CO-ADC equations becomes similar to the *dynamical mean field theory (DMFT)* [22].

6.4 Configuration selection

The convergence of the lattice sums occurring in the Feynman-Dyson perturbation series of the one-particle Green's function (5.13) is granted by the reasoning of Sun and Bartlett [166] in Section 3.3 for the crystal momentum representation of the Hamiltonian (3.4). The lattice sums also converge in the case of the Wannier representation (3.8) as it basically evolves from (3.4) by means of the inverse Wannier transformation (2.33).

Although the convergence of lattice sums is granted principally, I have to devise an algorithm for their proper truncation [1], a dynamical building of the configuration space is required which means to meet a chosen accuracy in the lattice sums for a given crystal. The appropriate truncation of lattice sums is an essential ingredient of all real *ab initio* methods for crystals and corresponds to a *configuration selection* procedure which ensures that the configuration space is sufficiently large for the desired accuracy of the $N \pm 1$ excited states but still sufficiently small to be tractable on present-day computers. In molecular physics, configuration selection has been introduced in the context of the configuration interaction method [255] which suffers from an exponentially growing configuration space with respect to the number of atoms in molecules. The techniques discussed in Reference [255] are not applicable here, as they are designed with the configuration interaction method in mind, but there are analogs for crystals which are similar in spirit.

In the incremental scheme for ground states of crystals [1,2,38,43–45,152] [Sections 3.3 and 3.4], the total configuration space of a crystal is partitioned into one-body orbital sets (3.14) which are used in a subsequent calculation of the correlation energy to yield energy increments (3.16) and (3.17). Frequently, explicit manual configuration selection is applied [Chapter 3]. This allows the partition of the configuration space to be chosen following chemical intuition. The situation is much more cumbersome for band structures because the number of distinct excited states grows with the number of correlated electrons, i.e., the number of orbitals which are considered in (6.6) or (6.16). In the local Hamiltonian approach, the number of states to be calculated is restricted to a fixed number which is treated in an incremental way [63–67,72]. Albrecht and Igarashi [68,69] ensure the convergence of an incremental series for the self-energy for $\omega = 0$, a criterion which is independent of the number of states actually described.

I devise here a configuration selection procedure that is perfectly adapted to the structure of the CO-ADC theory. For the CO-ADC in terms of Bloch orbitals [Sections 6.1.1 and 6.2.1], $\vec{k}$-points are chosen employing Born von Kármán boundary conditions which lead to a net of equidistant $\vec{k}$-points [3,6]. In this case, configuration selection means choosing a sufficiently dense net in conjunction with a cutoff criterion which is similar to the one for CO-ADC in terms of Wannier orbitals [Sections 6.1.2 and 6.2.2] discussed in the next paragraph. Yet, beforehand, one should interpret the impact of the number of $\vec{k}$-points used for Brillouin zone integration by recalling the transformation to the supercell form in Section 6.1.2. Using a given net of N_0 $\vec{k}$-points to carry out a Wannier transformation (2.33), a CO-ADC in Bloch orbitals can be immediately represented and analyzed in terms of the supercell form (6.12). However one should emphasize that the redundancies of this representation—which is utilized here for interpretation only—are not present in the Bloch orbital formulation of CO-ADC. The supercell form affords a tight-binding interpretation: within the supercell, the number of distinct neighbors to the origin cell is restricted by the volume of the supercell. Distinct interaction terms among the cells, i.e., the Fock matrix, and two-electron integrals, are thus also resticted and the number of $\vec{k}$-points employed can thus be understood to imply the number of nearest-neighbor cells treated in the interaction terms. These arguments generalize the tight-binding arguments given, e.g., in Reference [109], in conjunction with a single Brillouin zone integration of a crystal momentum dependent function, to the multi-dimensional case.

Configuration selection in crystal momentum representation is not intuitive and does not allow a fine grained selection of configurations within unit cells and between an origin cell and its neighbor cells. For crystals with large unit cells this is a significant restriction. To obtain a suitable cutoff criterion for CO-ADC in terms of Wannier orbitals, I evaluate the second order diagram of the retarded dynamic self-energy (5.24) [83,87] and examine the summand therein

$$\frac{V_{\vec{0}\,\varrho\,\vec{g}_1\,\kappa\,[\vec{g}_2\,\alpha\,\vec{g}_3\,\beta]}\,V^*_{\vec{R}\,\sigma\,\vec{g}_1\,\kappa\,[\vec{g}_2\,\alpha\,\vec{g}_3\,\beta]}}{\omega + \varepsilon_{\vec{g}_1\,\kappa} - \varepsilon_{\vec{g}_2\,\alpha} - \varepsilon_{\vec{g}_3\,\beta}}\,n_{\vec{g}_1\,\kappa}\,\bar{n}_{\vec{g}_2\,\alpha}\,\bar{n}_{\vec{g}_3\,\beta}\,. \tag{6.48}$$

The most delocalized occupied orbitals are the valence orbitals. Therefore, the occupied valence orbitals couple to the most important $2p1h$-configurations. Hence, ω can be assumed to be of the order of the band gap. The denominator in (6.48) is regarded to

be constant to a reasonable degree. It is thus considered as being part of the cutoff threshold. Therefore, if $V_{\vec{0}\,\varrho\,\vec{g}_1\,\kappa\,[\vec{g}_2\,\alpha\,\vec{g}_3\,\beta]}\,V^*_{\vec{R}\,\sigma\,\vec{g}_1\,\kappa\,[\vec{g}_2\,\alpha\,\vec{g}_3\,\beta]}\,n_{\vec{g}_1\,\kappa}\,\bar{n}_{\vec{g}_2\,\alpha}\,\bar{n}_{\vec{g}_3\,\beta}$ is above a certain cutoff threshold for some combination of $\vec{0}\,\varrho$ and $\vec{R}\,\sigma$, I include the corresponding $2p1h$-configuration $(\vec{g}_1\,\kappa, \vec{g}_2\,\alpha, \vec{g}_3\,\beta)$ in the configuration space. If the product is small for all external Wannier orbitals of the self-energy, $(\vec{g}_1\,\kappa, \vec{g}_2\,\alpha, \vec{g}_3\,\beta)$ is neglected completely by setting all two-electron integrals containing this configuration *exactly* to zero. By this, only a finite range of the residual Coulomb interaction, which is not treated in Hartree-Fock approximation, is explored. The same arguments hold for the selection of $2h1p$-configurations for the evaluation of the advanced dynamic self-energy.

Convergence of the configuration space, i.e., the number of unit cells contributing configurations to be considered in the cutoff criterion (6.48), is expected to be sufficiently quick as the two-electron matrix elements decay rapidly with the distance of a single Wannier orbital from the centroid of the $2p1h$- and $2h1p$-configurations. Long-range effects in the $N\pm1$ particle system, which are also present in the ground state of the N particle system, i.e., van der Waals dispersion interactions, are expected to be nearly equal in the N and the $N\pm1$ particle systems and thus almost cancel in quasiparticle band structure calculations. The long range effect, caused by the extra Coulomb charge that occurs in $N\pm1$ particle states, is nevertheless effective and causes an overall *polarization* of non-metallic crystals. It can be accounted for by adjusting the chemical potential $\mu^\pm$ of the added or removed electron, accordingly, using a continuum approximation [1, 2, 63, 64, 67, 71].

Having introduced a convenient method to truncate the configuration space for CO-ADC, I have to elucidate the physical impact of configuration selection. The modified coupling amplitudes (6.16b) in the band structure matrix (6.46) of a crystal carry two independent lattice vectors $\vec{g}_1'$ and $\vec{g}_2'$. If $\vec{g}_1'$ and $\vec{g}_2'$ are sufficiently far away from the origin cell, all two-electron matrix elements (6.19a) which contribute to the modified coupling amplitude $U^\pm_{\sigma\,;\,\vec{g}_1'\,\vec{g}_2'\,\kappa'\,\alpha'\,\beta'}(\vec{k})$ fall, for all σ, below the configuration selection threshold and are therefore zero. Because the modified interaction matrices (6.19c) vanish in CO-ADC(2,2) approximation and Equation (6.16c) thus denotes diagonal matrices, the eigenvalue associated with the configuration $(\vec{g}_1'\,\vec{g}_2'\,\kappa'\,\alpha'\,\beta')$ is simply given by the diagonal element $(\bar{\boldsymbol{K}}^\pm(\vec{k}))_{\vec{g}_1'\,\vec{g}_2'\,\kappa'\,\alpha'\,\beta'\,;\,\vec{g}_1'\,\vec{g}_2'\,\kappa'\,\alpha'\,\beta'}$, with an eigenvector being unity on position $\vec{g}_1'\,\vec{g}_2'\,\kappa'\,\alpha'\,\beta'$ and zero elsewhere. Consequently, such an eigenstate of $\boldsymbol{B}(\vec{k})$ is removed by deleting the column and the row $\vec{g}_1'\,\vec{g}_2'\,\kappa'\,\alpha'\,\beta'$ in $\boldsymbol{B}(\vec{k})$ because the transition amplitude (5.7) for the n-th state vanishes and thus it does not contribute to the spectral representation of the one-particle Green's function (6.47).

A further consequence of configuration selection involves the lattice summations over $\vec{R}$ in (6.16b) and (6.16c). In the first place, I consider a crystal with a macroscopic lattice constant which consists of N_0 unit cells. As a result of configuration selection, only Fock and two-electron matrix elements that involve Wannier orbitals from a single unit cell, specifically the origin cell, are non-zero. Therefore, in Equations (6.16b) and (6.16c), the lattice sums run over only the single term for $\vec{R}=\vec{0}$ with $\vec{g}_1=\vec{g}_2=\vec{0}$ and the resulting band structure matrix (6.46) is consequently independent of $\vec{k}$. As the Brillouin zone contains N_0 crystal momenta, I obtain a N_0-fold degenerate spectrum similarly to simple tight-binding models [3]. In typical crystals, interactions with neighboring unit cells are

important. Yet, a sufficiently large supercell which consist of n_0 unit cells can be chosen such that interactions between supercells are negligible leading to a N_0/n_0 fold degenerate spectrum. In other words, a cutoff threshold, to be used for the selection of Fock matrix elements and $2p1h$- and $2h1p$-configurations, implies a definition of degeneracy of the physical states in my model of the crystal.

To selectively diagonalize the band structure matrix, one uses an iterative eigenvalue solver, e.g., a *block-Lanczos algorithm* [127, 256, 257], that is capable of exploiting the sparsity of $\boldsymbol{B}(\vec{k})$. The most expensive step of the block-Lanczos algorithm is a matrix times vector product between $\boldsymbol{B}(\vec{k})$ and the *Lanczos vectors* which determines the overall performance of the eigenvalue solver [74, 127, 128, 257].[4] To investigate the scaling of a selective computation of eigenpairs, I consider a supercell consisting of two unit cells of the original lattice. Let me assume a crystal with a macroscopic lattice constant to investigate the asymptotic scaling behavior of the problem. Then, the configuration selection method of the previous paragraphs selects only configurations local to the individual unit cells. Hence, the resulting configuration space scales *linearly* with the system size, i.e., the number of atoms per unit cell. This is a necessary condition for the selective diagonalization of the band structure matrix (6.46) to scale linearly as well. The total Fock matrix of the supercell is also block-diagonal with the two identical Fock matrices of the constituting unit cells on its diagonal. Similarly, the modified coupling amplitudes (6.16b) only contain two non-zero blocks which describe the coupling of $2p1h$- and $2h1p$-configurations to the Fock matrix of each of the two constituting unit cells of the supercell such that the total band structure matrix decomposes into two subproblems that can be solved independently. A single matrix times vector product for the supercell requires twice as many floating point operations than are needed for a matrix times vector product for one of the two unit cells in the supercell. Hence, the computation of matrix times vector products scales *linearly* with the system size.[5] Yet, doubling the system size also usually means, that I am interested in twice as many excited states. Hence, the overall effort to determine all excited states of a crystal in a given energy range scales quadratically. It is a *quadratically* scaling problem, where linear scaling can only be achieved by an *a priori* restriction to a few excited states of the system.

For typical crystals, the Fock matrix of a supercell is not block-diagonal which implies another doubling of the number of floating point operations upon doubling the system size. Yet, this factor cancels in most cases as the number of $\vec{k}$-points needed for a given accuracy of the integration over the Brillouin zone of the supercell is halved because the volume of its Brillouin zone is half the volume of the Brillouin zone which corresponds to the original crystal lattice [3].

---

[4] Specifically in CO-ADC(2) for Bloch orbitals, a single matrix times vector operation requires $N_{\text{flops}} = 2\left[N_{\boldsymbol{F}(\vec{k})}^2 + (2N_{\boldsymbol{F}(\vec{k})} + 1)(N_{\boldsymbol{K}^+(\vec{k})} + N_{\boldsymbol{K}^-(\vec{k})})\right] = O(N_{\boldsymbol{F}(\vec{k})}N_{\boldsymbol{K}^+(\vec{k})})$ flops. Here $N_{\boldsymbol{A}}$ denotes the number of rows of the square matrix $\boldsymbol{A}$. By affixing bar accents to the matrices showing up in the expression for N_{flops}, I immediately obtain the corresponding formula for the number of flops required in the CO-ADC(2,2) approximation for Wannier orbitals.

[5] The number of (block-)Lanczos iterations, necessary to determine the eigenvalues and eigenvectors of the band structure matrix (6.46) with a given accuracy, is assumed to be the same for a single unit cell and a supercell consisting of two unit cells.

7 Hydrogen fluoride and lithium fluoride compounds

This chapter is devoted to the study of the energy levels of compounds that are formed by the elements hydrogen and lithium with fluorine. In the first place, I investigate the ionization potentials of isolated diatomic HF and LiF molecules in Section 7.1. Apart from test calculations in Section 7.1.2, electron affinities are not regarded, as they represent scattering states which are sensitive to the basis set and require a sophisticated non-Hermitian resonance treatment [67, 74, 128, 131, 132, 258].

Thereafter, the changes in the energy levels of the two molecules upon crystallization are studied. I turn to the single $(HF)_\infty$ chain of Chapter 4 which represents the simplest realistic model of a HF crystal in Section 7.2 and investigate bulk LiF in Section 7.3. I adopt a quasiparticle point of view to investigate the outer valence states and the lowest virtual states of the two solids.

7.1 Hydrogen fluoride and lithium fluoride molecules

7.1.1 Ionization potentials

Hydrogen fluoride and lithium fluoride are two diatomic molecules of $C_{\infty v}$ symmetry [259]. The experimental values for the internuclear distances are $0.91680\,\text{Å}$ for HF and $1.5639\,\text{Å}$ for LiF [259]. I carry out a *Mulliken* and a *Löwdin population analysis* [39–42, 260] of the Hartree-Fock density matrix utilizing GAMESS-UK [261] in conjunction with the cc-pVDZ basis set [48, 49]. The resulting *population numbers* are displayed in Table 7.1. HF turns out to be less ionic than LiF which can be understood by the difference in electronegativity between the elements hydrogen and lithium on the one hand and fluorine on the other hand. Hydrogen and lithium only have comparatively low electronegativities of 2.2 and 1.0, respectively, whereas fluorine is the element with the highest electronegativity 4.0 of all elements in the periodic table [230]. Therefore, fluorine draws electrons from hydrogen and lithium atoms whereby hydrogen donates substantially less partial charge to fluorine, -0.2 to -0.4. The by 71% larger internuclear distance in LiF compared to HF is traced back to the fact that only a bare proton with a diameter of $1\,\text{fm}$ would remain once hydrogen was fully ionized. Instead lithium attains to a helium configuration where the nuclear charge is still shielded by the lower lying Li $1s$ shell with a diameter which is orders of magnitude larger.

The ionization spectra of the two molecules are shown in Figure 7.1. They are obtained in two different ways, once directly by exploiting Koopmans' theorem [39–42, 143] and once by the Dyson ADC(3) program of Tarantelli [87, 262] which is based on canonical molecular orbitals. On the abscissa I give the IP while the ordinate indicates the pole

Compound	Atom	Nuclear charge	Mulliken population	Löwdin population
HF	H	1	0.76	0.89
	F	9	9.24	9.12
LiF	Li	3	2.38	2.64
	F	9	9.62	9.36

Table 7.1: Population numbers according to Mulliken and Löwdin for HF and LiF molecules.

strength of each hole state which is a measure of its one-particle character. It is unity for IPs resulting from Hartree-Fock theory.

Many of the characteristics of the ionization spectra of the two molecules can already be understood in terms of the independent particle model. The *outer valence region* of the molecules is formed by two distinct IPs in the range of 15–20 eV for HF and 10–15 eV for LiF. By inspecting the molecular orbitals, I find the lowest IPs of HF and LiF to correspond to an ionization from the two π-type lone pairs on fluorine which are twofold degenerate. Ionization from the third π-type lone pair of fluorine requires more energy as it is oriented towards either the hydrogen or the lithium atom and thus is attracted by their positive partial charges [Table 7.1]. The molecular orbital of predominantly F $2s$ character constitutes the *inner valence region* in both molecules which is situated around 40 eV in HF and around 35 eV in LiF. For the two ionization spectra, the differences between hydrogen and lithium atoms basically manifest in two effects. Firstly, there is an overall shift of all IPs of LiF to lower energies with respect to corresponding IPs in HF because in lithium the nuclear charge is shielded by the lower lying Li $1s$ shell.[1] Secondly, the larger internuclear distance in LiF than in HF causes a weaker interaction between lithium and fluorine atoms compared to the interaction between hydrogen and fluorine atoms. Consequently, I observe a smaller splitting of the outer valence IPs of LiF with respect to HF.

The simple independent particle view on the ionization spectra of HF and LiF changes considerably as soon as one accounts for electron correlations. They lead to a considerable shifting of the IPs of all main states to lower energies with respect to the corresponding Hartree-Fock values [1]. The shift of the IPs in the outer valence region with respect to their Hartree-Fock values is of the same magnitude for the two molecules. The energy splitting of the IPs from ADC(3) is slightly increased in HF whereas it is slightly decreased in LiF. The approximately uniform shift of the outer valence IPs of HF and LiF indicates that electron correlations for these states are dominated by the fluorine atom and is essentially unaltered upon formation of the molecular bond. This solidifies the given assignment for these IPs discussed in the previous paragraph.

The correlation effects in the inner valence region of both molecules are much more fascinating. Here a striking manifestation of many-particle effects occurs. In the ion-

---

[1]This observation can be compared to studies of the ionization spectra of the xenon fluorides where a shift of the inner valence (and core) IPs is also observed. There, the addition of fluorine atoms leads to a reduced screening of the nuclear charge of the xenon atom [74, 75].
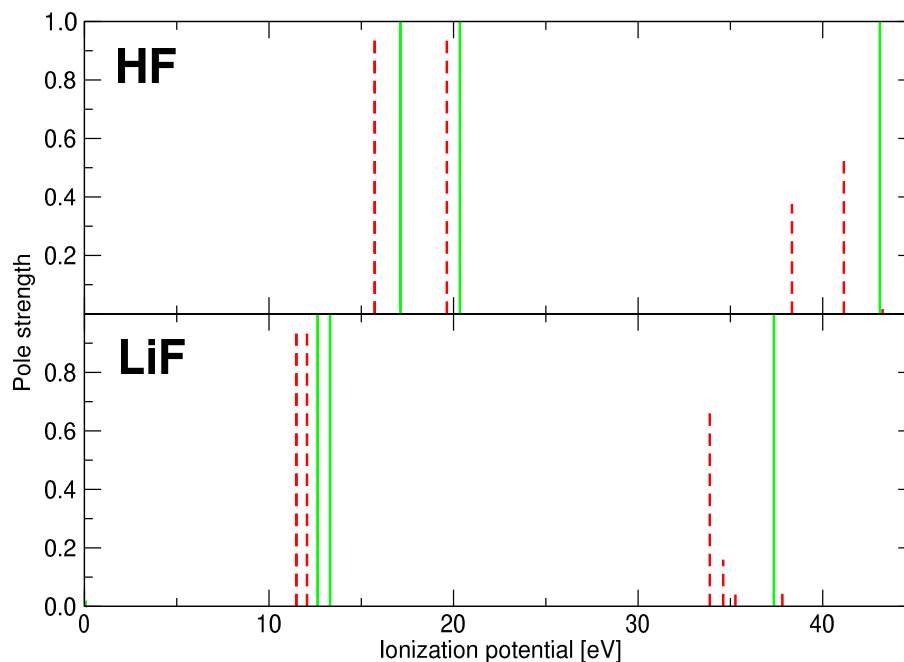
Figure 7.1: (Color) Ionization spectra of a HF and a LiF molecule. Solid green lines denote Hartree-Fock ionization potentials (Koopmans' theorem [39–42, 143]), dashed red lines depict results of the Dyson ADC(3) program of Tarantelli [87, 262] which is based on canonical molecular orbitals.

ization spectrum of HF, one observes a *shake-down satellite* at $\approx 38\,\mathrm{eV}$. The remnant of the independent particle state, the so-called *main state* is found at $\approx 41\,\mathrm{eV}$. This well-known phenomenon results from a strong admixture of two-particle-one-hole- and two-hole-one-particle-configurations ($2h1p$- and $2p1h$-configurations) to the description of the hole states and is termed *strong correlations* or *breakdown of the molecular orbital picture of ionization* [1, 1, 73–75]. In LiF, I observe a series of *shake-up satellites* aside of the main state at $38\,\mathrm{eV}$ but correlation effects seem to be less pronounced. For HF, the appreciable splitting of the independent particle state into two states of similar pole strength indicates that one may suggest a two-level-system-type of process as an explanation which is superimposed on the overall correlation effects. The canonical molecular orbital, which is mainly of F $2s$ type, is also of noticeable amplitude around the hydrogen nucleus. This suggests that the description of hole states that predominantly involve this orbital are influenced by both nuclei which leads to the observed splitting. The reasoning is supported further by the observation that the shift of the mean of the two inner valence IPs in HF with respect to the Hartree-Fock value is roughly the same as it is in LiF. Additionally, the nearly identical magnitude of the shifts implies that the correlation effects in the inner valence regions are also dominated by the fluorine atom. Moreover, the inner valence IPs are found to shift larger towards lower energies than the IP in the outer valence region.

$IP_{Koopmans}$	$IP_{2,2}$	$IP_{2,3}$	$IP_{2,\infty}$	$IP_{2,\infty}^{ND}$	PS
43.059	39.236	39.727	39.715	39.698	31.2
		38.183	38.157	38.142	60.4
20.300	18.922	18.638	18.549	18.597	94.6
(2×) 17.105	14.637	14.217	14.256	14.261	92.9

Table 7.2: Ionization potentials of a HF molecule as obtained in Hartree-Fock approximation $IP_{Koopmans}$ by Koopmans' theorem [39–42,143]) and various variants of ADC using all diagrams of the two-electron interaction up to second order in conjunction with off-diagonal elements of the Fock matrix being treated in second or third order of perturbation theory, $IP_{2,2}$ or $IP_{3,2}$, respectively, or exactly $IP_{\infty,2}$. The data from a non-Dyson ADC(∞,2) for canonical molecular orbitals is labelled as $IP_{\infty,2}^{ND}$. Here PS are the pole strengths.

$EA_{Koopmans}$	$EA_{2,2}$	$EA_{2,3}$	$EA_{2,\infty}$	PS
-4.985	-4.703	-4.685	-4.682	99.5
-21.962	-21.021	-20.922	-20.895	98.7

Table 7.3: Electron affinities of a HF molecule. Symbols are chosen as in Table 7.2 with "IP" replaced by "EA".

7.1.2 Local orbital algebraic diagrammatic construction

CO-ADC theory was devised for canonical (Bloch) orbitals (6.6), (6.22) and local (Wannier) orbitals (6.16), (6.39) in Chapters 5 and 6. Special care was required to handle the matrix representation of the Fock operator. It is diagonal (3.4) in canonical orbitals, however, becomes block-diagonal by the transition to local orbitals (3.8). Two ways were discussed in Chapter 6 to handle this situation. Once, I treated the full Fock matrix exactly in all stages of CO-ADC theory; the other time, I proposed a decomposition of the Fock matrix into a diagonal and an off-diagonal contribution with a subsequent perturbative treatment of the off-diagonal Fock matrix elements. The accuracy of the additional perturbative approximation in the latter approach has not been examined so far and still needs a critical assessment which is carried out in the following. There are a few well-tested ADC packages, which are based on canonical molecular orbitals like the Dyson ADC(3) program of Tarantelli [87, 262] used in the previous Section 7.1.1 or the non-Dyson ADC(2) program of Breidbach [263, 264]. Both programs employ canonical molecular orbitals. They are well suited to provide reference data. The accuracy of a perturbative treatment of the off-diagonal Fock matrix elements is studied for the simple HF molecule as a test case.

To this end, one has to devise a *local orbital ADC scheme* for molecules, first. This can most easily be done, both analytically and numerically, by starting from the CO-ADC equations described in Chapters 5 and 6. Let each unit cell of a crystal with a macroscopic lattice constant be occupied by a given molecule. Following the arguments of Section 6.4, only Fock matrix elements and two-electron integrals within the origin cell are selected for band structure calculations. In other words, all states are N_0 fold degenerate and the band structure matrix has only to be diagonalized at the Γ point to obtain all distinct

energy levels of the crystal. They can be identified with the energy levels of the molecule. By this line of argument, it is justified to drop the lattice sums and lattice vectors totally in Equations (6.16) and (6.39) to obtain analytical expressions for the local orbital ADC scheme.

The Hartree-Fock calculations are carried out with the WANNIER program [30,31] which yields *a priori* Wannier orbitals [Section 2.5]. Let the HF molecule constitute each unit cell of a one-dimensional lattice [Figure 2.1] with a constant of $1\,\mu$m. This assures that interactions with neighboring unit cells, which contain other HF molecules, are negligible. WANNIER [30, 31] diagonalizes the occupied block of the Fock matrix in the origin cell, so only the virtual block in terms of the crystal projected atomic orbitals of Section 2.6 contains off-diagonal matrix elements in the case of molecules. Based on the WANNIER program [30, 31], I wrote the CO-ADC program [97] which implements local molecular orbital ADC and local crystal orbital ADC. Following Sections 6.1.2 and 6.2.2, the off-diagonal Fock matrix elements and the two-electron integrals can be accounted for in different orders of perturbation theory for the construction of the ADC equations. This implies that the contributions which (partly) involve the one-electron interaction can be treated in order m and the contributions that exclusively represent the two-electron interaction can be treated in order n. This facilitates to take higher order terms into account for the more important part. The resulting approximations for molecules are denoted by local orbital ADC(m,n) scheme. A corresponding nomenclature is used for CO-ADC. To assess the perturbative treatment of off-diagonal Fock matrix elements of the virtual block, I calculate the IPs and EAs of HF using local orbitals. I employ the methods ADC(2,2), ADC(3,2) and an exact treatment of the off-diagonal terms of the Fock matrix denoted here by ADC(∞,2), instead of ADC(2), to be consistent with the notation introduced above. Furthermore, I make use of GAMESS-UK [261] and Breidbach's non-Dyson ADC(∞,2) program [263,264] for IPs which utilizes canonical molecular orbitals. These codes have been developed independently of WANNIER [30,31] and CO-ADC [97]; thus they provide reference data for ionization spectra.

The IPs and EAs are reported in Tables 7.2 and 7.3 and are plotted in Figure 7.2. Already ADC(2,2) yields satisfactory IPs and EAs with respect to ADC(∞,2). The largest difference in the outer valence and virtual states is found for the two-fold degenerate valence IPs in ADC(2,2) which deviate by 0.38 eV or 2.7% from the ADC(∞,2) data whereas the deviation of ADC(3,2) only is 0.04 eV or 0.3%, an improvement to ADC(2,2) by roughly one order of magnitude. In the inner valence region of HF, differences between ADC(2,2) and ADC(3,2) become more apparent. Although the former method is not able to describe the strong correlations observed for the F $2s$ main state accurately, it yields a mean IP nicely between the main state and the satellite found in ADC(∞,2) approximation that is far more accurate than the corresponding Hartree-Fock IP. In ADC(3,2) the description of the ionization process is significantly improved such that the impact of this approximation becomes negligible. Also the inner valence IPs can now hardly be distinguished graphically [Figure 7.2] from the corresponding IPs of ADC(∞,2). The non-Dyson ADC(∞,2) IPs of Table 7.2 are not included in Figure 7.2 because they differ from the Dyson ADC(∞,2) IPs by only a few hundredths of an electronvolt. The origin of the tiny deviations between corresponding IPs of Dyson and non-Dyson ADC is hard to fix. Firstly, the two Hartree-Fock programs GAMESS-UK [261] and WANNIER [30,31] differ. The
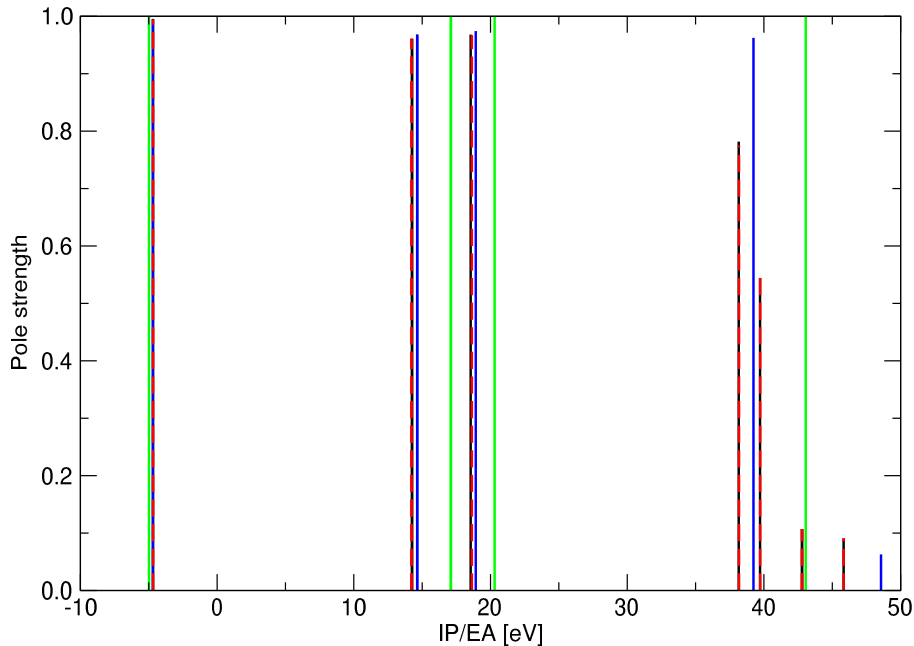
Figure 7.2: (Color) Comparison of the ionization potentials and electron affinities from several methods of a HF molecule. Solid green lines denote Hartree-Fock data (Koopmans' theorem [39–42, 143]) whereas results from correlation calculations are given by solid black lines: ADC(∞,2), solid blue lines: ADC(2,2) and dashed red lines: ADC(3,2).

former program employs conventional cartesian Gaussian functions [39–42] and canonical (virtual) orbitals while the latter employs Gaussian lobe functions [30,31,39,265,266] and projected atomic orbitals as virtual functions [Section 2.6]. Secondly, there is some difference between Dyson ADC [87] and non-Dyson ADC [263] theory which also contributes to the minute deviations found.

The central conclusion of the previous paragraphs is: the off-diagonal Fock matrix elements *can* be treated perturbatively! This result is very important for practical numerical applications because it renders the ADC matrices in my study of the HF molecule sparse where the *sparsity* is measured by

$$S = \frac{N_{\neq 0}}{N_{\mathbf{B}}^2} \ . \tag{7.1}$$

Here $N_{\neq 0}$ is the number of non-zero elements of the $N_{\mathbf{B}} \times N_{\mathbf{B}}$ matrix $\boldsymbol{B}$ is the equivalent to (6.46) for molecules. Values of only a few percent for ADC(2,2) and ADC(3,2) are found. In contrast, for ADC(∞,2) with localized orbitals, the matrix $\boldsymbol{B}$ is approximately half filled. The high value of S for ADC(∞,2) causes the matrix times vector product of a Lanczos vector with $\boldsymbol{B}$ to require a large amount of floating point operations which levels the performance gain of using a block-Lanczos algorithm over a full diagonalization. Consequently, the determination of the eigenvalues of the ADC(∞,2) matrix becomes prohibitively expensive [Section 6.4]. Fortunately, the ADC(∞,2) treatment with localized orbitals can be avoided.
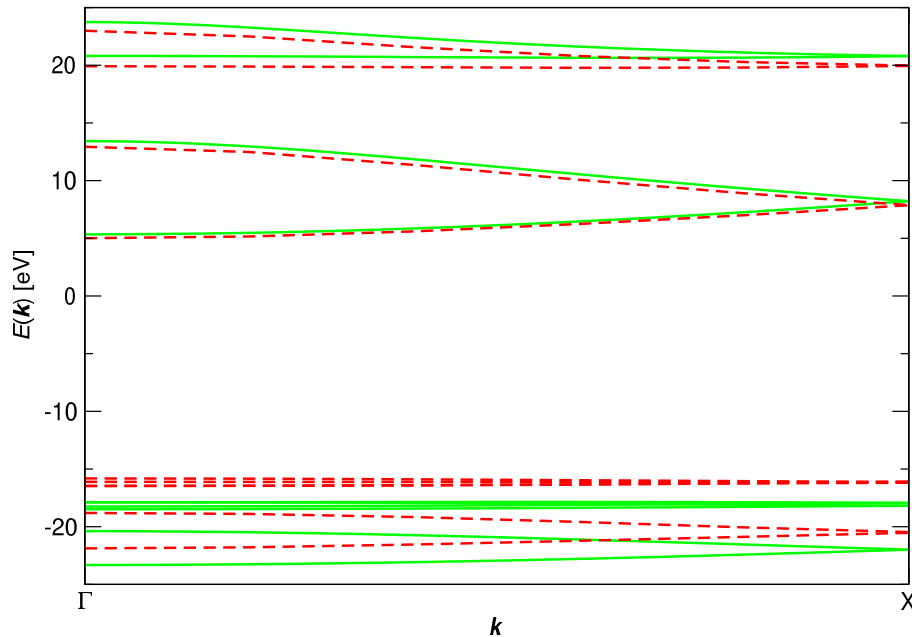
Figure 7.3: (Color) Band structure of a (HF)$_\infty$ chain. Hartree-Fock bands are given by solid green lines. The dashed red lines depict CO-ADC(2,2) quasiparticle bands which are determined by accounting for 2p1h- and 2h1p-configurations involving Wannier orbitals in the origin cell, the nearest and the next nearest-neighbor cells.

7.2 Hydrogen fluoride chain

The single, isolated hydrogen fluoride chain of Chapter 4 represents one of the simplest realistic models for an investigation of the excited states of a three-dimensional crystalline solid. I obtain the Hartree-Fock band structure with the WANNIER program [30, 31]. It is displayed in Figure 7.3. A closeup of the valence bands is shown in Figure 7.4. As a unit cell of the (HF)$_\infty$ chain comprises two HF monomers, the number of Hartree-Fock bands is twice the number of Hartree-Fock energy levels of the HF molecule [Figure 7.1 and Table 7.2]. The four low lying occupied bands, which mainly correspond to F 1s core states and F 2s inner valence states, are left out as well as the higher lying conduction bands.

The Hartree-Fock bands which are situated energetically around -18 eV are formed by the two-fold degenerate π-type lone pairs of mostly F 2p character of the isolated HF molecule at 17.105 eV [Figure 7.1 and Table 7.2]. By inspection of Figure 7.3, I see that the degeneracy of the molecular orbitals is lifted only slightly due to the crystal field upon formation of the infinite chain. The energy bands cross which is allowed because they belong two different irreducible representations with respect to the global mirror plane which contains the zig-zag chain [Figure 4.1].

The energy bands in the range -24 eV to -20 eV are constituted from the third outer valence orbital of the isolated monomer which is also predominantly of F 2p character at 20.300 eV [Figure 7.1 and Table 7.2]. The dispersion of the these two bands is much larger than the dispersion of the four bands discussed in the previous paragraph. It is also
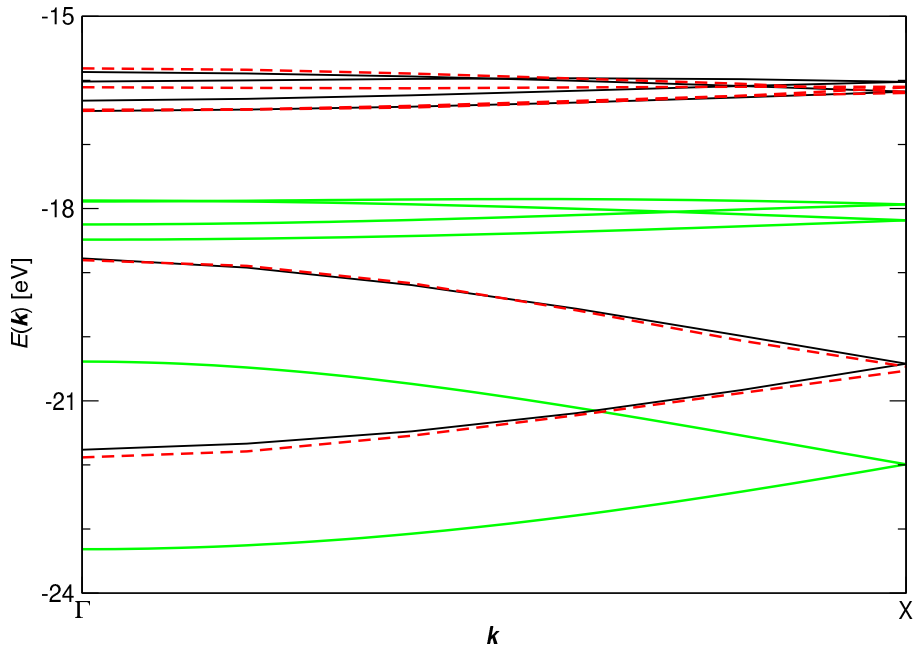
Figure 7.4: (Color) Valence band structure of a $(HF)_\infty$ chain. Zoom into Figure 7.3 where solid black lines denote additionally quasiparticle bands [98] which have been obtained using the local Hamiltonian approach [63–67, 71, 72].

considerably larger than the dispersion of the F $2s$ inner valence bands. This indicates that hydrogen bonding in the $(HF)_\infty$ chain is mainly mediated by the states which correspond to these two outer valence bands.

Berski and Latajka [224] report the Hartree-Fock band structure of the $(HF)_\infty$ chain for a series of basis sets. Among these, the 6-31+G(d,p) basis is of most comparable quality to the cc-pVDZ basis [48, 49]; the plot of the band structure of $(HF)_\infty$ in Figure 3 of Reference [224] agrees very well with the plot in my Figure 7.4. I read off the energy of the top of the valence bands at the Γ point from the plot of the band structure of Berski and Latajka [224]; it lies at -18.3 eV which is very close to my value of -17.9 eV from Table 7.4. The Hartree-Fock band structure of the $(HF)_\infty$ chain has also been studied by Liegener and Ladik [99] who use a double-ζ basis set [$(9s\,5p)\,/\,[3s\,2p]$ for fluorine and $(6s\,1p)\,/\,[2s\,1p]$ for hydrogen] to which they refer as DZP basis set. They obtain an energy of -17.57 eV for the top of the valence bands and 3.57 eV for the bottom of the conduction bands, i.e., the Hartree-Fock band gap amounts to 21.14 eV. The top of the valence bands is only by 0.3 eV smaller than my result at the Γ point and thus in good agreement. However, the bottom of the conduction bands is by 1.78 eV smaller than mine. The deviations between my results and those of Liegener and Ladik [99] can mainly be ascribed to the different basis sets employed cc-pVDZ and DZP, respectively, because the DZP basis set lacks a d-function on fluorine which is present for cc-pVDZ.

In order to investigate the effects of electron correlations in the $(HF)_\infty$ chain, I utilize my CO-ADC program [97], which implements the CO-ADC(2,2) theory of Chapters 5 and 6. The quasiparticle band structure of the $(HF)_\infty$ chain is obtained considering only a minimum fraction, a single unit cell, to form $2p1h$- and $2h1p$-configurations. This causes a

Cells	$E_{\text{top,v}}$	$E_{\text{bottom,c}}$	E_{gap}	$\Delta E_{\text{F}2p}^{<}$	$\Delta E_{\text{F}2p}^{>}$
0	-17.8762	5.3468	23.2230	2.923730	0.609874
1	-15.9747	5.1289	21.1036	2.993117	0.653985
3	-15.8146	5.0108	20.8254	3.077943	0.663644
5	-15.8125	5.0059	20.8184	3.078088	0.663573
7	-15.8122	5.0054	20.8175	3.078094	0.663572

Table 7.4: Convergence of the fundamental band gap E_{gap} and the bandwidth of the lower and upper F $2p$ valence band complexes $\Delta E_{\text{F}2p}^{<}$ and $\Delta E_{\text{F}2p}^{>}$, respectively, of a $(\text{HF})_\infty$ chain with respect to the number of unit cells included in the description of the quasiparticle band structure. "Cells" designates the number of unit cells taken into account in CO-ADC(2,2) calculations where zero refers to the original Hartree-Fock results. Unity denotes the $2p1h$- and $2h1p$-configurations from the origin cell only in correlation calculations. Three, five and seven indicate the additional inclusion of nearest, second nearest and third nearest-neighbor cells, respectively. The top of the valence bands $E_{\text{top,v}}$ and the bottom of the conduction bands $E_{\text{bottom,c}}$ are both situated at the Γ point. All data are given in electronvolt.

pronounced upwards shift by $1.90\,\text{eV}$ of the top of the valence bands whereas the bottom of the conduction bands shifts only by $0.22\,\text{eV}$ downwards. Subsequently, I enlarge the configuration space to include also configurations which extend to the nearest-neighbor cells leading only to slight changes; an additional shift of $0.16\,\text{eV}$ for the top of the valence bands and a shift of $0.12\,\text{eV}$ for the bottom of the conduction bands is observed. Further inclusion of second and third nearest-neighbor cells has only a minute effect. The convergence of several key quantities is summarized in Table 7.4. Namely, the top of the valence bands, the bottom of the conduction bands, the band gap and the width of the upper and the lower F $2p$ band complex. They are compared with the plain Hartree-Fock data (with "0" unit cells for the configuration selection). Clearly, they are fully converged with respect to the number of unit cells included in the CO-ADC(2,2) calculation.

There are two major reasons for the observed correlation corrections with a growing number of unit cells where configurations are regarded. Firstly, as a major effect, electrons successively delocalize over more and more unit cells. This accounts for an improved redistribution of the electrons, i.e., a polarization of the surrounding of the charged origin cell [1], as a reaction to the initial electron attachment or electron removal occurring in the one-particle Green's function (5.1) which propagates by means of electron correlations over the whole crystal.

Secondly, in Section 4.1, basis set convergence is discussed and especially the notion of basis set extension (BSE) [235] is introduced. It means that the description of the electronic structure of an atom is also improved by the one-particle basis sets which are centered on neighboring atoms in Hartree-Fock calculations. By allowing for configurations in neighboring unit cells, the number of configurations accounted for in the band structure matrix (6.46) is considerably enlarged which accordingly leads to BSE effects in correlation calculations as already observed for ground-state correlation energies. BSE becomes significant for the description of the ground-state of hydrogen-bonded crystals due to the weak bonding and the dense packing of the atoms [Chapter 4]. Yet, Table 7.4 reveals that BSE plays only a minor role for the quasiparticle bands of the $(\text{HF})_\infty$ chain

because the key quantities are already nearly converged employing configurations which involve only the Wannier orbitals in the origin cell.

The quasiparticle band structure of the $(HF)_\infty$ chain is shown aside of the Hartree-Fock band structure in Figures 7.3 and 7.4 whereby configurations in up to second nearest-neighbor cells are considered in the CO-ADC(2,2) calculation. Clearly, valence and conduction bands do not shift symmetrically, i.e., by the same amount, upwards and downwards, respectively. Instead, the former show a much stronger influence due to electron correlations.[2] However, the inclusion of nearest-neighbor cells in correlation calculations leads to essentially the same modification on both bands, i.e., this assumption becomes valid for long-range contributions [67].

Occupied Wannier orbitals are spatially less extended than virtual Wannier orbitals with a high probability of the electrons to be close to the nuclei of a crystal. The Hartree-Fock approximation becomes progressively worse the closer the electrons approach each other caused by an insufficient description of the Coulomb hole around the electrons which is especially important in the case of large spatial orbital overlaps [1]. Consequently, I observe pronounced corrections due to electron correlations for valence bands which manifest in a much larger upwards shift compared to the downwards shift of the conduction bands. This observation should also be compared to the discussion of the IPs and EAs of the HF monomer in Figure 7.2. There, I also find that the (outer valence) IPs shift noticeably less with respect to Hartree-Fock IPs than the corresponding shift of the lowest EAs with respect to the independent particle results. Moreover, the top of the F $2p$ band complex, that lies at the Γ point, shifts, due to electron correlations, by $2.1\,eV$ which is somewhat larger than the shift by $1.6\,eV$ of the top of the two inner valence bands also at the Γ point.

Although the quasiparticle bands are shifted appreciably with respect to the corresponding Hartree-Fock bands, they essentially maintain their shape. This observation is in contrast to the pronounced reduction of bandwidths due to electron correlations which are typically found in covalently bonded polymers like *trans*-polyacetylene [66, 71, 72].

In order to investigate the accuracy of the CO-ADC(2,2) method, I compare with theoretical results from other methods. The local Hamiltonian approach [63–67, 71, 72] has been used [98] to calculate quasiparticle bands for the same basis set. The resulting bands are displayed aside of the CO-ADC(2,2) bands in Figure 7.4. The overall excellent agreement is highly encouraging. A comparison of conduction bands is not feasible because the local Hamiltonian approach—in the way it is presently realized computationally—is not capable to deliver them.

Moreover, the outer valence Green's function (OVGF) method has been applied by Liegener and Ladik [99] to the $(HF)_\infty$ chain, employing the DZP basis set. For the top of the valence bands at the Γ point, they obtain $-15.10\,eV$ and $-3.05\,eV$ in second order OVGF and $-15.09\,eV$ and $3.03\,eV$ in third order OVGF. The latter two numbers correspond to an increase of the valence band energy by $2.48\,eV$ and a lowering of the conduction band energy by $0.54\,eV$. In contrast, CO-ADC(2,2) yields an increase by $2.08\,eV$

---

[2]For covalent crystals, it is assumed in Reference [67] that the treatment of electron correlations causes valence and conduction bands to shift by equal amounts upwards and downwards, respectively, at the Γ point to obtain a theoretical estimate of the (direct) band gap of diamond and silicon.

106
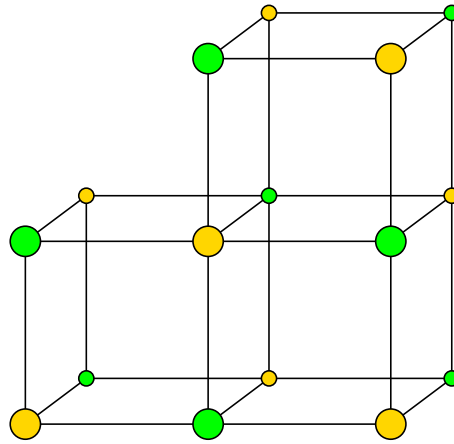
Figure 7.5: (Color) Geometry of a LiF crystal. The lithium and fluorine atoms are represented by yellow and green spheres, respectively.

and a lowering by $0.33\,\text{eV}$. The overall agreement between CO-ADC(2,2) and OVGF is satisfactory. The noticeable deviations between the results of both methods can, as already found for the Hartree-Fock band structures, be attributed predominantly to basis set artifacts.

7.3 Lithium fluoride crystal

As a first application of the CO-ADC method to a three-dimensional crystalline solid, I have chosen lithium fluoride which occurs in nature as the mineral *griceite*. LiF crystal-lizes in a *face-centered-cubic (fcc) rock-salt structure* described by the space group $Fm\bar{3}m$ [Figure 7.5]. The crystal lattice has a two-atomic basis: Li(0,0,0) and F$(\frac{1}{2},\frac{1}{2},\frac{1}{2})$ given in units of the lattice constant[3] $a = 3.990\,\text{Å}$. LiF not only has a wide range of technological applications like in x-ray monochromators or in filters for ultraviolet radiation, e.g., Reference [270] (and References therein), but is also interesting for a number of fundamental physical reasons. It is considered to be the "most ionic substance" and a prototypical insulator which manifests in its very large fundamental band gap (5.8) of[4] $14.1 \pm 0.1\,\text{eV}$ that is the largest one found in nature apart from exotic systems. Some authors even consider LiF to be comparable to a He–Ne rare-gas solid [270]. Its optical spectra show strong excitonic effects which complicates the experimental determination of the band

---

[3]This value for the lattice constant of a LiF crystal is utilized in References [31, 70, 267] and told to originate from the book of Wyckoff [268]. Yet, a value of $4.0173\,\text{Å}$ is reported therein which is consistent with early and recent experimental values. To facilitate comparison, I adopt the previously used value of $3.990\,\text{Å}$. Although the deviation is small, it has a quite noticeable influence on the fundamental band gap which decreased by $0.65\,\text{eV}$ when changing from $3.918\,\text{Å}$ to $4.026\,\text{Å}$ as reported in a recent density functional theory study at the LDA level [269].

[4]The experimental band gap of LiF is communicated in the early work of Roessler and Walker to be $13.60 \pm 0.06\,\text{eV}$ [271–273]. Piacentini [274] estimates the band gap of LiF to be $14.5\,\text{eV}$. This value is refined in Reference [275] to $14.2 \pm 0.2\,\text{eV}$. Shirley *et al.* [270] communicate $14.1 \pm 0.1\,\text{eV}$ from the dissertation of Himpsel.

Cells	$E_{\text{top,v}}$	$E_{\text{bottom,c}}$	E_{gap}	$\Delta E_{\text{F}\,2p}$
0	0	16.24	16.24	4.95
1	0.41	16.16	15.74	4.80
13	2.43	15.69	13.26	4.78
19	2.89	15.36	12.47	4.75

Table 7.5: Convergence of the fundamental band gap E_{gap} and the bandwidth of the F $2p$ valence band complex $\Delta E_{\text{F}\,2p}$ of a LiF crystal with respect to the number of unit cells included in the description of the quasiparticle band structure. Symbols are chosen as in Table 7.4 where there is only a single F $2p$ band complex for LiF and, in this case, thirteen and nineteen indicate the additional inclusion of nearest and second nearest-neighbor cells, respectively, in correlation calculations. All data are given in electronvolt.

gap [275] by optical spectroscopy. Similarly, many-particle effects have to be accounted for in the measurement of the widths of the F $2p$ and F $2s$ valence bands.

LiF has been thoroughly studied both experimentally [268, 272] and theoretically [31, 69, 70, 126, 179, 267, 269, 270, 273, 276]. Poole *et al.* survey early experimental and theoretical data [272, 273]. Recent studies of LiF comprise density functional theory calculations at the LDA level supplemented by an inclusion of correlation effects in terms of the GW approximation [269, 270]. *Ab initio* investigations comprise Hartree-Fock studies of ground-state properties [31, 126, 267] and of the band structure [69, 70, 276]. An accurate treatment of electron correlations for the ground state properties of LiF (and other alkali halides) has been carried out by Doll and Stoll [179]. Quasiparticle band structures have been obtained by Kunz [276] on the basis of Toyozawa's electronic polaron model [77] and by Albrecht [69, 70] with Igarashi's Green's function approach [62].

To investigate LiF with the new CO-ADC method (Reference [97], Chapters 5 and 6), I have chosen the simplest possible *ab initio* description. The main purpose here is to demonstrate the feasibility of the CO-ADC formulas for a three-dimensional crystalline solid. A minimal Gaussian STO-6G basis set [48, 277] is used which describes the lithium atom by a $(12s)\,/\,[2s]$ contraction and the fluorine atom by $(12s\,6p)\,/\,[2s\,1p]$. Each shell of the STO-6G basis set is constructed by fitting six Gaussian functions to each occupied orbital of the isolated atoms [277]. The $2s$ shell of a lithium atom is rather diffuse due to the single outer valence electron. As the lithium atoms are ionized in LiF crystals, I remove the two most diffuse Gaussian primitives in the Li $2s$ contraction because they do not reflect the physical situation of a compact Li$^+$ ion. I arrive at a $(10s)\,/\,[2s]$ contraction scheme.

The Hartree-Fock band structure that results from this minimal basis is shown in Figure 7.6. All band energies are given with respect to the Fermi energy. It is placed at the top of the valence bands which is located at the Γ point and is set to zero. Below zero there is a complex of three F $2p$ valence bands shown as a closeup in Figure 7.7. They originate from the three F $2p$ valence energy levels of the LiF molecule around $12\,\text{eV}$ where the lowest IP in Figure 7.1 is doubly degenerate. Upon crystallization, this degeneracy is lifted due to interactions with neighboring atoms and, except for the high symmetry lines Γ–L and Γ–X, one observes three distinct F $2p$ valence bands. As a minimal basis
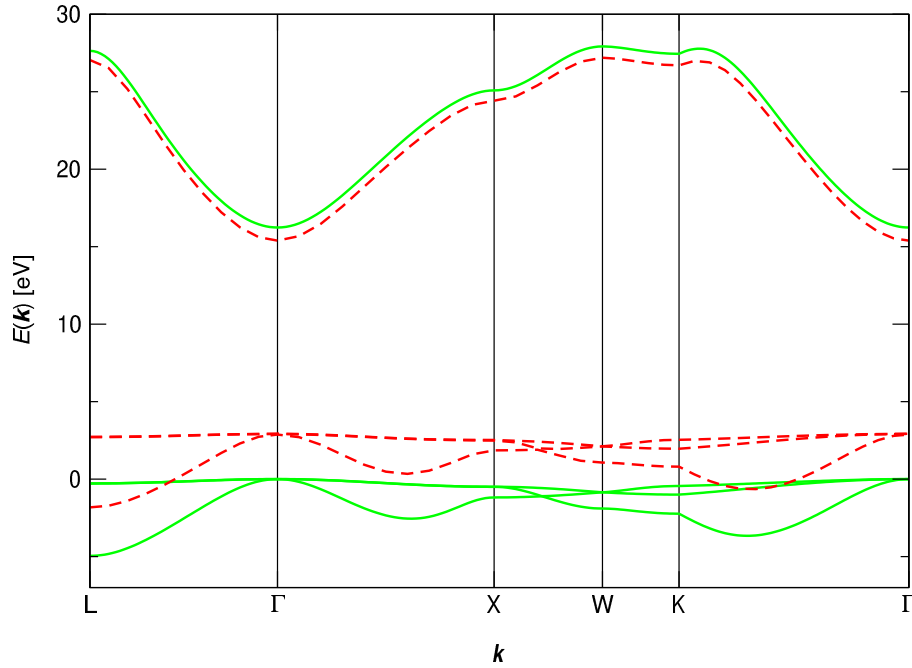
Figure 7.6: (Color) Band structure of a LiF crystal. The CO-ADC(2,2) quasiparticle bands are determined accounting for $2p1h$- and $2h1p$-configurations involving the Wannier orbitals in the origin cell, the nearest and the next nearest-neighbor cells. Line styles are chosen as in Figure 7.3.

set is utilized, there is only a single conduction band of mainly Li $2s$ character. A slight admixture of F $2p$ character to this band is observed in the W–K panel, by comparing with the band structure resulting from a richer basis set, e.g., the one of Reference [70], where a F $2p$ conduction band entangles with the Li $2s$ band. However, the single Li $2s$ conduction band represents the energetically lower edge of the conduction band complex well. LiF has a direct band gap, i.e., the maximum of the F $2p$ valence bands and the minimum of the Li $2s$ conduction band are located at the same crystal momentum, here at the Γ point.

Electron correlations are investigated by forming $2p1h$- and $2h1p$-configurations in the origin cell, first, and then successively including configurations involving nearest and next nearest-neighbor cells. The convergence, with respect to the number of unit cells where electron correlations are accounted for, is checked for the top of the valence bands, the bottom of the conduction band, the band gap and the width of the F $2p$ valence band complex in Table 7.5. The data are put into relation to the Hartree-Fock result which is indicated by "0" unit cells used for the configuration selection. Considering $2p1h$- and $2h1p$-configurations in the origin cell causes a slight upwards shift by 0.41 eV of the valence bands while the conduction band essentially remains unchanged. Upon inclusion of configurations in the nearest-neighbor cells, the band structure changes drastically. I observe a significant reduction of the band gap by 2.48 eV. Regarding second nearest-neighbor cells has three times less impact on the band gap which experiences a further reduction by 0.79 eV. Therewith, it can clearly be seen that the major contributions of electron correlations have been caught and that the effect of configurations which involve Wannier orbitals in unit cells beyond second nearest neighbors will yield a less significant
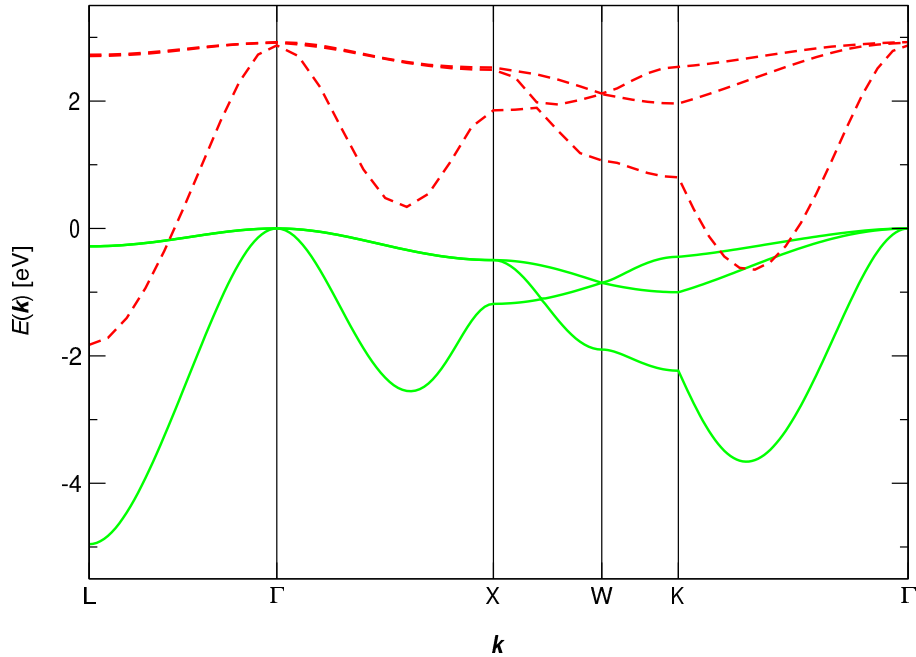
Figure 7.7: (Color) Valence band structure of a LiF crystal. Zoom into Figure 7.6.

enhancement of the quantities presented in Table 7.5.

The observation, that first and second nearest-neighbor cells make a significant contribution to the description of the quasiparticle bands of a LiF crystal, is in contrast to what is found for the $(HF)_\infty$ chain in Section 7.2 where configurations in the origin cell already represent the major influence of electron correlations and interactions with neighboring unit cells are only due to a weak hydrogen bond. However, there is a significant amount of interactions with neighboring unit cells for the ionic LiF crystal. Clearly, the effect of electron correlations, to delocalize the electrons over the whole crystal, is much more important for this compound [Section 7.2]. The successive inclusion of an increasing number of neighbor cells propagates the polarization of the solid that arises due to the extra charge occurring in the description of electron attachment and electron removal states. Another contribution to the large impact of neighboring cells for LiF can be ascied to basis set extension (BSE) [235]. BSE helps to describe the electrons from the Wannier orbitals in the origin cell by the basis functions centered on atoms in neighboring unit cells. BSE can be considered to play an appreciably pronounced role in the LiF crystal, compared with the $(HF)_\infty$ chain, as a minimal basis set is used to describe the former whereas a double-ζ basis set is employed for the latter.

The quasiparticle band structure of LiF is displayed in Figure 7.6 for the F $2p$ valence bands and the Li $2s$ conduction band. The former bands are additionally displayed on an enlarged scale in Figure 7.7. The data are taken from the most accurate computation with configurations in 19 unit cells. Valence and conduction bands do not shift by the same amount, upwards and downwards, respectively. The former show a much stronger influence due to electron correlations than the latter similarly to the $(HF)_\infty$ chain of Section 7.2. Although the quasiparticle bands are considerably shifted with respect to

110

the corresponding Hartree-Fock bands, they essentially keep their form. I also observe this effect for the $(HF)_\infty$ chain in Section 7.2. This is in contrast to the significant reduction of bandwidths observed for quasiparticle band structures of covalently bonded crystals like diamond [63, 64, 67], silicon [64, 67] and germanium [64] where electron correlations provide a energetically favorable redistribution of the electrons [1].

The minimal *ab initio* description of a LiF crystal provides valuable insights. The accuracy of this approach can be determined by comparing with experimental and theoretical data from related studies. The fundamental band gap is accessible by photoelectron spectroscopy and has been measured to be 14.1 eV. Another experimentally accessible quantity, the width of the F $2p$ valence band complex, was determined to lie in the range of 3.5–6 eV [276] and thus is inconclusive, unfortunately. With the STO-6G-like basis set, I find a Hartree-Fock band gap of 16.24 eV [Table 7.5] which is already considerably closer to the experimental band gap than the value of 22.7 eV communicated by Kunz [276] or the value of 22.4 eV reported by Albrecht [70]. Yet, I am interested in the correlation corrections to it, which are expected to be appreciably less than in other studies, for the band gap to come close to the experimental value. In the Hartree-Fock approximation, I find 4.95 eV for the width of the F $2p$ valence band complex [Table 7.5] which is appreciably larger than the value of 3 eV of Kunz [276] the value of 3.37 eV of Albrecht [70].

Including electron correlations, the quasiparticle band gap becomes 12.47 eV [Table 7.5] and thus falls short by 1.5 eV of the experimental value. Yet, it is in satisfactory agreement with the theoretical result of 13.5 eV by found Albrecht [70]. Sophisticated calculations of Kunz [276] yield a theoretical band gap of 14.0 eV, in excellent agreement with recent measurements. I obtain a width for the F $2p$ valence band complex of 4.75 eV which is nearly unchanged compared to the Hartree-Fock value [Table 7.5], a fact that has also been found in previous studies of LiF [70, 276]. Yet, my value of the width remains much higher than the value of 3.1 eV from Kunz [276] or the value of 3.40 eV from Albrecht [70].

In view of the fact that I follow a minimal *ab initio* approach, the band gap and the width of the F $2p$ band complex are already obtained with very promising accuracy. Increasing the size of the basis set in future work will substantially improve the CO-ADC(2,2) data. Yet, it is important to note that an understanding of the physics governing a LiF crystal is already provided by my first minimal *ab initio* approach and quantitative accuracy is achieved!

8 Conclusion

This dissertation is thematically centred around the theoretical first-principles description of the ground state, the electron attachment and the electron removal states of perfect semiconducting and insulating crystalline solids. The foundation of the many-particle theories described in this thesis is provided by the Hartree-Fock approximation. It is presented in detail elucidating the consequences of the characteristic translational symmetry. The canonical crystal orbitals, the plane-wave-like Bloch orbitals, extend over the whole solid. They are only a special view on the independent particle states of crystals; another view is given by localized crystal orbitals, the atomic-orbital-like Wannier orbitals. Appropriate Hartree-Fock equations are formulated that yield, *a priori*, Wannier orbitals. I prove that this approach is as efficient as the conventional *a posteriori* transformation of Bloch orbitals to Wannier orbitals [Chapter 2].

Based on the Hartree-Fock approximation, coupled-cluster theory [33–35] is introduced, to describe electron correlations in the ground-state of crystals. It provides size-consistent ansätze for wave functions of many-particle systems, that eventually reach the full configuration interaction result. I choose the well-established coupled-cluster singles and doubles (CCSD) correlation method [42, 158, 159] to treat crystals. I describe a means to truncate the lattice summations therein which is referred to as configuration selection. It leads to an incremental series of non-additive many-body energy contributions, the so-called energy increments. They are defined with respect to one-body orbital sets which are sets of Wannier orbitals that are identified with certain fractions, i.e., (groups of) atoms, in a unit cell of a crystal. A finite-cluster approximation is introduced which allows to approximate the Wannier orbitals with the help of a molecular cluster that represents a fraction of the solid. Configuration selection in conjunction with the finite-cluster approximation is referred to as incremental scheme [1, 2, 38, 43–45]. It allows to make use of existing quantum chemical program packages to study solids. A proof of the asymptotic linear scaling of the incremental scheme with the system size is given [Chapter 3].

Correlation effects in extended systems are generally classified into strong, short-range correlations that are mediated by spatial orbital overlaps and long-range van der Waals dispersion interactions. The incremental series provides a general framework to describe the interactions between fractions of the solid in terms of the many-body energy increments. I determine the constants of two-body dispersion interaction [162, 175, 178–180] which allow an interpretation of the two-body energy increments in terms of a dissociation process in a crystal. The van der Waals constants facilitate a partition of the energy increments into a short-range, van-der-Waals-reduced part and a long-range part that can be summed analytically to infinite distances. If the van der Waals constants are determined beforehand, the actual number of relevant energy increments is decreased by considering only the van-der-Waals-reduced energy increments. Furthermore, the long-range part turns out to be well-described using only a small (double-ζ) basis sets. The proposed treat-

ment of the long-range van der Waals interaction is also beneficial for the improvement of other local correlation methods which are presently developed for crystals [168]. They employ a multi-method treatment of the near, intermediate and distant contributions to the correlation energy to cope with the long-range contributions efficiently [Chapter 4].

Hydrogen bonding is of great importance for the physicochemical properties of (bio)-molecules, organic and inorganic crystals. I carry out a thorough analysis of the ground state of the infinite hydrogen fluoride and hydrogen chloride chains to provide a reliable grounding for the description of this type of bonding in future work. Thereby, the incremental scheme is based on the individual monomers in the chains; their orbitals are taken as one-body orbital sets. The scheme is shown to converge rapidly with respect to the number of monomers considered in an energy increment and the distance among them. In contrast to three-dimensional crystalline solids, the dominant contribution of electron correlations to the binding energy of the chains is already given by pair interactions between a monomer and its nearest and next nearest neighbors [Chapter 4].

A thorough analysis of the basis set convergence of the Hartree-Fock and the correlation energy in the infinite chains is undertaken. It reveals that data of predictive quality cannot be obtained with acceptable computational effort which requires theoretical advances. I show that Hartree-Fock [53] and correlation energies [42, 46, 55–59] follow corresponding relations found for small molecules like the dimers $(HF)_2$ and $(HCl)_2$ [42, 46, 55–59]. The known convergence properties facilitate an extrapolation of the energies to the basis set limit. The incremental scheme is particularly beneficial in conjunction with basis set extrapolation. As localized orbitals are used, selected terms in this decomposition of the correlation energy can be extrapolated individually. Specifically, energy increments which contain one-body orbital sets that are close nearby require an accurate description of the Coulomb hole in terms of a large one-particle basis set. However, energy increments with a larger distance among the one-body orbital sets are already represented in terms of basis sets of only moderate quality. The techniques allow to improve the reliability of binding energies by roughly an order of magnitude and provide a competitive accuracy in comparison with thermochemical data that can be achieved with a managable computational effort [Chapter 4].

For the $(HF)_\infty$ chain, the Hartree-Fock contribution dominates the total binding energy by 86% due to the large electrostatic contribution of the rather ionic HF monomers. The less polar HCl monomers cause the Hartree-Fock approximation to yield only 18% of the binding energy of the $(HCl)_\infty$ chain. This reflects the transitional character of hydrogen-bonded crystals in between of ionic and van der Waals bonding. The very weak hydrogen bonds in the $(HCl)_\infty$ chain bear a close resemblance to purely van der Waals bonded systems, like rare-gas solids [162, 174, 175, 278], where bonding is entirely caused by electron correlations. In fact, only the inclusion of electron correlations puts the binding energy per monomer of $(HCl)_\infty$ into the energy range conventionally ascribed to hydrogen bonding [173], namely 3–16 mE_h [Chapter 4].

Excited states of solids pose a *profoundly* more involved problem than ground states. The independent particle model of Hartree-Fock or Kohn-Sham theory still is the predominant intellectual device for the description and understanding of electron attachment and electron removal. Thereby, the characteristic symmetry properties for crystals are imprinted on the one-particle spectra. They are typically given with respect to the trans-

lational symmetry quantum number, the crystal momentum, and arrange graphically in terms of long energy bands, the so-called band structure. Although a considerable effort has been undertaken to go beyond the one-particle approximation, only few progress has been made in the rigorous *ab initio* description of the complex many-particle system a crystal represents [Chapter 5].

In order to formulate an *ab initio* foundation for the addition and removal of an electron from a crystal, I make a recourse to quantum field theory which provides the one-particle Green's function. Its pole positions represent the energies of the excited states. The Green's function is rewritten conveniently in terms of the Dyson's equation. To approximate the self-energy therein up to n-th order, I devise a crystal orbital formulation of the well-established *algebraic diagrammatic construction (ADC)* scheme [86–88] which is termed *crystal orbital ADC (CO-ADC)*. The required pole search is thereby recast into a Hermitian eigenvalue problem for the so-called *band structure matrix* which is a numerically stable and efficient formulation. It allows explorations of strong correlations beyond the quasiparticle picture which occur for the energetically lower lying states of crystals [Chapter 6].

I derive two CO-ADC approximations; the one expresses the self-energy completely in terms of Bloch orbitals and the other one uses Wannier orbitals. The derivation of the latter, local orbital CO-ADC method, sets out from the former CO-ADC method in terms of Bloch orbitals. Thereby, the Bloch orbitals are transformed to Wannier orbitals. I consider this line of argument to be compelling due to the close analogy of the equations in terms of Bloch orbitals to the equations of molecular physics. Alternatively, the derivation can be conducted by starting from the CO-ADC equations in terms of Wannier orbitals. A transformation of the equations to crystal momentum representation is then carried out by utilizing the inverse transformation. Both CO-ADC theories fully exploit translational symmetry [Chapter 6].

The lattice summations in the CO-ADC equations are required to be truncated to render the problem tractable. To this end, I devise a configuration selection procedure for excited states. Thereby, the Wannier orbital based scheme allows the fine grained truncation of the lattice sums which facilitates to exploit that electron correlations are predominantly local. The restriction of the configuration space is shown to lead to a definition of degeneracy among the states of a crystal. It can equally well be used to enable the calculation of ionization potentials and electron affinities of large molecules not amenable to a conventional treatment. The band structure matrix rapidly becomes too large for a full diagonalization and one has to resort to an iterative eigenvalue solver, e.g., a block-Lanczos algorithm, to obtain the eigenvalues in the desired spectral range. Such eigenvalue solvers only require the result of a matrix times vector product. The precise analysis of the scaling of the computational effort involved with a multiplication of a vector with the band structure matrix shows that the determination of excited states is a quadratically scaling problem which becomes a *linear* scaling problem, if one *a priori* restricts oneself to a few states [Chapter 6].

Localized orbitals lead to off-diagonal matrix elements in the Fock matrix which are treated either exactly or perturbatively. This represents an additional approximation that is not required if Bloch orbitals are used. The resulting scheme is termed CO-ADC(m,n) where m denotes the highest order of the diagrams which (partly) involve the one-particle

interaction, mediated by the off-diagonal elements of the Fock matrix, and n denotes the highest order diagrams exclusively describing the two-particle interaction, mediated by the two-electron integrals. ADC equations for local molecular orbitals can easily be derived from the CO-ADC equations for Wannier orbitals by simply assuming that the molecule occupies the unit cell of a crystal with a macroscopic lattice constant [Chapter 7].

I have developed a computer program [97] to carry out computations with the local orbital ADC and CO-ADC theories. The Fock matrix and the two-electron integrals in terms of Wannier orbitals are required. They are obtained from the *ab initio* Hartree-Fock program WANNIER [30–32] which has been written in Dresden. A new theory—and especially its implementation in a computer program—should be tested, if possible, on a problem where the results are precisely known beforehand. Therefore, a comparison of the ionization potentials and electron affinities of the hydrogen fluoride molecule is undertaken and an excellent agreement is found with respect to an exact treatment of the localized orbitals, denoted by ADC(∞,2). However, the ADC(∞,2) and CO-ADC(∞,2) approximation lead to a very low sparsity of the $\boldsymbol{B}$ matrix and band structure matrix, respectively, which causes the iterative diagonalization to become very expensive. Fortunately, the simplest perturbative approximation of the off-diagonal Fock matrix elements, ADC(2,2) and CO-ADC(2,2), that treats the one- and two-particle interactions both in second order of perturbation theory, is shown to provide already good results for outer valence bands and the first few conduction bands but not to properly account for strong correlations in the inner valence of the HF molecule. However, including third-order terms of the off-diagonal Fock matrix elements, the ADC(3,2) scheme, improves results from the ADC(2,2) approximation by an order of magnitude, with respect to ADC(∞,2) reference data, and also describes the strong correlations in the inner valence correctly [Chapter 7].

The ionization potentials of the hydrogen fluoride and lithium fluoride molecules are obtained in ADC(∞,3) approximation. The outer valence of both compounds is predominantly represented by the lone pairs of the fluorine atom. The pronounced differences between the spectra of both molecules which, clearly, are caused by the difference between the hydrogen and lithium atoms are discussed. Striking is the strong shake-down satellite in the HF molecule that splits off the F $2s$ independent-particle state and is not found in the LiF molecule. This smaller breakdown of the molecular orbital picture of ionization observed for the LiF compared with the HF molecule is ascribed mainly to the presence of the Li $1s$ shell [Chapter 7].

Using CO-ADC(2,2), the quasiparticle band structure of an infinite hydrogen fluoride chain is computed. The convergence of the configuration space turns out to be extremely rapid, requiring only nearest-neighbor cells to be included. The local Hamiltonian approach [2, 63–67, 69, 72] is utilized, additionally, to calculate the valence bands of $(HF)_\infty$ which agree excellently with those obtained by CO-ADC. Moreover, Liegener and Ladik [99] have published results for the $(HF)_\infty$ chain determined with the OVGF method. Their valence band energies agree very well with those of CO-ADC but there is some deviation between the data for the conduction bands which is most likely due to the different basis sets employed [Chapter 7].

The quasiparticle band structures of a lithium fluoride crystal is studied with CO-ADC(2,2) to demonstrate the feasibility of the method for three-dimensional crystalline solids in terms of a minimal *ab initio* approach. Successively, configurations in the origin

cell, the first and the second nearest-neighbor cells are accounted for and the rapid convergence of the configuration space is monitored. Concerning the fact that only a minimal basis set is used, the results obtained are in good agreement both with previous theoretical and experimental data which highly encourages further investigations [Chapter 7].

The advances made in this thesis offer a rich prospect for future research. CO-ADC theory is applicable to perfect crystals which are reasonably well described by a closed-shell Hartree-Fock ground-state wave function. The theory incorporates a full description of electron correlations thus facilitating to study strong correlations (breakdown of the one-particle picture) which occur when the inner valence bands are involved. Moreover, the decay of electronic resonances, like the Auger decay of core-ionized crystals, is described. Especially the interplay between intra- and interatomic Auger decay, as has been discussed recently by myself and others [74–76] in the case of the xenon fluoride molecules, allows deep insights into the complex many-particle effects of solids and represents a powerful analytical tool. It poses an intriguing perspective for future research. Interatomic decay processes can be conjectured to be of considerably greater impact on the crystalline Auger decay compared to the case of molecules and thus are important for the description of experimental photoelectron spectra [96].

Building on the results of this treatise, many more things can be achieved for excited states. The band structure matrix contains blocks of two-particle-one-hole and two-hole-one-particle-configurations where the former block is much larger than the latter. To reduce the computational effort, the advanced part and the retarded part of the one-particle Green's function can be independently evaluated diagrammatically [263]. This leads to a different, so-called non-Dyson CO-ADC scheme, which decouples the computation of occupied and virtual bands completely and results in two independent Hermitian matrix eigenvalue problems to be solved [279].

One can further benefit from the advances that have been achieved for the description of excited states of molecules. The molecular non-Dyson ADC scheme has recently been based on the Dirac-Hartree-Fock approximation to treat relativistic effects [280, 281]. Moreover, the Dyson equation based ADC scheme for molecules has been combined with the complex absorbing potential (CAP) method to treat electronic resonances [90, 131, 132]. The route offered in this thesis for the evaluation of the one-particle Green's function can be extended further to the two-particle Green's function and propagators derived from it. The particle-particle propagator up to third order allows to calculate double ionization and double attachment spectra [282, 283]. Excitonic spectra of molecules can be calculated with the polarization propagator which has been utilized to construct an ADC(2) approximation [86, 284]. The three-particle Green's function, finally, has been employed to calculate triple ionization potentials in terms of an ADC(2) scheme for the three-particle propagator [285].

9 Acknowledgments

Our receptionist, Rita DOHRMANN, always had a smile for me entering the institute. Heidrun NÄTHER, the spirit of our library, never understood why I liked to borrow *so* many books. My thanks are also extended to the system administrators Hubert SCHERRER, Torsten GOERKE and Helmut DEGGELMANN for support with computers. Regine SCHUPPE and Uta GNEISSE helped with administrative hurdles. Moreover, the endearing staff of our cafeteria should be noted who saved me from "starving" from time to time. I am indebted to all other members of this institute for the pleasant and inspiring atmosphere they created.

Bibliography

[1] P. Fulde, *Electron correlations in molecules and solids*, volume 100 of *Springer series in solid-state sciences*, Springer, Berlin, 3rd edition, 1995.

[2] P. Fulde, Wavefunction methods in electronic structure theory of solids, Adv. Phys. **51**, 909–948 (2002).

[3] N. W. Ashcroft and N. D. Mermin, *Solid state physics*, Cole, London, 1976.

[4] K. Richter and J.-M. Rost, *Komplexe Systeme*, Fischer Taschenbuch Verlag, Frankfurt am Main, 2002.

[5] C. Pisani, R. Dosevi, and C. Roetti, *Hartree-Fock ab initio treatment of crystalline systems*, volume 48 of *Lecture notes in chemistry*, Springer, Berlin, Heidelberg, 1988.

[6] J. Callaway, *Quantum theory of the solid state*, Academic Press, Boston, 2nd edition, 1991.

[7] C. Pisani, editor, *Quantum-mechanical ab initio calculation of the properties of crystalline materials*, volume 67 of *Lecture notes in chemistry*, Springer, Berlin, Heidelberg, 1996.

[8] P. Hohenberg and W. Kohn, Inhomogeneous electron gas, Phys. Rev. **136**, B864–B871 (1964).

[9] W. Kohn and L. J. Sham, Self-consistent equations including exchange and correlation effects, Phys. Rev. **140**, A1133–A1138 (1965).

[10] H. Eschrig, *Optimized LCAO method and the electronic structure of extended systems*, Research reports in physics, Springer, Berlin, 1989.

[11] W. Y. Ching, F. Gan, and M.-Z. Huang, Band theory of linear and nonlinear susceptibilities of some binary ionic insulators, Phys. Rev. B **52**, 1596–1611 (1995).

[12] R. Hott, GW-approximation energies and Hartree-Fock bands of semiconductors, Phys. Rev. B **44**, 1057–1065 (1991).

[13] V. I. Anisimov, F. Aryasetiawan, and A. I. Lichtenstein, First-principles calculations of the electronic structure and spectra of strongly correlated systems: the LDA+U method, J. Phys.: Condens. Matter **9**, 767–808 (1997).

[14] T. Grabo, T. Kreibich, S. Kurth, and E. K. U. Gross, Orbital functionals in density functional theory: The optimized effective potential method, in *Strong Coulomb correlations in electronic structure calculations*, edited by V. I. Anisimov, Advances in condensed matter science, pages 203–311, Taylor & Francis, London, 2000.

[15] M. Städele, M. Moukara, J. A. Majewski, P. Vogl, and A. Görling, Exact exchange Kohn-Sham formalism applied to semiconductors, Phys. Rev. B **59**, 10031–10043 (1999).

[16] Y. Kakehashi, Monte Carlo approach to the dynamical coherent-potential approximation in metallic magnetism, Phys. Rev. B **45**, 7196–7204 (1992).

[17] Y. Kakehashi, Dynamical coherent-potential approximation to the magnetism in a correlated electron system, Phys. Rev. B **65**, 184420 (2002).

[18] W. Metzner and D. Vollhardt, Correlated lattice fermions in $d = \infty$ dimensions, Phys. Rev. Lett. **62**, 324–327 (1989).

[19] W. Metzner and D. Vollhardt, Erratum: Correlated lattice fermions in $d = \infty$ dimensions, Phys. Rev. Lett. **62**, 1066 (1989).

[20] E. Müller-Hartmann, Correlated fermions on a lattice in high dimensions, Z. Phys. B **74**, 507–512 (1989).

[21] T. Pruschke, M. Jarrell, and J. K. Freericks, Anomalous normal-state properties of high-T_c superconductors: intrinsic properties of strongly correlated electron systems?, Adv. Phys. **44**, 187–210 (1995).

[22] A. Georges, G. Kotliar, W. Krauth, and M. J. Rozenberg, Dynamical mean-field theory of strongly correlated fermion systems and the limit of infinite dimensions, Rev. Mod. Phys. **68**, 13–125 (1996).

[23] M. Jarrell and H. R. Krishnamurthy, Systematic and causal corrections to the coherent potential approximation, Phys. Rev. B **63**, 125102 (2001).

[24] L. D. Faddeev, Sov. Phys. JETP **12**, 1014 (1961).

[25] P. Unger, J. Igarashi, and P. Fulde, Electronic excitations in 3d transition metals, Phys. Rev. B **50**, 10485–10497 (1994).

[26] W. M. C. Foulkes, L. Mitas, R. J. Needs, and G. Rajagopal, Quantum Monte Carlo simulations of solids, Rev. Mod. Phys. **73**, 33–83 (2001).

[27] J. J. Ladik, *Quantum theory of polymers as solids*, Plenum Press, New York, London, 1988.

[28] J. J. Ladik, Polymers as solids: a quantum mechanical treatment, Phys. Rep. **313**, 171–235 (1999).

[29] H. J. Monkhorst, GW method for extended, periodic systems with a mixed Slater-orbital/plane-wave basis and Fourier transform techniques, Adv. Quantum Chem. **48**, 35–45 (2005).

[30] A. Shukla, M. Dolg, H. Stoll, and P. Fulde, An *ab initio* embedded-cluster approach to electronic structure calculations on perfect solids: a Hartree-Fock study of lithium hydride, Chem. Phys. Lett. **262**, 213–218 (1996).

[31] A. Shukla, M. Dolg, P. Fulde, and H. Stoll, Obtaining Wannier functions of a crystalline insulator within a Hartree-Fock approach: applications to LiF and LiCl, Phys. Rev. B **57**, 1471–1483 (1998).

[32] A. Shukla, M. Dolg, P. Fulde, and H. Stoll, Wave-function-based correlated *ab initio* calculations on crystalline solids, Phys. Rev. B **60**, 5211–5216 (1999).

[33] F. Coester, Bound states of a many-particle system, Nucl. Phys. **7**, 421–424 (1958).

[34] F. Coester and H. Kümmel, Short-range correlations in nuclear wave functions, Nucl. Phys. **17**, 477–485 (1960).

[35] H. Kümmel, Compound pair states in imperfect Fermi gases, Nucl. Phys. **22**, 177–183 (1961).

[36] R. F. Bishop and H. Kümmel, The coupled-cluster method, Phys. Today **40**, 52–60 (1987).

[37] Science **271**, 920 (1996), Special issue on clusters.

[38] B. Paulus, *The method of increments – A wavefunction-based ab initio correlation method for solids*, Habilitation, Universität Regensburg, Naturwissenschaftliche Fakultät II – Physik der Universität Regensburg, Regensburg, Germany, 2005.

[39] A. Szabo and N. S. Ostlund, *Modern quantum chemistry: Introduction to advanced electronic structure theory*, McGraw-Hill, New York, 1st, revised edition, 1989.

[40] R. McWeeny, *Methods of molecular quantum mechanics*, Academic Press, London, 2nd edition, 1992.

[41] I. N. Levine, *Quantum chemistry*, Prentice Hall, Upper Saddle River, New Jersey 07458, 5th edition, 2000.

[42] T. Helgaker, P. Jørgensen, and J. Olsen, *Molecular electronic structure theory*, John Wiley & Sons, Chichester, New York, 2000.

[43] H. Stoll, Correlation energy of diamond, Phys. Rev. B **46**, 6700–6704 (1992).

[44] H. Stoll, The correlation energy of crystalline silicon, Chem. Phys. Lett. **191**, 548–552 (1992).

[45] H. Stoll, On the correlation energy of graphite, J. Chem. Phys. **97**, 8449–8454 (1992).

[46] W. Klopper, R12 methods, Gaussian geminals, in *Modern methods and algorithms of quantum chemistry*, edited by J. Grotendorst, volume 3 of *NIC series*, pages 181–229, Jülich, 2000, John von Neumann Institute for Computing, `www.fz-juelich.de/nic-series`.

[47] T. Kato, On the eigenfunctions of many-particle systems in quantum mechanics, Commun. Pure Appl. Math. **10**, 151–177 (1957).

[48] Basis sets were obtained from the Extensible Computational Chemistry Environment Basis Set Database, Version 02/25/04, as developed and distributed by the Molecular Science Computing Facility, Environmental and Molecular Sciences Laboratory which is part of the Pacific Northwest Laboratory, P.O. Box 999, Richland, Washington 99352, USA, and funded by the U.S. Department of Energy. The Pacific Northwest Laboratory is a multi-program laboratory operated by Battelle Memorial Institute for the U.S. Department of Energy under contract DE-AC06-76RLO 1830. Contact David Feller or Karen Schuchardt for further information, `www.emsl.pnl.gov/forms/basisform.html`.

[49] T. H. Dunning, Jr., Gaussian basis sets for use in correlated molecular calculations. I. The atoms boron through neon and hydrogen, J. Chem. Phys. **90**, 1007–1023 (1989).

[50] D. E. Woon and T. H. Dunning, Jr., Gaussian basis sets for use in correlated molecular calculations. III. The atoms aluminium through argon, J. Chem. Phys. **98**, 1358–1371 (1993).

[51] R. A. Kendall, T. H. Dunning, Jr., and R. J. Harrison, Electron affinities of the first-row atoms revisited. Systematic basis sets and wave functions, J. Chem. Phys. **96**, 6796–6806 (1992).

[52] D. E. Woon and T. H. Dunning, Jr., Gaussian basis sets for use in correlated molecular calculations. IV. Calculation of static electrical response properties, J. Chem. Phys. **100**, 2975–2988 (1994).

[53] F. Jensen, The basis set convergence of the Hartree-Fock energy for H_2, J. Chem. Phys. **110**, 6601–6605 (1999).

[54] R. N. Hill, Rates of convergence and error estimation formulas for the Rayleigh-Ritz variational method, J. Chem. Phys. **83**, 1173–1196 (1985).

[55] T. Helgaker, W. Klopper, H. Koch, and J. Noga, Basis-set convergence of correlated calculations on water, J. Chem. Phys. **106**, 9639–9646 (1997).

[56] A. Halkier, T. Helgaker, P. Jørgensen, W. Klopper, H. Koch, J. Olsen, and A. K. Wilson, Basis-set convergence in correlated calculations on Ne, N_2, and H_2O, Chem. Phys. Lett. **286**, 243–252 (1998).

[57] A. Halkier, W. Klopper, T. Helgaker, P. Jørgensen, and P. R. Taylor, Basis set convergence of the interaction energy of hydrogen-bonded complexes, J. Chem. Phys. **111**, 9157–9167 (1999).

[58] S. Y. Park and J. S. Lee, Basis set limit binding energies of dimers derived from basis set convergence of monomer energies, J. Chem. Phys. **116**, 5389–5394 (2002).

[59] S. B. Huh and J. S. Lee, Basis set limit binding energies of complexes derived from the basis set extrapolation of fragment correlation energies: applications to hydrogen-bonded systems, Chem. Phys. Lett. **369**, 466–471 (2003).

[60] A. J. May and F. R. Manby, An explicitly correlated second order Møller-Plesset theory using a frozen Gaussian geminal, J. Chem. Phys. **121**, 4479–4485 (2004).

[61] A. Karpfen, Cooperative effects in hydrogen bonding, in *Adv. Chem. Phys.*, edited by I. Prigogine and S. A. Rice, volume 123, pages 469–510, John Wiley & Sons, New York, 2002.

[62] J. Igarashi, P. Unger, K. Hirai, and P. Fulde, Local approach to electron correlations in ferromagnetic nickel, Phys. Rev. B **49**, 16181–16190 (1994).

[63] J. Gräfenstein, H. Stoll, and P. Fulde, Computation of the valence band of diamond by means of local increments, Chem. Phys. Lett. **215**, 611–616 (1993).

[64] J. Gräfenstein, H. Stoll, and P. Fulde, Valence-band structure of group-IV semiconductors by means of local increments, Phys. Rev. B **55**, 13588–13597 (1997).

[65] M. Albrecht, P. Reinhardt, and J.-P. Malrieu, Local-orbital based correlated *ab initio* band structure calculations in insulating solids, Theor. Chem. Acc. **100**, 241–252 (1998).

[66] M. Albrecht, *Elektronische Korrelationen im Grundzustand und bei angeregten Zuständen periodischer Systeme*, Dissertation, Bayerische Julius-Maximilians-Universität Würzburg, Fakultät für Physik und Astronomie, Würzburg, Germany, 1999.

[67] M. Albrecht, P. Fulde, and H. Stoll, An ab initio estimate of correlation effects on the band gap of covalent semiconductors: diamond and silicon, Chem. Phys. Lett. **319**, 355–362 (2000).

[68] M. Albrecht and J. Igarashi, Local-orbital based correlated *ab initio* band structure calculations in insulating solids, J. Phys. Soc. Jpn. **70**, 1035–1044 (2001).

[69] M. Albrecht and P. Fulde, Local *ab initio* schemes to include correlations in the calculated band structure of semiconductors and insulators, phys. stat. sol. (b) **234**, 313–328 (2002).

[70] M. Albrecht, Local-orbital-based correlated ab initio band structure calculations in insulating solids: LiF, Theor. Chem. Acc. **107**, 71–79 (2002).

Bibliography

[71] V. Bezugly, *Wavefunction-based method for excited-state electron correlations in periodic systems*, Dissertation, Technische Universität Dresden, Fakultät Mathematik und Naturwissenschaften, Dresden, Germany, 2003.

[72] V. Bezugly and U. Birkenheuer, Multireference configuration interaction treatment of excited-state electron correlation in periodic systems: The band structure of *trans*-polyacetylene, Chem. Phys. Lett. **399**, 57–61 (2004), `arXiv: cond-mat/0407382`.

[73] L. S. Cederbaum, W. Domcke, J. Schirmer, and W. von Niessen, Correlation effects in the ionization of molecules: Breakdown of the molecular orbital picture, in *Adv. Chem. Phys.*, edited by I. Prigogine and S. A. Rice, volume 65, pages 115–159, John Wiley & Sons, New York, 1986.

[74] C. Buth, Non-Hermitian perturbation theory for the electronic decay of excited and ionized molecules and identification of the electronic decay processes in the Auger decay of core-ionized xenon fluorides, Diplomarbeit, Ruprecht-Karls-Universität Heidelberg, Theoretische Chemie, Physikalisch-Chemisches Institut, Im Neuenheimer Feld 229, 69120 Heidelberg, Germany, 2002, `www.ub.uni-heidelberg.de/archiv/ 3004`.

[75] C. Buth, R. Santra, and L. S. Cederbaum, Ionization of the xenon fluorides, J. Chem. Phys. **119**, 7763–7771 (2003), `arXiv:physics/0306123`.

[76] C. Buth, R. Santra, and L. S. Cederbaum, Impact of interatomic electronic decay processes on the width of the Xe $4d$ lines in the Auger decay of the xenon fluorides, J. Chem. Phys. **119**, 10575–10584 (2003), `arXiv:physics/0303100`.

[77] Y. Toyozawa, Prog. Theor. Phys. (Kyoto) **12**, 422 (1954).

[78] S. Suhai, Quasiparticle energy-band structures in semiconducting polymers: Correlation effects on the band gap in polyacetylene, Phys. Rev. B **27**, 3506–3518 (1983).

[79] J.-Q. Sun and R. J. Bartlett, Second-order many-body perturbation-theory calculations in extended systems, J. Chem. Phys. **104**, 8553–8565 (1996).

[80] S. Hirata and R. J. Bartlett, Many-body Green's-function calculations on the electronic excited states of extended systems, J. Chem. Phys. **112**, 7339–7344 (2000).

[81] R. Pino and G. E. Scuseria, Laplace-transformed diagonal Dyson correction to quasiparticle energies in periodic systems, J. Chem. Phys. **121**, 2553–2557 (2004).

[82] L. S. Cederbaum, One-body Green's function for atoms and molecules: theory and application, J. Phys. B: At. Mol. Phys. **8**, 290–303 (1975).

[83] L. S. Cederbaum and W. Domcke, Theoretical aspects of ionization potentials and photoelectron spectroscopy: A Green's function approach, in *Adv. Chem. Phys.*, edited by I. Prigogine and S. A. Rice, volume 36, pages 205–344, John Wiley & Sons, New York, 1977.

[84] W. von Niessen, J. Schirmer, and L. S. Cederbaum, Computational methods for the one-particle Green's function, Comp. Phys. Rep. **1**, 57–125 (1984).

[85] C.-M. Liegener, Third-order many-body perturbation theory in the Møller-Plesset partitioning applied to an infinite alternating hydrogen chain, J. Phys. C: Solid State Phys. **18**, 6011–6022 (1985).

[86] J. Schirmer, Beyond the Random-phase Approximation: A New Approximation Scheme for the Polarization Propagator, Phys. Rev. A **26**, 2395–2416 (1982).

[87] J. Schirmer, L. S. Cederbaum, and O. Walter, New approach to the one-particle Green's function for finite fermi systems, Phys. Rev. A **28**, 1237–1259 (1983).

[88] L. S. Cederbaum, Green's functions and propagators for chemistry, in *Encyclopedia of computational chemistry*, edited by P. v. R. Schleyer, volume 2, pages 1202–1211, John Wiley & Sons, Chichester, New York, 1998.

[89] J. Schirmer and G. Angonoa, On Green's function calculations of the static self-energy part, the ground state energy and expectation values, J. Chem. Phys. **91**, 1754–1761 (1989).

[90] R. Santra and L. S. Cederbaum, Complex absorbing potentials in the framework of electron propagator theory. I. General formalism, J. Chem. Phys. **117**, 5511–5521 (2002).

[91] J. Schirmer, Closed-form intermediate representations of many-body propagators and resolvent matrices, Phys. Rev. A **43**, 4647–4659 (1991).

[92] J. Schirmer and F. Mertins, Size consistency of an algebraic propagator approach, Int. J. Quantum Chem. **58**, 329–339 (1996).

[93] F. Mertins and J. Schirmer, Algebraic propagator approaches and intermediate-state representations. I. The biorthogonal and unitary coupled-cluster methods, Phys. Rev. A **53**, 2140–2152 (1996).

[94] M. S. Deleuze and L. S. Cederbaum, Formation of satellite bands in the ionization spectra of extended systems, Phys. Rev. B **53**, 13326–13339 (1996).

[95] A. Golod, M. S. Deleuze, and L. S. Cederbaum, Valence correlation bands of model oligomers of polyethylene: A Green's function study by the band-Lanczos approach, J. Chem. Phys. **110**, 6014–6024 (1999).

[96] R. Santra, J. Zobeley, and L. S. Cederbaum, Electronic decay of valence holes in clusters and condensed matter, Phys. Rev. B **64**, 245104 (2001).

[97] C. Buth, CO-ADC *user's manual*, Max-Planck-Institut für Physik komplexer Systeme, Nöthnitzer Straße 38, 01187 Dresden, Germany, 2004, with contributions by Martin Albrecht, Hans-Dieter Meyer, Uwe Riss and Thomas Sommerfeld.

Bibliography

[98] C. Buth, V. Bezugly, M. Albrecht, and U. Birkenheuer, Quasi-particle band structure of hydrogen fluoride chains, manuscript in preparation.

[99] C.-M. Liegener and J. J. Ladik, Ab initio calculations on bent-chain models of solid hydrogen fluoride, Phys. Rev. B **35**, 6403–6408 (1987).

[100] P. J. Mohr and B. N. Taylor, CODATA recommended values of the fundamental physical constants: 2002, Rev. Mod. Phys. **77**, 1–107 (2005).

[101] D. R. Hartree, Proc. Camb. Phil. Soc. **24**, 328 (1928).

[102] J. C. Slater, Note on Hartree's method, Phys. Rev. **35**, 210–211 (1930).

[103] V. A. Fock, Z. Phys. **15**, 126 (1930).

[104] M. Born and J. R. Oppenheimer, Ann. Phys. (Leipzig) **84**, 457 (1927).

[105] C. Cohen-Tannoudji, B. Diu, and F. Laloë, *Quantum mechanics*, John Wiley & Sons, New York, 1977.

[106] P. Pyykkö, Relativistic effects in structural chemistry, Chem. Rev. **88**, 563–594 (1988).

[107] K. Balasubramanian, *Relativistic effects in chemistry: Theory and techniques*, John Wiley & Sons, New York, 1997.

[108] F. Bloch, Z. Physik **52**, 555 (1928).

[109] H. J. Monkhorst and J. D. Pack, Special points for Brillouin-zone integrations, Phys. Rev. B **13**, 5188–5192 (1976).

[110] V. Heine, *Group theory in quantum mechanics*, International series of monographs in pure and applied mathematics, Pergamon, London, New York, 1960.

[111] J. J. Sakurai, *Modern quantum mechanics*, Addison-Wesley, Reading (Massachusetts), 2nd edition, 1994.

[112] A. A. Abrikosov, L. P. Gorkov, and I. E. Dzyaloshinski, *Methods of quantum field theory in statistical physics*, Dover, New York, 1963.

[113] A. L. Fetter and J. D. Walecka, *Quantum theory of many-particle systems*, International series in pure and applied physics, edited by Leonard I. Schiff, McGraw-Hill, New York, 1971.

[114] R. D. Mattuck, *A guide to Feynman diagrams in the many-body problem*, McGraw-Hill, New York, 2nd edition, 1976.

[115] E. K. U. Gross, E. Runge, and O. Heinonen, *Many-particle theory*, Adam Hilger, Bristol, 1991.

[116] P.-O. Löwdin, Band theory, valence bond, and tight-binding calculations, J. Appl. Phys. **33**, 251–280 (1962).

[117] C. C. J. Roothaan, New developments in molecular orbital theory, Rev. Mod. Phys. **23**, 69 (1951).

[118] G. G. Hall, Proc. Roy. Soc. A **208**, 328 (1951).

[119] J. A. Pople and R. K. Nesbet, Self-consistent orbitals for radicals, J. Chem. Phys. **22**, 571–572 (1954).

[120] D. Feller and E. R. Davidson, Basis sets for ab initio molecular orbital calculations and intermolecular interactions, in *Reviews in computational chemistry*, edited by K. B. Lipkowitz and D. B. Boyd, volume 1, pages 1–43, VCH Publishers, New York, 1990.

[121] G. H. Wannier, The structure of electronic excitation levels in insulating crystals, Phys. Rev. **52**, 191–197 (1937).

[122] N. Marzari and D. Vanderbilt, Maximally localized generalized Wannier functions for composite energy bands, Phys. Rev. B **56**, 12847–12865 (1997).

[123] C. M. Zicovich-Wilson, R. Dovesi, and V. R. Saunders, A general method to obtain well localized Wannier functions for composite energy bands in linear combination of atomic orbital periodic calculations, J. Chem. Phys. **115**, 9708–9719 (2001).

[124] A. Abdurahman, *Correlated ground state ab initio studies of polymers*, Dissertation, Technische Universität Dresden, Fakultät Mathematik und Naturwissenschaften, Dresden, Germany, 2000.

[125] C. Edmiston and K. Ruedenberg, Localized atomic and molecular orbitals, Rev. Mod. Phys. **35**, 457–464 (1963).

[126] A. Shukla, *Ab initio* Hartree-Fock Born effective charges of LiH, LiF, LiCl, NaF, and NaCl, Phys. Rev. B **61**, 13277–13282 (2000).

[127] G. H. Golub and C. F. van Loan, *Matrix computations*, Johns Hopkins University Press, Baltimore, 3rd edition, 1996.

[128] C. Buth, R. Santra, and L. S. Cederbaum, Non-Hermitian Rayleigh-Schrödinger perturbation theory, Phys. Rev. A **69**, 032505 (2004), `arXiv:physics/0401081`.

[129] E. R. Davidson, The iterative calculation of a few of the lowest eigenvalues and corresponding eigenvectors of large real-symmetric matrices, J. Comp. Phys. **17**, 87–94 (1975).

[130] R. Santra, J. Breidbach, J. Zobeley, and L. S. Cederbaum, Parallel filter diagonalization: A novel method to resolve quantum states in dense spectral regions, J. Chem. Phys. **112**, 9243–9252 (2000).

[131] R. Santra, *Non-Hermitian Many-Particle Theory for Investigating Electronic Decay of Valence Holes in Clusters*, Dissertation, Ruprecht-Karls-Universität Heidelberg, Theoretische Chemie, Physikalisch-Chemisches Institut, Im Neuenheimer Feld 229, 69120 Heidelberg, Germany, 2001, Published as Ref. [132].

[132] R. Santra and L. S. Cederbaum, Non-Hermitian Electronic Theory and Applications to Clusters, Phys. Rep. **368**, 1–117 (2002).

[133] P. P. Ewald, Ann. Phys. (Leipzig) **64**, 253 (1921).

[134] F. Mertins, Potentials in low-dimensional and semi-infinite crystals, Ann. Phys. (Leipzig) **8**, 261–300 (1999).

[135] A. Shukla, M. Dolg, P. Fulde, and H. Stoll, Towards a quantum-chemical description of crystalline insulators: A Wannier-function-based Hartree-Fock study of Li_2O and Na_2O, J. Chem. Phys. **108**, 8521–8527 (1998).

[136] A. Abdurahman, M. Albrecht, A. Shukla, and M. Dolg, *Ab Initio* Study of structural and cohesive properties of polymers: polyiminoborane and polyaminoborane, J. Chem. Phys. **110**, 8819–8824 (1999).

[137] M. Albrecht, A. Shukla, M. Dolg, P. Fulde, and H. Stoll, A Hartree-Fock ab initio band-structure calculation employing Wannier-type orbitals, Chem. Phys. Lett. **285**, 174–179 (1998).

[138] A. Abdurahman, A. Shukla, and M. Dolg, *Ab initio* treatment of electron correlations in polymers: Lithium hydride chain and beryllium hydride polymer, J. Chem. Phys. **112**, 4801–4805 (2000).

[139] J. M. Foster and S. F. Boys, Canonical configurational interaction procedure, Rev. Mod. Phys. **32**, 300–302 (1960).

[140] S. F. Boys, Construction of some molecular orbitals to be approximately invariant for changes from one molecule to another, Rev. Mod. Phys. **32**, 296–299 (1960).

[141] I. Souza, N. Marzari, and D. Vanderbilt, Maximally localized generalized Wannier functions for composite energy bands, Phys. Rev. B **65**, 035109 (2002).

[142] J. Pipek and P. G. Mezey, A fast intrinsic localization procedure applicable for *ab initio* and semiempirical linear combination of atomic orbital wave functions, J. Chem. Phys. **90**, 4916–4926 (1989).

[143] T. Koopmans, Über die Zuordnung von Wellenfunktionen und Eigenwerten zu den einzelnen Elektronen eines Atoms, Physica **1**, 104–113 (1933).

[144] P. Pulay, Localizability of dynamic electron correlation, Chem. Phys. Lett. **100**, 151–154 (1983).

[145] S. Saebø and P. Pulay, Local treatment of electron correlation, Annu. Rev. Phys. Chem. **44**, 213–236 (1993).

[146] C. Hampel and H.-J. Werner, Local treatment of electron correlation in coupled cluster theory, J. Chem. Phys. **104**, 6286–6297 (1996).

[147] M. Albrecht, private communication, 2004.

[148] P. Knowles, M. Schütz, and H.-J. Werner, Ab initio methods for electron correlation in molecules, in *Modern methods and algorithms of quantum chemistry*, edited by J. Grotendorst, volume 3 of *NIC series*, pages 97–179, Jülich, 2000, John von Neumann Institute for Computing, `www.fz-juelich.de/nic-series`.

[149] G. Del Re, J. J. Ladik, and G. Biczó, Self-consistent-field tight-binding treatment of polymers. I. Infinite three-dimensional case, Phys. Rev. **155**, 997–1003 (1967).

[150] J.-M. André, L. Gouverneur, and G. Leroy, L'étude théorique des systèmes périodique. II. La méthode LCAO-SCF-CO, Int. J. Quantum Chem. **1**, 451–461 (1967).

[151] M. Yu, S. Kalvoda, and M. Dolg, An incremental approach for correlation contributions to the structural and cohesive properties of polymers. Coupled-cluster study of *trans*-polyacetylene, Chem. Phys. **224**, 121–131 (1997).

[152] C. Willnauer and U. Birkenheuer, Quantum chemical ab initio calculations of correlation effects in complex polymers: Poly(para-phenylene), J. Chem. Phys. **120**, 11910–11918 (2004).

[153] E. N. Adams, II, Motion of an electron in a perturbed periodic potential, Phys. Rev. **85**, 41–50 (1952).

[154] E. N. Adams, II, The crystal momentum as a quantum mechanical operator, J. Chem. Phys. **21**, 2013–2017 (1953).

[155] J. Čížek, On the correlation problem in atomic and molecular systems. calculation of wavefunction components in Ursell-type expansion using quantum-field theoretical methods, J. Chem. Phys. **45**, 4256–4266 (1966).

[156] J. Čížek, in *Adv. Chem. Phys.*, volume 14, page 35, John Wiley & Sons, New York, 1969.

[157] R. J. Bartlett, Many-body perturbation theory and coupled cluster theory for electron correlation in molecules, Ann. Rev. Phys. Chem. **32**, 359.–401 (1981).

[158] G. D. Purvis III and R. J. Bartlett, A full coupled-cluster singles and doubles model: The inclusion of disconnected triples, J. Chem. Phys. **76**, 1910–1918 (1982).

[159] C. Hampel, K. A. Peterson, and H.-J. Werner, A comparison of the efficiency and accuracy of the quadratic configuration interaction (QCISD), coupled cluster (CCSD), and Brueckner coupled cluster (BCCD) methods, Chem. Phys. Lett. **190**, 1–12 (1992).

[160] K. Raghavachari, G. W. Trucks, J. A. Pople, and M. Head-Gordon, A fifth-order perturbation comparison of electron correlation theories, Chem. Phys. Lett. **157**, 479–483 (1989).

[161] K. Fink, *Korrelationseffekte in ein- und zweidimensionalen periodischen Systemen*, Dissertation, Ruhr-Universiät Bochum, Fakultät für Chemie, Bochum, Germany, 1995.

[162] K. Fink and V. Staemmler, *Ab initio* calculations of van der Waals interactions in one- and two-dimensional infinite periodic systems, J. Chem. Phys. **103**, 2603–2614 (1995).

[163] W. Förner, Formulation of the coupled cluster theory with localized orbitals in correlation calculations on polymers, Int. J. Quantum Chem. **43**, 221–250 (1992).

[164] W. Förner, R. Knab, J. Čížek, and J. Ladik, Numerical application of the coupled cluster theory with localized orbitals to polymers. IV. Band structure corrections in model systems and polyacetylene, J. Chem. Phys. **106**, 10248–10264 (1997).

[165] S. Hirata, R. Podeszwa, M. Tobita, and R. J. Bartlett, Coupled-cluster singles and doubles for extended systems, J. Chem. Phys. **120**, 2581–2592 (2004).

[166] J.-Q. Sun and R. J. Bartlett, Convergence of many-body perturbation methods with lattice summations in extended systems, J. Chem. Phys. **106**, 5554–5563 (1997).

[167] B. Paulus, *Elektronische Korrelationen in Halbleitern*, Dissertation, Universität Regensburg, Naturwissenschaftliche Fakultät II – Physik der Universität Regensburg, Regensburg, Germany, 1995.

[168] C. Pisani, Local techniques for the ab initio quantum-mechanical descriptions of the chemical properties of crystalline materials, J. Mol. Struct. (THEOCHEM) **621**, 141–147 (2003).

[169] K. Doll, *Berechnung von Korrelationsenergien von ionischen Festkörpern*, Dissertation, Universität Stuttgart, Fakultät für Physik, Stuttgart, Germany, 1995.

[170] S. Kalvoda, *Lokale elektronische Korrelationen in Gadoliniumnitrid und anderen periodischen Systemen*, Dissertation, Technische Universität Dresden, Fakultät Mathematik und Naturwissenschaften, Dresden, Germany, 1998.

[171] B. Paulus, Wave-function-based ab initio correlation treatment for the Buckminsterfullerene C_{60}, Int. J. Quantum Chem. **100**, 1026–1032 (2004).

[172] S. Kalvoda, B. Paulus, M. Dolg, H. Stoll, and H.-J. Werner, Electron correlation effects on structural and cohesive properties of *closo*-hydroborate dianions $(B_nH_n)^{2-}$ ($n = 5$–12) and (B_4H_4), Phys. Chem. Chem. Phys. **3**, 514–522 (2001).

[173] L. Pauling, *The nature of the chemical bond and the structure of molecules and crystals*, Cornell University Press, Ithaca (New York), 3rd edition, 1993.

[174] K. Rościszewski, B. Paulus, P. Fulde, and H. Stoll, *Ab initio* calculation of ground-state properties of rare-gas crystals, Phys. Rev. B **60**, 7905–7910 (1999).

[175] K. Rościszewski, B. Paulus, P. Fulde, and H. Stoll, *Ab initio* coupled-cluster calculations for the fcc and hcp structures of rare-gas solids, Phys. Rev. B **62**, 5482–5488 (2000).

[176] H. M. Evjen, On the stability of certain heteropolar crystals, Phys. Rev. **39**, 675–687 (1932).

[177] K. Doll, M. Dolg, P. Fulde, and H. Stoll, Correlation effects in ionic crystals: The cohesive energy of MgO, Phys. Rev. B **52**, 4842–4848 (1995).

[178] K. Doll and M. Dolg, Correlation effects in MgO and CaO: Cohesive energies and lattice constants, Phys. Rev. B **54**, 13529–13535 (1996).

[179] K. Doll and H. Stoll, Cohesive properties of alkali halides, Phys. Rev. B **56**, 10121–10127 (1997).

[180] K. Doll and H. Stoll, Ground-state properties of heavy alkali halides, Phys. Rev. B **57**, 4327–4331 (1998).

[181] K. Rościszewski, K. Doll, B. Paulus, P. Fulde, and H. Stoll, Ground-state properties of rutile: Electron-correlation effects, Phys. Rev. B **57**, 14667–14672 (1998).

[182] K. Doll, M. Dolg, P. Fulde, and H. Stoll, Quantum chemical approach to cohesive properties of NiO, Phys. Rev. B **55**, 10282–10288 (1997).

[183] K. Doll, P. Pyykkö, and H. Stoll, Closed-shell interaction in silver and gold chlorides, J. Chem. Phys. **109**, 2339–2345 (1998).

[184] S. Kalvoda, M. Dolg, H.-J. Flad, P. Fulde, and H. Stoll, *Ab initio* approach to cohesive properties of GdN, Phys. Rev. B **57**, 2127–2133 (1998).

[185] Dank auch an Dresdens Nachtleben! Viele schöne Stunden habe ich in den Kneipen Planwirtschaft, Schwalbennest und Westside sowie den Diskos Downtown, Platinum, Flowerpower, Vollbier, Lyra und Die Treppe verbracht.

[186] B. Paulus, P. Fulde, and H. Stoll, Electron correlations for ground-state properties of group-IV semiconductors, Phys. Rev. B **51**, 10572–10578 (1995).

[187] B. Paulus, F.-J. Shi, and H. Stoll, A correlated *ab initio* treatment of the zinc-blende wurtzite polytypism of SiC and III-V nitrides, J. Phys.: Condens. Matter **9**, 2745–2758 (1997).

[188] B. Paulus, P. Fulde, and H. Stoll, Cohesive energies of cubic III-V semiconductors, Phys. Rev. B **54**, 2556–2560 (1996).

[189] S. Kalvoda, B. Paulus, P. Fulde, and H. Stoll, Influence of electron correlations on ground-state properties of III-V semiconductors, Phys. Rev. B **55**, 4027–4030 (1997).

[190] M. Albrecht, B. Paulus, and H. Stoll, Correlated *ab initio* calculations for ground-state properties of II-VI semiconductors, Phys. Rev. B **56**, 7339–7347 (1997).

[191] B. Paulus, Towards an ab initio incremental correlation treatment for metals, Chem. Phys. Lett. **371**, 7–14 (2003).

[192] B. Paulus, K. Rościszewski, N. Gaston, P. Schwerdtfeger, and H. Stoll, Convergence of the *ab initio* many-body expansion for the cohesive energy of solid mercury, Phys. Rev. B **70**, 165106 (2004).

[193] C. Schwartz, Importance of angular correlations between atomic electrons, Phys. Rev. **126**, 1015–1019 (1962).

[194] D. P. Carroll, H. J. Silverstone, and R. M. Metzger, Piecewise polynomial configuration interaction natural orbital study of $1\,s^2$ helium, J. Chem. Phys. **71**, 4142–4163 (1979).

[195] W. Kutzelnigg and J. D. Morgan III, Rates of convergence of the partial-wave expansions of atomic correlation energies, J. Chem. Phys. **96**, 4484–4508 (1992).

[196] W. Kutzelnigg and J. D. Morgan III, Erratum: Rates of convergence of the partial-wave expansions of atomic correlation energies [J. Chem. Phys. 96, 4484 (1992)], J. Chem. Phys. **97**, 8821 (1992).

[197] M. Atoji and W. N. Lipscomb, The crystal structure of hydrogen fluoride, Acta. Cryst. **7**, 173–175 (1954).

[198] S. P. Habuda and Y. V. Gagarinsky, Nuclear magnetic resonance data on proton positions in solid HF, Acta. Cryst. **B27**, 1677–1678 (1971).

[199] M. W. Johnson, E. Sándor, and E. Arzi, The crystal structure of deuterium fluoride, Acta. Cryst. **B31**, 1998–2003 (1975).

[200] P. Otto and E. O. Steinborn, Binding energy of solid hydrogen fluoride, Solid State Communications **58**, 281–284 (1986).

[201] I. Panas, On the solid state of hydrogen fluoride: a self-consistent crystal field study, Int. J. Quantum Chem. **46**, 109–118 (1993).

[202] S. Berski and Z. Latajka, On the difference between hydrogen fluoride and hydrogen chloride crystals, J. Mol. Struct. **450**, 259–263 (1998).

[203] E. Sándor and R. F. C. Farrow, Crystal structure of solid hydrogen chloride and deuterium chloride, Nature **213**, 171–172 (1967).

[204] E. Sándor and R. F. C. Farrow, Crystal structure of cubic deuterium chloride, Nature **215**, 1265–1266 (1967).

[205] E. Sándor and R. F. C. Farrow, Neutron diffraction study of molecular motion in solid deuterium chloride, Disc. Faraday Soc. **48**, 78–86 (1969).

[206] W. C. Hamilton and J. A. Ibers, *Hydrogen bonding in solids*, Benjamin, New York, Amsterdam, 1968.

[207] S. Scheiner, *Hydrogen bonding—A theoretical perspective*, Oxford University Press, New York, Oxford, 1997.

[208] D. Hadži, editor, *Theoretical treatments of hydrogen bonding*, John Wiley & Sons, Chichester, New York, 1997.

[209] M. S. Gordon and J. H. Jensen, Understanding the hydrogen bond using quantum chemistry, Acc. Chem. Res. **29**, 536–543 (1996).

[210] R. W. Jansen, R. Bertoncini, A. I. Pinnick, David A. Katz, R. C. Hanson, O. F. Sankey, and M. O'Keeffe, Theoretical aspects of solid hydrogen halides under pressure, Phys. Rev. B **35**, 9830–9846 (1987).

[211] M. Springborg, First-principles examination of hydrogen bonds: polymeric hydrogen fluoride, Phys. Rev. Lett. **59**, 2287–2290 (1987).

[212] M. Springborg, Energy surfaces and electronic properties of hydrogen fluoride, Phys. Rev. B **38**, 1483–1503 (1988).

[213] A. Zunger, Band structure, crystal conformation, and hydrogen bond potentials for solid HF, J. Chem. Phys. **63**, 1713–1731 (1975).

[214] M. Kertész, J. Koller, and A. Ažman, Ab initio crystal orbital treatment of hydrogen fluoride (HF) chains, Chem. Phys. Lett. **36**, 576–579 (1975).

[215] A. Karpfen and P. Schuster, Ab initio studies on infinite linear hydrogen fluoride chains, Chem. Phys. Lett. **44**, 459–464 (1976).

[216] A. Blumen and C. Merkel, Comparative calculations on ferroelectric HCl and HF, Solid State Commun. **20**, 755–758 (1976).

[217] A. Blumen and C. Merkel, Energy band calculations on helical systems, phys. stat. sol. (b) **83**, 425–431 (1977).

[218] M. Kertész, J. Koller, and A. Ažman, Ab-initio crystal orbital study of hydrogen fluoride chain. Basis set dependence, Z. Naturforsch. A **33**, 249–250 (1978).

[219] A. Karpfen, Ab initio studies on hydrogen bonded chains. I. Equilibrium geometry of the infinite, linear chain of hydrogen fluoride molecules, Chem. Phys. **47**, 401–406 (1980).

[220] A. Karpfen, A. Beyer, and P. Schuster, Hydrogen bonding in clusters and molecular crystals, Int. J. Quantum Chem. **19**, 1113–1119 (1981).

[221] A. Beyer and A. Karpfen, Ab initio studies on hydrogen bonded chains. II. Equilibrium geometry and vibrational spectra of the bent chain of hydrogen fluoride molecules, Chem. Phys. **64**, 343–357 (1982).

[222] Y. J. I'haya, S. Narita, Y. Fujita, and H. Ujino, Ab initio crystal orbital calculations on $4(CH)_n$ and $(HF)_n$ with extended basis set., Int. J. Quantum Chem. Symp. **18**, 153–159 (1984).

[223] I. Mayer, G. Räther, and S. Suhai, The chemical Hamiltonian approach for infinite chains, Chem. Phys. Lett. **270**, 211–216 (1997).

[224] S. Berski and Z. Latajka, Periodic Hartree-Fock study of $(HF)_\infty$ chain, J. Mol. Struct. (Theochem) **389**, 147–154 (1997).

[225] S. Hirata and S. Iwata, Ab initio Hartree-Fock and density functional studies on the structures and vibrations of an infinite hydrogen fluoride polymer, J. Phys. Chem. A **102**, 8426–8436 (1998).

[226] D. Jacquemin, J.-M. André, and B. Champagne, Long-range effects in optimizing the geometry of stereoregular polymers. II. Hydrogen fluoride chains as a working example, J. Chem. Phys. **111**, 5324–5330 (1999).

[227] A. Blumen and C. Merkel, Electronic band structure of ferroelectric HCl, Chem. Phys. Lett. **45**, 47–49 (1977).

[228] S. Berski and Z. Latajka, Periodic Hartree-Fock studies on $(HCl)_\infty$ chain, Polish J. Chem. **72**, 1540–1550 (1998).

[229] G. Schaftenaar and J. H. Noordik, Molden: a pre- and post-processing program for molecular and electronic structures, J. Comput.-Aided Mol. Design **14**, 123–134 (2000).

[230] N. Wiberg, A. F. Holleman, and E. Wiberg, *Inorganic chemistry*, Academic Press, New York, 2001.

[231] V. R. Saunders, R. Dovesi, C. Roetti, R. Orlando, C. M. Zicovich-Wilson, N. M. Harrison, K. Doll, B. Civalleri, I. J. Bush, P. D'Arco, and M. Llunell, CRYSTAL03 *User's Manual*, University of Torino, Torino, 2003.

[232] R. D. Amos, A. Bernhardsson, A. Berning, P. Celani, D. L. Cooper, M. J. O. Deegan, A. J. Dobbyn, F. Eckert, C. Hampel, G. Hetzer, P. J. Knowles, T. Korona, R. Lindh, A. W. Lloyd, S. J. McNicholas, F. R. Manby, W. Meyer, M. E. Mura, A. Nicklass, P. Palmieri, R. Pitzer, G. Rauhut, M. Schütz, U. Schumann, H. Stoll, A. J. Stone, R. Tarroni, T. Thorsteinsson, and H.-J. Werner, MOLPRO, a package of *ab initio* programs designed by H.-J. Werner and P. J. Knowles, version 2002.6, 2002.

[233] H. B. Jansen and P. Ros, Non-empirical molecular orbital calculations on the protonation of carbon monoxide, Chem. Phys. Lett. **3**, 140–143 (1969).

[234] S. F. Boys and F. Bernardi, The calculation of small molecular interactions by the differences of separate total energies. Some procedures with reduced errors, Mol. Phys. **19**, 553–566 (1970).

[235] F. B. van Duijneveldt, J. G. C. M. van Duijneveldt-van de Rijdt, and J. H. van Lenthe, State of the art in counterpoise theory, Chem. Rev. **94**, 1873–1885 (1994).

[236] L. Rincón, R. Almeida, D. García-Aldea, and H. Diez y Riega, Hydrogen bond cooperativity and electron delocalization in hydrogen fluoride clusters, J. Chem. Phys. **114**, 5552–5561 (2001).

[237] M. L. Klein and J. A. Venables, editors, *Rare gas solids*, volume 1, Academic Press, London, 1976.

[238] J. J. Moré, The Levenberg-Marquardt algorithm: Implementation and theory, in *Numerical analysis*, edited by G. A. Watson, volume 630 of *Lecture notes in mathematics*, pages 105–116, Springer-Verlag, Berlin, New York, 1977.

[239] B. M. Axilrod and E. Teller, Interaction of the van der Waals type between three atoms, J. Chem. Phys. **11**, 299–300 (1943).

[240] C. Pisani and U. Birkenheuer, Unrestricted Hartree-Fock treatment of paramagnetic defect centers in non-magnetic crystals VI, Comput. Phys. Commun. **96**, 152–166 (1996).

[241] U. Birkenheuer, F. Corà, C. Pisani, E. Scorza, and G. Perego, Embedded-cluster study of core-level binding energies of magnesium and alkali impurities at the surface of MgO, Surf. Sci. **373**, 393–408 (1997).

[242] M. Gell-Mann and F. Low, Bound states in quantum field theory, Phys. Rev. **84**, 350–354 (1951).

[243] G. C. Wick, The evaluation of the collision matrix, Phys. Rev. **80**, 268–272 (1950).

[244] R. P. Feynman, The theory of positrons, Phys. Rev. **76**, 749–759 (1949).

[245] R. P. Feynman, Space-time approach to quantum electrodynamics, Phys. Rev. **76**, 769–789 (1949).

[246] K. A. Brueckner, Many-body problem for strongly interacting particles. II. Linked cluster expansion, Phys. Rev. **100**, 36–45 (1955).

[247] J. Goldstone, Derivation of the Brueckner many-body theory, Proc. R. Soc. London., Ser. A **239**, 267–279 (1957).

[248] F. J. Dyson, The radiation theories of Tomonaga, Schwinger, and Feynman, Phys. Rev. **75**, 486–502 (1949).

Bibliography

[249] F. J. Dyson, The S Matrix in Quantum Electrodynamics, Phys. Rev. **75**, 1736–1755 (1949).

[250] S. Ethofer and P. Schuck, The six-point Green function and the application of Faddeev's theory to the many body problem, Z. Physik **228**, 264–285 (1969).

[251] J. Winter, Study of core excitations in one-particle and one-hole nuclei by means of the six-point Green function, Nucl. Phys. A **194**, 535–551 (1972).

[252] L. van Hove, N. M. Hugenholtz, and L. Howland, *Quantum theory of many-particle systems*, Benjamin, New York, 1961.

[253] N. M. Hugenholtz, Quantum theory of many-body systems, Rep. Prog. Phys. **28**, 201–247 (1965).

[254] M. S. Deleuze, The issue of size and charge consistency and the implications of translation symmetry in advanced Green's function theories, Int. J. Quantum Chem. **93**, 191–211 (2003).

[255] R. J. Buenker and S. D. Peyerimhoff, Individualized configuration selection in CI calculations with subsequent energy extrapolation, Theoret. Chim. Acta (Berl.) **35**, 33–58 (1974).

[256] C. Lanczos, An iteration method for the solution of the eigenvalue problem of linear differential and integral operators, J. Res. Nat. Bur. Stand. **45**, 255–282 (1950).

[257] J. K. Cullum and R. A. Willoughby, *Lanczos algorithms for large symmetric eigenvalue computations*, Birkhäuser, Boston, 1985, two volumes.

[258] V. I. Kukulin, V. M. Krasnopol'sky, and J. Horáček, *Theory of resonances*, Kluwer, Dordrecht, 1989.

[259] K. P. Huber and G. H. Herzberg, *Molecular spectra and molecular structure. IV. Constants of diatomic molecules*, Van Nostrand-Reinhold, New York, 1979.

[260] R. S. Mulliken, Electronic population analysis on LCAO—MO molecular wave functions. I, J. Chem. Phys. **23**, 1833–1840 (1955).

[261] GAMESS-UK is a package of *ab initio* programs written by M. F. Guest, J. H. van Lenthe, J. Kendrick, K. Schoffel, and P. Sherwood, with contributions from R. D. Amos, R. J. Buenker, H. J. J. van Dam, M. Dupuis, N. C. Handy, I. H. Hillier, P. J. Knowles, V. Bonacic-Koutecky, W. von Niessen, R. J. Harrison, A. P. Rendell, V. R. Saunders, A. J. Stone, D. J. Tozer, and A. H. de Vries. The package is derived from the original GAMESS code due to M. Dupuis, D. Spangler and J. Wendoloski, NRCC Software Catalog, Vol. 1, Program No. QG01 (GAMESS), 1980.

[262] F. Tarantelli, private communication, 2004.

[263] J. Schirmer, A. B. Trofimov, and G. Stelter, A non-Dyson third-order approximation scheme for the electron propagator, J. Chem. Phys. **109**, 4734–4744 (1998).

[264] J. Breidbach, private communication, 2004.

[265] H. Preuss, Bemerkungen zum Self-consistent-field-Verfahren und zur Methode der Konfigurationenwechselwirkung in der Quantenchemie, Z. Naturforschg. **11A**, 823–831 (1956).

[266] J. L. Whitten, Gaussian expansion of Hydrogen-atom wavefunctions, J. Chem. Phys. **39**, 349–352 (1963).

[267] M. Prencipe, A. Zupan, R. Dovesi, E. Aprà, and V. R. Saunders, *Ab initio* study of the structural properties of LiF, NaF, KF, LiCl, NaCl, and KCl, Phys. Rev. B **51**, 3391–3396 (1995).

[268] R. W. G. Wyckoff, *Crystal structures*, volume I, Wiley, New York, 2nd edition, 1968.

[269] N.-P. Wang, M. Rohlfing, P. Krüger, and J. Pollmann, Quasiparticle band structure and optical spectrum of LiF(001), Phys. Rev. B **67**, 115111 (2003).

[270] E. L. Shirley, L. J. Terminello, J. E. Klepeis, and F. J. Himpsel, Detailed theoretical photoelectron angular distributions for LiF(100), Phys. Rev. B **53**, 10296–10309 (1996).

[271] D. M. Roessler and W. C. Walker, Electronic spectrum of crystalline lithium fluoride, J. Phys. Chem. Solids **28**, 1507–1515 (1967).

[272] R. T. Poole, J. G. Jenkin, J. Liesegang, and R. C. G. Leckey, Electronic band structure of the alkali halides. I. Experimental parameters, Phys. Rev. B **11**, 5179–5189 (1975).

[273] R. T. Poole, J. Liesegang, R. C. G. Leckey, and J. G. Jenkin, Electronic band structure of the alkali halides. II. Critical survey of theoretical calculations, Phys. Rev. B **11**, 5190–5196 (1975).

[274] M. Piacentini, A new interpretation of the fundamental exciton region in LiF, Solid State Commun. **17**, 697–700 (1975).

[275] M. Piacentini, D. W. Lynch, and C. G. Olson, Thermoreflectance of LiF between 12 and 30 eV, Phys. Rev. B **33**, 5530–5543 (1976).

[276] A. B. Kunz, Study of the electronic structure of twelve alkali halide crystals, Phys. Rev. B **26**, 2056–2069 (1982).

[277] W. J. Hehre, R. F. Stewart, and J. A. Pople, Self-consistent molecular-orbital methods. I. Use of Gaussian expansions of Slater-type atomic orbitals, J. Chem. Phys. **51**, 2657–2664 (1969).

[278] K. Rościszewski and B. Paulus, Influence of three-body forces and anharmonic effects on the zero-point energy of rare-gas crystals, Phys. Rev. B **66**, 092102 (2002).

[279] U. Birkenheuer and C. Buth, manuscript in preparation, 2005.

[280] M. Pernpointner and A. B. Trofimov, The one-particle Green's function method in the Dirac-Hartree-Fock framework. I. Second-order valence ionization energies of Ne through Xe, J. Chem. Phys. **120**, 4098–4106 (2004).

[281] M. Pernpointner, The one-particle Green's function method in the Dirac-Hartree-Fock framework. II. Third-order valence ionization energies of the noble gases, CO and ICN, J. Chem. Phys. **121**, 8782–8791 (2004).

[282] J. Schirmer and A. Barth, Higher-order approximations for the particle-particle propagator, Z. Phys. A **317**, 267–279 (1984).

[283] A. Tarantelli and L. S. Cederbaum, Particle-particle propagator in the algebraic diagrammatic construction scheme at third order, Phys. Rev. A **39**, 1656–1664 (1989).

[284] A. B. Trofimov and J. Schirmer, An efficient polarization propagator approach to valence electron excitation spectra, J. Phys. B **28**, 2299–2324 (1995).

[285] A. Tarantelli and L. S. Cederbaum, Approximation scheme for the three-particle propagator, Phys. Rev. A **46**, 81–94 (1992).

Index

Summary

This dissertation focuses on *ab initio* theories for the ground state, electron attachment and electron removal states of perfect semiconducting and insulating crystals. In part one, I study the ground-state of the hydrogen-bonded infinite chains $(HF)_\infty$ and $(HCl)_\infty$ with the help of basis set extrapolation. In part two, a local orbital Green's function method is derived and applied to the HF and LiF molecules, the infinite $(HF)_\infty$ chain and the LiF crystal.

The Hartree-Fock approximation is presented in detail elucidating the consequences of translational symmetry. The canonical crystal orbitals, the Bloch orbitals, are plane-wave-like functions which extend over the whole crystal. Another view on independent particle states is provided by localized crystal orbitals, the atomic-orbital-like Wannier orbitals. Computational methods to obtain Wannier orbitals are discussed. Thereby, I particularly focus on their *a priori* determination by deriving Hartree-Fock equations which directly yield Wannier orbitals.

The coupled-cluster singles and doubles correlation method is chosen. It is formulated in terms of Wannier orbitals to treat electron correlations in the ground-state of crystals. In the energy expression of the correlation energy, lattice summations lead to an incremental series of energy contributions in terms of the residual interaction between fragments of growing size in the crystal, the so-called energy increments. This infinite series is truncated, denoted as configuration selection, and a molecular cluster is used to represent a fraction of the solid. This procedure is frequently referred to as incremental scheme. I can harness existing quantum chemical program packages for computations on crystals. The incremental series provides a general framework to describe interactions in crystals. I determine the constants of two-body dispersion interaction. They allow partition of the two-body energy increments into a short-range, van-der-Waals-reduced part and a long-range part that can be summed analytically to infinite distances. Thereby, I show that the actual number of relevant energy increments is reduced notably.

A thorough analysis of the basis set convergence of the Hartree-Fock energy and the correlation energy in the ground-state of the infinite $(HF)_\infty$ and $(HCl)_\infty$ chains is undertaken. I show that both energies follow relations found for small molecules. The now known convergence properties allow an extrapolation of the results from truncated one-particle basis sets towards the complete basis set limit which improves the accuracy of binding energies by roughly an order of magnitude.

The theoretical description of excited states of solids poses a *profoundly* more involved problem than the description of the ground state. The one-particle model of Hartree-Fock or Kohn-Sham theory still is the predominant intellectual device for their description and interpretation. The orbital energies are typically plotted with respect to the crystal momentum which graphically leads to long bands, the so-called band structures.

A rigorous *ab initio* description is feasible using methods of quantum field theory. Specifically, the pole positions of the one-particle Green's function represent the exact energies of excited states. I evaluate the Green's function in terms of the Dyson equation where the self-energy therein is approximated in a certain order of perturbation theory. A crystal orbital formulation of the well-established *algebraic diagrammatic construction (ADC)* which I term *crystal orbital ADC (CO-ADC)* is used to sum these contributions to infinite orders in addition to the summation carried out by the Dyson equation. The pole search of the one-particle Green's function is recast into a sparse Hermitian eigenvalue problem which is a numerically stable and efficient formulation. CO-ADC theory is derived for both Bloch and Wannier orbitals.

The formulation in terms of Wannier orbitals is particularly beneficial as it allows to apply cutoff criteria even within the unit cell. To this end, I devise a configuration selection procedure to restrict the configurations that have to be accounted for in a description of electron attachment and electron removal states at a given accuracy. Configuration selection is shown to lead to a definition of degeneracy among the states of a crystal. The performance of iterative diagonalization algorithms, e.g., the block-Lanczos algorithm I employ, is determined by the scaling of the matrix times vector product. Its precise analysis leads to the conclusion that the determination of excited states is a quadratically scaling problem that becomes a *linear* scaling problem, if one *a priori* restricts oneself to a few states.

Moreover, a new ADC scheme for localized molecular orbitals follows immediately from the CO-ADC equations in terms of Wannier orbitals. The scheme is suitable to calculate the ionization potentials and electron affinities of large molecules which are not accessible by conventional methods.

I have developed a computer program to carry out computations with the CO-ADC theory. Ionization potentials of the molecules HF and LiF are determined. Striking is the strong shake-down satellite in HF that splits off the $F\,2s$ independent-particle state and is not found in LiF. This makes HF particularly suitable to assess the additional perturbative treatment employed to account for the off-diagonal elements of the Fock matrix in terms of localized orbitals. I show the high reliability of this approximation by means of a comparison to the ionization potentials obtained with established canonical molecular orbital based ADC programs.

Using CO-ADC, the quasiparticle band structure of an infinite hydrogen fluoride chain is computed. The convergence of the configuration space turns out to be extremely rapid, requiring only nearest-neighbor cells to be included. A completely different method, the local Hamiltonian approach, is utilized to independently obtain the valence bands of $(HF)_\infty$. A good agreement between the results of the two methods is found.

Finally, the quasiparticle band structure of a three-dimensional lithium fluoride crystal is studied in terms of a minimal *ab initio* approach. Successively, configurations in the origin cell, the first and second nearest-neighbor cells are accounted for in the CO-ADC method, observing a rapid convergence of the fundamental band gap and the width of the $F\,2p$ band complex. Concerning the fact that only a minimal basis set is used, the obtained results are in good agreement both with previous theoretical and with experimental data.

2

Curriculum vitae

Personal details

Name	Christian Buth (Dipl. Phys.)
Date and place of birth	15 February 1975 in Mönchengladbach, Germany
Nationality	German
Marital status	Single

School

1 Sep 1981 – 1 Jul 1985	Grundschule [primary school] Katterbach, Bergisch Gladbach, Germany
1 Sep 1985	Städtisches Nicolaus-Cusanus-Gymnasium [secondary school], Bergisch Gladbach, Germany
1 Sep 1995	Allgemeine Hochschulreife (Abitur) [diploma from secondary school qualifying for university admission]

Community service

3 Jul 1995 – 31 Jul 1996	Zivildienst [community service as a replacement for military service] in the Gemeinnützige Werkstätten Köln, Bergisch Gladbach, Germany

University

30 Sep 1996	Studying physics at the Ruprecht-Karls-Universität Heidelberg, Heidelberg, Germany
3 Sep 1998	Diplom-Vorprüfung [intermediate examination] in physics
2 Oct 1998 – 25 Jun 1999	One year of studying physics at the University of Edinburgh, Edinburgh, Scotland, Great Britain
18 Oct 1999	Continued studying physics at the Ruprecht-Karls-Universität Heidelberg, Heidelberg, Germany
12 Sep 2002	Diplom [diploma] in physics. Diplomarbeit [diploma thesis] at the Theoretische Chemie, Physikalisch-Chemisches Institut with Prof. Lorenz S. CEDERBAUM

1 Dec 2002 – 10 Nov 2005	Research for the Ph.D. thesis [Dissertation] at the Max-Planck-Institut für Physik komplexer Systeme, Dresden, Germany, with Prof. Peter FULDE

Internships

29 Jun 1999 – 3 Sep 1999	Summer student program at the Organisation Européenne pour la recherche nucléaire (CERN), Geneva, Switzerland

Teaching

13 Oct 2003 – 7 Feb 2004	Supervising the experiment "Reversion pendulum" at the Technische Universität Dresden, Dresden, Germany
5 Apr 2004 – 17 Jul 2004	Tutorial "Theoretical Electrodynamics" at the Technische Universität Dresden, Dresden, Germany
Since 15 Nov 2004	Tuition of a master student at the Max-Planck-Institut für Physik komplexer Systeme, Dresden, Germany

Scholarships and grants

1 Oct 1997 – 12 Sep 2002	Grundförderung [scholarship for undergraduate students], Friedrich-Ebert-Stiftung, Bonn, Germany
Since 16 May 2001	Online-scholarship, e-fellows.net GmbH & Co. KG, München, Germany
5 – 18 Mar 2005	Kongress- und Vortragsreise [travel to a congress and a lecture tour], Deutsche Forschungsgemeinschaft (DFG), Bonn, Germany, references KON 324/2005 and BU 1865/1-1

Awards

9 Mar 2005	IBM-Zerner Fellowship, 45th Sanibel Symposium organized by the Quantum Theory Project, University of Florida, Gainesville, Florida, United States of America

Publications

1. Christian Buth, *Non-Hermitian perturbation theory for the electronic decay of excited and ionized molecules and identification of the electronic decay processes in the Auger decay of core-ionized Xenon Fluorides*, Diplomarbeit, Ruprecht-Karls-Universität Heidelberg, Theoretische Chemie, Physikalisch-Chemisches Institut, Im Neuenheimer Feld 229, 69120 Heidelberg, Germany, 2002, `www.ub.uni-heidelberg.de/archiv/3004`.

2. Christian Buth, Robin Santra, and Lorenz S. Cederbaum, *Ionization of the Xenon Fluorides*, J. Chem. Phys. **119**, 7763–7771 (2003), `arXiv:physics/0306123`.

3. Christian Buth, Robin Santra, and Lorenz S. Cederbaum, *Impact of interatomic electronic decay processes on the width of the Xe 4d lines in the Auger decay of the xenon fluorides*, J. Chem. Phys. **119**, 10575–10584 (2003), `arXiv:physics/0303100`.

4. Republication of Reference 3, Virtual Journal of Ultrafast Science **2**, issue 12, (2003).

5. Christian Buth, Robin Santra, and Lorenz S. Cederbaum, *Non-Hermitian Rayleigh-Schrödinger perturbation theory*, Phys. Rev. A **69**, 032505 (2004), `arXiv:physics/0401081`.

6. Christian Buth and Beate Paulus, *Basis set convergence in extended systems: infinite hydrogen fluoride and hydrogen chloride chains*, Chem. Phys. Lett. **398**, 44–49 (2004), `arXiv:cond-mat/0408243`.

7. Christian Buth, Uwe Birkenheuer, Martin Albrecht, and Peter Fulde, Ab initio *Green's function formalism for band structures*, Phys. Rev. B **72**, 195107 (2005), `arXiv:cond-mat/0409078`.

Talks

Invited

1. *Green's function approach to* ab initio *band structures*, Center for Computational Materials Science (CMS), Lecture for the Science College of CMS, 11 Oct 2004, Universität Wien, Vienna, Austria

2. *Algebraic diagrammatic construction for band structures*, Oberseminar zur theoretischen Chemie, 18 Jan 2005, Ruprecht-Karls-Universität Heidelberg, Heidelberg, Germany

3. *Green's function approach to* ab initio *band structures*, Quantum Theory Project – Seminar series, 16 Mar 2005, University of Florida, Gainesville, Florida, United States of America

Contributed

1. *Nichthermitesche Multireferenz-Störungstheorie zur Berechnung elektronischer Resonanzzustände in Molekülen*, Frühjahrstagung der Deutschen Physikalischen Gesellschaft 4 to 8 Mar 2002, Fachverband Molekülphysik, Osnabrück, Germany

2. *A Green's function formalism for* ab initio *band structure calculations in semiconductors and insulators*, Electronic-correlations tea seminar, 6 Aug 2003, Max-Planck-Institut für Physik komplexer Systeme, Dresden, Germany

3. *Green's function approach to* ab initio *band structures*, Doktorandentag, 18 Dec 2003, Max-Planck-Institut für Physik komplexer Systeme, Dresden, Germany

4. *Green's function approach to* ab initio *band structures*, Doktorandentag, 16 Dec 2004, Max-Planck-Institut für Physik komplexer Systeme, Dresden, Germany

Posters

1. *Green's function approach to* ab initio *band structures of HF and HCl chains*, *Ab initio* modeling in solid state chemistry (MSSC2003), 7 to 13 Sep 2003, Torino, Italy

2. *Green's function approach to* ab initio *band structures of HF and HCl chains*, Molecular spectroscopy and dynamics, 39th Symposium on Theoretical Chemistry (STC2003), 28 Sep to 2 Oct 2003, Gwatt Lake Thun, Switzerland

3. *Green's function approach to* ab initio *band structures*, Local correlation methods: From molecules to crystals (LCC2004), 9 to 11 Sep 2004, Torino, Italy

4. *Green's function approach to* ab initio *band structures*, Korrelationstage 2005 (Korrel05), 28 February to 5 Mar 2005, Dresden, Germany

5. *Green's function approach to* ab initio *band structures*, 45th Sanibel Symposium, 5 to 11 Mar 2005, St. Simons Island, Georgia, United States of America

6. *Green's function approach to* ab initio *band structures*, Strong correlations and ARPES: Recent progress in theory and experiment (CORPES05), Seminar: 29 Mar to 6 May 2005, Workshop: 4 to 8 April 2005, Dresden, Germany

Dresden, 14 June 2005

Versicherung

a) Hiermit versichere ich, dass ich die vorliegende Arbeit ohne unzulässige Hilfe Dritter und ohne Benutzung anderer als der angegebenen Hilfsmittel angefertigt habe; die aus fremden Quellen direkt oder indirekt übernommenen Gedanken sind als solche kenntlich gemacht.

b) Die vorliegende Arbeit wurde am Max-Planck-Institut für Physik komplexer Systeme, Dresden unter der wissenschaftlichen Betreuung von Herrn Prof. Dr. Peter Fulde angefertigt.

c) Die Arbeit wurde bisher weder im Inland noch im Ausland in gleicher oder ähnlicher Form einer anderen Prüfungsbehörde vorgelegt.

d) Hiermit erkläre ich, dass ich die Promotionsordnung der Fakultät Mathematik und Naturwissenschaften der Technischen Universität Dresden anerkenne.

Dresden, 14.06.2005   ....
                                                              Unterschrift